2018-02-26

Understanding Human Erythrocyte Glucose Transporter (GLUT1) Mediated Glucose Transport Phenomena Through Structural Analysis

Kenneth P. Lloyd
University of Massachusetts Medical School

Understanding Human Erythrocyte Glucose Transporter (GLUT1) Mediated Glucose Transport Phenomena Through Structural Analysis.

A Dissertation Presented By:

Kenneth P. Lloyd

Abstract

GLUT1-mediated, facilitated sugar transport is proposed to be an example of transport by a carrier that alternately presents exofacial (e2) and endofacial (e1) substrate binding sites, commonly referred to as the alternating access carrier model. This hypothesis is incompatible with observations of co-existent exo- and endofacial ligand binding sites, transport allostery, and e1 ligand (e.g. cytochalasin B) induced GLUT1 sugar occlusion. The fixed-site carrier model proposes co-existent, interacting e2 and e1 ligand binding sites but involves sugar translocation by geminate exchange through internal cavities. Demonstrations of membrane-resident dimeric and tetrameric GLUT1 and of e2, e1 and occluded GLUT conformations in GLUT crystals of monodisperse, detergent-solubilized proteins suggest a third model. Here, GLUT1 is an alternating access carrier but the transporter complex is a dimer of GLUT1 dimers, in which subunit interactions produce two e2 and two e1 conformers at any instant. The crystallographic structures in different conformations can be utilized to further understand the transport cycle, ligand binding behavior and complex kinetics observed in GLUT1. Specifically, the GLUT1 crystal structure and homology models based upon related major facilitator superfamily proteins were used in this study, to understand inhibitor binding, ligand binding induced GLUT1 transport allostery and the existence of helix packing/oligomerization motifs and glycine induced flexibility. These studies suggest that GLUT1 functions as an oligomeric allosteric carrier where cis-allostery is an intramolecular behavior and trans-allostery is an intermolecular behavior. Additionally, mutations of a dynamic glycine affect the turnover of the transporter while mutations to helix packing motifs affect affinity.

Acknowledgements

First, I would like to thank my mentor Dr. Anthony Carruthers for his support, advice, and encouragement. I am thankful for his guidance through allowing me to pursue the research areas that most interested me while always being available to discuss ideas and answer questions. Thank you for allowing me to grow as both a scientist and a person.

I would like to thank the members of the Carruthers lab: Dr. Julie DeZutter, Dr. Ogooluwa Ojelabi, Dr. Andrew Simon, and Dr. Jay Sage. I must single out Dr. Julie DeZutter for all of the advice, guidance and teaching that you gave me throughout my gradute career.

I would like to thank my TRAC committee Dr. Reid Gilmore, Dr. Francesca Massi and Dr. Scott Shaffer for your advice and help with my thesis research.

I would like to thank Dr. Kendall Knight for joining my dissertation exam committee.

I would like to thank Dr. Jeffrey Pessin for agreeing to be my outside examiner, for venturing to Massachusetts during January, and for always coming to view my poster(s) at FASEB meetings.

I would like to thank the members of the UMassMed Mass Spectrometry facility Karin Greene, Dr. John Leczyk, and Dr. Kristin Boggio for assisting me with all of my mass spectrometry experiments and questions. I wish that the experiments had been more productive but it wasn't for lack of trying.

Finally, I must thank my family. My parents Ken and Joan for all of the support and encouragement in life and throughout my time in graduate school. I must thank my sister Janice, for her support in listening to me whenever anything went wrong in lab or life, for helping me stay focused, and for always being there to help me with anything I needed. I could not have finished this program without their help.

Table of Contents

List of Figures

List of Tables

Abbreviations

β-D-Glc .....β-D-glucose

β-NG .....nonyl-β-D-glucopyranoside

1DeO-FSK 1-deoxy-forskolin

2DG.....2-deoxy-D-glucose

3MG 3-O-methyl-D-glucose

6A-FSK 6-acetyl-forskolin

7DeA-FSK 7-deacetyl-forskolin

7FPA-FSK..... 7-fluorophenylacetyl-forskolin

AAT .....alternating access transporter

AMP .....adenosine monophosphate

ATP .....adenosine triphosphate

BBB.....blood brain barrier

BCA ..... bicinchoninic acid assay

BRET .....bioluminescent forster resonance energy transfer

CB .....cytochalasin B

C(X) .....cytochalasins

C-AB .....polyclonal antibody corresponding to GLUT4 residues 498-509

DTT.....dithiothreitol

DMEM ..... dulbecco's modified eagle medium

e1.....endofacial

e1o..... endofacial occluded

e2.....exofacial

e2o ..... exofacial occluded

ECG ..... epicatechin gallate

EE ..... equilibrium exchange

EGCG ..... epigallocatechin gallate

FBS ..... fetal bovine serum

FSK ..... forskolin

FST ..... fixed-site transporter

GLUT ..... facilitative glucose transporter

GLUT1 ..... human erythrocyte facilitative glucose transporter

$GLUT1_{Q282A}$ ..... GLUT1 containing Q282A mutant

$GLUT1_{(GLUT3\text{-}H9)}$ ..... tetramerization deficient GLUT1 mutant

$GLUT1_{(GLUT3\text{-}H9)Q282A}$ ..... tetramerization deficient GLUT1 + Q282A mutant

G1DS ..... GLUT1 deficiency syndrome

GS ..... GlideScore

H# ..... transmembrane alpha-helix #

IC ..... infinite-cis

IMP ..... integral membrane protein

MFS ..... major facilitator superfamily

NaKATPase ..... sodium potassium ATPase

PBS ..... phosphate buffered saline

PBS-Mg ..... phosphate buffered saline + magnesium chloride

PBS-T ..... phosphate buffered saline + tween

RBC ..... red blood cell

SDS-PAGE ..... sodium dodecyl sulfate-polyacrylamide gel electrophoresis

SGLT..... sodium driven glucose transporter

SLC50 ..... SWEET transporter

TM..... transmembrane alpha helix

WT ..... wild-type GLUT1

wtGLUT1 ..... wild-type GLUT1

WZB117..... 2-fluoro-6-(m-hydroxybenzoyloxy)phenyl m-hydroxybenzoate

XylE ..... xylose/H+ symporter

ZT..... zero-trans

CHAPTER 1:

Introduction:

Glucose Transport Protein Literature Review

Why Study Carrier Mediated Transport?

Homeostasis is the process through which the internal environment of cells is maintained at a steady-state, wherein flux and consumption are balanced. In order to maintain this balance, cells rely upon integral membrane proteins (IMP) to catalyze the transport of molecules across the cell membrane. Investigating the relationships between IMP structure, ligand binding and transport mechanism is necessary if our goal is to understand a vast number of biological processes including metabolism, cell signaling, and cellular/organismal homeostasis. The importance of understanding the relationships between IMPs and cellular and organismal homeostasis is also of fundamental interest to the pharmaceutical industry as more than 50% of drug targets fall within this class of proteins (1). This thesis will focus on the human erythrocyte facilitative glucose transporter (GLUT1), a member of the major facilitator superfamily (MFS), and an IMP which plays a central role in cellular and organismal homeostasis and is implicated in both cancer and metabolic diseases.

The Plasma Membrane

Both prokaryotic and eukaryotic cells are surrounded by a plasma membrane that seals the cell from its external environment and maintains the internal volume and composition of the cell. The membrane is composed of amphipathic lipids, specifically: phospholipids, sterols and glycolipids. Phospholipids, the most abundant lipid in membranes, combine a hydrophilic phosphate head group with a hydrophobic tail of uncharged, non-polar long chain fatty acids. The fatty acid chains self-associate to form a hydrophobic bilayer while the hydrophilic head groups interact with both the interstitium and the cytoplasm. The continuous envelope of lipid bilayer is interspersed with glycolipids and sterols. Glycolipids, a lipid moiety modified with a sugar, primarily serve as recognition sites for cell-cell interaction. Sterols, a subgroup of steroids,

the most well-known of which is cholesterol are necessary to maintain the plasticity of the membrane (2).

Transport across Cell Membranes

Molecules can cross the cell membrane in several ways. Non-Stokesian diffusion is one such process whereby molecules must first partition into the bilayer, diffuse across the bilayer then partition out at the opposite, trans-side of the membrane (3). Partitioning into and out of the bilayer is governed by the membrane solubility of the molecular diffusant - hydrophobic molecules are characterized by lower standard chemical potentials in hydrophobic solvents and thus accumulate more readily in the bilayer. Diffusion across the bilayer is governed by molecular diffusant size. The bilayer core behaves as a polymer and thus the rate of diffusion is governed by the probability of a diffusant encountering a void volume of sufficient size to permit diffusant entry (3). The average volume of void spaces in the human erythrocyte bilayer is a mere 8.4 cm^3/mol - the size of a methylene group and smaller than the van der Waal's volume of water [3]. These principles explain why transbilayer molecular diffusion of only the smallest and most hydrophobic of biological substrates (e.g. O_2, CO_2) is sufficient to explain physiological rates of transport. For most other molecules (sugars, amino acids, nucleosides, ions) transbilayer diffusion is too slow and nonspecific to be compatible with cellular function [3]. These molecules use IMPs to cross the membrane in a process referred to as protein-mediated transport.

IMPs catalyze two types of membrane transport. Passive transport (sometimes referred to as facilitated diffusion) results in the transmembrane movement of molecules down an electrochemical gradient. Active transport results in the net transport of molecules against an electrochemical gradient and requires an energy input to catalyze the movement of a solute

against its electrochemical gradient [3]. This is accomplished in nature in two ways: 1) by coupling uphill transport to an exergonic process such as ATP hydrolysis (primary active transport) or 2) by coupling uphill transport to the transport of a second molecule down a favorable electrochemical gradient (a process known as secondary active transport) [3]. Within these general classifications of passive and active transport mechanisms, there exists three different operational transport modes: 1) uniport, where the transport of a molecule does not require the transport of a counter species in the opposite direction; 2) symport, where multiple different molecules are transported across the membrane in the same direction, and 3) antiport, where two or more different molecules are transported across the membrane in opposite directions [3].

Membrane Proteins

The plasma membrane comprises a lipid bilayer with associated peripheral and integral membrane proteins. Peripheral membrane proteins non-covalently attach to the cell membrane, primarily at the cytoplasmic surface (4). Integral membrane proteins may be subdivided into three types: monotopic IMPs, bitopic IMPs and transmembrane proteins (5). Monotopic IMPs are permanently attached to one side of the plasma membrane and penetrate the bilayer without crossing it. Bitopic or single-pass IMPs cross the membrane only once and have N- and C-termini on opposite sides of the membrane. Transmembrane or multi-pass IMPs cross the membrane multiple times and can have N- and C-termini at the same or opposite sides of the membrane. Coupled together the plasma membrane and associated proteins function to limit and regulate the passage of molecules and information into and out of the cell.

Three types of membrane transport proteins mediate transport: pores, channels and carriers. (Figure 1.1) These proteins differ in their transport mechanism, permeation pathway and form of

solute movement. While all three protein types mediate facilitated diffusion, only carriers can mediate active transport [3]. Pore proteins stabilize an opening in the membrane, presenting simultaneous access at both sides of the plasma membrane to molecules compatible with the size and charge constraints of the membrane pore [3]. Similarly, channel proteins transport ions across the cell membrane by stabilizing an opening in the cell membrane. However, in the case of channel proteins, access to both sides of the membrane is temporary and conditional. Channels exist in either an open or closed state triggered by a small conformational change. Open channels are much like pores in that they are open to both sides of the membrane simultaneously allowing a continuous flow of solutes without interruption. A selectivity filter controls what class and type of ions can pass through the open-channel pore. Sodium, potassium, calcium, and chloride are common ions that enter and exit the cell through channels. Unlike pores and channels, carriers are thought not to present simultaneous access to both the intra- and extracellular environments. Carrier proteins instead undergo a series of conformational changes to facilitate translocation of substrate. Both the rate of the conformational change and stoichiometry of binding combine to limit the number of molecules transported per event.

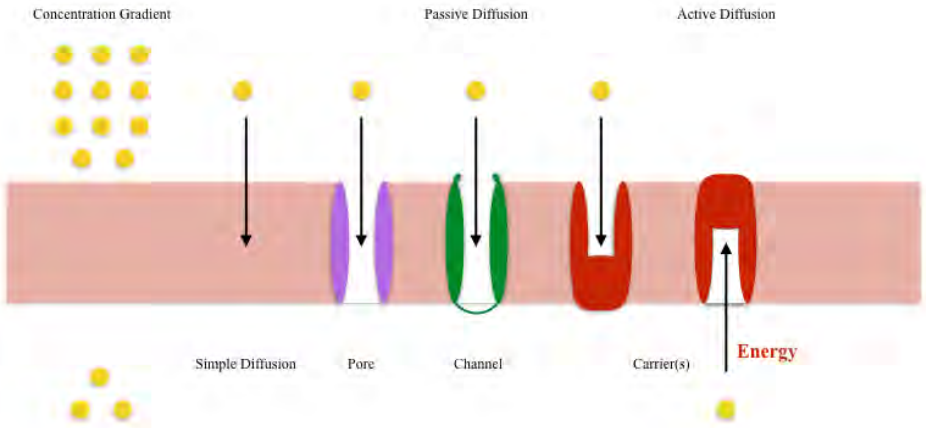

Figure 1.1: Diffusion across a membrane bilayer. A lipid bilayer is shown (pink) providing a barrier between extracellular (above) and intracellular space (below). The yellow circles represent the substrate and are at a higher concentration outside the cell. Passive diffusion processes, simple of facilitated diffusion (pores, channels, carriers), don't require an energy input and mediate transport from high to low concentrations. Active transport, mediated by carriers requires an energy input to transport the ligand against the concentration gradient.

The Major Facilitator Superfamily

Carrier proteins can be further sub-categorized as subclasses or superfamilies of proteins based upon function and structure. GLUT1 is a member of the major facilitator superfamily (MFS) (6). These proteins are ubiquitously expressed across all three domains of organisms: Archaea, Bacteria, and Eukaryota. They catalyze both passive or secondary active transport of a variety of molecules including simple sugars, complex oligosaccharides, drugs, amino acids, ions and other molecules utilizing uniport, antiport and symport mechanisms (7). They share a common fold, with the majority containing 12 membrane spanning α-helices and cytoplasmic N- and C-termini. The proteins average a length of 400-600 amino acids and comprise two six helix halves connected by a large intracellular loop between transmembrane domains 6 and 7 (8,9).

Glucose Homeostasis

Glucose occupies a central role in mammalian energy metabolism serving as a preferred metabolite in the brain and exercising skeletal muscle. Mammals maintain blood glucose within narrow limits (4-12 mM) despite continuously variable carbohydrate ingestion and elimination (10). Fifty to seventy-five percent of total glucose metabolism is used to fuel brain metabolism (11).

Why Study Glucose Transport?

Glucose through its role as a substrate for ATP synthesis is a critical energy source for life on Earth. The human brain consumes approximately 50-75% of the glucose supply in the human body while comprising ~2% of total body mass [11]. In addition, glucose serves as an important precursor for biomolecule synthesis and plays a significant role in cell signaling. Through different mechanisms, glucose can regulate gene transcription, enzyme activity, hormone secretion and the activity of glucoregulatory neurons (12). The cellular uptake of glucose

precedes any events involving metabolism and signaling and is controlled by the level of glucose transporter expression at the cell surface. Three families of transporters have been identified for glucose transport: the sodium driven glucose transporter (SGLT), the SWEET transporters (SLC50), and the facilitative glucose transporters (GLUT) (13).

The Glucose Transporter Family

The GLUT family of passive sugar transporters maintains glucose hemostasis throughout all cell types but in a tissue specific manner (12,14). The GLUT transporter family comprises 14 members that can be grouped into 3 different classes based upon sequence similarity: class I: GLUT1-4 and GLUT14 a gene duplication of GLUT3, class II: GLUT5, 7, 9, and 11 and class III: GLUT6, 8, 10, 12, and 13, (GLUT13 is the proton driven myoinositol transporter HMIT) (Table 1) (12,14). Each class is characterized by variable substrate specificities including several aldoses, myo-inositol, urate, glucosamine, and ascorbate (12,14). The entire family has a sequence identity ranging from 28 to 65% and shares specific sugar transporter sugar motifs (12,14). All GLUTs have the canonical MFS transporter fold and a single N-linked glycosylation site. Class III can be differentiated from class I and II by the position of the glycosylation site which is found in exofacial loop 1 in class I and II GLUTs and in exofacial loop 5 in class III GLUTs (15).

GLUT1 is expressed in almost all human cell types but is most highly concentrated in erythrocytes and at the blood brain barrier (16). GLUT1 was one of the first membrane transporters to be identified, purified, and cloned (17-19). GLUT2 has a low apparent affinity for glucose, can also transport galactose, mannose and fructose with low affinity but transports glucosamine with high affinity (20,21). GLUT2 is the major glucose transporter of hepatocytes, and is expressed in intestinal absorptive cells, kidney cells, and some neurons and astrocytes (22-

24). Although GLUT2 is highly expressed in rodent pancreatic α- and β- cells, GLUT1 is the major transporter expressed in human pancreatic α- and β- cells (22,25). GLUT3 displays higher apparent affinity and high maximum turnover number for glucose than the other class I proteins, and its principal physiological substrate is D-glucose (26). GLUT3 is the primary mediator of glucose uptake in neurons (27). GLUT4 is expressed most prominently in adipocytes, skeletal muscle and cardiomyocytes, residing primarily in intracellular membrane compartments (28). GLUT4 is the insulin-responsive glucose transporter. Defects in insulin-mediated GLUT4 translocation to the plasma membrane coupled with a defect in insulin secretion from pancreatic beta cells and insulin resistance in the liver results in type 2 diabetes (29). GLUT5 was the first of the class II GLUTs identified and it has a high specificity for fructose but does not transport glucose or galactose (30-32). The small intestine regulates dietary fructose absorption where GLUT5 mediates fructose transport across the apical membrane (33). It is present in low levels in kidney, brain, fat, testes, and muscle (33). GLUT9 has two forms GLUT9a and GLUT9b with different cytoplasmic tails. Both forms are expressed in the liver and kidney while GLUT9a is also expressed in the intestine, leukocytes and chondrocytes (34). GLUT9 is a urate transporter and transport is not competitively inhibited by glucose or fructose (35). GLUT9-mediated urate transport is inhibited by phloretin but not by cytochalasin B (CB) (36). GLUT8 is only expressed in an intracellular compartment (37). GLUT8 mutations resulting in its cell surface expression suggest that GLUT8 has a high affinity for glucose, while also showing affinity for fructose and galactose and inhibition by CB (37). GLUT8 is expressed at high levels in the testis and at lower levels in the cerebellum, adrenal gland, liver, spleen, brown adipose tissue, and lung (38).

GLUT13 or HMIT is a H+/myo-inositol co-transporter (39). While transport by HMIT is inhibited by phloretin, phlorizin, and CB, HMIT does not transport glucose [39]. It is expressed

most highly in the brain but also in brown adipose tissue and in the kidney [39]. GLUTs 6, 7, 10, 11, 12, and 14 were identified through the sequencing of the human genome. While each is capable of transporting hexoses when expressed in Xenopus oocytes the primary physiological substrates for most of these proteins have not been identified definitively (40).

GLUTs and Disease

Due to the ubiquitous expression of GLUTs and their role in maintaining glucose homeostasis, disruption to both the regulation of GLUT localization/expression and mutations in GLUT transporter gene sequences can have effects on both sugar metabolism and the physiology of organ systems where the GLUTs are expressed.

While mutations in glucose transporter genes are rare, they can result in severe diseases that render sugar consumption impossible. For example, mutations in both GLUT1, resulting in GLUT1 deficiency syndrome, and GLUT2, resulting in Fanconi-Bickel syndrome, eliminate the ability to ingest sugar without deleterious effects. The first case of GLUT1 deficiency syndrome (G1DS) was found to have a null allele producing hemizygosity and haploinsufficiency of the GLUT1 gene (41). As of 2012, there were approximately 200 known cases of G1DS resulting from different mutations to the GLUT1 gene (42). These mutations give rise to a wide array of phenotypes, but they are generally characterized by a low cerebral glucose supply, due to the role GLUT1 plays in transporting glucose across the blood brain barrier (43). Lifelong adherence to a ketogenic diet can mitigate some of these symptoms if the disease is detected early enough. Fanconi-Bickel syndrome is an autosomal recessive disorder where patients can suffer from hepatomegaly, nephropathy, fasting hypoglycemia, sugar intolerance, and growth retardation (44). For some of the identified mutations, GLUT2 function is abolished and these patients do not tolerate simple sugars in their diets (45).

In addition to diseases directly arising from mutations of GLUTs, glucose transporters and their trafficking also play a significant role in metabolic disorders. For example, in type II diabetes, glucose uptake into muscle and fat is impaired due to insulin resistance (46). The transport of glucose into muscle and fat tissue is the rate-limiting step for glucose metabolism in these tissues and is mediated by GLUT4 (47). In response to impaired insulin secretion GLUT4 trafficking to the cell-surface is downgraded, disrupting GLUT4 mediated entry of glucose into fat and muscle cells (48,49). An understanding of how GLUT4 is trafficked and transports sugar is central to our ability to treat type II diabetes and remains under active investigation.

Cancer cells depend on glucose metabolism for energy production and the synthesis of biomass to sustain proliferation. The "Warburg effect" refers to human and animal tumor cells preference for conversion of glucose to lactate in the presence of oxygen for energy production (50). Studies have demonstrated elevated expression of glucose transporters in most cancers and some cancers show abnormal transporter expression patterns compared to healthy tissues (12,15,51). In particular, high expression of GLUT1 has been documented in a wide range of cancer types including lung, brain, breast, bladder, cervical, colorectal, esophageal, hepatocelluar, head and neck, gastric, ovarian, renal cell, pancreatic, thyroid, penile, and uterine cancers (51). GLUTs pose an interesting avenue both as biomarkers and drug targets for cancer therapeutics.

GLUT1 as an Ideal Model System

Studying glucose transport is complicated for a number of reasons. Most tissues express multiple GLUTs and the profile of cellular glucose transporter expressions alters upon cell isolation and culture. Furthermore, cell culture conditions can promote hypoxia-induced gene expression, the up regulation of glycolysis and changes in the level of cell-surface GLUT

expression. In addition to phenotypic changes, cell culture can result in a heterogeneous population of cell sizes with an attendant range of surface area:volume ratios that make accurate transport determinations difficult to achieve.

On the other hand, the human red blood cell (RBC) provides an ideal model system for studying glucose flux. GLUT1 comprises 10-20% of RBC integral membrane proteins and mediates >99% of glucose transport across the plasma membrane (52). RBCs are relatively uniform in size and shape, are easily isolated form whole blood and, because rates of glucose transport are some 500-fold greater than rates of glucose metabolism, human RBCs are not subject to isolation-promoted phenotypic changes in metabolism (53,54). Importantly, an established purification protocol was developed by two groups that produces a significant amount of pure functional GLUT1 reconstituted in native erythrocyte lipids at greater than 90% purity (17,18). The availability of human erythrocytes, coupled with their uniformity in both size and surface area and a robust purification protocol have resulted in more than 70 years of sophisticated kinetic and biophysical analyses of GLUT1. However, analysis of the role of primary structure of GLUT1 requires alternative cell systems as mutagenesis of GLUT1 and its expression in red cells is not practical.

GLUT1 Localization and Function

GLUT1 is expressed most highly in erythrocytes, cardiac muscle cells, smooth muscle, astrocytes and in the blood brain barrier (BBB) endothelial cells (55). Human red blood cells contain 250,000-500,000 copies of GLUT1, where it catalyzes glucose and galactose transport (56-58). Due to its presence in the BBB, GLUT1 plays a fundamental role in delivering glucose to the central nervous system (59,60). Approximately 20-40% of total cellular GLUT1 is expressed at the cell surface of cardiomyocytes, BBB endothelial cells, adipocytes and astrocytes

(61-64). Intracellular GLUT1 is located within the endoplasmic reticulum, the Golgi, and endosomes, where endosomal GLUT1 cycles between the plasma membrane and endosomal compartments in cardiomyocytes in an AMP kinase and phosphatidylinositol 3-kinase dependent manner (61).

Glucose uptake is rate-limiting for metabolism in cells where glucose transport capacity is low relative to the rate of sugar metabolism. These cells typically respond acutely to metabolic stress with accelerated net sugar uptake and increased glucose metabolism (64-66). In cardiomyocytes, smooth muscle, and astrocytes glucose transport is rate limiting and transport regulation is integral for maintaining metabolic homeostasis. In erythrocytes and endothelial cells, however, glucose is transported some 50-500 times more rapidly than it is metabolized (53,67). Yet, RBCs respond to ATP depletion with 4- to 10-fold increased glucose uptake, and endothelial cells respond to acute hypoglycemia with 4- to 10-fold increased glucose uptake and respond to chronic hypoglycemia with increased GLUT1 expression (16,68-71). These observations have resulted in the rejection of earlier lore that glucose transport is only regulated in cells where transport is rate-limiting for cellular glucose metabolism (72). Rather, glucose transport appears to be regulated both in cells where transport is rate-limiting for cellular glucose metabolism and in cells which serve to deliver glucose to other tissues where glucose is a primary metabolic fuel (55,73).

GLUT1 Substrate Specificity

GLUT1 transports both D-glucose and D-galactose, but it has a 10-fold higher affinity for D-glucose (74). Competitive inhibition studies suggest that the hydroxyl groups at C1 and C6 of D-glucose are solvent exposed at the sugar uptake site in the exofacial (e2) conformation while the hydroxyl at C1 is solvent exposed in the e1 conformation at the sugar exit site (74,75).

Hydrogen bonding is suggested at the hydroxyl groups at C1, C3, and possibly C4 at the uptake site while the hydroxyl group at C6 is involved in hydrogen bonding at the e1 site (74,75). Additionally, both transport and crystallization studies of GLUT1 demonstrate that there is no difference in the binding and transport behavior by GLUT1 towards α- and β-D-glucose suggesting that the position of the C1 hydroxyl is unimportant for hydrogen bond formation (76,77).

GLUT1 Ligand Binding

GLUT1 ligand binding studies allow for the direct quantitation of the number of ligand-binding sites per transporter and allow for analysis of possible drug targets for GLUT1. Determination of the sidedness of ligand binding to GLUT1 can be accomplished using two approaches: direct measurements of ligand binding to GLUT1 to examine the effects of exo- and endofacial substrates on ligand binding or by examining the effects of inhibitors on glucose transport. GLUT1 interacts with and is regulated and/or inhibited by several different molecules. Disaccharides such as maltose and oligosaccharides, such as maltotriose are inhibitors of GLUT1 mediated sugar transport (78). As the size of the oligosaccharide increases the strength of inhibition decreases (78). The exofacial site of GLUT1 can also interact with and become inhibited by a diverse array of molecules including: phloretin, ethylidene glucose, green tea catechins, and flavonoids (79-82). Similarly, the endofacial site of GLUT1 interacts with and is inhibited by cytochalasin B, forskolin, and methylxanthines including caffeine (83-85). In addition, the transporter interacts with and is allosterically inhibited by ATP (86,87).

Building upon earlier kinetic and transport studies of NaKATPase that recognized that the enzyme isomerized between at least two states - e1 and e2- and that these states presented ligand binding cavity at endofacial and exofacial surfaces of the membrane respectively, the sugar

transport community has termed the endofacial and exofacial conformations of the glucose transporter e1 and e2 conformations respectively (88-90).

Early purifications of red blood cell GLUT1 demonstrated that cytochalasin B and exofacial inhibitor binding to GLUT1 are mutually exclusive (91-93). However, later studies using purified GLUT1, red cell membranes, and intact red cells showed interacting, negatively cooperative, e2 (exofacial) and e1 (endofacial) ligand binding sites (79,83,94). For example, phloretin, an e2 ligand, exerts a strongly negatively cooperative effect on CB binding to the endofacial site (79). At low concentrations, maltose and ethylidene glucose enhance CB binding to GLUT1, but at higher concentrations these ligands have a negative cooperative effect, suggesting that the e2 and e1 sites are not mutually exclusive (79,80). Additional studies of CB binding to purified GLUT1 showed a stoichiometry of 1 molecule of CB per 2 molecules of GLUT1. Treatment of the purified transporter with reductant changed the binding stoichiometry to 1 molecule of CB to 1 molecule GLUT1 (17,95,96).

GLUT1 Kinetics

Due to the absence of a 3-dimensional structure, GLUT1 behavior and transport models have been developed using kinetic measurements. Several common experimental methods were developed to analyze the transport behavior of GLUT1, and obtain the V_{MAX} and K_M for both sugar exit and entry under different conditions (89,97,98). Three main types of experiments have been developed: zero-trans (ZT), equilibrium exchange (EE) and infinite-cis (IC). ZT experiments measure unidirectional transport of sugar over a wide range of concentrations of sugar from one side (cis) of the cell to the other (trans) where no sugar is initially present. ZT experiments can be used to determine kinetic parameters for both sugar uptake and efflux. In EE experiments the total concentration of sugar is varied but is the same on both sides of the

membrane (i.e. the system is at equilibrium), and the unidirectional transport of radio-tracer sugar is measured. IC experiments begin with saturating concentrations of sugar on one side and vary the concentration of sugar on the other side of the membrane. IC experiments then measure either the rate of net or unidirectional transport from the saturating sugar concentration to the opposite side. Infinite cis-exit, for example, measures that concentration of sugar which half-maximally inhibits saturated net exit.

GLUT1 Steady-State Kinetics

In order to study steady-state kinetics (the concentration dependence) of sugar transport, the concentrations of GLUT1 sugar intermediates involved in transport must be unchanged during the transport assay. In practice, this means that transport measurements must be made at very early time points where the amount of sugar in the cell increases or decreases linearly with time. This requires either making measurements in <1s at 37 °C, lowering the temperature to 4 °C, or using sugar analogs that are transported at slower rates. Despite these challenges, GLUT1 is the most extensively characterized of the GLUTs due to the experimental advantages posed by the human erythrocyte (99). Transport measurements of metabolizable sugars are simplified in red cells due to their slower metabolic processes compared to conventional cells (100). However, GLUT1 mediated transport has also been characterized in a variety of systems including *Xenopus* oocytes, mammalian cell lines, and yeast (101-105).

Studying glucose transport necessitates the use of radiolabeled glucose analogs as tracers for sugar movements and the use of specific inhibitors to arrest transport. In order to more effectively measure transport rates, glucose analogs are used that are not metabolically processed. Two such analogs are 2-deoxy-D-glucose (2DG) and 3-O-methyl-D-glucose (3MG) (106). 2DG is used to simplify undirectional sugar uptake measurements as it is phosphorylated

by hexokinase to form 2-deoxy-D-glucose-6-phosphate, which is not a substrate for further metabolism and is trapped inside the cell (107). 3MG is not metabolized and can be used to measure transport into or out of the cell (108).

Transport Kinetic Asymmetry

GLUT1 is an asymmetric transporter (109). This means that V_{MAX} and K_M for sugar exit into sugar sugar-free medium (ZT exit) are not identical to V_{MAX} and K_M for entry into sugar-free cells (ZT entry). This behavior does not violate the passive nature of transport because under equilibrium exchange conditions (where intracellular [sugar] = extracellular [sugar]), uptake must equal efflux and, at sub saturation [sugar],

$$\text{uptake} = \text{efflux} = k[\text{sugar}] \text{ where } k = V_{MAX} / K_M$$

Thus, the only requirement of an asymetric, passive transporter is that: V_{MAX} / K_M for exit = V_{MAX} / K_M for entry. At low temperatures GLUT1 sugar transport in human red cells is increasingly asymmetric. At 4 °C V_{MAX} and K_M for exit are 10X greater than the equivalent parameters for entry (109). In red cell ghosts asymmetry is greatly diminished, due to the loss of allosteric regulation by cytoplasmic ATP (86,87,110). Simulations of sugar transport demonstrate that asymmetric red cell glucose transport allows cells to equilibrate much more rapidly with extracellular sugar, such that glucose-depleted red cells emerging from glucose-consuming organs such as the brain or placenta are more readily refilled upon reentering glucose-rich circulation (87,111).

Accelerated Exchange

Accelerated exchange transport describes the stimulatory effect that the presence of sugar at the *trans* side of the membrane exerts on the rate of unidirectional sugar flux from the *cis* to the trans side. In red cells preloaded with sugar, unidirectional sugar uptake is accelerated several

fold when compared with unloaded cells, similarly unidirectional sugar exit is accelerated by extracellular sugar (112). In EE accelerated exchange experiments, intracellular [sugar] = extracellular [sugar], and unidirectional sugar uptake/exit is measured using tracer sugars, while in infinite trans experiments the concentration of sugar at the *trans* side is saturating and the concentration of sugar at the *cis* side is varied. Unidirectional radio tracer sugar flux is then measured in the direction *cis* to *trans.* At 4 °C, V_{MAX} and K_M for EE are 50-fold greater than for ZT sugar uptake and 5- to 10-fold greater than for ZT sugar exit (113). As temperature increases, the difference between exchange and net transport parameters decreases (109). The availability of cytoplasmic ATP exaggerates accelerated exchange in red blood cells by suppressing the maximum rate of ZT sugar uptake and by decreasing K_M for EE (114). Unlike GLUT1, GLUT4 does not demonstrate trans-acceleration (115). Substitution of GLUT4 transmembrane (TM) domain 6 into GLUT1 eliminates trans-acceleration in GLUT1 while substitution of GLUT1 TM6 into GLUT4 enables GLUT4 to catalyze trans-acceleration. This demonstrates the GLUT1 TM6 is necessary and sufficient for trans-acceleration, possibly by slowing transport associated conformational changes in the absence of intracellular sugar (116).

Transient Kinetics

Transient kinetic studies allow for monitoring of the transition of one conformational state of GLUT1 to another. Transient kinetic studies of purified reduced GLUT1 by intrinsic tryptophan fluorescence demonstrated that exofacial ligands can trap GLUT1 in one conformational state that subsequently relaxes to a second state upon dilution of exofacial ligand (117). Studies with non-reduced purified GLUT1 demonstrate that micromolar levels of exofacial ligand promote one conformational state whereas higher micromolar levels promote a second inhibited state (118). Rapid quench transport measurements in red cells show transient

acceleration of glucose uptake after dilution of extracellular maltose. Quench-flow analysis of sugar uptake by red cells demonstrates three observable, sequential phases of sugar uptake: the first, a rapid but quantitatively small phase describing sugar association with GLUT1 (1 mol sugar: 1 mol GLUT1), the second, fast phase, shows sugar import into cytosol and accounts for 2/3 sugar uptake by red cells and the third slowest phase shows a slowing of transport as endofacial sugar binding sites become saturated (119). This same study also demonstrated the ability of GLUT1 to occlude or "trap" a sugar molecule within a central cavity when conformational changes are "stopped" by CB or phloretin (119).

GLUT1 Cooperativity

Sugar and ligand binding to the transporter have been demonstrated to exert a cooperative effect on binding of a second ligand or on sugar transport. Both *cis*- and *trans*-cooperative effects are seen. Specifically, *trans*-cooperative effects are seen on both entry and exit of unidirectional sugar flux. The experimentally determined K_M for infinite *trans* glucose or 3MG exit from RBCs is consistently 5- to 10-fold lower than predicted by standard transport models based on measurements from ZT and EE sugar transport experiments, suggesting that saturation of the external sugar binding site increases the affinity of the internal sugar binding site(s) for sugar (114,120-123). A second *trans* effect has been demonstrated by the e1 inhibitors CB and forskolin. At low concentrations, both ligands increase sugar uptake compared to unliganded GLUT1 while inhibiting transport as the concentration is raised (80). Similarly, exofacial maltose or maltotriose stimulate sugar uptake at low concentrations before inhibiting uptake as the concentration is raised, thus unidirectional sugar uptake is stimulated by the presence of both extra- and intracellular inhibitors at low concentrations (78). Additionally, ligand binding also demonstrates both *cis*- and *trans*-cooperativity. Phloretin has a strong negatively cooperative

effect on CB binding (79). Similarly, maltose and ethylidene glucose have a negatively cooperative effect on CB binding at high concentrations but a positively cooperative effect at low concentrations of maltose and ethylidene glucose (79,80). Similarly, at the endofacial site, derivatives of the e1 ligand forskolin have different effects on CB binding. While forskolin is a direct inhibitor of CB binding to GLUT1, derivatives of forskolin can have a stimulatory effect (7DeA-FSK) and a stimulatory followed by inhibition effect (1DeO-FSK) (84).

Kinetic and Ligand Binding Derived GLUT1 Transport Models.

In absence of a 3D crystal structure, the majority of transport models for GLUT1 were developed using kinetic and ligand binding experiments. The two most widely described models to explain carrier-mediated transport are the alternating conformer or simple carrier model and the fixed-site carrier model.

The first proposed model was the mobile carrier hypothesis, where a glucose specific molecule bound glucose on one side of the membrane, moved across the membrane and deposited the translocated glucose molecule inside the cell (124). While this model was physically improbable, it led to the development of the alternating access carrier model (Figure 1.2). The alternating access carrier model proposes that the transporter alternately presents sugar import (e2) and sugar export sites (e1). Sugar binding to the e2 site catalyzes a conformational change that results in the sugar molecules translocation across the membrane and released from the e1 site. Multiple rounds of transport are processed either by reconversion of e1 to e2 conformation or substrate binding and translocation. However, the GLUT1 monomer presents only one site, e1 or e2 at any one time (125). Further kinetic analysis suggested an intermediate occluded state (119). Thus, the transporter when in an e2 conformation binds sugar, and then undergoes a conformational change through an occluded state to the e1 state where the sugar is

released

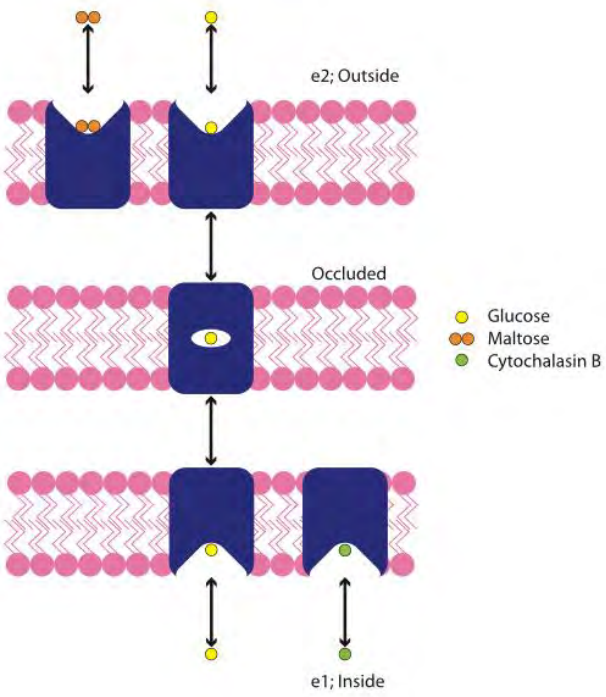

Figure 1.2: The alternating access carrier model. GLUT1 presents either an e2 outward facing site or e1 inward facing site. Glucose molecules represented by yellow circles are transported by binding at the e2 site, inducing a conformational change through an occluded state to the e1 state where the sugar is released. Transport inhibitors maltose (e2, orange) and cytochalasin B (e1 green) bind to the transporter and lock it in e2 or e1 conformations, respectively.

inside the cell. In order to continue translocating sugar into the cell the transporter must relax from e1 to the occluded state and then to the e2 state where it binds sugar again to repeat the cycle. However, the simple carrier is not compatible with all experimental observed transport and ligand binding studies, specifically the demonstrated ability of the transporter to interact with multiple substrates simultaneously.

Alternatively, the fixed-site carrier model predicts that ligands or sugars can bind at both the e1 and e2 sites simultaneously (Figure 1.3) (125,126). This model proposes a higher-affinity exofacial binding site and a lower-affinity endofacial binding site, allowing for the greater V_{MAX} and K_M observed for sugar exit than entry under saturating extracellular sugar concentrations. This model allows sugar or inhibitors to interact with the transporter at both sides of the membrane at the same time. During transport, bound sugars are released into a central cavity whence they exchange with e1 and e2 binding. The sugars then dissociate from the carrier to be released at the opposite side of the membrane.

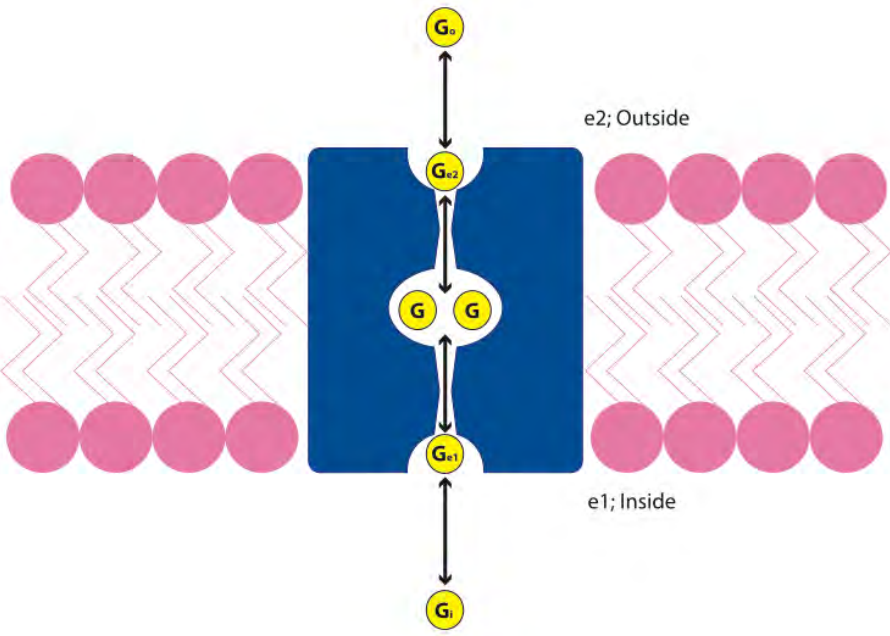

Figure 1.3: The fixed-site carrier model. In the fixed site carrier model sugar (yellow circles) can bind at either the e2 or e1 site simultaneously. Transport is accomplished through a central cavity with room for two glucose molecules to pass each other.

The fixed-site carrier explains how the V_{MAX} for exchange can be equal for two substrates with dissimilar translocation rates. Additionally, it is compatible with the multiphase nature of transport, specifically the rapid, fast and slow phases of glucose transport, potentially describing binding at e2, translocation and rebinding at e1, and the slow release of the substrate into the cytosolic domain of the transporter.

However, neither the simple nor fixed site carrier models can explain the low intracellular K_M observed in infinite-cis entry or infinite-trans exit experiments. In addition, the fixed site carrier model fails to explain allosteric phenomena such as the cooperative binding of modulators or inhibitors like ATP, CB, and maltose.

GLUT1 Structure Function Relationship

GLUT1 is a 492 amino acid protein with the canonical MFS protein fold containing 12 membrane spanning alpha-helices, N- and C-termini in the cytoplasm, an N-linked-glycosylation site at asparagine 45 and a large intracellular loop connecting transmembrane domains 6 and 7. (Figure 1.4) Due to the difficulty of membrane protein crystallography, early studies focused on hydropathy analysis, scanning glycosylation mutagenesis, mass spectrometry of GLUT1 proteolytic cleavage sites, circular dichroism, fourier transform infrared spectroscopy, and analysis of the crystal structures of other MFS transporters combined with homology modeling techniques (127-130). Together, these analyses suggested that there are 12 hydrophobic TMs, with 8 TMs being highly amphipathic forming a water filled channel for sugar translocation (75). TMs 1 and 8 are poised at the limits of membrane solubility, such that TM1 is released by trypsin digestion of GLUT1 and TM8 is released by addition of endofacial ligand to trypsinized GLUT1 (128).

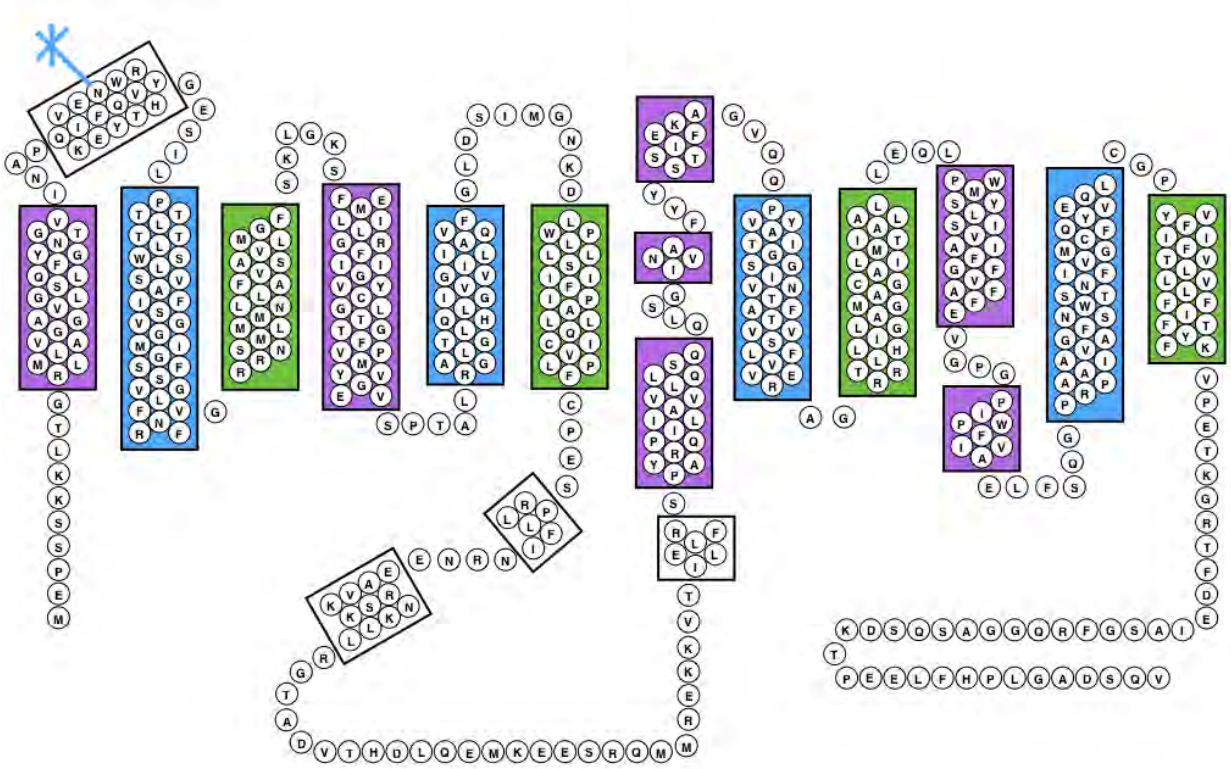

Figure 1.4: GLUT1 primary amino acid sequence and membrane topology from 4PYP crystal structure. Transmembrane domains are color-coded based upon their role in the transporter. TMs 1, 4, 7, and 10 are colored purple and with TMs 2, 5, 8, and 11, colored blue, form the aqueous pore. TMs 3, 6, 9, and 12 act as scaffold domains outside the transport pore. The N-linked Glycosylation site at N45 is represented as is the large intracellular loop connecting TMs 6 and 7 and containing three short helical regions.

MFS Structure

Membrane protein crystallography has been much more technically challenging than that of soluble proteins. Only 1.7% of over 130,000 structural coordinates deposited in the Protein Data Bank (PDB) represents membrane proteins. Of these only 707 out of 2250 are from unique proteins. The first MFS transporters crystalized were the lactose/H+ symporter LacY in both e1 open and e2 partially occluded conformations and the glycerol-3-phosphate/Pi antiporter GlpT in an e1 open conformation (8,9). In total, 20 different MFS proteins have been crystalized in different liganded states and conformations including: e1 open, e1 partially occluded, e2 open, and e2 partially occluded.

Sugar Transport Protein Structure

Sugar transport proteins from both bacteria and human have been crystalized. The xylose/H+ symporter, XylE from *Escherichia coli* was crystallized in e2 occluded, e1 occluded, and e1 open conformations with multiple different ligands (6,131). It shares 25% sequence homology and 58% sequence similarity with GLUT1. The fucose/H+ symporter (FucP) from *E. coli* was crystalized in an e2 open conformation (132). From, *Bos taurus* and *Rattus norvegicus*, GLUT5, a fructose uniporter and member of the GLUT family, was crystalized in both an inward open and outward open conformation (133). From *Homo sapiens* GLUT3, a glucose uniporter was crystalized in both e2 open and e2 occluded conformations (134). Finally, GLUT1 was crystalized in an e1 open conformation with both β-NG, a glycodetergent and CB (4PYP, 5EQI) (77,135). All of these structures contained the canonical MFS fold with 12 TM alpha helices, N- and C- termini in the cytoplasm, and a large semi-structured loop between TMs 6 and 7.

GLUT1 Structure

The first crystal structure of GLUT1 was obtained in 2014 in an inward-open conformation at 3.15 Å resolution. (Figure 1.5) This was aided by the elimination of the N45 glycosylation, a point mutation at E329Q which was predicted to lock the transporter in an inward open conformation, by crystallization at 4 °C to restrain conformational changes, and using the detergent nonyl-β-D-glucopyranoside (β-NG) to further stabilize the inward open conformation (77). The structures with inhibitors were described in 2016 with inhibitors occupying the central cavity replacing the β-NG (135). Structures of GLUT1, GLUT3, GLUT5 and the related sugar binding MFS proteins all support the alternating access simple carrier model although alternative interpretations of the crystal structure are available (136).

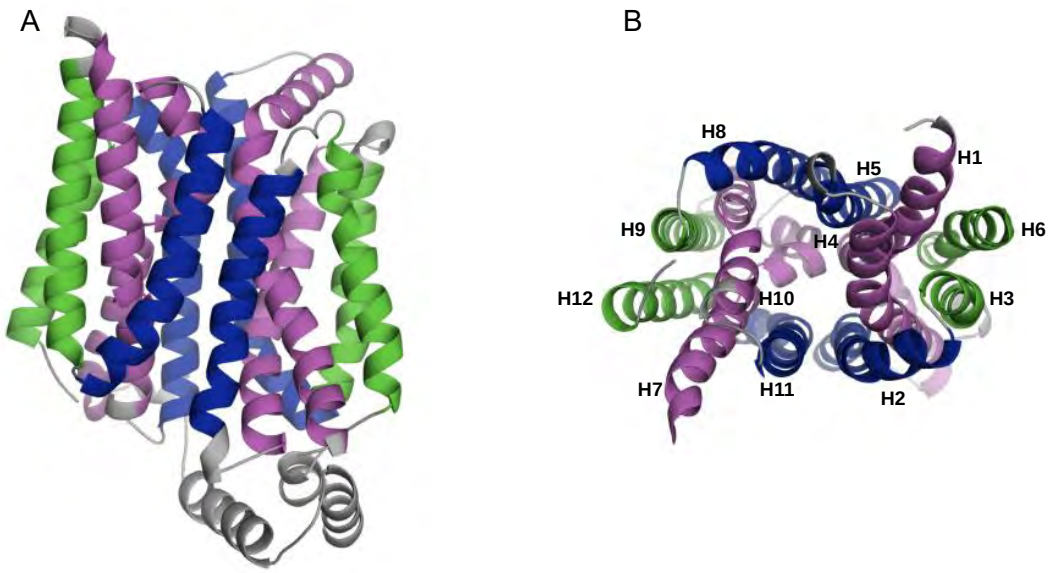

Figure 1.5: Crystal structure of GLUT1. A. The crystal structure of GLUT1 in an e1 open conformation, pdb code 4PYP. Scaffold helices (3, 6, 9, 12) are colored green. Aqueous pore helices are colored pink (1, 4, 7, 10) and blue (2, 5, 8, 11). B. GLUT1 inward open conformation viewed from the cytoplasm. Helices are labeled H1 – H12.

Oligomeric Structure

The crystal structure of GLUT1 represents the monomeric form of GLUT1 suggesting that the catalytic unit of the transporter is a monomer. Freeze-fracture electron microscopy and hydrodynamic size analysis of detergent-solubilized GLUT1 suggest that purified, non-reduced GLUT1 is a tetramer and reduced GLUT1 is a dimer (95,102,122,137). Chemical cross linking and Bioluminescent Forster Resonance Energy Transfer (BRET) support this conclusion (102,138). Additionally, purified GLUT1 binds 0.5 mol CB per mol GLUT1 while reduced purified GLUT1 binds 1 mol CB per mol GLUT1, suggesting that reduced dimeric GLUT1 is an unlinked dimeric protein comprising one catalytic site per monomer (17,95,96). While GLUT1 forms homo-oligomers, the available evidence suggests that it does not form hetero-oligomers with GLUT3 (139). Chimeric proteins of GLUT1 and GLUT3 were used to probe the regions necessary for homo-oligomerization. Substitution of GLUT1 TM9 into GLUT3 led to tetramerization of GLUT3 while substitution of GLUT3 TM9 into GLUT1 converted GLUT1 into a dimer. However, $GLUT1_{(GLUT3\ TM9)}$ was still able to catalyze cis-allosteric behavior with maltose stimulation of sugar uptake(140).

GLUT1 Tetramerization Model

Neither the simple carrier nor the fixed-site carrier can fully explain all of the kinetic and ligand binding behavior observed in GLUT1. To address the allosteric, and cooperative behaviors, CB binding stoichiometry, and oligomerization, a hybrid model of simple and fixed site carriers has been proposed. In this model, each individual monomer of GLUT1 functions as a simple carrier. The carrier subunits are functionally coupled in an obligate anti-parallel fashion where each tetramer is made up of a dimer of dimers (Figure 1.6) (141). Each subunit would only present a single substrate binding site either e2 or e1. Ligand induced conformational

changes would necessitate an equal and opposite conformational change from its functionally linked subunit. Sugar would be transported in both directions or unidirectional uptake would proceed with two subunit undergoing the conformational change in the absence of sugar.

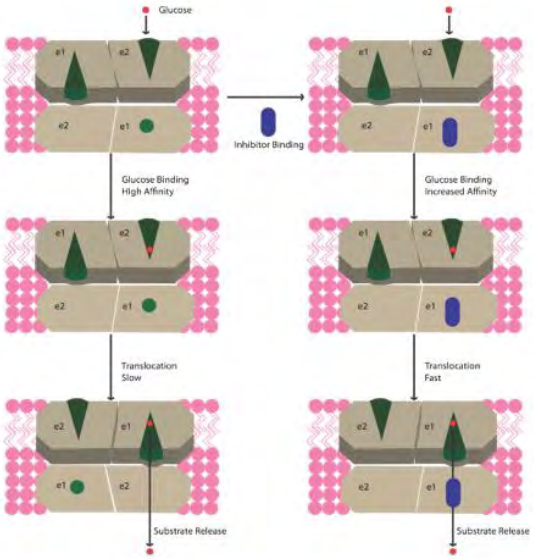

Figure 1.6: GLUT1 tetramer transport model. The GLUT1 tetramer is shown as a dimer of 4 alternating access carriers. The two upper molecules are shown as a cross-section and the two lower molecules are shown from inside the cell. In the absence of inhibitor, glucose (red) binds at the high affinity binding site inducing a slow conformational change where it is released inside the cell. All four subunits undergo the conformational change. In the presence of low concentrations of inhibitor (blue) glucose binds with increased affinity and translocation is faster than in the absence of inhibitor. The inhibitor locks two subunits in their original orientation.

Overall Conclusions and Research Purpose

Understanding the relationship between GLUT1 structure and function is critical to reconciling kinetic, biochemical and structural information. While the available structural information would confirm the simple-carrier model, we know that the simple carrier model does not allow for simultaneous ligand binding at opposite sides of the membrane. It is therefore necessary to understand the shortcomings in both the biochemical and structural analysis. Utilizing the available crystal structures of GLUT1 and other MFS transporters, it is possible to more closely examine potential substrate binding sites and transporter transitions.

This work attempts to use structural information to understand several interesting phenomena observed in GLUT1. Specifically, we utilized molecular docking to search for residues that interact with glucose and other ligands in the transport cycle. While molecular docking can suggest important residues for hydrogen bonding and steric interference it is necessary to validate this through biochemical testing. To this end, we disrupted the potential hydrogen bonding residue Q282 observed to form hydrogen bonds with glucose in all four conformations of GLUT1. Not only did this mutation decrease glucose transport, it also eliminated *cis*-allostery observed by maltose stimulation of 2DG uptake. However, this mutation did not eliminate *trans*-allostery.

In addition to studying ligand binding through structural analysis, the transitions between exo- and endofacial conformations of the GLUT1 structure were also examined. Studies in other membrane proteins have suggested an important role for the amino acid glycine in both stabilizing alpha-helices in the form of GXXXG motifs and in acting as gating hinges. This work examines disruptions to GXXXG motifs, dynamic alpha-helix resident glycines and glycines that

are conserved throughout the GLUT family through the ability to transport 2DG.

Finally, while examining the monomeric GLUT1 structure is important to understanding ligand binding it cannot give a full understanding of transport behavior. This work uses transport deficient GLUT chimeras to examine both cis- and trans-allostery and the role that oligomerization plays. Utilizing this knowledge helps to develop a full model for the GLUT1 mediated glucose transport cycle.

CHAPTER 2:

Reconciling contradictory findings: Glucose transporter 1 (GLUT1) functions as an oligomer of allosteric, alternating access transporters

This chapter was published in the *Journal of Biological Chemistry* in 2017, and can be found using the following reference:

Lloyd, K., et al., *Reconciling contradictory findings: Glucose transporter 1 (GLUT1) functions as an oligomer of allosteric, alternating access transporters.* J Biol Chem, 2017.

Research was supported using NIH Grants: DK36081 and DK44888

Abstract

Recent structural studies suggest that glucose transporter 1 (GLUT1)-mediated sugar transport is mediated by an alternating access transporter that successively presents exofacial (e2) and endofacial (e1) substrate-binding sites. Transport studies, however, indicate multiple, interacting (allosteric), and co-existent, exo- and endofacial GLUT1 ligand-binding sites. The present study asks whether these contradictory conclusions result from systematic analytical error or reveal a more fundamental relationship between transporter structure and function. Here, homology modeling supported the alternating access transporter model for sugar transport by confirming at least four GLUT1 conformations, the so-called outward, outward-occluded, inward-occluded, and inward GLUT1 conformations. Results from docking analysis suggested that outward and outward-occluded conformations present multiple β-D-glucose and maltose interaction sites, whereas inward-occluded and inward conformations present only a single β-D-glucose interaction site. Gln-282 contributed to sugar binding in all GLUT1 conformations via hydrogen bonding. Mutating Gln-282 to alanine (Q282A) doubled the $K_{M(app)}$ for 2-deoxy-D-glucose uptake, eliminated *cis*-allostery (stimulation of sugar uptake by subsaturating extracellular maltose) but not *trans*-allostery (uptake stimulation by subsaturating cytochalasin B). *Cis*-allostery persisted, but *trans*-allostery was lost in an oligomerization-deficient GLUT1 variant in which we substituted membrane helix 9 with the equivalent GLUT3 sequence. Moreover, Q282A eliminated *cis*-allostery in the oligomerization variant. These findings reconcile contradictory conclusions from structural and transport studies by suggesting that GLUT1 is an oligomer of allosteric, alternating access transporters in which 1) *cis*-allostery is mediated by intra-subunit interactions and 2) *trans*-allostery requires inter-subunit interactions.

Introduction

Glucose plays a crucial role in mammalian energy metabolism serving as a preferred metabolic substrate in brain and exercising skeletal muscle (100). However, the molecular mechanism by which glucose enters and exits cells is the subject of considerable controversy (136). Blood brain barrier, glial and erythrocyte sugar transport are mediated by the transport protein GLUT1 (19). Recent structural studies suggest that GLUT1-mediated sugar transport is mediated by a carrier that alternately presents exofacial (e2) and endofacial (e1) substrate binding sites (77,131,133,134,142). Transport studies, on the other hand, demonstrate multiple, interacting, co-existent exo- and endofacial ligand binding sites and e1 ligand-induced sugar occlusion within GLUT1 (78-80,83,84,113,119,143,144). The present study asks whether these apparently contradictory conclusions are mutually exclusive and thus indicative of some form of systematic error in analysis or, rather, are revealing of a more fundamental relationship between transporter structure and function.

GLUT1 comprises 492 amino acids, is a member of the major facilitator superfamily (MFS) of proteins and shares the common MFS fold of 12 transmembrane domains, cytoplasmic N- and C-termini and a long, partially structured intracellular loop connecting membrane spanning helices 6 and 7 (124,145,146). GLUT1 has been crystalized in an inward open (e1 or endofacial) conformation (77). Additional members of the MFS family have been crystalized in outward open (e2 or exofacial) and outward (e2o) and inward (e1o) partially occluded conformations. These members include human GLUT3 (e2, e2o (134)), GLUT5 (e1, e2 (133)) and the bacterial xylose transporter XylE (e1, e1o, e2o (6,131)). Each structure supports the hypothesis that the sugar translocation pathway consists of eight amphipathic, membrane spanning α-helices (H1, H2, H4, H5, H7, H8, H10 and H11) coordinated by a scaffold of 4

hydrophobic α-helices (H3, H6, H9 and H12). The N- and C-terminal membrane-spanning α-helices share a similar topology and are related by a two-fold symmetry (8).

Two competing hypotheses have been presented to explain glucose transporter behavior: the simple, alternating access carrier which sequentially presents mutually exclusive exofacial and endofacial substrate binding sites (124,145), or the fixed-site transporter with coexistent exofacial and endofacial sugar binding sites (143,147). Initial studies using purified GLUT1 suggested that exofacial and endofacial inhibitors bind at mutually exclusive binding sites thereby supporting the simple carrier model (91,92). Erythrocyte sugar transport and ligand binding studies (78,79,83,113) and studies using non-reduced, purified transporter (79,83) suggest GLUT1 behaves like a fixed site transporter with interacting, cooperative binding sites.

Cell membrane resident GLUT1 forms non-covalent homodimers and tetramers (95,102,137,140). Purified, non-reduced GLUT1 forms a mixture of dimeric and tetrameric species while reduced purified GLUT1 is largely dimeric. GLUT1 and GLUT3 co-expressed in the same cells do not form heterocomplexes (139,140) but substitution of GLUT3 membrane spanning α-helix 9 (H9) into GLUT1 shifts the GLUT1 population from a tetrameric/dimeric mixture with high transport capacity to a dimeric population with reduced transport capacity suggesting H9 is involved in GLUT1 oligomerization. Conversely, substitution of GLUT1 H9 into GLUT3 converts GLUT3 into a tetramer and increases its transport capacity to GLUT1 levels confirming the pivotal role of H9 in determining GLUT quaternary structure and catalytic function (140).

Ligand binding studies with non-reduced and reduced GLUT1 provide further insights into the subunit organization of the transport complex (95). The sugar transport inhibitor cytochalasin B (CB) and intracellular sugar compete for binding at the GLUT1 endofacial sugar binding site

(148). Purified tetrameric GLUT1 binds 0.5 mol CB per mol GLUT1 while purified dimeric GLUT1 binds one mol CB per mol GLUT1 (95). This contradiction is explained by the suggestion (137) that each subunit of tetrameric GLUT1 undergoes the e2 ⇌ e1 catalytic cycle but, at any instant two subunits must present the e1 conformation and two must adopt the e2 conformation. In dimeric GLUT1, each subunit is functionally unconstrained by its neighbor and free to adopt either the e1 or e2 conformation. Thus, both subunits of dimeric GLUT1 bind CB when [CB] is saturating.

This suggestion is reinforced by demonstrations of functional coupling between GLUT1 ligand and substrate binding sites. Trans-allostery is observed when low concentrations of GLUT1 endofacial site inhibitors (e.g. forskolin or CB) increase the affinity of the external site for transported sugar (80). As inhibitor concentration is further increased, transport is inhibited. Exofacial cis-allostery is observed when extracellular maltose (a non-transportable disaccharide which binds at the exofacial sugar binding site), stimulates sugar uptake at low maltose concentrations but inhibits uptake as its concentration is raised (78). Endofacial cis-allostery is seen when endofacial ligand binding (e.g. forskolin) increases the affinity of GLUT1 for a second e1 ligand (e.g. CB, (80,84)). These findings suggest that GLUT1 presents multiple, co-existent endo- and exofacial ligand binding sites and/or that oligomerization promotes subunit cooperativity.

This study interrogates crystal and homology-modeled GLUT1 structures to ask whether GLUT1 can present multiple substrate and ligand interaction sites. Then, using insights gained from this analysis, we mutagenize GLUT1 to examine its impact on cis-and trans-allostery. We conclude that exofacial cis-allostery is an intramolecular phenomenon resulting from cross-talk between multiple, co-existent ligand interaction sites present in the exofacial cavity of each

GLUT1 protein whereas trans-allostery and endofacial cis-allostery require ligand-induced subunit-subunit interactions.

Materials and Methods

Reagents

[^{3}H]-2-deoxy-D-glucose ([^{3}H]-2DG) was purchased from American Radiolabeled Chemicals (St. Louis, MO). Unlabeled 2DG, maltose, Cytochalasin B (CB) and phloretin were purchased from Sigma-Aldrich (St. Louis, MO). All primers were purchased from Integrated DNA Technologies. Herculase polymerase, XL1-Blue Competent cells, and QuikChange Multisite-directed Mutagenesis kits were obtained from Agilent Technologies. SuperSignal Pico West, NeutrAvidin Gel, micro-BCA kits, spin columns, and EZ-Link Sulfo-NHS-ss-Biotin were from Pierce.

Solutions

Phosphate-buffered saline (PBS) comprised 140 mM NaCl, 10 mM Na_2HPO_4, 3.4 mM KCl, 1.84 mM KH_2PO_4, pH 7.3. Solubilization buffer comprised PBS medium with 0.5% Triton X-100 and 5 mM $MgCl_2$. Stop solution comprised PBS-Mg medium plus CB (CB; 10 μM) and phloretin (100 μM). Sample buffer contained 0.125 M Tris-HCl (pH 6.8), 4% SDS, 20% glycerol, and 50 mM DTT. Transfer buffer comprised 12 mM Tris Base, 96 mM Glycine, 20% methanol.

Antibodies

A custom-made (New England Peptide) affinity-purified goat polyclonal antibody (C-Ab) raised against a peptide corresponding to GLUT4 C-terminal residues 498-509 was used at 1:10,000 dilution (86). Horseradish peroxidase-conjugated donkey anti-goat secondary antibody (Jackson ImmunoResearch) was used at 1:50,000 dilution.

Tissue Culture

HEK293 cells were maintained in Dulbecco's modified Eagle's medium (DMEM) supplemented with 10% fetal bovine serum, 100 units/mL penicillin, and 100 μg/mL streptomycin in a 37 °C humidified 5% CO_2 incubator as described previously (149). All experiments were performed with confluent cells. Plates were subcultured into 12-well plates at a ratio of 1:2-1:5 2-4 days prior to transfections. Passages 4-20 were used for all experiments.

Mutagenesis

GLUT1-encoding cDNA was inserted into the EcoRV-NotI restriction sites of PCDNA 3.1(+). As described previously (140), the C-terminal 13 amino acids of this GLUT1 construct are substituted using the C-terminal 13 amino acids of GLUT4 to facilitate detection of heterologously expressed GLUT1 against a low level background expression of endogenous GLUT1. Mutagenesis was as described previously (116) using QuikChange Multi-site-directed Mutagenesis kits and was verified by sequencing. The GLUT1 construct in which H9 is substituted with GLUT3 H9 sequence was described previously (140)**.**

Transient Transfection

Cells (70-90% confluence) were transfected with 2 μg (12 well plates) or 5 μg of DNA per well (6 well plates). Transfections were performed 36-48 hr prior to analysis of sugar uptake or protein expression. Sugar uptake and cell-surface biotinylation measurements were performed in tandem. GLUT1, GLUT3, GLUT1/GLUT3 chimeras tagged with a GLUT4-specific epitope and their associated mutations were constructed and heterologously expressed in HEK293 cells as described previously (116,140).

Cell-Surface Expression Measurements

Three days post-transfection, 6-Well plates of HEK cells were washed twice with ice-cold

PBS and incubated on ice with ice-cold PBS containing 5 mM EZ-Link Sulfo-NHS-ss-Biotin for 30 min with gentle rocking. Reactions were quenched by adjusting each well to 12.5 mM Trizma (Tris base). Cells were harvested, re-suspended in biotin lysis buffer, and lysates were bound to Neutravidin Gel in spin columns according to kit instructions. Protein was eluted from spin columns using reductant, the eluate protein concentration was determined spectrophotometrically. Normalized loads were analyzed by Western blotting.

Western Blotting

GLUT1 expression in whole cell lysates and cell surface expression by biotinylation were analyzed by western blot as previously described (73). Total and isolated biotinylated proteins were normalized for total protein concentration by BCA and resolved by SDS-PAGE on a 10% NuPage gel in NuPage running buffer. Gels were transferred onto PVDF membranes blocked with 3% bovine serum albumin in PBS-T, probed with primary antibody overnight at 4°C, probed with secondary antibody for 1 hr at room temperature, and developed using SuperSignal Pico West Chemiluminescent substrate. Blots were imaged on a FujiFilm LAS-3000 and relative band densities were quantitated using ImageJ32 software.

2-Deoxy-D-glucose Uptake

2-deoxy-D-glucose (2-DG) uptake was measured as described previously (140). Briefly, 36-48 hr post transfections, confluent 12-well plates of HEK-293 cells were serum- and glucose-starved for 2 hr at 37°C in FBS and penicillin/streptomycin-free DMEM lacking glucose. Cells were washed with 1.0 mL of DPBS-Mg at 37°C for 15 min, then exposed to 0.4 ml of [^{3}H]2-DG uptake solution at various 2-DG concentrations (0.1 - 20 mM) for 5 min at 37°C. Uptake was stopped by addition of 1 ml of ice-cold stop solution. Cells were washed twice with ice-cold stop solution and lysed with Triton lysis buffer. Total protein content was analyzed in duplicate by

BCA. Each sample was counted in duplicate by liquid scintillation spectrometry. Each mutant was analyzed in triplicate on at least 3 separate occasions.

Cis- and trans-allostery experiments measured 0.1 mM 2-DG uptake in cells exposed to [maltose] or [CB] respectively.

Homology Modeling

We modeled GLUT1 e2, e2-occluded and e1-occluded structures respectively using the human GLUT3 (4ZWC) structure (134) and the XylE e2-occluded (4GBZ) and e1-occluded (4JA3) structures (6,131). We removed ligands and used chain A as the template for each modeled structure. Sequence alignments were generated using ClustalX. Homology models were built using Modeller-9.9 and analyzed using PROCHECK. The GLUT1 e1 structure (4PYP (77)) was used directly.

Cavity analysis

Cavities for ligand docking were calculated using the CastP server (http://sts.bioe.uic.edu/castp/) (150) and the grid was centered on the residues forming the cavity.

Stochastic Docking

β-D-glucose, maltose and CB structures were obtained from ZINC (http://zinc.docking.org). The WZB117 structure was generated using the 3D structure generator Corina from Molecular Networks GmbH (http://www.molecular-networks.com). Docking was performed using the Schrodinger software suite. No restraints were used during the docking. The protein structure was preprocessed with the Protein Preparation Wizard, bond orders were assigned, hydrogens added and the H-bond network was optimized. The system was energy minimized using the OPLS 2005 force field. Ligand structures were prepared with the LigPrep module and the pKa of the ligands was calculated using the Epik module. Computational

docking was performed by the GLIDE module in standard-precision (SP) mode and default values for grid generation. Grids were mapped using CastP cavity analysis and ligand positions from the original crystal structures.

Data analysis

Data analysis was undertaken using GraphPad Prism (version 7.0c, GraphPad Software, Inc.). Curve fitting was by non-linear regression using the following equations:

1. Concentration dependence of 2-deoxy-D-glucose uptake:

$$v_{21} = \frac{V_{\max}[S]}{K_{m(app)} + [S]} \qquad \text{eqn 1}$$

where [S] is [2DG] and V_{max} and $K_{m(app)}$ have the usual meaning.

2. Exofacial Cis-Allostery and Endofacial trans-allostery are expressed as normalized 2DG uptake which is described by

$$\frac{v_i}{v_c} = \frac{K_1 + [I]\left(K_2 + [I]\right)}{K_1 + [I]\left(K_3 + [I]K_4\right)} \qquad \text{eqn 2}$$

where v_i/v_c is uptake in the presence of inhibitor divided by uptake in the absence of inhibitor, [I] is the concentration of cis- or trans-inhibitor and interpretation of constants is model dependent and described in (151).

3. When simple saturable inhibition of transport is observed, normalized 2DG uptake is described by

$$\frac{v_i}{v_c} = K_1 - \frac{K_2[I]}{K_3 + [I]} \qquad \text{eqn 3}$$

where v_i/v_c is uptake in the presence of inhibitor divided by uptake in the absence of inhibitor, K_1 is uptake in the absence of inhibitor I, K_2 is the difference between K_1 and uptake in the presence of saturating [I] and K_3 is $K_{I(app)}$ for uptake inhibition by I.

Results

Homology Modeled GLUT1 structures

GLUT1 and GLUT3 structures have been described previously (77,134). The current study presents and interrogates three homology-modeled GLUT1 structures - the so-called outward, outward-occluded and inward-occluded conformations of GLUT1 plus the experimentally derived inward conformation of GLUT1 (4PYP (77); Figure 2.1). These conformations present a striking physical correspondence to the proposed kinetic intermediates in the alternating access carrier catalytic cycle named e2, e2o, e1o and e1 (99,100,111), argue strongly for sugar movements through a central translocation pore and are henceforth termed GLUT1-e2, GLUT1-e2o, GLUT1-e1o and GLUT1-e1.

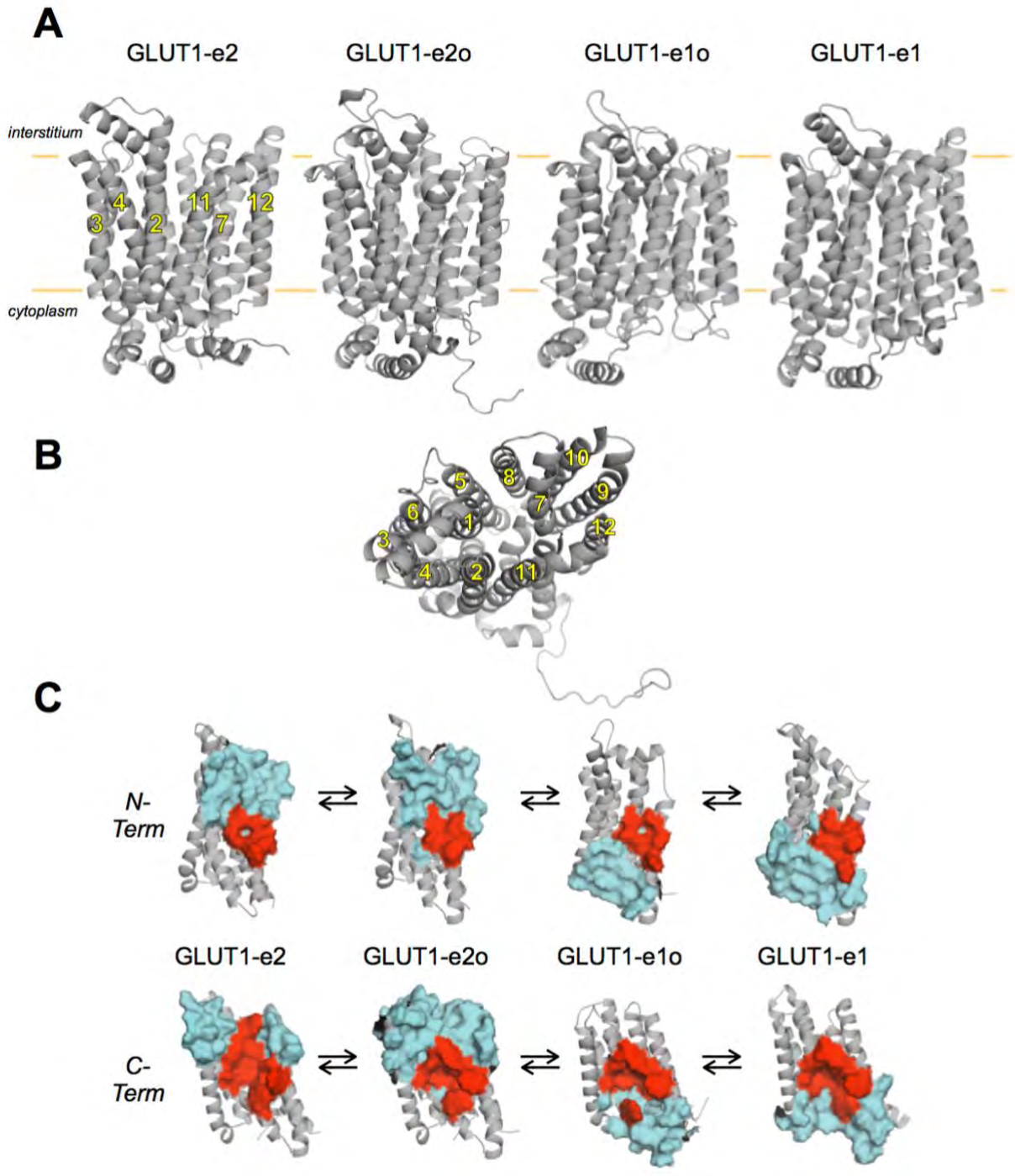
A
GLUT1-e2
GLUT1-e2o
GLUT1-e1o
GLUT1-e1
interstitium
cytoplasm
3
4
2
11
7
12
B
10
5
8
9
6
1
7
12
3
4
2
11
C
N-
Term
GLUT1-e2
GLUT1-e2o
GLUT1-e1o
GLUT1-e1
C-
Term

Figure 2.1: Homology-modeled GLUT1 conformations. A. GLUT1 is shown in cartoon representation normal to the bilayer plane (horizontal orange lines), membrane spanning α-helices (H 2, 3, 4, 7, 11 and 12) are indicated, and locations of the interstitium and cytoplasm are highlighted. Four conformations are depicted: exofacial (GLUT1-e2), exofacial-occluded (GLUT1-e2o), endofacial-occluded (GLUT1-e1o) and endofacial (GLUT1-e1). **B.** A second depiction of GLUT1-e1 is shown along the bilayer normal from the cytoplasmic side. Membrane spanning α-helices (H1-12) are indicated. **C.** Representation of ligand-interaction cavities present in all 4 GLUT1 conformations shown normal to the bilayer plane. N- and C-terminal halves (H1-6 and H7-12 respectively shown in gray in cartoon representation) of each conformation are indicated. Solvent-exposed residues in the ligand interaction cavities of each conformation are shown as surface maps colored cyan. Residues common to all 4 cavities are shown as surface maps colored red and include: N-terminal residues Gly-26, Thr-30 (of helix 1), Gln-161, Ile-164, Val-165, and Ile-168 (of helix 5); C-terminal residues: Gln-282, Gln-283, Ile-287, Asn-288, Phe-291, Tyr-292 (of helix 7), Asn-317 (of helix 8), Phe-379, Trp-388 (of helix 10) and Asn-411, Trp-412 and Asn415 (of helix 11).

Docking analysis of GLUT1-substrate interactions

Docking analysis first requires the location of GLUT1 pockets of sufficient size to permit ligand entry and coordination. Cavity analysis of all 4 homology-modeled GLUT1 conformations suggests the existence of a translocation pore that transitions from one contiguous with the interstitium but excluded from cytosol in GLUT1-e2 through intermediate, occluded cavity forms in GLUT1-e2o and GLUT1-e1o to a cavity contiguous with the cytosol but excluded from the interstitium in GLUT1-e1 (Figure 2.1). Translocation pore volume increases in the occluded state. Computed cavity volumes (Figure 2.1) are GLUT1-e2 = 2,850.8 $Å^3$, GLUT1-e2o = 4,397.5 $Å^3$, GLUT1-e1o = 3,029.4 $Å^3$, and GLUT1-e1 = 2,845.9 $Å^3$. For comparison, the molecular volume of β-D-glucose (β-D-Glc) based on its self-diffusion coefficient is 433 $Å^3$ (152). Loop 6-7 was not included in cavity calculations for the GLUT1-e1 conformation. The side chains of several residues line the cavities in all 4 conformations (Figure 2.1C).

A

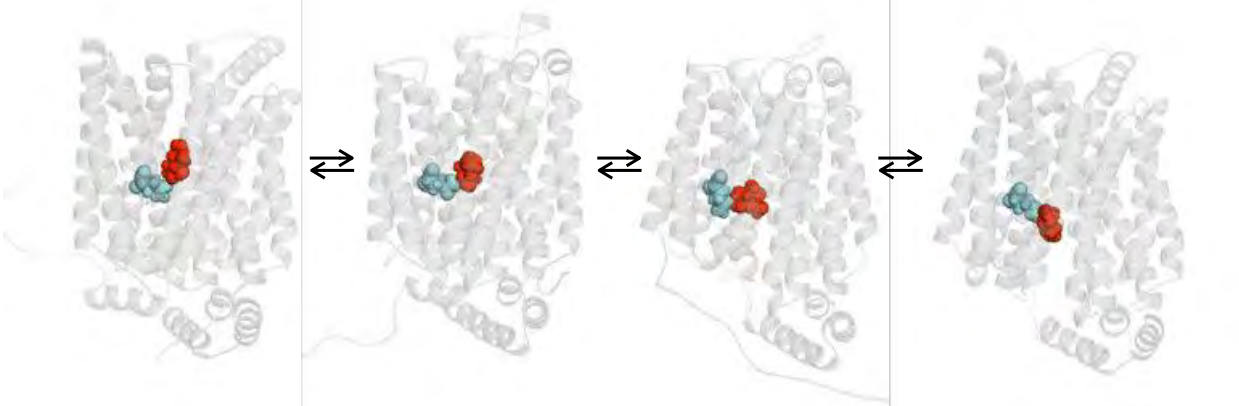

GLUT1-e2S GLUT1-e2o(S) GLUT1-e1o(S) GLUT1-e1S

B

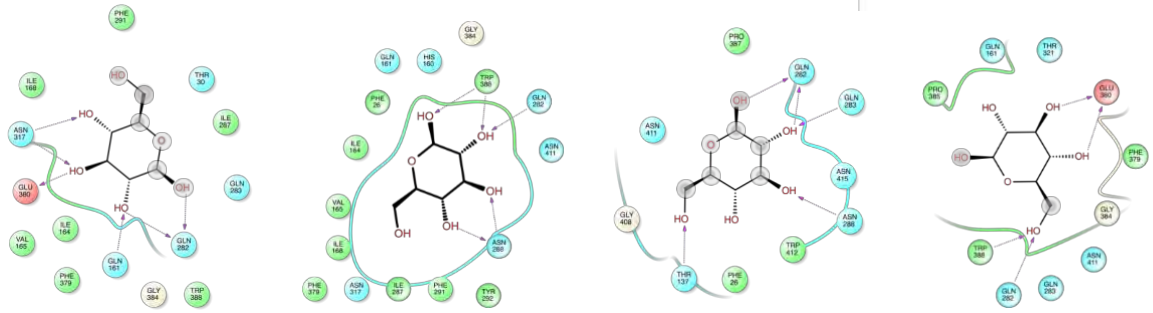

GLUT1-e2o(S)

C

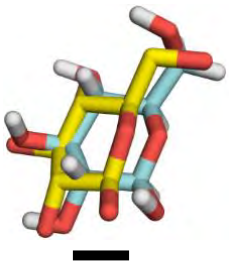

Figure 2.2: β-D-Glc docking to homology-modeled GLUT1 conformations. A. Each GLUT1 conformation is shown complexed with β-D-Glc (shown in red as a space-filling representation). The location of GLUT1 Q282 is shown in cyan in space-filling format. Conformation nomenclature is indicated beneath each structure where β-D-Glc is represented by the letter S and occluded β-D-Glc (by convention) by the letter S in parenthesis. **B**. β-D-Glc docking to GLUT1 conformations in which Glc is shown as a 2D structure, coordinating GLUT1 residues are shown as circles and are colored according to their properties (green=hydrophobic, cyan=polar, red=negative), GLUT1 backbone as green or blue ribbons, solvent exposed regions of β-D-Glc are indicated by gray-shaded circles and H-bonds shared between amino acid side chain amines, carbonyls or hydroxyls with β-D-Glc and their directionality are represented as red arrows. **C**. Alignment of XylE containing a co-crystallized β-D-Glc (4GBZ; (*7*); XyleE-e2o(S)) with homology-modeled GLUT1-e2o containing its docked β-D-Glc (GLUT1-e2o(S)). Both proteins are hidden to show the proximity of co-crystallized and docked sugars. XylE-bound β-D-Glc lacks hydrogens and its carbons are colored yellow. GLUT1-bound β-D-Glc carbons are colored cyan. The black scale bar indicates the length of a single C-C bond (0.154 Å).

GLIDE software was developed to optimize ligand docking to rigid protein structures using co-crystallized ligand-protein complexes as comparative standards (153,154). GlideScores for computed ligand/protein pairs are useful for selecting the best docked poses but can under- or over-estimate ΔG for binding by 2 kcal/mol (30-fold; (155)).

Transport studies show that β-D-Glc binding at the GLUT1 exofacial sugar binding site involves H-bonding to pyranose ring C1, C3 and C4 oxygens (74,75). Similarly, ligand binding at the endofacial sugar binding site involves H-bonding with OH groups at C3 and C4 in the pyranose ring and is inhibited by bulky substitutions at C6 (74). Docking analysis of β-D-Glc interactions with GLUT1-e2, GLUT1-e2o, GLUT1-e1o and GLUT1-e1 conformations is shown in Figures 2.2A and 2.2B. The illustrated interactions conform to the aforementioned stereospecificity of GLUT1-ligand binding. Gln-282 (Q282) is the one residue whose side chain interacts with β-D-Glc in all 4 GLUT1 conformations. Figure 2.2C shows the relative positions of β-D-Glc in the XylE-e2o-β-D-Glc co-crystal structure (131) and of β-D-Glc docked to the homology-modeled GLUT1-e2o structure following alignment of the two protein structures. The agreement is excellent and exceeds the resolution (2.9 Å) of the XyleE-e2o structure.

Additional glucose interaction sites

β-D-Glc docking to GLUT1-e2 reveals additional potential interaction sites which we call intermediate and peripheral sites (Figure 2.3A). The intermediate site persists in GLUT1-e2o but not in e1o and e1 suggesting that an extra sugar (in addition to the core or transported sugar) is excluded in e1o and e1 states. If occupancy of the intermediate site modifies GLUT1 catalytic behavior, this could explain how extracellular sugar allosterically modulates sugar uptake. How it affects exit is more difficult to explain (78,80). β-D-Glc docking to GLUT1-e1o and GLUT1-e1 (Figures 2.3C and 2.3D) suggests that each conformation presents a single interaction

envelope. This precludes simultaneous occupancy of endofacial conformations by two intracellular sugars.

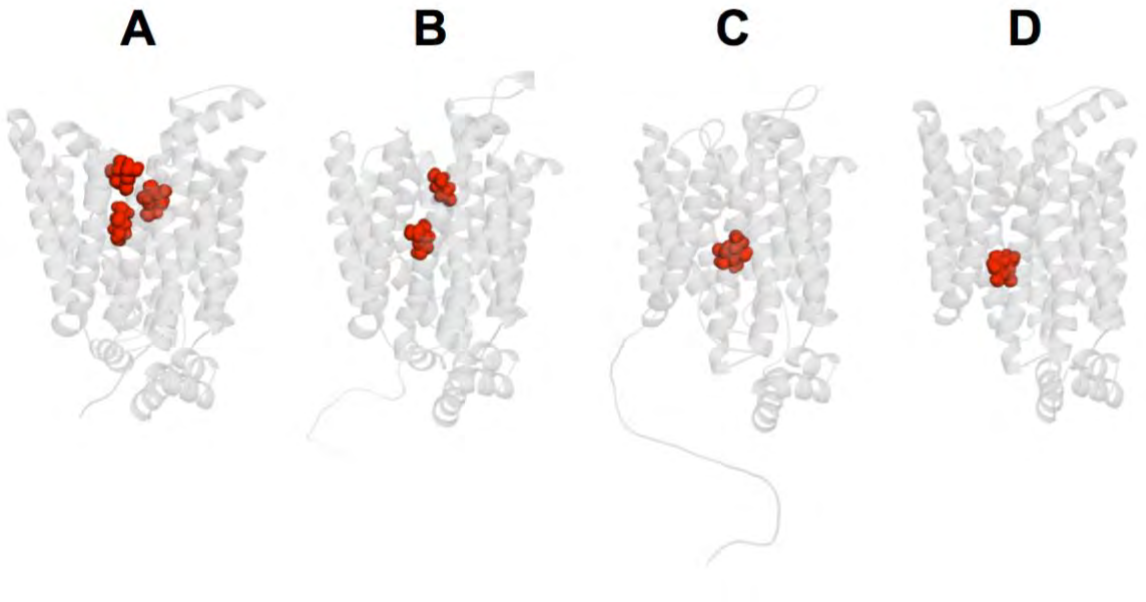

Figure 2.3: GLUT1 presents additional β-D-Glc binding sites. GLUT1 is oriented as in Figure 1A. **A.** β-D-Glc (in red) docking to GLUT1-e2 reveals 3 potential sites termed peripheral, intermediate and core. Computed GlideScores (GS) for ligand binding: peripheral GS = -5.1 kcal/mol, intermediate GS = -5.1 kcal/mol, core GS = -4.9 kcal/mol. **B**. β-D-Glc (in red) docking to GLUT1-e2o reveals 2 potential sites termed peripheral and core. Computed GS for ligand binding: peripheral GS = -6.0 kcal/mol, core GS = -5.8 kcal/mol. **C**. β-D-Glc (in red) docking to GLUT1-e1o reveals 1 potential site with computed GS for ligand binding = -5.1 kcal/mol. **D**. β-D-Glc (in red) docking to GLUT1-e1 Computed GS for ligand binding: core 1 GS = -5.4 kcal/mol.

Interpretation of $K_{M(app)}$ for transport is model-dependent and includes both binding and translocation rate constants (111). GlideScores for β-D-Glc interaction at these sites range from -4.9 to -6 kcal/mol suggesting $K_{D(app)}$ for β-D-Glc binding of 18 - 135 μM. $K_{D(app)}$ for β-D-Glc binding to GLUT1 is 0.5 mM (113). Computed $K_{D(app)}$ for xylose docking to each of the 8 known XylE structures ranges from 4 μM to 90 μM (136) yet $K_{D(app)}$ for xylose binding to XylE is 0.4 mM (131). As previously discussed, GlideScores for computed ligand/protein can under- or over-estimate ΔG for binding by 2 kcal/mol (30-fold; (155)).

Docking analysis of GLUT1-inhibitor interactions

Maltose and CB are non-transported inhibitors of GLUT1-mediated sugar transport acting at exofacial and endofacial sites respectively (83). Molecular docking of β-maltose to GLUT1-e2 suggests two maltose interaction domains: 1) the core β-D-Glc site and, 2) an outer location comprising peripheral and intermediate β-D-Glc interaction sites (Figure 2.4A). These sites do not sterically clash suggesting that GLUT1-e2 can form a complex with 2 maltose molecules. GLUT1-e2o can also accommodate a core β-D-Glc or core β-maltose plus an outer β-maltose (Figure 2.4B). GlideScores for maltose interaction with core and outer sites range from -6.1 to -3.4 kcal/mol corresponding to $K_{D(app)} \approx 15$ μM to 2 mM. Maltose stimulates then inhibits GLUT1-mediated sugar uptake with $K_{0.5}$ of 32 μM and 3.2 mM respectively (78) indicating close agreement between GlideScores and $K_{D(app)}$ when the interfering exofacial ligand is non transportable.

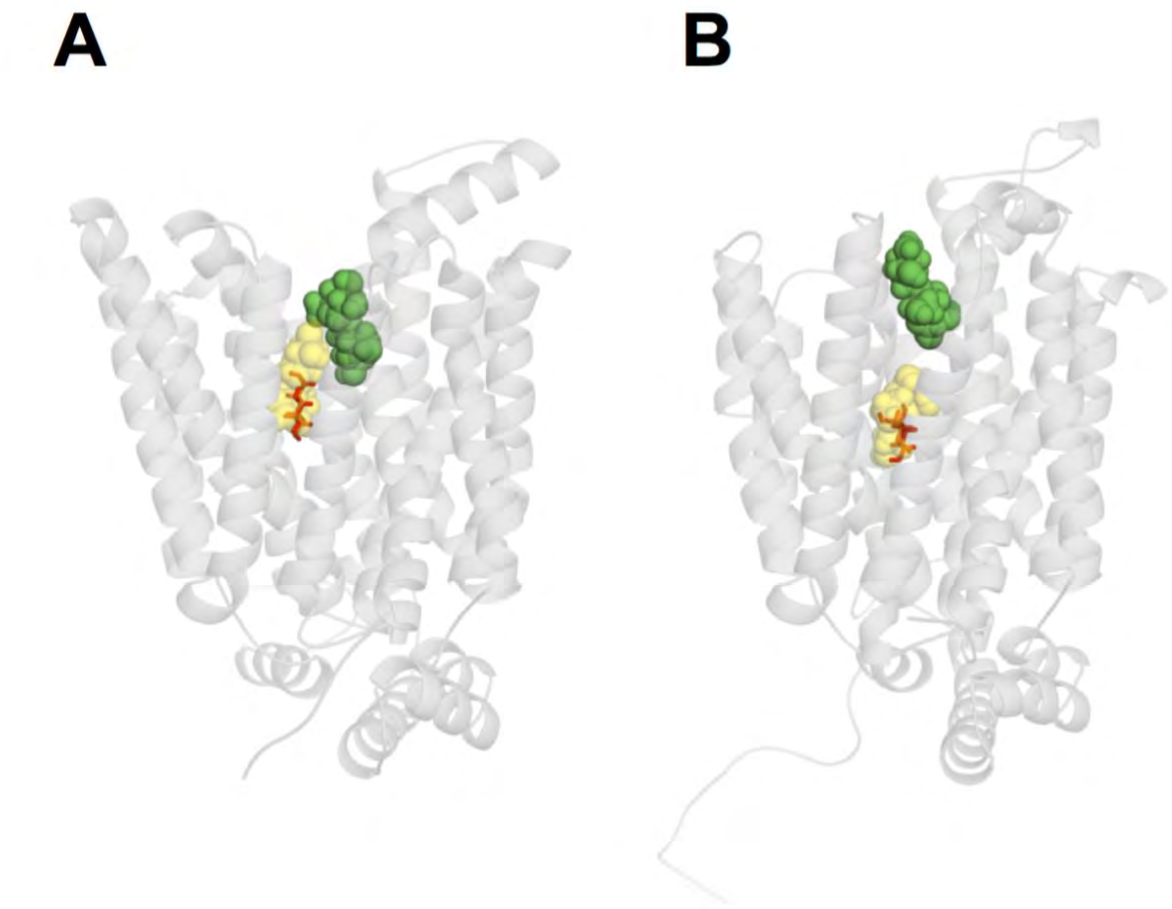
A
B

Figure 2.4: Maltose binding to the exofacial conformation of GLUT1. GLUT1 is oriented as in Figure 1A. **A.** β-Maltose binding. Maltose (a disaccharide comprising two glucose units joined with an α(1→4) bond) can occupy two sites in GLUT1-e2: a site (shown in yellow) comprising the core β-D-Glc site and extending into additional space or a site (shown in green) comprising intermediate and peripheral β-D-Glc sites. β-D-Glc is indicated as a stick figure occupying its core site. GlideScores for Maltose binding core and intermediate sites are -6.1 kcal/mol and -5.6 kcal/mol respectively. **B**. Maltose occupies two sites in GLUT1-e2o comprising core (yellow) and peripheral (green) sites. GlideScores for maltose binding at core and peripheral sites are -3.4 kcal/mol and -5.0 kcal/mol respectively. β-D-Glc is indicated as a stick figure occupying the core site.

Docking analysis of CB - GLUT1-e1 interactions suggests two possible orientations for CB coordination (Figure 2.5). Each sterically clashes with the core, GLUT1-e1 β-D-Glc interaction envelope (Figure 2.5) thus explaining competition between CB and β-D-Glc for binding. GlideScores for CB interaction with GLUT1-e1 are consistent with $K_{D(app)}$ for CB binding of 0.1 to 5 µM. $K_{D(app)}$ for CB binding to GLUT1 ranges from 150 - 180 nM (91,156)

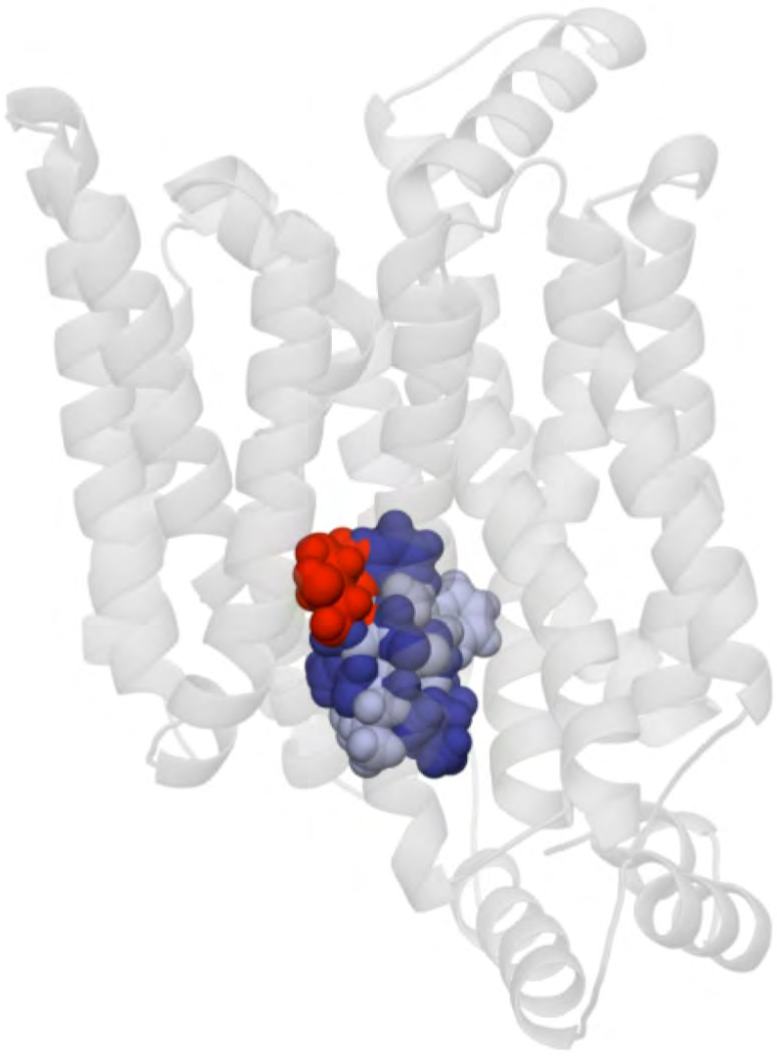

Figure 2.5: CB interaction sites in GLUT1-e1. GLUT1 is oriented as in Figure 1A. CB adopts two overlapping coordinations in GLUT1-e1. These are shown as space-filling molecules in dark blue (CB site 1) and light blue (CB site 2). GS for CB binding to sites 1 and 2 are -7.2 kcal/mol and -6.6 kcal/mol respectively. Both CB sites suggest steric hindrance with the core β-D-Glc binding site (shown as a space-filling molecule in red).

Effects of inhibitors on sugar transport

The predicted involvement of Q282 in β-D-Glc coordination by all GLUT1 conformations suggests that this residue plays a central role in sugar transport. We therefore mutagenized Q282 to alanine. The concentration dependence of the initial rate of 2-deoxy-D-glucose (2DG) uptake by HEK293 cells expressing wtGLUT1 or GLUT1 containing the Q282A mutation ($GLUT1_{Q282A}$) is well approximated by Michaelis-Menten kinetics (Figure 2.6A). V_{max} for net 2DG uptake (wtGLUT1 = $3.18 \times 10^{-12} \pm 0.25 \times 10^{-12}$ mol/μg protein/min) is unaffected by the Q282A mutation ($V_{max} = 3.38 \times 10^{-12} \pm 0.28 \times 10^{-12}$ mol/μg protein/min). However, $K_{m(app)}$ for net sugar uptake by wtGLUT1 (0.89 ± 0.18 mM) is doubled in $GLUT1_{Q282A}$ ($K_{m(app)}$ = 1.59 ± 0.28 mM). Cell-surface GLUT1 biotinylation studies confirm that HEK293 cells express similar levels of wtGLUT1 and $GLUT1_{Q282A}$ (Figure 2.6B). Replicate analysis (n = 5; Figure 2.6C) reveals that $K_{m(app)}$ is significantly increased in $GLUT1_{Q282A}$ (paired T-test, P = 0.0046) but V_{max} is unchanged (P = 0.2036).

Two types of "allostery" have been described for GLUT1-mediated sugar import. Cis-allostery obtains when extracellular inhibitors (e.g. maltose), stimulate sugar uptake at low concentrations but inhibit uptake at higher concentrations (78). Trans-allostery describes sugar uptake stimulation by subsaturating levels of endofacial inhibitors (e.g. CB, forskolin; (80)).

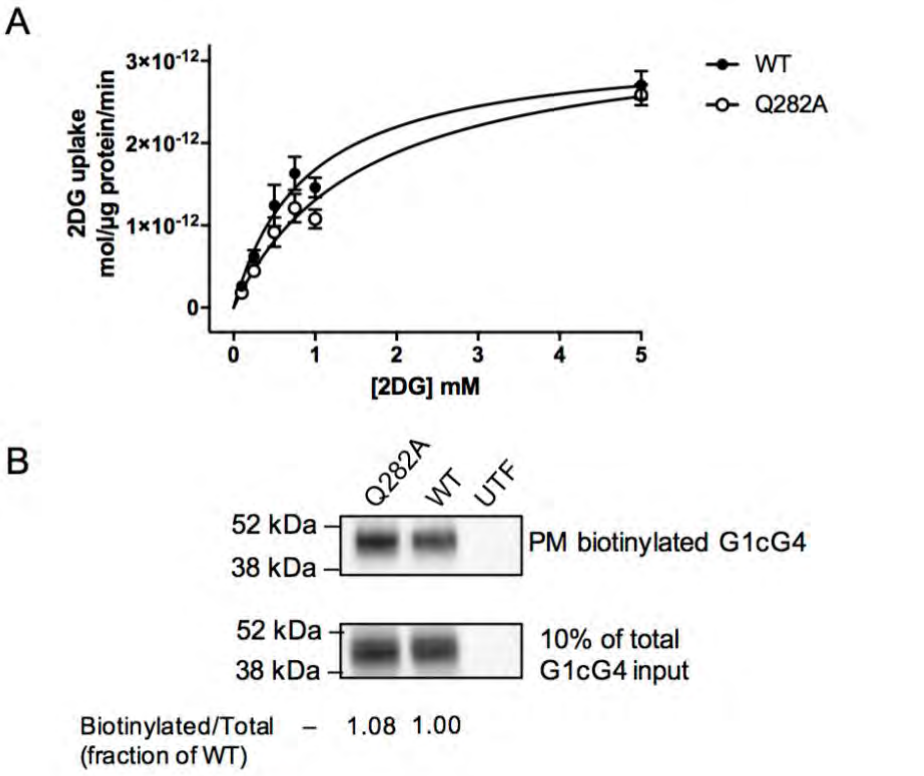
A
2DG uplake
mol/µg protein/min
3×10-12
2×10-12
1×10-12
0
0
1
2
3
4
5
[2DG] mM
WT
Q282A
B
Q282A
WT
UTF
52 kDa
38 kDa
PM biotinylated G1cG4
52 kDa
38 kDa
10% of total
G1cG4 input
Biotinylated/Total – 1.08 1.00
(fraction of WT)
C
Km(app) mM
3
2
1
0
GLUT1
GLUT1Q282A
6×10-12
4×10-12
2×10-12
0
Vmax
mol/µg protein/min
GLUT1
GLUT1Q282A

Figure 2.6: Sugar transport in HEK293 cells heterologously expressing wtGLUT1 or GLUT1$_{Q282A}$. A. Michaelis-Menten kinetics of zero-trans 2-deoxy-D-glucose (2DG) uptake in cells expressing wtGLUT1 (●), or GLUT1$_{Q282A}$ (○). 2DG uptake in µmol/µg cell protein/min is plotted versus [2DG] in mM. Each data point is the mean ± SEM of 3 or more duplicate measurements and is corrected for 2DG uptake in mock-transfected cells. Curves were computed by nonlinear regression assuming Michaelis-Menten uptake kinetics (equation 1) and have the following constants: wtGLUT1 (●):V_{max} = 3.2 ± 0.02 pmol/µg protein/min, $K_{m(app)}$ = 0.89 ± 0.18 mM, R^2 = 0.884, standard error of regression = 0.31 pmol/µg protein/min; GLUT1$_{Q282A}$ (○):V_{max} = 3.4 ± 0.3 pmol/µg protein/min, $K_{m(app)}$ = 1.59 ± 0.28 mM, R^2 = 0.926, standard error of regression = 0.24 pmol/µg protein/min. **B**. Cell surface expression of wtGLUT1 and GLUT1$_{Q282A}$ in HEK293 cells. The mobility of molecular weight markers is indicated at the left of the blot which shows GLUT1 levels present in biotinylated membrane proteins collected from untransfected (UTF), wtGLUT1-expressing (wt) and GLUT1$_{Q282A}$ (Q282A) expressing HEK293 cells. **C.** $K_{m(app)}$ but not V_{max} for 2DG transport is affected in GLUT1$_{Q282A}$. The results of 5 separate experiments are shown as scatter dot plots for both $K_{m(app)}$ and V_{max}. Results are shown as mean ± SEM. Paired t-test analysis (dashed lines indicate paired measurements) indicates that V_{max} is not significantly affected by the Q282A mutation (p = 0.2036) but that $K_{m(app)}$ increases 2-fold (p = 0.0046).

Cis-Allostery is eliminated in GLUT1$_{Q282A}$

Subsaturating extracellular maltose (10 to 50 μM) stimulates wtGLUT1-mediated 2DG uptake (Figure 2.7A) but higher concentrations inhibit transport. Low concentrations of maltose are without effect on sugar uptake by GLUT1$_{Q282A}$ but higher concentrations inhibit transport (Figure 2.7A).

Trans-Allostery persists in GLUT1$_{Q282A}$

CB stimulates 2DG uptake at low concentrations (0.025 μM CB) in both wtGLUT1 and GLUT1$_{Q282A}$ but inhibits transport at higher concentrations (Figure 2.7B).

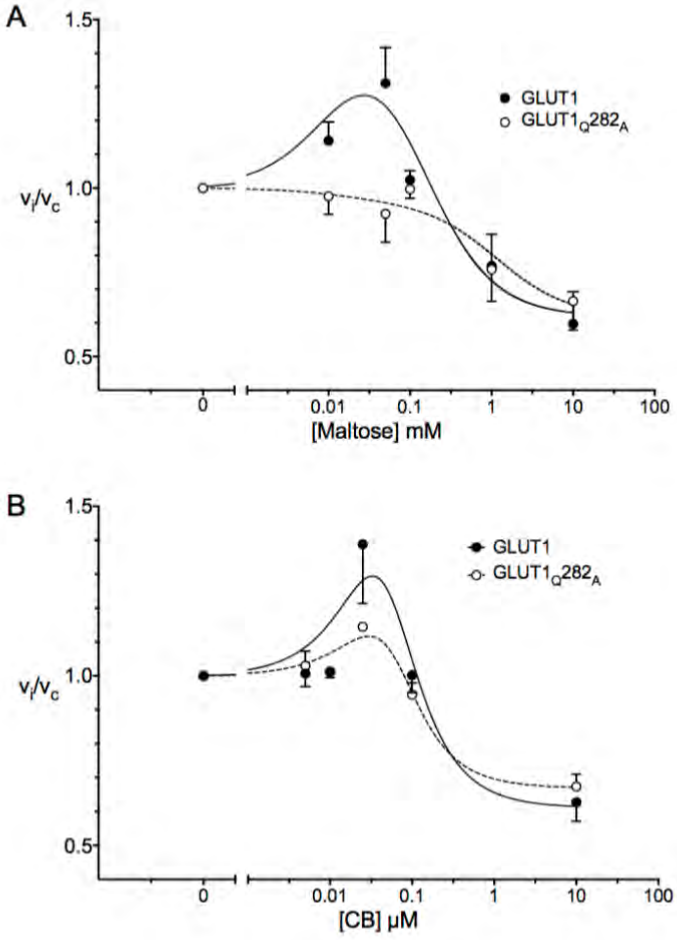
A
1.5
1.0
0.5
v_i/v_c
GLUT1
$GLUT1_Q282_A$
0
0.01
0.1
1
10
100
[Maltose] mM
B
1.5
1.0
0.5
v_i/v_c
GLUT1
$GLUT1_Q282_A$
0
0.01
0.1
1
10
100
[CB] μM

Figure 2.7: Cis- and trans-allostery in wtGLUT1 (●) and GLUT1$_{Q282A}$ (○). A. *Cis-Allostery*. Concentration dependence of maltose-modulation of 2DG influx. Normalized 2DG uptake (v_i/v_c) is plotted as a function of [Maltose] (mM) on a log scale. The curves drawn through the points (solid lines for wtGLUT1 (●) and dashed lines for GLUT1$_{Q282A}$ (○)) were computed by nonlinear regression using equation 2 and have the following constants: wtGLUT1 (●) K1 = 0.0028, K2 = 0.31 mM^{-1}; K3 = 0.197 mM^{-1}, K4 = 1.62 mM^{-2}, R^2 = 0.582, standard error of regression = 0.147; GLUT1$_{Q282A}$ (○) K1 = 0.028, K2 = 1.83 mM^{-1}; K3 = 1.911 mM^{-1}, K4 = 1.62 mM^{-2}, R^2 = 0.582, standard error of regression = 0.147. **B. *Trans-Allostery***. Concentration dependence of CB-modulation of 2DG influx. Normalized 2DG uptake (v_i/v_c) is plotted as a function of [CB] (μM) on a log scale. The curves drawn through the points (solid lines for wtGLUT1 (●) and dashed lines for GLUT1$_{Q282A}$ (○)) were computed by nonlinear regression using equation 2 and have the following constants: wtGLUT1 (●) K1 = 0.0041 μM^2, K2 = 0.073 μM; K3 = 2 x 10^{-12} μM, K4 = 1.64, R^2 = 0.637, standard error of regression = 0.179; GLUT1$_{Q282A}$ (○) K1 = 0.0050 μM^2, K2 = 0.039 μM; K3 = 8.3 x 10^{-14} μM, K4 = 1.495, R^2 = 0.849, standard error of regression = 0.067.

Cis- and trans-allostery in a GLUT1-oligomerization mutant.

GLUT1 forms a mixture of homo-tetramers and homo-dimers in red cell membranes and in CHO and HEK293 cells (102,140). GLUT1 tetramerization (but not sugar transport) is eliminated in a GLUT1/GLUT3 chimera in which GLUT1 membrane spanning helix 9 is substituted with GLUT3 membrane spanning helix 9 sequence (140). We used this tetramerization-deficient mutant ($GLUT1_{(GLUT3\text{-}H9)}$) to ask whether cis- or trans-allostery require GLUT1 tetramerization.

Subsaturating levels of maltose stimulate both GLUT1- and $GLUT1_{(GLUT3\text{-}H9)}$-mediated 2DG uptake whereas higher concentration of maltose inhibit uptake (Figure 2.8A). Introduction of the Q282A mutation to the $GLUT1_{(GLUT3\text{-}H9)}$ background eliminates sugar uptake stimulation by subsaturating [maltose] (Figure 2.8A).

While cis-allostery persists in the oligomerization-deficient mutant, sub-saturating [CB] no longer stimulates 2DG uptake in $GLUT1_{(GLUT3\text{-}H9)}$ or $GLUT1_{(GLUT3\text{-}H9)Q282A}$ expressing HEK293 cells (Figure 2.8B).

The effects of stimulating levels of maltose (10 and 50 μM) and CB (25 nM) on 2DG uptake in GLUT1, $GLUT1_{Q282A}$, $GLUT1_{(GLUT3\text{-}H9)}$ and $GLUT1_{(GLUT3\text{-}H9)Q282A}$ are summarized in Figure 2.9. Stimulation by maltose but not by CB is eliminated in $GLUT1_{Q282A}$. Stimulation by maltose but not by CB persists in $GLUT1_{(GLUT3\text{-}H9)}$ and all stimulations are lost in $GLUT1_{(GLUT3\text{-}H9)Q282A}$.

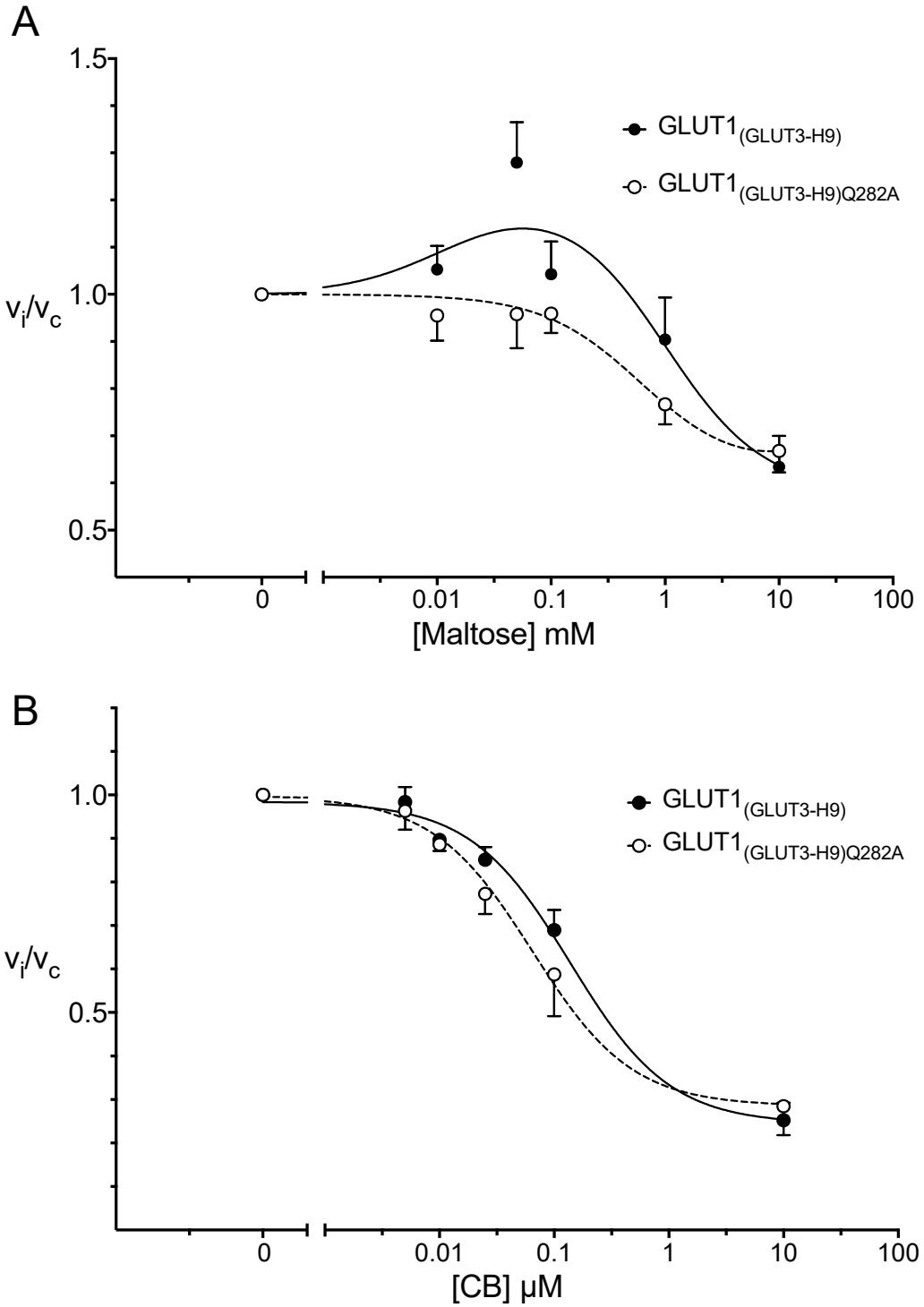
A
1.5
1.0
0.5
v_i/v_c
GLUT1(GLUT3-H9)
GLUT1(GLUT3-H9)Q282A
0
0.01
0.1
1
10
100
[Maltose] mM
B
1.0
0.5
v_i/v_c
GLUT1(GLUT3-H9)
GLUT1(GLUT3-H9)Q282A
0
0.01
0.1
1
10
100
[CB] µM

Figure 2.8: Cis- and trans-allostery in a GLUT1 oligomerization-deficient background. $GLUT1_{(GLUT3\text{-}H9)}$ and $GLUT1_{(GLUT3\text{-}H9)Q282A}$ expressed in HEK293 cells were tested for their ability to mediate cis-and trans-allostery. **A. *Cis-Allostery.*** Concentration dependence of maltose-modulation of 2DG influx. Normalized 2DG uptake (v_i/v_c) is plotted versus [Maltose] (mM) on a log scale. The curves drawn through the points (solid lines for $GLUT1_{(GLUT3\text{-}H9)}$ and dashed lines for $GLUT1_{(GLUT3\text{-}H9)Q282A}$) were computed by nonlinear regression using equation 2 and have the following constants: $GLUT1_{(GLUT3\text{-}H9)}$ (●) K1 = 0.0022, K2 = 2.052 mM^{-1}; K3 = 1.707 mM^{-1}, K4 = 1.72 mM^{-2}, R^2 = 0.656, standard error of regression = 0.137; $GLUT1_{(GLUT3\text{-}H9)Q282A}$ (○) K1 = 0.081, K2 = 0.63 mM^{-1}; K3 = 0.626 mM^{-1}, K4 = 1.528 mM^{-2}, R^2 = 0.747, standard error of regression = 0.080. **B. *Trans-Allostery.*** Concentration dependence of CB-modulation of 2DG influx. Normalized 2DG uptake (v_i/v_c) is plotted versus [CB] (μM) on a log scale. The curves drawn through the points (solid lines for $GLUT1_{(GLUT3\text{-}H9)}$ and dashed lines for $GLUT1_{(GLUT3\text{-}H9)Q282A}$) were computed by nonlinear regression using equation 3 and have the following constants: $GLUT1_{(GLUT3\text{-}H9)}$ (●) K1 = 0.984 μM/s, K2 = 0.740 μM/s; K3 = 0.138 μM, R^2 = 0.963, standard error of regression = 0.058; $GLUT1_{(GLUT3\text{-}H9)Q282A}$ (○) K1 = 0.996 μM/s, K2 = 0.711 μM/s; K3 = 0.065 μM, R^2 = 0.904, standard error of regression = 0.093.

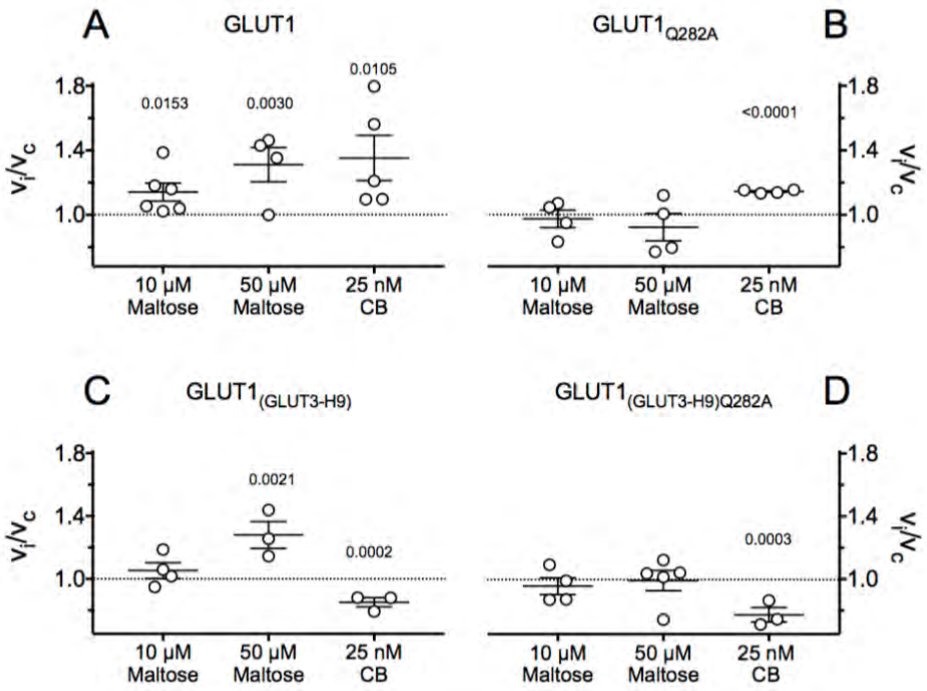

Figure 2.9: Scatter plots of the effects of maltose (10 and 50 µM) and CB (25 nM) on 0.1 mM 2DG uptake in **A** GLUT1, **B** GLUT1$_{Q282A}$, **C** GLUT1$_{(GLUT3\text{-}H9)}$ and **D** GLUT1$_{(GLUT3\text{-}H9)Q282A}$ expressing cells. Normalized uptake (v_i/v_c) is plotted versus concentrations of maltose and CB applied during 2DG uptake measurements. Results are shown as the averages of paired replicates ($n = 4$) and mean ± SEM of multiple experiments ($n \geq 3$). Data were examined by unpaired t-test analysis comparing the effect of treatment to no treatment ($v_i/v_c = 1$ as indicated by the dashed horizontal line) and the computed significance levels are indicated above the points for treatments resulting in $P < 0.05$.

Discussion

As more sugar transporter structures become available, the weight of evidence supporting the alternating access transporter model for sugar transport grows. Each study (6,8,77,131,133,157) has interpreted transporter structures in the context of this model (99,124,145) in which the transporter cycles between conformations presenting either an exofacial cavity to extracellular sugars or an endofacial cavity to cytoplasmic sugars. Sugar binding to exofacial (e2) or endofacial (e1) conformations promotes gating transitions which occlude the bound sugar from the interstitium (forming the e2o state) or from the cytoplasm (forming the e1o state). Occlusion triggers rigid body movements leading to e2o conversion to e1o and vice versa. The trans-gate then opens releasing bound sugar at the opposite side of the membrane. The catalytic cycle concludes via the reverse sequence of conformational changes with or without bound sugar as cargo.

This interpretation of the structural data has excited criticism (78-80,83,84,113,136,143) for 3 reasons: 1) We do not yet have crystal structures of each GLUT conformation complexed with a transported sugar; 2) Available sugar transport data demonstrate that GLUT1 simultaneously presents exofacial and endofacial ligand binding sites; 3) Transport and ligand binding studies demonstrate that the transporter interacts with more than one exofacial ligand (e.g. β-D-Glc plus maltose) and more than one endofacial ligand (e.g. CB plus forskolin) at any instant.

Ligand interaction sites

We therefore asked whether available crystal structures support the idea that e2 and e1

forms of GLUT1 can simultaneously bind multiple ligands in exo- or endofacial cavities. While a crystal structure for GLUT1-e1 is available (77), it was necessary to model GLUT1-e2, GLUT1-e2o and GLUT1-e1o structures using the human GLUT3 (4ZWC) structure (134) and the XylE e2-occluded and e1-occluded structures (6,131) respectively.

Molecular docking reveals that the GLUT1-e2 exofacial cavity presents 3 potential, non-overlapping β-D-Glc interaction sites and two non-overlapping maltose interaction sites. β-D-Glc interaction envelopes are located at peripheral, intermediate and core locations within the exofacial cavity. One maltose interaction envelope overlaps with the core β-D-Glc interaction envelope and the second is more peripherally located in the exofacial cavity. Docking suggests that GLUT1-e2 can simultaneously accommodate core β-D-Glc and peripheral maltose. These three β-D-Glc sites may represent progressive steps in β-D-Glc binding or 3 co-existent interaction sites. The latter hypothesis is consistent with the observation that the transporter can bind extracellular maltose and transported sugar simultaneously (see (78) and this study).

We next asked if GLUT1-e1 or GLUT1-e2 simultaneously interact with endofacial and exofacial ligands. Molecular docking analysis indicates that this is highly improbable. Finally, we asked whether GLUT1-e1 interacts with more than one endofacial ligand simultaneously. GLUT1-e1 presents a single potential, CB interaction envelope which accommodates CB in either of 2 possible but mutually exclusive orientations. Both orientations sterically clash with the GLUT1-e1 β-D-Glc interaction envelope providing a rationale for competition between intracellular β-D-Glc and CB for binding to GLUT1 (92). CB interaction envelopes also sterically clash with the forskolin interaction envelope explaining competition between CB and forskolin for binding to GLUT1 (84).

A model for allostery

Cis- and trans-allostery (sugar import stimulation at low [inhibitor] followed by inhibition at high [inhibitor]) require that GLUT1 must bind inhibitors at at least two sites. This is readily explicable for cis- (maltose-dependent) allostery because GLUT1-e2 presents 2 co-existent, exofacial maltose interaction sites and β-D-Glc competes with maltose for binding at both sites. Trans-(CB-dependent) allostery is more difficult to explain because GLUT1-e1 presents only one CB interaction site. We therefore conclude that each GLUT1 molecule is an alternating access transporter capable of exofacial cis-allostery but incapable of trans-allostery when catalyzing sugar import. How then do we explain trans-allostery?

Previous work (95,102,122,140,158-160) demonstrates that GLUT1 forms mixtures of dimeric and tetrameric GLUT1 complexes. When purifying RBC GLUT1, the ratio of dimeric:tetrameric GLUT1 is affected by cellular redox status with reducing conditions favoring the dimeric form (95,102). GLUT1 cysteines 347 and 421 may form mixed disulfides under non-reducing conditions [95, 102] and GLUT1 transmembrane helix 9 contains GLUT1-specific sequence essential for tetramerization (140). Reduced, dimeric GLUT1 presents 1 CB binding site per GLUT1 molecule whereas nonreduced, tetrameric GLUT1 presents only 0.5 CB binding sites per GLUT1 molecule [95, 102]. Extracellular reductant inhibits RBC sugar import by 80-90% [95, 102] and eliminates trans- but not cis-allostery (80).

The molecular mechanisms by which Q282 and membrane spanning helix 9 (TM9) promote cis- and trans-allostery respectively are unknown. However, our observations support the following model. Dimeric GLUT1 comprises two physically associated but functionally independent GLUT1 molecules. Each subunit displays cis- but not trans-allostery in net sugar uptake, binds 1 molecule of CB and, because transport is rate-limited by conformational changes

between unliganded e1 and e2 states (relaxation (99)), transport is characterized by a low k_{cat}. Tetrameric GLUT1 comprises a noncovalent dimer of two associated and functionally coupled GLUT1 molecules. Intra-dimer subunit interactions produce a functional, anti-parallel arrangement of subunits. If one GLUT1 molecule presents an e2 conformation, its cognate partner in the dimer must present an e1 conformation and vice versa. When an e2 subunit of any dimer interacts with extracellular sugar to undergo the eS2 → eS1 conformational change, its cognate partner undergoes the e1 → e2 conformational change thereby coupling transport via one subunit to the regeneration of an e2 conformation in the cognate subunit, bypassing slow relaxation, and accelerating net sugar transport. Because only two subunits in tetrameric GLUT1 can present the e1 conformation, the stoichiometry of CB binding is 0.5 mol CB per mol GLUT1. Each subunit functions as an allosteric alternating access transporter in import mode. Trans-allostery in sugar import obtains when one e1 subunit interacts with high affinity with an endofacial ligand (e.g. CB or forskolin). The dimer presenting this liganded e1 conformation is locked in an inhibited state but its occupancy is communicated to the adjacent dimer, increasing that dimer's affinity for extracellular β-D-Glc or k_{cat} for transport. As the endofacial ligand concentration is raised, the remaining free e1 subunit in the adjacent dimer is occupied and both dimers are inhibited. Endofacial cis-allostery obtains when the affinity of an unliganded e1 subunit in one dimer is increased by occupancy of the e1 subunit of the adjacent dimer.

In conclusion, GLUT1 functions as an oligomer of allosteric, alternating access transporters. Cis- and trans-allostery require intra- and inter-subunit interactions respectively. Each GLUT1 molecule appears to present a core, catalytic sugar binding site. The exofacial confomer of GLUT1 presents at least one and possibly two additional sugar interaction sites whose occupancy allosterically affects transport via the catalytic site. Trans-allostery requires at

least one subunit to bind an endofacial ligand and one to bind an extracellular, imported sugar. Preventing GLUT1-GLUT1 interactions in an oligomerization-deficient mutant, eliminates trans- but not cis-allostery. Mutating Gln-282 to alanine eliminates cis-allostery but not trans-allostery

CHAPTER 3:

Kinetic basis of Cis- and Trans-Allostery in GLUT1-mediated sugar transport

This chapter was published in the *Journal of Membrane Biology* in 2017, and can be found using the following reference:

Lloyd, K., et al., *Kinetic basis of Cis- and Trans-Allostery in GLUT1-mediated sugar transport.* J Membr Biol, 2017.

Research was supported using NIH Grants: DK36081 and DK44888

Abstract

A growing body of evidence demonstrates that GLUT1-mediated erythrocyte sugar transport is more complex than widely assumed and that contemporary interpretations of emergent GLUT1 structural data are incompatible with the available transport and biochemical data. This study examines the kinetic basis of one such incompatibility -transport allostery - and in doing so suggests how the results of studies examining GLUT1 structure and function may be reconciled. Three-types of allostery are observed in GLUT1-mediated, human erythrocyte sugar transport: 1) Exofacial cis-allostery in which low concentrations of extracellular inhibitors stimulate sugar uptake while high concentrations inhibit transport; 2) Endofacial cis-allostery in which low concentrations of intracellular inhibitors enhance cytochalasin B binding to GLUT1 while high concentrations inhibit binding and, 3) Trans-allostery in which low concentrations of ligands acting at one cell surface stimulate ligand binding at or sugar transport from the other surface while high concentrations inhibit these processes. We consider several kinetic models to account for these phenomena. Our results show that an inhibitor can only stimulate then inhibit sugar uptake if: 1) the transporter binds 2 or more molecules of inhibitor; 2) high affinity binding to the first site stimulates transport and, 3) low affinity binding to the second site inhibits transport. Reviewing the available structural, transport and ligand binding data, we propose that exofacial cis-allostery results from cross-talk between multiple, co-existent ligand interaction sites present in the exofacial cavity of each GLUT1 protein whereas trans-allostery and endofacial cis-allostery require ligand-induced subunit-subunit interactions.

Introduction

Human erythrocyte facilitative sugar transport is mediated by the sugar transport protein GLUT1 (18) (161)and displays three-types of allostery: 1) Exofacial cis-allostery in which low concentrations of extracellular maltose and WZB117 stimulate sugar uptake while high concentrations inhibit transport (78,149,162); 2) Endofacial cis-allostery in which low concentrations of intracellular inhibitors such as forskolin and related molecules enhance binding of the intracellular inhibitor cytochalasin to GLUT1 while high concentrations inhibit binding (80,84) and, 3) Trans-allostery in which low concentrations of ligands such as cytochalasin B or forskolin acting at one cell surface stimulate ligand binding at or sugar transport from the other surface while high concentrations inhibit these processes (80,118,149). These behaviors are incompatible with the predictions of the simple/alternating access (99,124,145) and the fixed site transporters (143,147) and are routinely ignored in discussions of emergent glucose transport structures (6,77,131,133) (but see (136,163)).

The present study considers several kinetic explanations for GLUT1 allostery. These models range from the simple, alternating access transporter (AAT, which alternately exposes an exofacial sugar binding site or an endofacial sugar binding site) and the fixed site transporter (FST, which simultaneously exposes exo-and endo-facial sugar binding sites) through progressively more complex variants of the AAT and FST presenting catalytic and allosteric ligand binding sites at either side of the membrane. We conclude that an exofacial or endofacial inhibitor can only stimulate then inhibit sugar uptake if: 1) the transporter binds 2 or more molecules of inhibitor at exofacial or endofacial binding sites respectively; 2) high affinity binding to the first site stimulates transport and, 3) low affinity binding to the second site inhibits transport.

We then examine available structural, transport and biochemical evidence and propose: 1) that exofacial cis-allostery is an intramolecular phenomenon; 2) that trans-allostery and endofacial-cis allostery are intermolecular behaviors, and 3) that the available data may be reconciled by a model in which the transporter comprises an oligomer of interacting subunits in which each subunit is an allosteric alternating access transporter.

Methods

Each model was schematized in King-Altman form and then analyzed assuming rapid-equilibrium kinetics or when appropriate by the method of Cha (164,165). Sugar uptake was expressed as zero-trans sugar uptake (intracellular sugar is absent at zero-time) and cast as the ratio of uptake in the presence of inhibitor (v_i) relative to uptake in the absence of inhibitor (v_c), i.e. as $\frac{v_i}{v_c}$.

Analysis

Tools

In order to proceed with our analysis we must first consider some of the basic tools employed in studies of GLUT1-mediated sugar transport and ligand binding. These include:

1. Cytochalasin B (CB) - an "e1" ligand (binds at the endofacial surface of GLUT1) (79,83,92).
2. Maltose - an "e2" ligand (cell impermeant and binds at the exofacial surface of GLUT1) (78,83,118).
3. β-D-Glucose (βGlc) and 3-O-methylglucose (3MG) - GLUT1 substrates that bind at both endofacial (e1) and exofacial (e2) binding sites (89,125).
4. The human erythrocyte - a cell whose membrane contains approximately 500,000 copies of GLUT1 (166) and whose sugar transport properties have been studied exhaustively

(89,97,100,125,141).

5. Purified and membrane-resident GLUT1 - exists in 2 forms of noncovalent oligomers:

i) Dimeric GLUT1, isolated in the presence of reductant and binds 1 mol CB per mol GLUT1 (95,102)

ii) Tetrameric GLUT1, isolated in the absence of reductant and binds 0.5 mol CB per mol GLUT1 [95, 102].

6. Tetramerization-deficient GLUT1 mutants - GLUT1 forms in which membrane spanning helix 9 is substituted with GLUT3 membrane spanning helix 9 resulting in dissociation into GLUT1 dimers (140) and the loss of trans-allostery but retention of exofacial cis-allostery (162).

Models

We must then consider several models for sugar transport:

1. **The Simple Carrier:** The transporter (or carrier, Figure 3.1A) is an alternating access transporter (AAT; (145)) alternately presenting e2 (external) and e1 (internal) substrate binding sites. Inhibitors bind competitively to e2 and/or e1.

2. **The Fixed Site Transporter (FST):** The transporter (Figure 3.1B) presents sugar uptake and sugar exit sites simultaneously (147). Inhibitor binding at uptake and exit sites is competitive with sugar binding at the same sites.

3. **Intermolecular cis-allostery:** The transporter is an FST but comprises a dimer of FSTs (Figure 3.2A). The occupancy state of one subunit affects the transport and ligand binding properties of adjacent subunits.

4. **Intramolecular cis-allostery:** The transporter is an FST but additionally contains an exofacial allosteric activator site (Figure 3.2B) at which sugar or inhibitors compete for binding and whose occupancy activates transport (either via an affinity or catalytic effect).

5. **Intramolecular trans-allostery 1:** The transporter is an FST. An allosteric activator site that can bind sugar or inhibitors is present at the endofacial surface of each subunit (Figure 3.3A) and its occupancy activates transport (either via an affinity or catalytic effect) and enhances ligand binding at the exofacial site.

6. **Intramolecular trans-allostery 2:** The transporter is an FST containing endofacial, mutually-exclusive, allosteric sites that can bind sugar or inhibitors (Figure 3.3B). High affinity occupancy of the first site activates transport. Low affinity occupancy of the second site inhibits transport.

7. **Intramolecular trans-allostery 3:** The transporter is an FST containing two allosteric sites that can bind sugar or inhibitors (competitively) at the endofacial surface of each subunit (Figure 3.3C). High affinity occupancy of the first site activates transport. Low affinity occupancy of the second site inhibits transport. The low affinity site could also represent the endofacial sugar binding site.

8. **Intermolecular trans-allostery:** The transporter is a dimer of dimers (a tetramer) of alternating access transporters in which each dimer presents an e2 subunit and an e1 subunit (Figure 3.4A). If an e1 subunit of a dimer undergoes the e1 to e2 conformational change, the adjacent e2 subunit within the same dimer must undergo the e2 to e1 conformational change. If one dimer contains an inhibitor in the e1 subunit, the dimer is locked in an inactive state. The occupancy states of any one dimer is communicated to the adjacent dimer.

9. **Exofacial, Allosteric Alternating Access Transporter:** A simple carrier that contains an additional exofacial allosteric site at which sugars and inhibitors compete for binding (Figure 3.4B). Occupancy of the allosteric site stimulates transport.

A

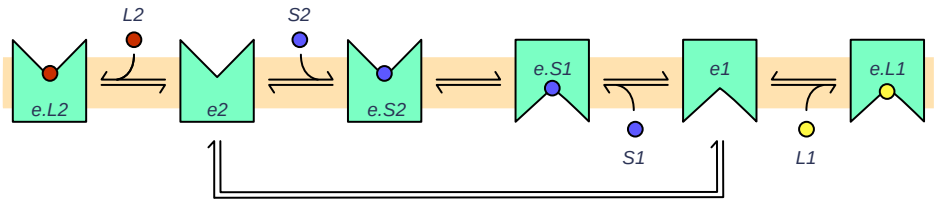
L2
S2
e.L2
e2
e.S2
e.S1
e1
e.L1
S1
L1

B

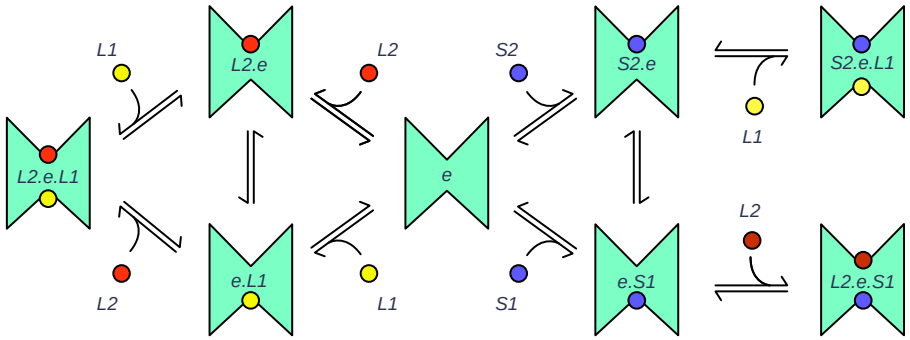
L1
L2.e
L2
S2
S2.e
S2.e.L1
L1
L2.e.L1
e
L2
e.L1
L1
S1
e.S1
L2
L2.e.S1

Figure 3.1: The Alternating Access Transporter (AAT) and the Fixed Site Transporter (FST). A. The AAT. The carrier alternates between conformations exposing an exofacial sugar binding site (e2) and an endofacial sugar binding site (e1). Extracellular inhibitor (L2) and extracellular sugar (S2) compete for binding to e2. intracellular inhibitor (L1) and intracellular sugar (S1) compete for binding to e1. Conformational changes between e2 and e1 are called "translocation" when sugar is bound and "relaxation" when no sugar is bound. **B**. The FST. The carrier, e, presents exofacial and endofacial sugar binding sites simultaneously. Extracellular sugar (S2) and inhibitor (L2) compete for binding at the exofacial site. Intracellular sugar (S1) and inhibitor (L1) compete for binding at the endofacial site. The carrier can form ternary complexes with intra- and extracellular sugars (S2.e.S1, intra- and extracellular inhibitors (L2.e.L1), or with sugars and inhibitors (L2.e.S1, S2.e.L1).

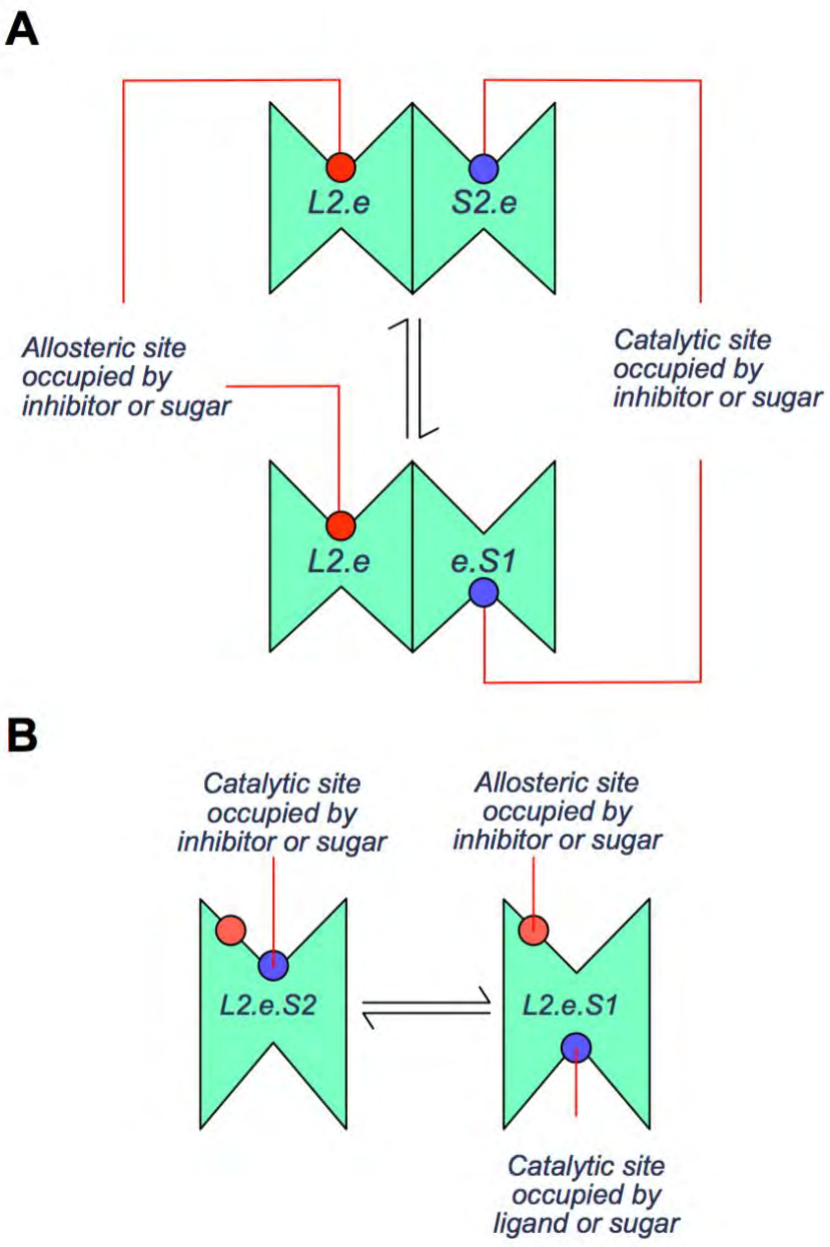
A
L2.e
S2.e
Allosteric site
occupied by
inhibitor or sugar
Catalytic site
occupied by
inhibitor or sugar
L2.e
e.S1
B
Catalytic site
occupied by
inhibitor or sugar
Allosteric site
occupied by
inhibitor or sugar
L2.e.S2
L2.e.S1
Catalytic site
occupied by
ligand or sugar

Figure 3.2: Models for cis-allostery A. Intermolecular cis-allostery The transporter is an FST but comprises a dimer of FSTs (Figure 3.2A). The occupancy state of one subunit affects the transport and ligand binding properties of adjacent subunits. Thus occupancy of subunit 1 by an exofacial inhibitor to form L2.e traps that subunit in an inhibited state but increases the affinity of the adjacent subunit for extracellular sugar and/or accelerates the rate of transport via the adjacent subunit. **B. Intramolecular cis-allostery**. The transporter is an FST which additionally contains an exofacial allosteric activator site at which sugars or inhibitors compete for binding and whose occupancy activates transport (either via an affinity or catalytic effect). Thus L2.e.S2 transports faster or with higher affinity for substrate than does e.S2.

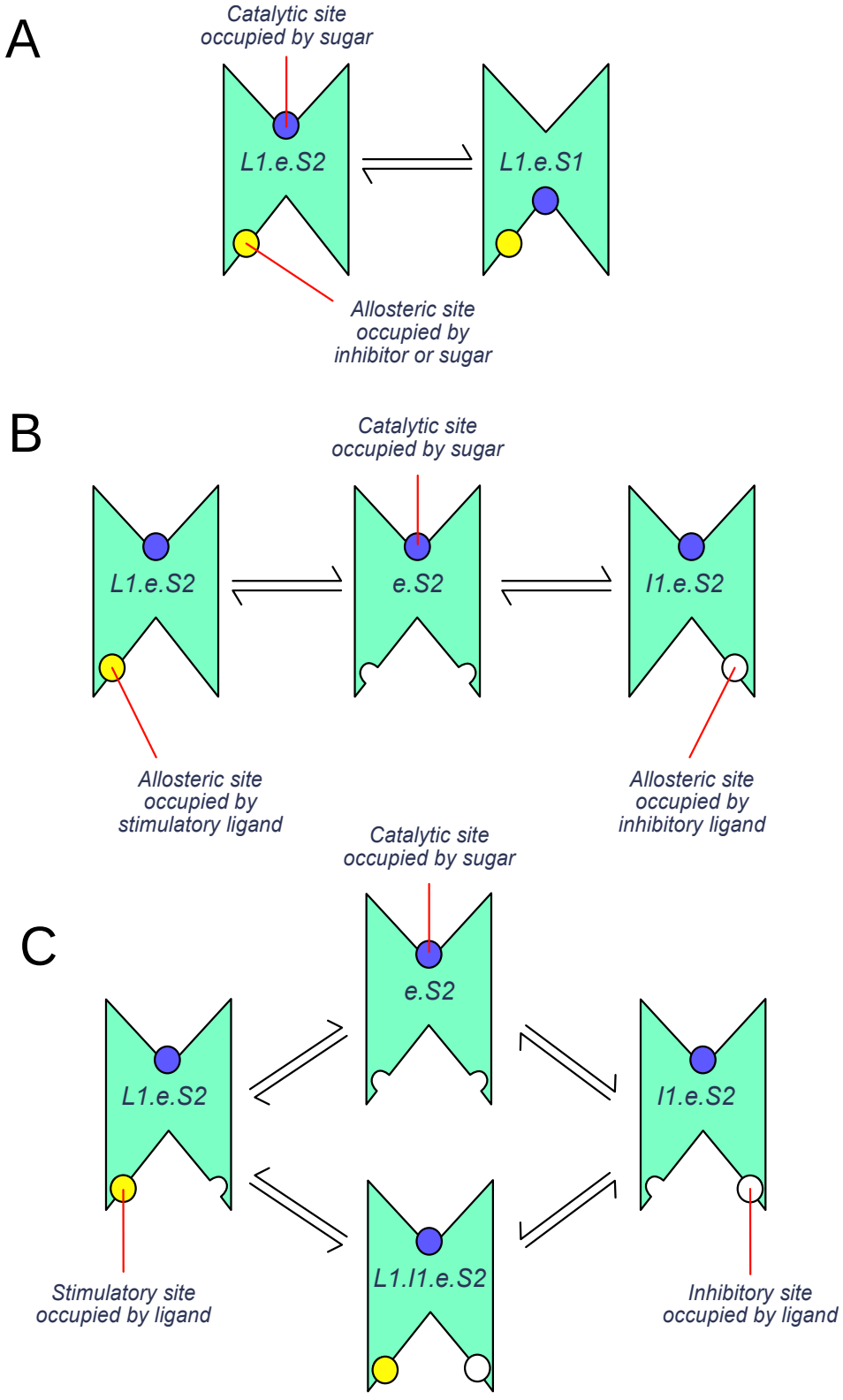
A
Catalytic site
occupied by sugar
L1.e.S2
L1.e.S1
Allosteric site
occupied by
inhibitor or sugar
B
Catalytic site
occupied by sugar
L1.e.S2
e.S2
I1.e.S2
Allosteric site
occupied by
stimulatory ligand
Allosteric site
occupied by
inhibitory ligand
C
Catalytic site
occupied by sugar
e.S2
L1.e.S2
I1.e.S2
L1.I1.e.S2
Stimulatory site
occupied by ligand
Inhibitory site
occupied by ligand

Figure 3.3: Intramolecular trans-allostery models. A. Model 1 The transporter is an FST. An allosteric activator site that can bind sugar or inhibitors is present at the endofacial surface of each subunit and, when occupied by ligand, activates transport (either via an affinity or catalytic effect) and enhances ligand binding at the exofacial site. **B. Model 2** The transporter is an FST containing mutually-exclusive, endofacial, allosteric sites that can bind sugar or ligands. High affinity occupancy of the first site by an activating ligand (L1) activates transport. Low affinity occupancy of the second site by an inhibitory ligand (I1) inhibits transport. The transporter cannot be occupied by both activator and inhibitor simultaneously. **C. Model 3** The transporter is an FST containing two allosteric sites that can bind sugar or inhibitors (competitively) at the endofacial surface of each subunit. High affinity occupancy of the first site by an activator (L1) activates transport. Low affinity occupancy of the second site by an inhibitory ligand (I1) inhibits transport. The transporter may be occupied by both activator and inhibitor simultaneously (forming L1.I1.e) and the net effect on transport depends on the relative potency of activator and inhibitor.

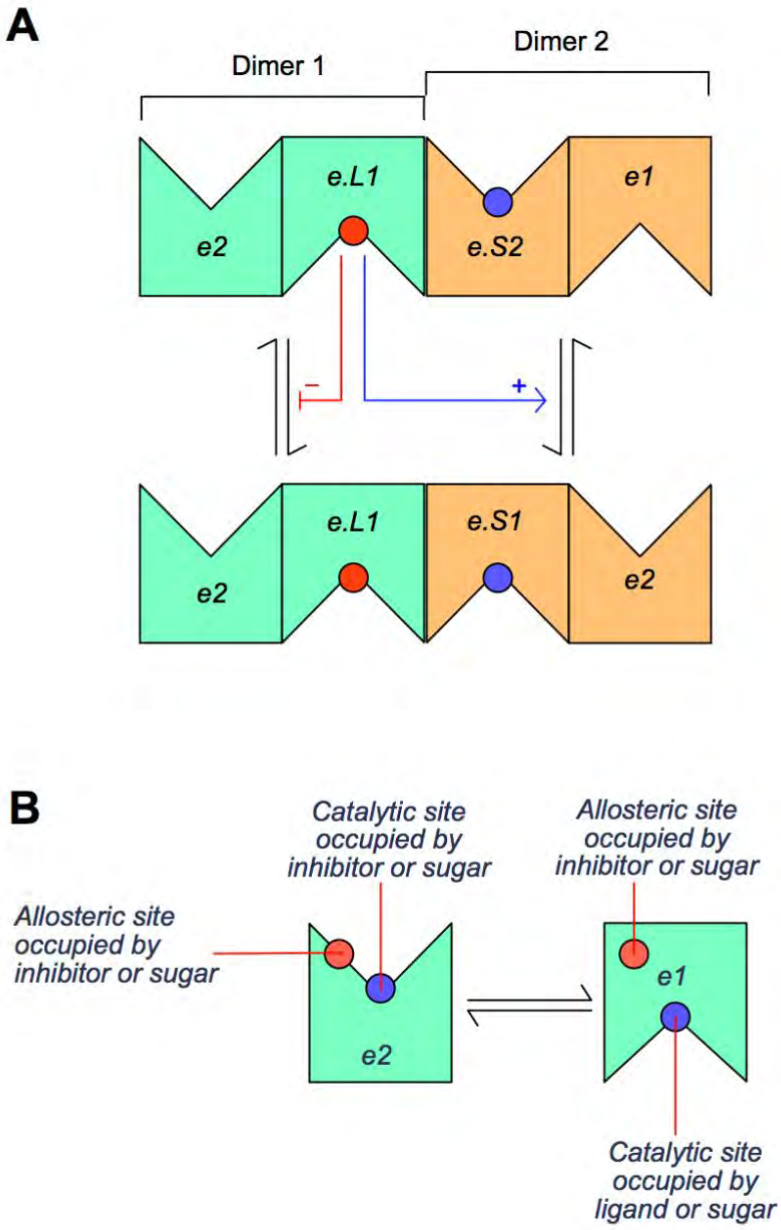
A
Dimer 1
Dimer 2
e.L1
e1
e2
e.S2
–
+
e.L1
e.S1
e2
e2
B
Catalytic site occupied by inhibitor or sugar
Allosteric site occupied by inhibitor or sugar
Allosteric site occupied by inhibitor or sugar
e1
e2
Catalytic site occupied by ligand or sugar

Figure 3.4: Trans-allostery Models A. Intermolecular trans-allostery The transporter is a dimer of dimers (a tetramer) of alternating access transporters in which each dimer must present subunits in opposite conformations (e.g. one subunit presents an e2 conformation and the second an e1 conformation or vice versa). If an e1 subunit of a dimer undergoes the e1 to e2 conformational change, the adjacent e2 subunit within the same dimer must undergo the e2 to e1 conformational change. If a dimer contains an inhibitor in its e1 subunit (e.L1), that dimer is trapped in an inhibited state. If the adjacent dimer does not contain an inhibitory ligand (i.e. its e1 subunit is ligand-free), the occupancy state of the neighboring liganded dimer is communicated to the uninhibited dimer and transport of sugar via the e2 subunit is accelerated either via increased affinity of sugar binding or via increased translocation. **B. Exofacial, Allosteric Alternating Access Transporter** An AAT containing an additional exofacial allosteric site at which sugars and inhibitors compete for binding. Occupancy of the allosteric site (which may persist throughout the transport cycle) stimulates transport via the catalytic center.

King-Altman Schema

The King-Altman schema corresponding to each of these models are illustrated in Schema 1 through 10 (Figure 3.5 - 10).

Scheme 1

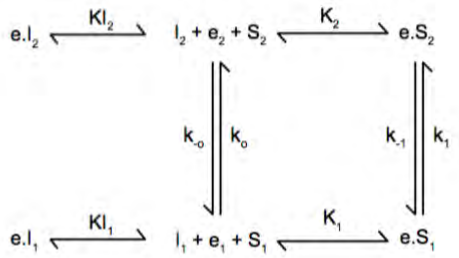

Scheme 2

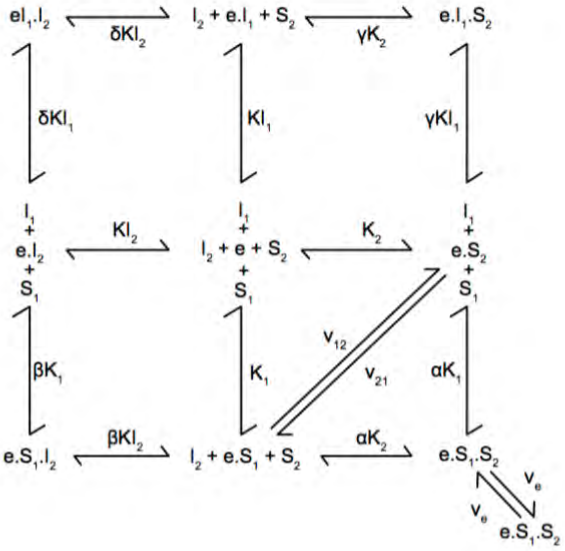

Figure 3.5: King-Altman representations of the AAT and FST. Scheme 1. The AAT. The carrier e isomerizes between exofacial (e2) and endofacial (e1) conformations. The dissociation constants for extracellular sugar and inhibitor binding to e_2 are K_2 and KI_2 respectively. The dissociation constants for intracellular sugar and inhibitor binding to e_1 are K_1 and KI_1 respectively. First order relaxation rate constants are k_{-o} and k_o and first order translocation rate constants are k_{-1} and k_1 **Scheme 2. The FST**. The carrier e exposes an exofacial site at which extracellular sugar (S_2) and inhibitor (I_2) compete for binding and an endofacial site at which intracellular sugar (S_1) and inhibitor (I_1) compete for binding. Dissociation constants for S_2, I_2, S_1 and I_1 binding are K_2, KI_2, K_1 and KI_1 respectively. Binding of I_2 to e affects the dissociation constant for S_1 binding by the cooperativity factor β and for I_1 binding by the cooperativity factor δ. Binding of I_1 to e affects the dissociation constant for S_2 binding by the cooperativity factor γ. Binding of S_2 to e affects the dissociation constant for S_1 binding by the cooperativity factor α. k_{cat} for net sugar import, net sugar export and for exchange transport are v_{21}, v_{12} and v_e respectively.

Scheme 3

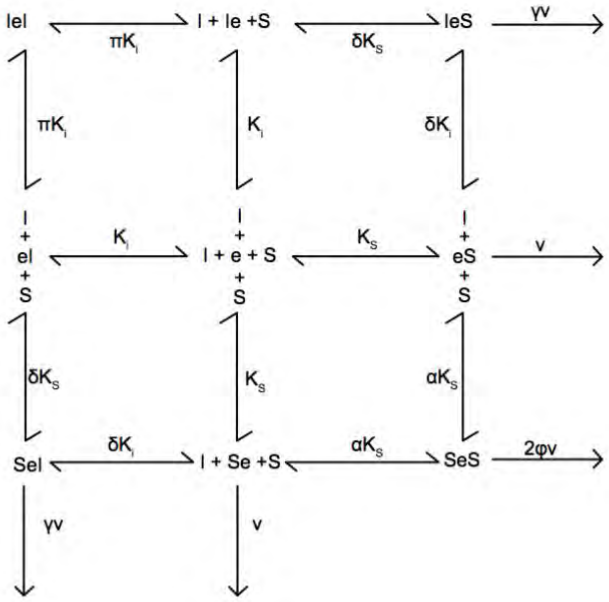

Scheme 4

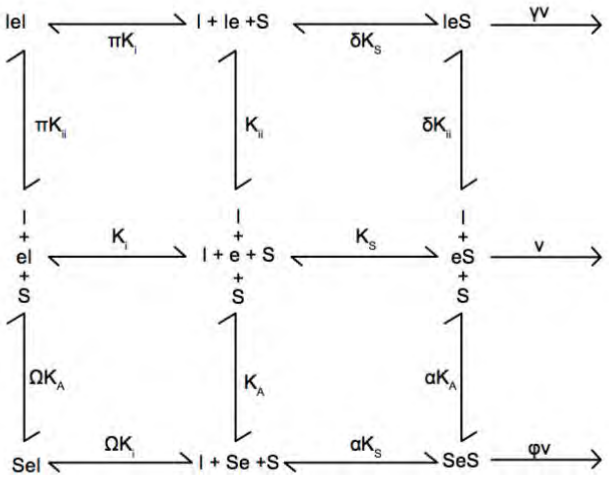

Figure 3.6: King-Altman representations of inter- and intramolecular cis-allostery.

Scheme 3. Intermolecular cis-allostery GLUT1 is an FST but the transporter comprises a dimer of FSTs. Binding of extracellular inhibitor (I) or sugar (S) to subunit 1 is represented as an addition to the left of e. Binding of extracellular inhibitor (I) or sugar (S) to subunit 2 is represented as an addition to the right of e. Dissociation constants for I or S binding to either subunit are K_I and K_S respectively. Binding of S to either subunit affects the dissociation constants for S and I binding to the adjacent subunit by the cooperativity factors α and δ respectively. Binding of I to either subunit affects the dissociation constant for I binding to the adjacent subunit by the cooperativity factor π. k_{cat} for transport by S.e and e.S is v. k_{cat} for transport by S.e.I and I.e.S is γv. k_{cat} for transport by S.e.S is 2φv. **Scheme 4. Intramolecular cis-allostery**. GLUT1 is an FST which additionally contains an exofacial allosteric activator site at which sugars or inhibitors compete for binding and whose occupancy activates transport (either via an affinity or catalytic effect). Binding of inhibitor (I) or sugar (S) at the allosteric site is shown to the left of e. Binding of inhibitor (I) or sugar (S) at the catalytic center is shown to the right of e. Dissociation constants for I or S binding at the allosteric site are K_{II} and K_A respectively. Dissociation constants for I or S binding at the catalytic center are K_I and K_S respectively. Sugar binding at the allosteric site affects dissociation constants for S and I binding at the catalytic center by cooperativity factors α and Ω respectively. Inhibitor binding at the allosteric site affects dissociation constants for S and I binding at the catalytic center by cooperativity factors δ and π respectively. k_{cat} for transport by e.S is v., for transport by I.e.S is γv and for transport by S.e.S is φv.

Scheme 5

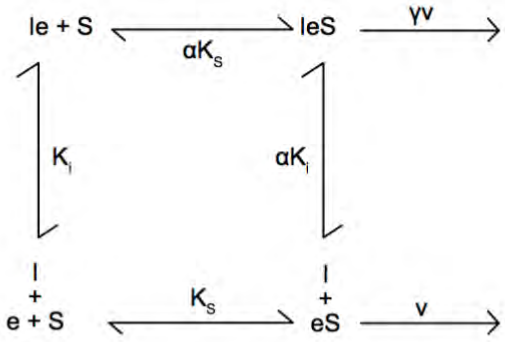

Scheme 6

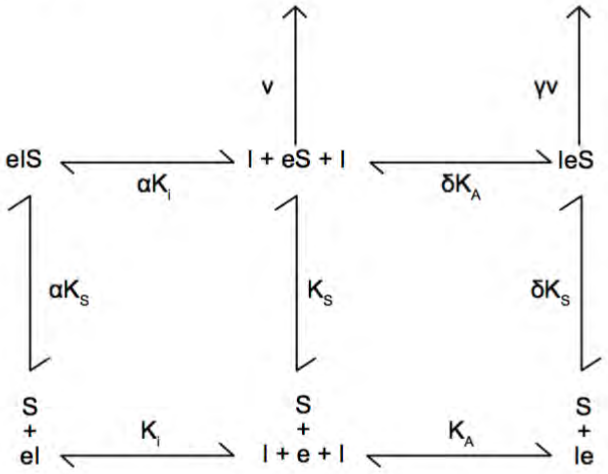

Figure 3.7: King-Altman representations of intramolecular trans-allostery. Scheme 5. Intramolecular trans-allostery model 1. GLUT1 is an FST which contains an allosteric site for intracellular ligand. Dissociation constants for binding of intracellular inhibitor (I) or extracellular sugar (S) are K_I and K_S respectively. Binding of S affects the dissociation constant for I binding by the cooperativity factor α and vice versa. k_{cat} for transport by eS is v. k_{cat} for transport by IeS is γv. **Scheme 6.** Intramolecular trans-allostery model 2. GLUT1 is an FST containing mutually exclusive, endofacial, allosteric activator and inhibitor binding sites at which sugars or inhibitors compete for binding. Occupancy of the activator and inhibitory sites stimulates and inhibits transport respectively. Binding of activating ligand (I) is shown to the left of e (Ie) and of inhibitory ligand (I) to the right of e (eI). Binding of sugar (S) at the catalytic center is shown to the right of e. Dissociation constants for I binding at the activating and inhibitory sites are K_A and K_i respectively. The dissociation constant for S binding at the catalytic center is K_S. Sugar binding at its catalytic center affects dissociation constants for I binding at the activating and inhibitory sites by cooperativity factors δ and α respectively. k_{cat} for transport by eS is v., for transport by IeS is δv. eIS is catalytically inactive.

Scheme 7

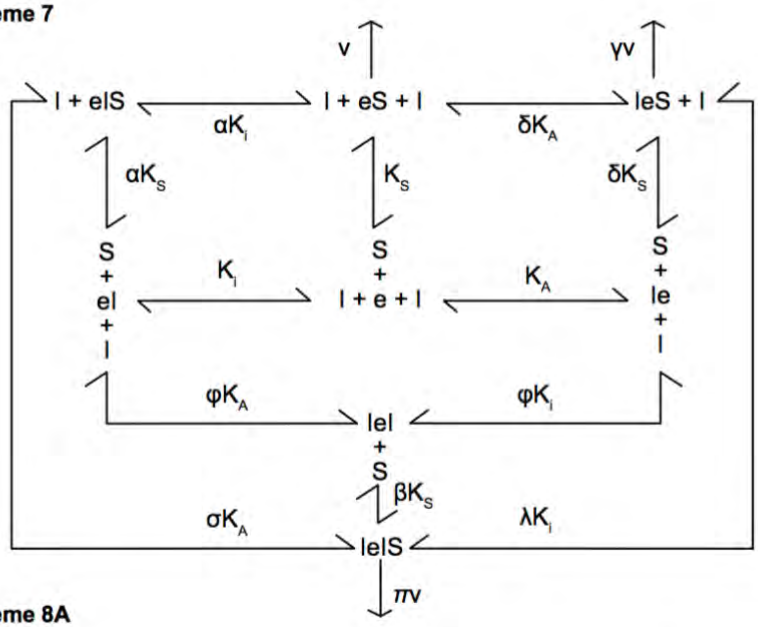

Scheme 8A

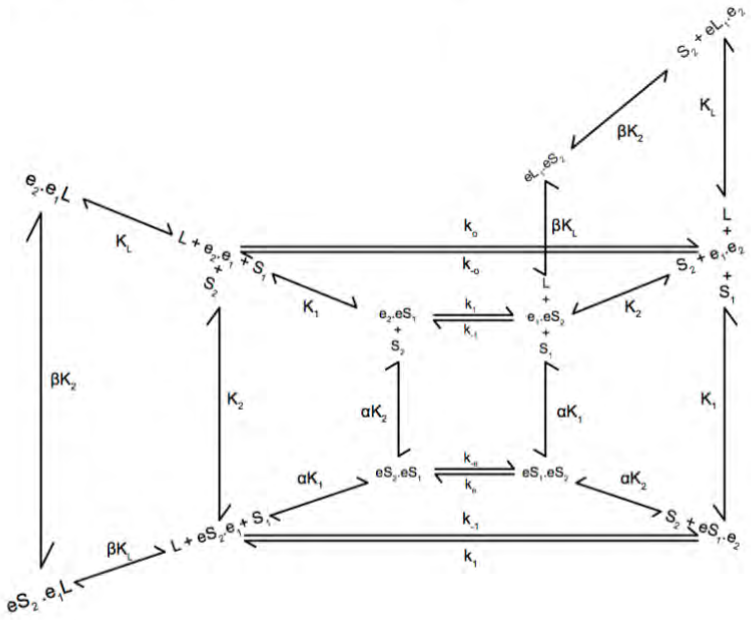

Figure 3.8: King-Altman representations of intra- and inter-molecular trans-allostery.

Scheme 7. GLUT1 is an FST containing two co-existent allosteric sites that competitively bind sugar (S) or inhibitors (I) at the endofacial surface of each subunit. High affinity occupancy of the first site (shown as binding to the left of e) activates transport. Low affinity occupancy of the second site (shown as binding to the right of e) inhibits transport. Binding of sugar (S) at the catalytic center is shown to the right of e. Dissociation constants for I binding at the activating and inhibitory sites are K_A and K_i respectively. The dissociation constant for S binding at the catalytic center is K_S. Sugar binding at its catalytic center affects dissociation constants for I binding at the activating and inhibitory sites by cooperativity factors δ and α respectively. I binding at the activating site affects the dissociation constant for I binding at the inhibitory site by cooperativity factor φ. The dissociation constant for I binding at the activating site in the eIS ternary complex is affected by the cooperativity factor σ. The dissociation constant for I binding at the inhibitory site in the IeS ternary complex is affected by the cooperativity factor λ. The dissociation constant for S binding at the catalytic center of the IeI ternary complex is affected by the cooperativity factor β. The rule of microscopic reversibility (45) requires that $\alpha\,\sigma = \delta\,\lambda = \varphi\,\beta$. k_{cat} for transport by eS is v, for transport by IeS is δv and for transport by IeIS is πv. eIS is catalytically inactive. **Scheme 8A.** Inter-molecular trans-allostery. The transporter comprises a dimer of GLUT1 dimers. Each GLUT1 subunit is an AAT. Each dimer is independent of the other although subunit occupancy states are communicated across the dimer/dimer interface. Inhibitor L interacts only with e1 conformations of GLUT1. When one e1 subunit of a dimer contains a bound inhibitor (L) its adjacent e2 partner within the dimer (termed the cognate subunit) is, like its liganded partner, locked and thus inactive. However, the occupancy state of e_1L is transmitted to the adjacent

dimer and allows the e_2 subunit of the adjacent dimer to bind S_2 with higher affinity or to transport S_2 (k_{-1}) with greater speed. This scheme portrays intracellular ligand (L) and extra- and intracellular sugar (S_2 and S_1) binding to a single dimer in the tetrameric complex. First-order translocation rate constants for sugar uptake and exit are k_{-1} and k_1 respectively. First order translocation rate constants for relaxation are k_{-o} and k_o. Dissociation constants for S_1, S_2 and L binding to the dimer are K_1, K_2 and K_L respectively. S_2 binding to the dimer affects the dissociation constants for S_1 and L binding to the adjacent e1 subunit by the cooperativity factors α and β respectively. The law of microscopic reversibility requires the following: $k_o\ k_{-1}\ K_1 = k_{-o}\ k_1\ K_2$. All other microscopic reversibility requirements derive from this specific relationship.

A Scheme 8B

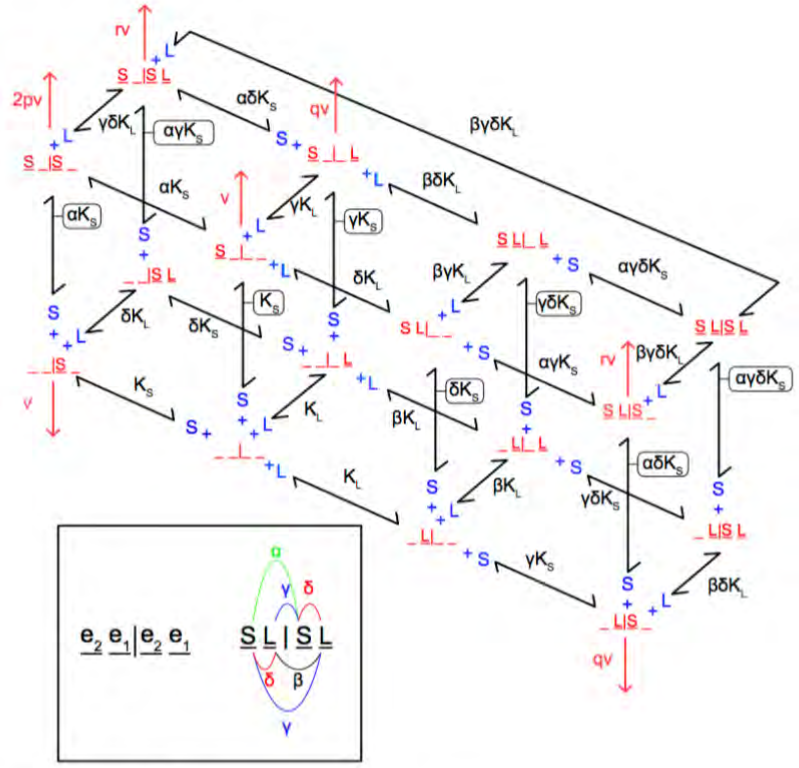

B Scheme 8C

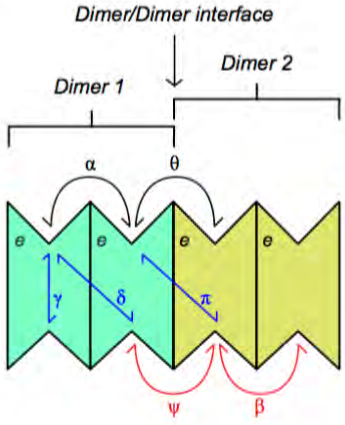

Figure 3.9: King-Altman representation of intermolecular trans-allostery. A. Scheme 8B. King-Altman representation of alternative model for intermolecular trans-allostery. The transporter comprises a dimer of GLUT1 dimers. Each GLUT1 subunit is an AAT. Each dimer is independent of the other although subunit occupancy states are communicated across the dimer/dimer interface. Each dimer adopts the $e_2.e_1$ or $e_1.e_2$ conformation. There are 4 possible configurations of unliganded tetramer ($e_2.e_1|e_2.e_1$, $e_2.e_1|e_1.e_2$, $e_1.e_2|e_2.e_1$ and $e_1.e_2|e_1.e_2$). The scheme in here illustrates only the $e_2.e_1|e_2.e_1$ conformation. The unliganded transporter ($e_2.e_1|e_2.e_1$) is depicted as _ _ | _ _ where each underscore represents an unliganded site. An e2 site can become liganded with extracellular sugar S (e.g. S _ | _ _ or _ _ | S _ or S _ | S _) whereas the e1 site can become liganded with L (e.g. _ L | _ _ or _ _ | _ L or _ L | _ L). Only dimers in which the cognate e1 subunit is not complexed with L are capable of transport. Dissociation constants for S and L binding are K_S and K_L respectively. The inset summarizes cooperative interactions. S biding to one dimer affects S binding to the adjacent dimer by the cooperativity constant α. L biding to one dimer affects L binding to the adjacent dimer by the cooperativity constant β. S and L biding to the same dimer is cooperative and described by the cooperativity constant δ. S and L biding to different dimers within the complex is cooperative and is described by the cooperativity constant γ. The factors p, q and r describe how k_{cat} (v) for sugar uptake by the tetramer is affected when the tetramer contains: 1) 2 sugars, 2) a sugar in 1 dimer plus an inhibitor in the adjacent dimer and 3) 2 sugars and one inhibitor respectively. **B. Scheme 8C.** A FST tetramer comprising a dimer of FST dimers. This transporter can bind up to 4 exofacial sugars (S) and 4 endofacial ligands (L). Exofacial cooperativity is shared within subunits of each dimer (binding of the first sugar affects K_S for binding of the second by the

cooperativity factor α) and between dimers (binding of a sugar to one dimer affects K_S for binding of a second sugar to a subunit in the adjacent dimer by the cooperativity factor θ. In a similar way, endofacial cooperativity is shared within subunits of each dimer (binding of the first ligand affects K_L for binding of the second by the cooperativity factor β) and between dimers (binding of a ligand to one dimer affects K_L for binding of a second ligand to a subunit in the second dimer by the cooperativity factor ψ. Finally, cooperativity may exist between endofacial and exofacial sites (trans-allostery) within the same subunit (γ) between subunits of the same dimer (δ) and between subunits in different dimers (π).

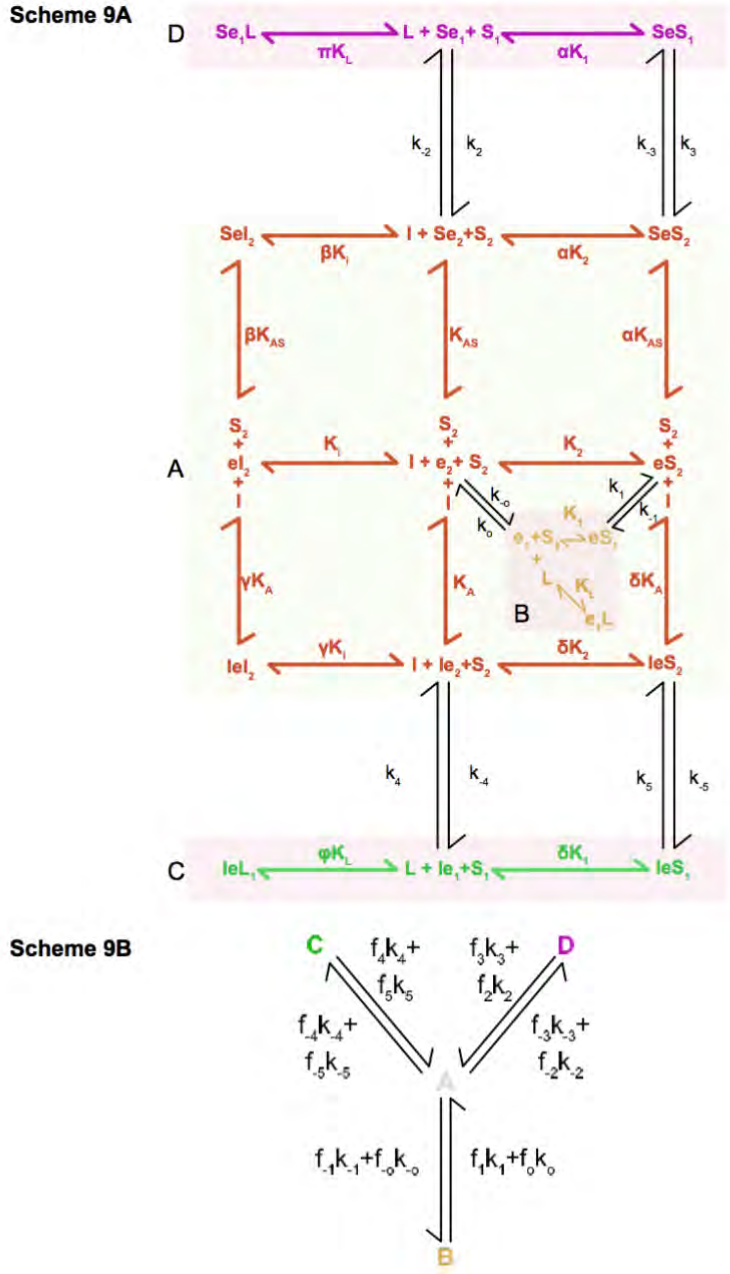

Figure 3.10: King-Altman representation of the exofacial allosteric AAT. Scheme 9A A simple carrier that contains an additional exofacial allosteric site at which sugars and inhibitors

compete for binding. Occupancy of the allosteric site stimulates transport. Ligand binding to the catalytic center is shown as an addition to the right of e. Ligand binding to the allosteric site is shown as an addition to the left of e. Dissociation constants for S_1, S_2 and I (exofacial inhibitor) binding to e are as described in Figure 5 (K_1, K_2 and K_i respectively). Intracellular inhibitor (L) binding to e1 is described the the dissociation constant K_L. Dissociation constants for S_2 and I binding to the exofacial allosteric site are K_{AS} and K_A respectively. Binding of I to the allosteric site affects the dissociation constant for S_2 and I binding to the catalytic center of e_2 by the cooperativity factors δ and γ respectively. Binding of S_2 to the allosteric site affects the dissociation constant for S_2 and I binding to the catalytic center of e_2 by the cooperativity factors α and β respectively. When the allosteric site is occupied by S_2 the relaxation rate constants (k_o and k_{-o}) become k_2 and k_{-2} and the translocation rate constants (k_1 and k_{-1}) become k_3 and k_{-3}. Dissociation constants for L and S_1 binding to Se_1 are affected by the cooperativity factors π and α respectively. When the allosteric site is occupied by I the relaxation rate constants (k_o and k_{-o}) become k_4 and k_{-4} and the translocation rate constants (k_1 and k_{-1}) become k_5 and k_{-5}. Dissociation constants for L and S_1 binding to Ie_1 are affected by the cooperativity factors φ and δ respectively. The law of microscopic reversibility requires the following: $K_2\ k_{-2}\ k_3 = K_1\ k_2\ k_{-3}$ and $K_2\ k_{-4}\ k_5 = K_1\ k_4\ k_{-5}$. **Scheme 9B** A simplified version of Scheme 9A according to the method of Cha. Scheme 9A is subdivided into 4 rapid equilibrium segments - A, B, C and D (see Scheme 9A). The components of segments A, B, C and D (that interchange with other segments via the indicated first order rate constants are described in the solution to Model 9.

Results

Both the alternating access transporter (model 1) and the fixed site transporter (model 2) have been analyzed previously (78,80,83,118,147,149,167) and neither can reproduce transport stimulation at low [inhibitor] followed by inhibition at higher [inhibitor] without significant modification. Only transport inhibition is possible with either of these models when inhibitors (cis or trans) are introduced (83).

Our general conclusion from the subsequent analyses we present below is that when the effect of inhibitor on transport is cast as the ratio of inhibited sugar uptake (v_i) : control sugar uptake (v_c) the equations that reproduce stimulation followed by inhibition take one of two general forms. In the absence of transbilayer sugar leakage (i.e. when non GLUT1-mediated sugar trans- bilayer diffusion is absent)

$$\frac{v_i}{v_c} = \frac{Const_1 + [I]Const_2}{Const_1 + [I](Const_3 + [I]Const_4)} \qquad \text{eqn 1}$$

Or, when non-specific leakage of sugar across the cell membrane is considered,

$$\frac{v_i}{v_c} = \frac{Const_1 + [I](Const_2 + [I])}{Const_1 + [I](Const_3 + [I]Const_4)} \qquad \text{eqn 2}$$

where the specific interpretation of $Const_1$ - $Const_4$ is model-dependent. An extension of equation 1 also results when the transporter can bind multiple ligands and transported sugars (see result for model 8C).

Solutions for models 3 - 9

Model 3 - Intermolecular cis-allostery

Assuming rapid equilibrium kinetics, sugar uptake in the presence of extracellular inhibitors (v_i) is given by

$$\frac{v_i}{[e]_t} = \frac{2v\left(\frac{[S]}{K_S} + \phi\frac{[S]^2}{\alpha K_S^2} + \gamma\frac{[I][S]}{\delta K_S K_I}\right)}{\left(1 + \frac{2[S]}{K_S} + \frac{[S]^2}{\alpha K_S^2} + \frac{2[I]}{K_I} + \frac{[I]^2}{\pi K_I^2} + \frac{2[I][S]}{\delta K_S K_I}\right)} \qquad \text{eqn 3}$$

where $[e]_t$ is the concentration of membrane resident GLUT1, [S] and [I] are concentrations of extracellular transported sugar and transport inhibitor respectively and the remaining constants are as defined in Scheme 3. When inhibitors are absent, control uptake (vc) is given by

$$\frac{v_c}{[e]_t} = \frac{2v\left(\frac{[S]}{K_S} + \phi\frac{[S]^2}{\alpha K_S^2}\right)}{\left(1 + \frac{2[S]}{K_S} + \frac{[S]^2}{\alpha K_S^2}\right)} \qquad \text{eqn 4}$$

Thus, the ratio of inhibited to control transport is given by:

$$\frac{v_i}{v_c} = \frac{[I]Const_1 + Const_2}{[I](Const_3 + [I]Const_4) + Const_2} \qquad \text{eqn 1}$$

Where the constants have the following solutions:

$$Const_1 = \left(1 + \frac{2[S]}{K_S} + \frac{[S]^2}{\alpha K_S^2}\right)\left(\frac{[S]}{K_S} + \phi\frac{[S]^2}{\alpha K_S^2}\right) \quad Const_2 = \left(1 + \frac{2[S]}{K_S} + \frac{[S]^2}{\alpha K_S^2}\right)\gamma\frac{[S]}{\delta K_S K_I}$$

$$Const_3 = \frac{2}{K_I}\left(1 + \frac{[S]}{\delta K_S}\right)\left(\frac{[S]}{K_S} + \phi\frac{[S]^2}{\alpha K_S^2}\right)$$

$$Const_4 = \frac{\left(\frac{[S]}{K_S} + \phi\frac{[S]^2}{\alpha K_S^2}\right)}{\pi K_I^2}$$

This model successfully reproduces transport stimulation followed by transport inhibition as [I] is raised from 0 to saturating levels but seems unlikely given that cis-allostery persists in the GLUT1 tetramerization-null mutant (162).

Model 4 - Intramolecular cis-allostery

Assuming rapid equilibrium kinetics, sugar uptake in the presence of extracellular inhibitors (v_i) is given by

$$\frac{v_i}{[e]_t} = \frac{v\left(\frac{[S]}{K_S} + \phi\frac{[S]^2}{\alpha K_S^2} + \gamma\frac{[I][S]}{\delta K_S K_I}\right)}{\left(1 + \frac{[S]}{K_S} + \frac{[S]}{K_A} + \frac{[S]^2}{\alpha K_A K_S} + \frac{[I]}{K_I} + \frac{[I]}{K_{II}} + \frac{[I]^2}{\pi K_I K_{II}} + \frac{[I][S]}{\delta K_S K_{II}} + \frac{[I][S]}{\Omega K_A K_I}\right)} \qquad \text{eqn 5}$$

where $[e]_t$ is the concentration of membrane resident GLUT1, [S] and [I] are concentrations of extracellular transported sugar and transport inhibitor respectively and the remaining constants are as defined in Scheme 4. When inhibitors are absent, control uptake (v_c) is given by:

$$\frac{v_c}{[e]_t} = \frac{v\left(\frac{[S]}{K_S}+\phi\frac{[S]^2}{\alpha K_S^2}\right)}{\left(1+\frac{[S]}{K_S}+\frac{[S]}{K_A}+\frac{[S]^2}{\alpha K_A K_S}\right)} \qquad \text{eqn 6}$$

Thus the ratio of inhibited to control transport is given by:

$$\frac{v_i}{v_c} = \frac{[I]Const_1+Const_2}{[I](Const_3+[I]Const_4)+Const_2} \qquad \text{eqn 1}$$

Where the constants have the following solutions:

$$Const_1 = \left(1+[S]\left(\frac{1}{K_S}+\frac{1}{K_A}+\frac{[S]}{\alpha K_A K_S}\right)\right)\left(\frac{[S]}{K_S}+\phi\frac{[S]^2}{\alpha K_A K_S}\right)$$

$$Const_2 = \left(1+[S]\left(\frac{1}{K_S}+\frac{1}{K_A}+\frac{[S]}{\alpha K_A K_S}\right)\right)\gamma\frac{[S]}{\delta K_S K_{II}}$$

$$Const_3 = \left(\frac{[S]}{\Omega K_A K_I}+\frac{[S]}{\delta K_S K_{II}}+\frac{1}{K_I}+\frac{1}{K_{II}}\right)\left(\frac{[S]}{K_S}+\phi\frac{[S]^2}{\alpha K_A K_S}\right)$$

$$Const_4 = \frac{\left(\frac{[S]}{K_S}+\phi\frac{[S]^2}{\alpha K_A K_S}\right)}{\pi K_I K_{II}}$$

This reproduces transport stimulation followed by transport inhibition as [I] is raised from 0 to saturating levels (the equation is of the correct form) and is consistent with the finding that the exofacial cavity presents 3 sugar binding sites - peripheral (P), intermediate (I) and core (C) (149,162). The core site is proposed to be catalytic and the peripheral and intermediate are thought to be allosteric (maltose, WZB117 and other molecules can occupy P+I and I+C; (78,149,162).

Model 5 - Intramolecular trans-allostery 1

Assuming rapid equilibrium kinetics, uptake (v_i) in the presence of intracellular inhibitors (I) is

given by:

$$\frac{v_i}{[e]_t} = \frac{v\left(\frac{[S]}{K_S} + \gamma\frac{[I][S]}{\alpha K_S K_I}\right)}{\left(1 + \frac{[S]}{K_S} + \frac{[I]}{K_I} + \frac{[I][S]}{\alpha K_S K_I}\right)} \qquad \text{eqn 7}$$

where $[e]_t$ is the concentration of membrane resident GLUT1, [S] and [I] are concentrations of extracellular transported sugar and intracellular transport inhibitor respectively and the remaining constants are as defined in Scheme 5. When inhibitors are absent, control uptake (v_c) is given by:

$$\frac{v_c}{[e]_t} = \frac{v\left(\frac{[S]}{K_S}\right)}{\left(1 + \frac{[S]}{K_S}\right)} \qquad \text{eqn 8}$$

Thus the ratio of inhibited to control transport is given by:

$$\frac{v_i}{v_c} = \frac{[I]Const_1 + Const_2}{[I]Const_3 + Const_2} \qquad \text{eqn 9}$$

Where the constants have the following solutions:

$$Const_1 = \frac{\gamma}{K_I}\left(1 + \frac{[S]}{\alpha K_S}\right)$$

$$Const_2 = 1 + \frac{[S]}{K_S}$$

$$Const_3 = \frac{1}{\mathrm{K}_I}\left(1 + \frac{[S]}{\alpha K_S}\right)$$

Equation 9 can only produce transport inhibition ($\gamma < 1$) or stimulation ($\gamma > 1$) thus this model is rejected.

Model 6 - Intramolecular trans-allostery 2

Assuming rapid equilibrium kinetics, sugar uptake (v_i) in the presence of intracellular inhibitors is given by:

$$\frac{v_i}{[e]_t} = \frac{v\left(\frac{[S]}{K_S} + \gamma\frac{[I][S]}{\delta K_S K_I}\right)}{\left(1 + \frac{[S]}{K_S} + \frac{[I]}{K_I} + \frac{[I]}{K_A} + \frac{[I][S]}{K_S}\left(\frac{1}{\alpha K_I} + \frac{1}{\delta K_A}\right)\right)} \qquad \text{eqn 10}$$

where $[e]_t$ is the concentration of membrane resident GLUT1, [S] and [I] are concentrations of extracellular transported sugar and transport inhibitor respectively and the remaining constants are as defined in Scheme 6. When inhibitors are absent, control uptake (v_c) is given by

$$\frac{v_c}{[e]_t} = \frac{v\left(\frac{[S]}{K_S}\right)}{\left(1+\frac{[S]}{K_S}\right)} \qquad \text{eqn 11}$$

Thus the ratio of inhibited to control transport is given by:

$$\frac{v_i}{v_c} = \frac{[I]Const_1+Const_2}{[I]Const_3+Const_2} \qquad \text{eqn 9}$$

Where the constants have the following solutions:

$$Const_1 = \frac{\gamma}{\delta K_A}\left(1+\frac{[S]}{K_S}\right)$$

$$Const_2 = 1+\frac{[S]}{K_S}$$

$$Const_3 = \frac{1}{K_I}+\frac{1}{K_A}+\frac{[S]}{K_S}\left(\frac{1}{\alpha K_I}+\frac{1}{\delta K_A}\right)$$

As with Model 5, Model 6 can only produce transport inhibition ($\gamma < 1$) or stimulation ($\gamma > 1$) thus this model is rejected.

Model 7 - Intramolecular trans-allostery 3

Assuming rapid equilibrium kinetics, sugar uptake (v_i) in the presence of intracellular inhibitors (I) is given by:

$$\frac{v_i}{[e]_t} = \frac{v\left(\frac{[S]}{K_S}+\gamma\frac{[I][S]}{\delta K_S K_A}+\pi\frac{[I]^2[S]}{\delta\gamma K_S K_A K_S K_I}\right)}{\left(1+\frac{[S]}{K_S}+\frac{[I]}{K_I}+\frac{[I]}{K_A}+\frac{[I]^2}{\phi K_I K_A}+\frac{[I][S]}{K_S}\left(\frac{1}{\alpha K_I}+\frac{1}{\delta K_A}\right)+\frac{[I]^2[S]}{\delta\lambda K_S K_A K_I}\right)} \qquad \text{eqn 12}$$

where $[e]_t$ is the concentration of membrane resident GLUT1, [S] and [I] are concentrations of extracellular transported sugar and intracellular transport inhibitor respectively and the remaining constants are as defined in Scheme 7. When inhibitors are absent, control uptake (v_c) is given by

$$\frac{v_c}{[e]_t} = \frac{v[S]}{K_S+[S]}$$

Thus the ratio of inhibited to control transport is given by:

$$\frac{v_i}{v_c} = \frac{Const_1+[I](Const_2+[I]Const_3)}{Const_1+[I](Const_4+[I]Const_5)} \qquad \text{eqn 1.1}$$

Where the constants have the following solutions:

$$Const_1 = \alpha\delta\gamma\lambda\phi K_A K_I(K_S + [S])$$

$$Const_2 = \alpha\gamma\lambda\phi K_I(K_S + [S])$$

$$Const_3 = \alpha\pi\phi(K_S + [S])$$

$$Const_4 = \alpha\delta\lambda\phi K_S\{(K_A + K_I) + \lambda\phi[S](\delta \mathrm{K}_A + \alpha K_I)\}$$

$$Const_5 = \alpha(\delta\gamma K_S + \phi[S])$$

When $\pi = 0$,

$$\frac{v_i}{v_c} = \frac{Const_1+[I]Const_2}{Const_1+[I](Const_4+[I]Const_5)} \qquad \text{eqn 1}$$

These equations (eqns 1 and 1.1) take the correct form (eqn 1) to permit transport stimulation followed by transport inhibition as [I] is raised from subsaturating to saturating levels. This model seems unlikely, however, because dimeric GLUT1 binds 1 mol CB per mol GLUT1 while tetrameric GLUT1 binds 0.5 mol CB per mol GLUT1 (95,102). The binding capacity of this carrier would be 2 mol CB per mol GLUT1.

Model 8 - Intermolecular trans-allostery

In this model, the transporter comprises a dimer of GLUT1 dimers. Each dimer is essentially independent of the other although subunit occupancy states are communicated across the dimer/dimer interface. When one e1 subunit of a dimer contains a bound inhibitor (L) its adjacent e2 partner within the dimer (termed the cognate subunit) is, like its liganded partner, locked and thus inactive. However, the occupancy state of e1L is transmitted to the adjacent

dimer and allows the e2 subunit of the adjacent dimer to bind S_2 with higher affinity or to transport S_2 (k-1) with greater speed.

This model is more challenging to solve. The probability of dimer 1 or 2 having S_2 bound in a catalytically active form is given by

$$P_{S2} = \frac{\frac{S_2}{K_2}}{D_A} \text{where} D_A = 1 + \frac{[S_1]}{K_1} + \frac{[S_2]}{K_2} + \frac{[S_1][S_2]}{\alpha K_1 K_2} + \frac{[L]}{K_L} + \frac{[L][S_2]}{\beta K_L K_2}$$

The probability of dimer 1 or 2 having S1 plus S2 bound in a catalytically active form is given by:

$$P_{SS} = \frac{\frac{[S_1][S_2]}{\alpha K_1 K_2}}{D_A}$$

The probability of dimer 1 or 2 having L bound is given by

$$P_L = \frac{\frac{[L]}{K_L} + \frac{[L][S_2]}{\beta K_L K_2}}{D_A}$$

And the probably of either being free of ligand is 1-P_L.

Assuming only transport rates are affected (not affinity at this point)

$$v_{21} = v_i = (1 - P_L)(k_{-1}P_{S2} + k_e P_{SS}) + P_L(k^*_{-1}P_{S2} + k^*_e P_{SS})$$

$$\text{where} \frac{k^*_{-1}}{k_{-1}} \text{and} \frac{k^*_e}{k_e} > 1 = \gamma$$

When $S_1 = 0$

$$P_L = \frac{\frac{[L]}{K_L} + \frac{[L][S_2]}{\beta K_L K_2}}{1 + \frac{[S_2]}{K_2} + \frac{[L]}{K_L} + \frac{[L][S_2]}{\beta K_L K_2}} \text{and} 1 - P_L = \frac{1 + \frac{[S_2]}{K_2}}{1 + \frac{[S_2]}{K_2} + \frac{[L]}{K_L} + \frac{[L][S_2]}{\beta K_L K_2}}; P_{S2}$$

$$= \frac{\frac{[S_2]}{K_2}}{1 + \frac{[S_2]}{K_2} + \frac{[L]}{K_L} + \frac{[L][S_2]}{\beta K_L K_2}}; P_{SS} = 0$$

$$v_c = \frac{k_{-1}\frac{[S_2]}{K_2}}{1+\frac{[S_2]}{K_2}}; v_i = \frac{\left(1+\frac{[S_2]}{K_2}\right)k_{-1}\frac{[S_2]}{K_2} + \frac{[L]}{K_L}\left(1+\frac{[S_2]}{\beta K_2}\right)\gamma k_{-1}\frac{[S_2]}{K_2}}{D_A D_A}$$

$$\frac{v_i}{v_c} = \frac{\left[\left(1+\frac{[S_2]}{K_2}\right)k_{-1}\frac{[S_2]}{K_2} + \frac{[L]}{K_L}\left(1+\frac{[S_2]}{\beta K_2}\right)\gamma k_{-1}\frac{[S_2]}{K_2}\right]\left(1+\frac{[S_2]}{K_2}\right)}{D_A D_A k_{-1}\frac{[S_2]}{K_2}}$$

$$\frac{v_i}{v_c} = \frac{\left(1+\gamma\frac{[L]}{K_L}+\frac{2[S_2]}{K_2}+\gamma\frac{[L][S_2]}{K_L K_2}+\gamma\frac{[L][S_2]}{\beta K_L K_2}+\frac{[S_2]^2}{K_2^2}+\gamma\frac{[L][S_2]^2}{\beta K_L K_2^2}\right)}{\left(1+\frac{[L]}{K_L}+\frac{[S_2]}{K_2}+\frac{[L][S_2]}{\beta K_L K_2}\right)^2} \quad \text{eqn 13}$$

$$\frac{v_i}{v_c} = \frac{\beta K_L(K_2+[S_2])(\gamma[L][S_2]+\beta(K_2(K_L+\gamma[L])+K_L[S_2]))}{(\beta(K_2(K_L+[L])+\beta K_L[S_2]+[L][S_2])^2} \quad \text{eqn 14}$$

$$\frac{v_i}{v_c} = \frac{Const_1+[L]Const_2}{Const_1+[L](Const_3+[L]Const_4)} \quad \text{eqn 1.1}$$

where

$$Const_1 = \beta^2 K_L^2(K_2+[S_2])^2$$

$$Const_2 = \beta\gamma K_L(K_2+[S_2])(\beta K_L+[S_2])$$

$$Const_3 = 2\beta K_L(K_2+[S_2])(\beta K_2+[S_2])$$

$$Const_4 = (\beta K_2+[S_2])^2$$

Equation 1.1 is analogous to eqn 1 thereby permitting transport stimulation followed by transport inhibition as [L] is raised from subsaturating to saturating levels.

A variant of this scheme (Scheme 8B) is shown in Figure 3.9A. Here the tetramer is shown as a dimer of dimers in which each subunit is an AAT but where each dimer adopts the $e_2.e_1$ or $e_1.e_2$ conformation. There are 4 possible configurations of unliganded tetramer ($e_2.e_1|e_2.e_1$, $e_2.e_1|e_1.e_2$, $e_1.e_2|e_2.e_1$ and $e_1.e_2|e_1.e_2$). The scheme in Figure 3.9 illustrates only the $e_2.e_1|e_2.e_1$ conformation. It should be noted, however, that this represents only one half cycle of AAT-mediated transport (we assume rapid equilibrium kinetics to simplify the analysis).

Assuming rapid equilibrium, uptake in the absence of intracellular inhibitor, L, is given by:

$$v_c = \frac{\frac{2v[S]}{K_S} + \frac{2pv[S]^2}{\alpha K_S^2}}{1 + \frac{2[S]}{K_S} + \frac{[S]^2}{\alpha K_S^2}}$$

and uptake in the presence of intracellular inhibitor L is described by

$$v_i = \frac{\frac{2v[S]}{K_S} + \frac{2pv[S]^2}{\alpha K_S^2} + \frac{2qv[L][S]}{\gamma K_L K_S} + \frac{2rv[L][S]^2}{\alpha\delta\gamma K_L K_S^2}}{1 + 2\frac{[S]}{K_S} + \frac{[S]^2}{\alpha K_S^2} + 2\frac{[L]}{K_L} + \frac{[L]^2}{\beta K_L^2} + 2\frac{[L][S]}{\gamma K_L K_S} + 2\frac{[L][S]}{\delta K_L K_S} + 2\frac{[L]^2[S]}{\beta\delta\gamma K_L^2 K_S} + 2\frac{[L][S]^2}{\alpha\delta\gamma K_L K_S^2} + \frac{[L]^2[S]^2}{\alpha\beta\delta^2\gamma^2 K_L^2 K_S^L}}$$

Thus v_i/v_c is:

$$\frac{v_i}{v_c} = \frac{\left(\frac{2v[S]}{K_S} + \frac{2pv[S]^2}{\alpha K_S^2} + \frac{2qv[L][S]}{\gamma K_L K_S} + \frac{2rv[L][S]^2}{\alpha\delta\gamma K_L K_S^2}\right)\left(1 + \frac{2[S]}{K_S} + \frac{[S]^2}{\alpha K_S^2}\right)}{\left(1 + 2\frac{[S]}{K_S} + \frac{[S]^2}{\alpha K_S^2} + 2\frac{[L]}{K_L} + \frac{[L]^2}{\beta K_L^2} + 2\frac{[L][S]}{\gamma K_L K_S} + 2\frac{[L][S]}{\delta K_L K_S} + 2\frac{[L]^2[S]}{\beta\delta\gamma K_L^2 K_S} + 2\frac{[L][S]^2}{\alpha\delta\gamma K_L K_S^2} + \frac{[L]^2[S]^2}{\alpha\beta\delta^2\gamma^2 K_L^2 K_S^L}\right)\left(\frac{2v[S]}{K_S} + \frac{2pv[S]^2}{\alpha K_S^2}\right)}$$

which reduces to

$$\frac{v_i}{v_c} = \frac{\beta\delta\gamma K_L(\alpha K_S\{K_S + 2[S]\} + [S]^2)(\alpha\delta K_S\{\gamma K_L + [L]q\} + [S]\{\delta\gamma K_L p + [L]r\})}{(\alpha K_S + p[S])(\alpha\delta\gamma K_S(\beta K_L(\delta\{\gamma K_L K_S + 2\gamma K_L[S] + 2\gamma K_S[L] + 2[L][S]\} + 2\gamma[L][S]) + [L]^2\{\delta\gamma K_S + 2[S]\}) + [S]^2(\beta\delta\gamma K_L\{\delta\gamma K_L + 2[L]\} + [L]^2)}$$

and subsequently to the form of equation 1

$$\frac{v_i}{v_c} = \frac{Const_1 + Const_2[L]}{Const_1 + [L](Const_3 + [L]Const_4)} \qquad \text{eqn 1}$$

where:

$$Const_1 = \beta\delta^2\gamma^2 K_L{}^2(\alpha K_S + p[S])([S]^2 + \alpha K_S\{K_S + 2[S]\})$$

$$Const_2 = \beta\delta\gamma K_L(\alpha\delta K_S q + r[S])([S]^2 + \alpha K_S\{K_S + 2[S]\})$$

$$Const_3 = 2\beta\delta\gamma K_L(\alpha K_S + p[S])\left([S]^2 + \alpha K_S(\gamma[S] + \delta\{\gamma K_S + [S]\})\right)$$

$$Const_4 = (\alpha K_S + p[S])([S]^2 + \alpha\delta\gamma K_S\{\delta\gamma K_S + 2[S]\})$$

If the trans-action of L is to increase V_{MAX} for net sugar uptake, the parameters q and r > 1 while the cooperativity factors α, β, δ and γ = 1. If the trans-action of L is to increase affinity for substrate in net sugar uptake, the parameters q = r = 1 while the cooperativity factors δ and γ = < 1. This model allows for endofacial cis-allostery when β < 1.

As described, this model is also kinetically equivalent to a dimer of FSTs. While we think the latter model is inappropriate because trans-allostery is lost when GLUT1 forms only dimers (162), this model could be expanded to allow for a tetramer of FSTs in which trans-allostery requires cooperative interactions from all 4 subunits. Such a model (Scheme 8C) is shown in Figure 3.9B. This transporter can bind up to 4 exofacial sugars (S) and 4 endofacial ligands (L). Exofacial cooperativity is shared within subunits of each dimer (binding of the first sugar affects K_S for binding of the second by the cooperativity factor α) and between dimers (binding of a sugar to one dimer affects K_S for binding of a second sugar to a subunit in the second dimer by the cooperativity factor θ. In a similar way, endofacial cooperativity is shared within subunits of each dimer (binding of the first ligand affects K_L for binding of the second by the cooperativity factor β) and between dimers (binding of a ligand to one dimer affects K_L for binding of a second ligand to a subunit in the second dimer by the cooperativity factor ψ. Finally, cooperativity could be expressed between endofacial and exofacial sites (trans-allostery) in the same subunit (γ) between subunits of the same dimer (δ) and between subunits in different dimers (π). Since trans-allostery and endofacial cis allostery are absent in dimeric GLUT1, this eliminates a role for trans-cooperativity factors ∂ and γ) and trans-allostery must (according to this model) be strongly dependent on cooperativity factor π. The endofacial cis-allostery constant ψ must be

restored to unity in dimeric GLUT1.

Capable of binding up to 8 ligands simultaneously, this transporter complex can exist in as many as 256 (2^8) different liganded states and the solution is correspondingly complex. Measuring uptake of extracellular sugar, S, in the absence of intracellular sugar but in the presence of endofacial ligand, L, and assuming that any individual subunit complexed with L is catalytically inactive, the ratio v_i/v_c is given by:

$$\frac{v_i}{v_c} = \frac{Const_1 + L(Const_2 + L(Const_3 + L))}{Const_1 + L(Const_4 + L(Const_5 + L(Const_6 + LConst_7)))} \qquad \text{eqn 1.2}$$

where:

$$\mathrm{Const}_1 = \frac{\beta\psi^2\delta^3\gamma^3{K_L}^3\pi^6\{S^3 + 3\alpha K_S S^2\theta^2 + \alpha^2{K_S}^3\theta^4 + \alpha{K_S}^2 S\theta^3(2\alpha+\theta)\}}{S^3 + \alpha\gamma K_S\pi(2\delta+\pi)S^2\theta^2 + \alpha^2\psi\delta^2\gamma^3{K_S}^3\pi^4\theta^4 + \alpha\delta\gamma^2{K_S}^2\pi^2 S\theta^3(2\alpha\pi+\delta\theta)}$$

$$\mathrm{Const}_2 = \frac{\beta\psi^2\delta^2\gamma^2\pi^4{K_L}^2\begin{pmatrix}\alpha^2\gamma\pi\theta^4(2\delta+\pi){K_S}^3 + \alpha\theta^3(2\alpha\pi(\delta+2\gamma){K_S}^2 S \\ +\theta(2\delta\gamma+\pi^2)) + \alpha\theta^2(2\delta+3\gamma+4\pi)K_S S^2 + 3S^3\end{pmatrix}}{\alpha^2\psi\delta^2\gamma^3\pi^4\theta^4{K_S}^3 + \alpha\delta\gamma^2\pi^2\theta^3(2\alpha\pi+\delta\theta){K_S}^2 S + \alpha\gamma\pi\theta^2(2\delta+\pi)K_S S^2 + S^3}$$

$$Const_3 = \frac{\psi\delta\gamma K_L\pi^2\begin{pmatrix}(2\beta+\psi)S^3 + \alpha\theta^2\big(2\beta(\delta+2\gamma)\pi + \psi(2\delta\gamma+\pi^2)\big)K_S S^2 \\ +2\alpha^2\beta\gamma(2\delta+\gamma)\pi^2\theta^3{K_S}^2 S + \alpha\delta\gamma{K_S}^2(\alpha\gamma K_S\pi^2(\psi\delta+2\beta\pi) + (\psi\delta\gamma + (\beta+\psi)\pi^2)S)\theta^4\end{pmatrix}}{S^3 + \alpha\gamma K_S\pi(2\delta+\pi)S^2\theta^2 + \alpha^2\psi\delta^2\gamma^3{K_S}^3\pi^4\theta^4 + \alpha\delta\gamma^2{K_S}^2\pi^2 S\theta^3(2\alpha\pi+\delta\theta)}$$

$$Const_4 = \frac{4\beta\psi^2\delta^2\gamma^2{K_L}^2\pi^4\big(S^3 + 3\alpha K_S S^2\theta^2 + \alpha^2{K_S}^3\theta^4 + \alpha{K_S}^2 S\theta^3(2\alpha+\theta)\big)\big(S^4 + \alpha K_S(\delta+\gamma+2\pi)S^3\theta^2 + \alpha^2\delta\gamma{K_S}^4\pi^2\theta^4 + \alpha^2{K_S}^3\pi(\gamma\pi+\delta(2\gamma+\pi))S\theta^4 + \alpha{K_S}^2 S^2\theta^3(2\alpha(\delta+\gamma)\pi + (\delta\gamma+\pi^2)\theta)\big)}{\big(S^4 + 4\alpha K_S S^3\theta^2 + \alpha^2{K_S}^4\theta^4 + 4\alpha^2{K_S}^3 S\theta^4 + 2\alpha{K_S}^2 S^2\theta^3(2\alpha+\tau)\big)\big(S^3 + \alpha\gamma K_S\pi(2\delta+\pi)S^2\theta^2 + \alpha^2\psi\delta^2\gamma^3{K_S}^3\pi^4\theta^4 + \alpha\delta\gamma^2{K_S}^2\pi^2 S\theta^3(2\alpha\pi+\delta\theta)\big)}$$

$$Const_5 = \frac{2\psi\delta\gamma K{l_L}\pi^2\begin{pmatrix}(2\beta+\psi)S^4 + 2\alpha K_S(2\beta(\delta+\gamma)\pi + \psi(\delta\gamma+\pi^2))S^3\theta^2 + 2\alpha^2\beta(\delta^2+4\delta\gamma+\gamma^2){K_S}^2\pi^2 S^2\theta^3 + \alpha{K_S}^2((2\beta\delta\gamma\pi^2 + \psi(\delta\gamma+\pi^2)^2)S^2) \\ +\alpha\delta\gamma K_S\pi^2((2\beta+\psi)\delta\gamma K_S\pi^2 + 2(\psi\delta\gamma + 2\beta\gamma\pi + (\psi+2\delta)\pi^2)S))\theta^4\end{pmatrix}\big(S^3 + 3\alpha K_S S^2\theta^2 + \alpha^2{K_S}^3\theta^4 + \alpha{K_S}^2 S\theta^3(2\alpha+\theta)\big)}{\big(S^4 + 4\alpha K_S S^3\theta^2 + 4\alpha^2{K_S}^2 S^2\theta^3 + \alpha{K_S}^2(2S^2 + \alpha K_S(K_S+4S))\theta^4\big)\big(S^3 + \alpha\gamma K_S\pi(2\delta+\pi)S^2\theta^2 + \alpha^2\psi\delta^2\gamma^3{K_S}^3\pi^4\theta^4 + \alpha\delta\gamma^2{K_S}^2\pi^2 S\theta^3(2\alpha\pi+\delta\theta)\big)}$$

$$Const_6 = \frac{4\psi\left(S^4 + \alpha\pi K_S S^2(\psi^2\delta\gamma\pi^3 K_S + \theta^2(2\delta\gamma + (\delta+\gamma)\pi)S) + 2\alpha^2\delta\gamma(\delta+\gamma)\pi^3\theta^3 K_S{}^2 S^2 + \alpha\delta^2\gamma^2\pi^2 K_S{}^2\left(S^2 + \alpha\psi\pi^2 K_S(\delta\gamma K_S\pi^2 + (\delta+\gamma+2\pi)S)\right)\theta^4\right)}{\left(S^3 + 3\alpha\theta^2 K_S S^2 + \alpha^2\theta^4 K_S{}^3 + \alpha\theta^3(2\alpha+\theta)K_S{}^2 S\right)}$$

$$\left(S^4 + 4\alpha K_S S^3\theta^2 + 4\alpha^2 K_S{}^2 S^2\theta^3 + \alpha\theta^4 K_S{}^2\left(2S^2 + \alpha K_S(K_S + 4S)\right)\right)$$

$$\left(S^3 + \alpha\gamma\pi\theta^2(2\delta+\pi)K_S S^2 + \alpha^2\psi\delta^2\gamma^3\pi^4\theta^4 K_S{}^3 + \alpha\delta\gamma^2\pi^2\theta^3(2\alpha\pi + \delta\theta)K_S{}^2 S\right)$$

$$Const_7 = \frac{\left(S^3 + 3\alpha K_S S^2\theta^2 + \alpha^2 K_S{}^3\theta^4 + \alpha K_S{}^2 S\theta^3(2\alpha+\theta)\right)}{\beta\psi^2\delta\gamma K_L\pi^2\left(S^4 + 4\alpha K_S S^3\theta^2 + 4\alpha^2 K_S{}^2 S^2\theta^3 + \alpha K_S{}^2\left(2S^2 + \alpha K_S(K_S+4S)\right)\theta^4\right)}$$

$$\left(S^4 + 4\alpha\delta\gamma K_S\pi^2 S^3\theta^2 + \alpha^2\psi^2\delta^4\gamma^4 K_S{}^4\pi^8\theta^4 + 4\alpha\delta^3\gamma^4 K_S{}^3\pi^6 S\theta^4 + 2\alpha\delta^2\gamma^2 K_S{}^2\pi^4 S^2\theta^3(2\alpha+\theta)\right)$$

$$\left(S^3 + \alpha\gamma K_S\pi(2\delta+\pi)S^2\theta^2 + \alpha^2\psi\delta^2\gamma^3 K_S{}^3\pi^4\theta^4 + \alpha\delta\gamma^2 K_S{}^2\pi^2 S\theta^3(2\alpha\pi + \delta\theta)\right)$$

This model allows for trans-allostery (stimulation of sugar uptake by endofacial ligand (e.g. CB) when all allostery constants are set to unity but ∂ (trans allostery between S and L binding sites in neighboring subunits of each dimer) or π (trans allostery between S and L binding sites in subunits of neighboring dimers) are <1. Since trans-allostery is lost in dimeric GLUT1, we assume that ∂ =1 and that π is the dominant trans-cooperativity constant in this model.

Model 9 - Exofacial, Allosteric Alternating Access Transporter

This is a standard alternating access transporter with the proviso that the e2 conformation presents 2 binding sites - an allosteric site which can be occupied by sugar or inhibitor and a catalytic site which can be occupied by sugar or inhibitor. Occupancy of the allosteric site can stimulate or inhibit transport and affect the affinity of the catalytic site in both e1 and e2 for substrate or inhibitor. Occupancy of the allosteric site and its effects persist through the e2 to e1 conformational change. However, S or I can only dissociate from the allosteric site in the e2 conformation.

This model is more challenging to solve. Assuming segments A, B, C and D of scheme 9 (Figure 3.10; for simplicity, only one of the 4 subunits is illustrated) are in rapid equilibrium, we can define the following:

f_{-1} is fraction of A existing as eS2

f_{-o} is fraction of A existing as e2

f_{-2} is fraction of A existing as Se2

f_{-3} is fraction of A existing as SeS2

f_{-4} is fraction of A existing as Ie2

f_{-5} is fraction of A existing as IeS2

f_1 is fraction of B existing as eS1

f_o is fraction of B existing as e1

f_4 is fraction of C existing as Ie1

f_5 is fraction of C existing as IeS1

f_2 is fraction of D existing as Se1

f_3 is fraction of D existing as SeS1

The King-Altman figure reduces to Scheme 9B and uptake

$$\frac{v_{21}}{e_{total}} = \frac{(f_{-1}k_{-1} + f_{-3}k_{-3} + f_{-5}k_{-5})A}{A + B + C + D}$$

$$\frac{v_{21}}{e_{total}} = \frac{\left(k_{-3}\frac{[S_2]^2}{\alpha K_2 K_{AS}} + k_{-1}\frac{[S_2]}{K_2} + k_{-5}\frac{[I][S_2]}{\delta K_2 K_A}\right)\left(k_4 + k_5\frac{[S_1]}{\delta K_1}\right)\left(k_2 + k_3\frac{[S_1]}{\alpha K_1}\right)\left(k_o + k_1\frac{[S_1]}{K_1}\right)}{\left(\begin{array}{c}\left(k_4 + k_5\frac{[S_1]}{\delta K_1}\right)\left(k_2 + k_3\frac{[S_1]}{\alpha K_1}\right)\left(k_o + k_1\frac{[S_1]}{K_1}\right)D_A + \left(k_4 + k_5\frac{[S_1]}{\delta K_1}\right)\left(k_2 + k_3\frac{[S_1]}{\alpha K_1}\right)\left(k_{-o} + k_{-1}\frac{[S_1]}{\delta K_1}\right)D_B \\ + \left(k_o + k_1\frac{[S_1]}{K_1}\right)\left(k_{-4}\frac{[I]}{K_A} + k_{-5}\frac{[I][S_2]}{\delta K_A K_2}\right)\left(k_2 + k_3\frac{[S_1]}{\alpha K_1}\right)D_C + \left(k_4 + k_5\frac{[S_1]}{\delta K_1}\right)\left(k_o + k_1\frac{[S_1]}{K_1}\right)\left(k_{-2}\frac{[S_2]}{K_{AS}} + k_3\frac{[S_2]^2}{\alpha K_2 K_{AS}}\right)D_D\end{array}\right)}$$

where

$$D_A = 1 + \frac{[S_2]}{K_2} + \frac{[I]}{K_i} + \frac{[I]}{K_A} + \frac{[S_2]}{K_{AS}} + \frac{[S_2][I]}{\beta K_{AS} K_i} + \frac{[S_2]^2}{\alpha K_{AS} K_2} + \frac{[S_2][I]}{\delta K_A K_2} + \frac{[I]^2}{\gamma K_A K_i}$$

$$D_B = 1 + \frac{[S_1]}{K_1} + \frac{[L]}{K_L}$$

$$D_C = 1 + \frac{[S_1]}{\delta K_1} + \frac{[L]}{\phi K_L}$$

$$D_D = 1 + \frac{[S_1]}{\alpha K_1} + \frac{[L]}{\pi K_L}$$

When $S_1 = L = I = 0$

$$\frac{v_{21}}{e_{total}} = v_c = \frac{[S_2]k_o k_2 k_4(\alpha K_{AS} k_{-1} + [S_2]k_{-3})}{[S_2]^2 k_o k_4(k_2 + k_{-3}) + [S_2](k_o k_2 \alpha K_2 + k_2 \alpha K_{AS}(k_{-1} + k_o) + k_o k_{-2} k_4 \alpha K_2) + k_o k_2 k_{-4} \alpha K_2 K_{AS} + k_2 k_4 \alpha K_2 K_{AS}(k_o + k_{-o})}$$

$$= \frac{[S_2](Const_2 + [S_2])}{Const_1 + [S_2](Const_3 + [S_2]Const_4)}$$

where

$$Const_1 = \frac{\alpha K_2 K_{AS}(k_o k_{-4} + k_4(k_o + k_{-o}))}{k_o k_{-3} k_4}$$

$$Const_2 = \frac{\alpha k_1 k_{-1} K_{AS}}{k_2 k_{-3}}$$

$$Const_3 = \frac{\alpha(k_o k_{-2} k_4 K_2 + k_2(k_o K_2 + K_{AS}(k_o + k_{-1})))}{k_o k_2 k_{-3} k_4}$$

$$Const_4 = \frac{1}{k_2} + \frac{1}{k_{-3}}$$

When $S_1 = I = 0$ but $L > 0$

$$\frac{v_{21}}{e_{total}} = v_i$$

$$= \frac{[S_2]k_o k_2 k_4\left(\frac{k_{-1}}{K_2} + [S_2]\frac{k_{-3}}{\alpha K_2 K_{AS}}\right)}{k_o k_2 k_{-4}\left(1 + \frac{[L]}{K_L}\right) + k_2 k_4\left(1 + \frac{[L]}{K_L}\left(k_{-o} + \frac{k_{-1}[S_2]}{K_2}\right)\right) + k_o k_2 k_4\left(1 + \frac{[S_2]}{K_2} + \frac{[S_2]}{K_{AS}} + \frac{[S_2]^2}{\alpha K_2 K_{AS}}\right)}$$
$$+ k_o k_4\left(1 + \frac{[L]}{\pi K_L}\right)\left(\frac{k_2[S_2]}{K_{AS}} + \frac{k_{-3}[S_2]^2}{\alpha K_2 K_{AS}}\right)$$

Thus

$$\frac{v_i}{v_c} = \frac{[S_2]k_o k_2 k_4\left(\frac{k_{-1}}{K_2} + [S_2]\frac{k_{-3}}{\alpha K_2 K_{AS}}\right)}{\left(\left[S_2\right]^2 k_o k_4(k_2 + k_{-3}) + [S_2](k_o k_2 \alpha K_2 + k_2 \alpha K_{AS}(k_{-1} + k_o) + k_o k_{-2} k_4 \alpha K_2) + k_o k_2 k_{-4} \alpha K_2 K_{AS} + k_2 k_4 \alpha K_2 K_{AS}(k_o + k_{-o})\right)}{[S_2]k_o k_2 k_4(\alpha K_{AS} k_{-1} + [S_2]k_{-3})}$$
$$\left(k_o k_2 k_{-4}\left(1 + \frac{[L]}{K_L}\right) + k_2 k_4\left(1 + \frac{[L]}{K_L}\left(k_{-o} + \frac{k_{-1}[S_2]}{K_2}\right)\right) + k_o k_2 k_4\left(1 + \frac{[S_2]}{K_2} + \frac{[S_2]}{K_{AS}} + \frac{[S_2]^2}{\alpha K_2 K_{AS}}\right) + k_o k_4\left(1 + \frac{[L]}{\pi K_L}\right)\left(\frac{k_2[S_2]}{K_{AS}} + \frac{k_{-3}[S_2]^2}{\alpha K_2 K_{AS}}\right)\right)$$

Expanding terms then gathering around L terms yields the following:

$$\frac{v_i}{v_c} = \frac{R_1 + [S_2](R_2 + [S]_2)}{R_1 + [S_2](R_2 + [S_2] + [L]\{R_3 + [S_2]R_4\}[S_2]) + [L]R_5}$$

$$\frac{v_i}{v_c} = \frac{Const_1}{Const_1 + [L]Const_2} \qquad \text{eqn 15}$$

where

$$Const_1 = R_1 + [S_2](R_2 + [S_2])$$

$$= \frac{\alpha k_2 K_2 K_{AS}\left(k_o k_{-4} + k_4(k_o + k_{-o})\right)}{k_o k_4(k_2 + k_{-3})}$$

$$+ [S_2]\left(\frac{\alpha(k_{-1} k_2 K_{AS} + k_o k_2(K_2 + K_{AS}) + k_o k_{-2} K_2)}{k_o(k_2 + k_{-3})} + [S_2]\right)$$

$$Const_2 = R_5 + [S_2]\{R_3 + [S_2]R_4\}$$

$$= \frac{\alpha K_2 K_{AS}(k_o k_2 k_{-4} + \phi k_{-o} k_2 k_4)}{\phi k_o k_4 K_L(k_2 + k_{-3})} + [S_2]\left(\frac{\alpha(k_o k_{-2} K_2 + \pi k_{-1} k_2 K_{AS})}{\pi k_o K_L(k_2 + k_{-3})} + [S_2]\frac{k_{-3}}{\pi K_L(k_2 + k_{-3})}\right)$$

Finally, let's consider that S1 = L = 0 but I > 0. Under these conditions:

$$\frac{v_{21}}{e_{total}} = v_i = \frac{k_o k_2 k_4 \left(k_{-1}\frac{[S_2]}{K_2} + k_{-5}\frac{[I][S_2]}{\delta K_2 K_A} + k_{-3}\frac{[S_2]^2}{\alpha K_2 K_{AS}}\right)}{k_2 k_4 \left(k_{-o} + k_{-1}\frac{[S_2]}{K_2}\right) + k_o k_2 \left(k_{-4} + k_{-5}\frac{[I][S_2]}{\delta K_2 K_A}\right)}$$
$$+k_o k_2 k_4 \left(1 + \frac{[I]}{K_A} + \frac{[I]}{K_i} + \frac{[I]^2}{\gamma K_i K_A} + \frac{[S_2]}{K_2} + \frac{[I][S_2]}{\delta K_2 K_A} + \frac{[S_2]}{K_{AS}} + \frac{[I][S_2]}{\beta K_{AS} K_i} + \frac{[S_2]^2}{\alpha K_2 K_{AS}}\right)$$
$$+k_o k_4 \left(k_{-2}\frac{[S_2]}{K_{AS}} + k_{-3}\frac{[S_2]^2}{\alpha K_2 K_{AS}}\right)$$

Dividing by v_c expanding then gathering terms around I, we obtain:

$$\frac{v_i}{v_c} = \frac{Const_1 + [I]Const_2}{Const_1 + [I](Const_3 + [I]Const_4)} \qquad \text{eqn 1}$$

where

$$Const_1 = \alpha^2\beta\gamma^2\delta k_{-1}k_2K_2K_AK_{AS}^2K_i\left(k_ok_{-4} + k_4(k_o + k_{-o})\right)$$
$$+ [S_2]\Big(\alpha\beta\gamma\delta K_AK_{AS}K_i\Big(\alpha k_{-1}k_4(k_{-1}k_2K_{AS} + k_ok_2(K_2 + K_{AS}) + k_ok_{-2}K_2)$$
$$+ k_2k_{-3}K_2\left(k_ok_{-4} + k_4(k_o + k_{-o})\right)\Big)\Big)$$
$$+ [S_2]\Big(\alpha\beta\gamma\delta k_4K_AK_i\Big(k_ok_{-3}(k_{-1}K_{AS} + k_{-2}K_2)$$
$$+ k_2\left(k_{-1}k_{-3}K_{AS} + k_ok_{-3}K_2 + k_oK_{AS}(k_{-1} + k_{-3})\right)\Big)\Big)$$
$$+ [S_2]\left(\beta\gamma\delta k_ok_{-3}k_4K_AK_i(k_2 + k_{-3})\right)$$

$$Const_2 = \alpha^2\beta\gamma k_2k_{-5}K_2K_{AS}^2K_i\left(k_ok_{-4} + k_4(k_o + k_{-o})\right)$$
$$+ [S_2]\Big(\alpha^2\beta\gamma k_4k_{-5}K_{AS}K_i(k_{-1}k_2K_{AS} + k_ok_2(K_2 + K_{AS}) + k_ok_{-2}K_2)$$
$$+ [S_2]\left(\alpha\beta\gamma k_ok_4k_{-5}K_{AS}K_i(k_2 + k_{-3})\right)\Big)$$

$$Const_3 = \alpha^2\beta\gamma\delta k_o k_{-1} k_2 k_4 K_2 K_{AS}^2 (K_A + K_i)$$
$$+ [S_2]\Big(\alpha\gamma k_o k_2 K_{AS}\Big(\beta\delta k_{-3} k_4 K_2 (K_A + K_i)$$
$$+ \alpha k_{-1}\big(\delta k_4 K_2 K_A + \beta K_{AS} K_i (k_4 + k_{-5})\big)\Big)$$
$$+ [S_2]\Big(\alpha\gamma k_o k_2 k_{-3}\big(\delta k_4 K_2 K_A + \beta K_{AS} K_i (k_4 + k_{-5})\big)\Big)\Big)$$

$$Const_4 = \alpha^2\beta\delta k_o k_{-1} k_2 k_4 K_2 K_{AS}^2 + [S_2](\alpha\beta\delta k_o k_2 k_{-3} k_4 K_2 K_{AS})$$

This model explains why exofacial cis-allostery persists in the TM9 (tetramerization-null) mutant (162) and in dimeric GLUT1 (80) and allows for allosteric stimulation of sugar uptake by the transport substrate. The model also explains sugar occlusion in the presence of CB (119). The model does not allow for intramolecular, endofacial trans-allostery because the equation for the effect of L on uptake takes the form

$$\frac{v_i}{v_c} = \frac{Const_1}{Const_1 + [L]Const_2}$$

Consideration of non-specific transport

We occasionally observe a component of transport (typically measured as uptake of radiolabeled sugar) that is neither inhibited by saturating concentrations of inhibitors (e.g. cytochalasin B or forskolin) nor by saturating concentrations of sugars (e.g. D-glucose or 3-O-methylglucose) (168). This could represent protein-independent, trans-bilayer diffusion or non-specific association with the cell surface or with plasticware used in transport determinations. Such non-specific "transport" is well-described as

$$v = k[S] \quad \text{eqn 16}$$

where k is a first order rate constant which is insensitive to inhibitor. We examine the effect of inclusion of non-specific transport in our analyses by reviewing its impact on Model 4 -

intramolecular cis-allostery.

Assuming rapid equilibrium kinetics, sugar uptake in the presence of extracellular inhibitors (v_i) is given by:

$$\frac{v_i}{[e]_t} = k[S] + \frac{v\left(\frac{[S]}{K_S} + \phi\frac{[S]^2}{\alpha K_S^2} + \gamma\frac{[I][S]}{\delta K_S K_{II}}\right)}{\left(1 + \frac{[S]}{K_S} + \frac{[S]}{K_A} + \frac{[S]^2}{\alpha K_A K_S} + \frac{[I]}{K_I} + \frac{[I]}{K_{II}} + \frac{[I]^2}{\pi K_I K_{II}} + \frac{[I][S]}{\delta K_S K_{II}} + \frac{[I][S]}{\Omega K_A K_I}\right)}$$

eqn 17

where $[e]_t$ is the concentration of membrane resident GLUT1, [S] and [I] are concentrations of extracellular transported sugar and transport inhibitor respectively and the remaining constants are as defined in Scheme 4. When inhibitors are absent, control uptake (v_c) is given by:

$$\frac{v_c}{[e]_t} = k[S] + \frac{v\left(\frac{[S]}{K_S} + \phi\frac{[S]^2}{\alpha K_S^2}\right)}{\left(1 + \frac{[S]}{K_S} + \frac{[S]}{K_A} + \frac{[S]^2}{\alpha K_A K_S}\right)} \qquad \text{eqn 18}$$

$$\frac{v_i}{v_c} = \frac{Const_1 + [I](Const_2 + [I])}{Const_1 + [I](Const_3 + [I]Const_4)} \qquad \text{eqn 2}$$

where:

$$Const_1 = \frac{K_I K_{II}\pi(\alpha\{k\langle K_S[S] + K_A(K_S + [S])\rangle + K_A v\} + [S](k[S] + \phi v))}{\alpha k K_A K_S}$$

$$Const_2 = \frac{\pi(\delta k\Omega K_A\{K_I + K_{II}\} + K_{II}[S] + \Omega K_A K_I\{k[S] + \gamma v\})}{\delta k\Omega K_A K_S}$$

$$Const_3 = \frac{\pi(\alpha\{k\langle K_A(K_S + [S]) + K_S[S]\rangle + K_A v\} + [S](k[S] + \phi v))(\delta K_S\{K_A\Omega(K_I + K_{II}) + K_{II}[S]\} + K_A K_I\Omega[S])}{\delta k\Omega K_A K_S(\alpha\langle K_A(K_S + [S]) + K_S[S]\rangle + [S]^2)}$$

$$Const_4 = \frac{\alpha(k\{K_S[S] + K_A(K_S + [S])\} + K_A v) + [S](k[S] + \phi v)}{k([S]^2 + \alpha\{K_S[S] + K_A\langle K_S + [S]\rangle\})}$$

Behavior of Models

Models 1, 2, 3, 5, 6 and 7 were eliminated in the Results section either because the resulting equations cannot reproduce the transport behavior (Models 1, 2, 5, 6) or because the available biochemical evidence (ligand binding) is incompatible with the model's predictions (Models 3 and 7). This leaves models 4, 8 and 9 for consideration. Because each of the remaining models is described by a common set of equations, we consider the simplest models for cis-allostery (Model 4) and trans-allostery (Model 8B) although the general conclusions for Models 4 and 8B are also applicable to Models 9 and 8A/8C respectively.

Figure 3.11A (intramolecular cis-allostery - the affinity affect) illustrates how subsaturating levels of extracellular maltose stimulate GLUT1-mediated 3-O-methylglucose uptake in human erythrocytes then, as extracellular maltose levels increase, how sugar uptake is inhibited. This was modeled simply as two binding sites for maltose - a high affinity allosteric site whose occupancy reduces $K_{D(app)}$ for 3-O-methylglucose binding to the catalytic center by the factor δ and a lower affinity catalytic site at which maltose and 3-O-methylglucose compete for binding. At low [maltose], the allosteric site is occupied reducing $K_{D(app)}$ for transport and thus stimulating sub-saturated transport. As [maltose] is further increased, maltose and 3-O-methylglucose compete for binding to the catalytic site and transport is inhibited. Using parameters that are consistent with previously published affinity constants for 3-O-methylglucose and maltose (3–5), Figure 3.11A (intramolecular cis-allostery - the affinity affect) illustrates that reducing δ from 1 to 0.7 produces a 1.4-fold increase in transport that peaks at approximately 50 μM maltose followed by robust transport inhibition with an IC_{50} of approximately 5 mM. Conversely, we can model the same effect by eliminating any affect of high affinity maltose binding on 3-O-methylglucose binding (δ is fixed at 1) but progressively

increasing γ from 1 to 1.4. (Figure 3.11B Intramolecular cis-allostery the k_{cat} effect). This increases k_{cat} for transport thereby stimulating transport until [maltose] is increased sufficiently to compete with 3-O-methylglucose for binding at the catalytic center.

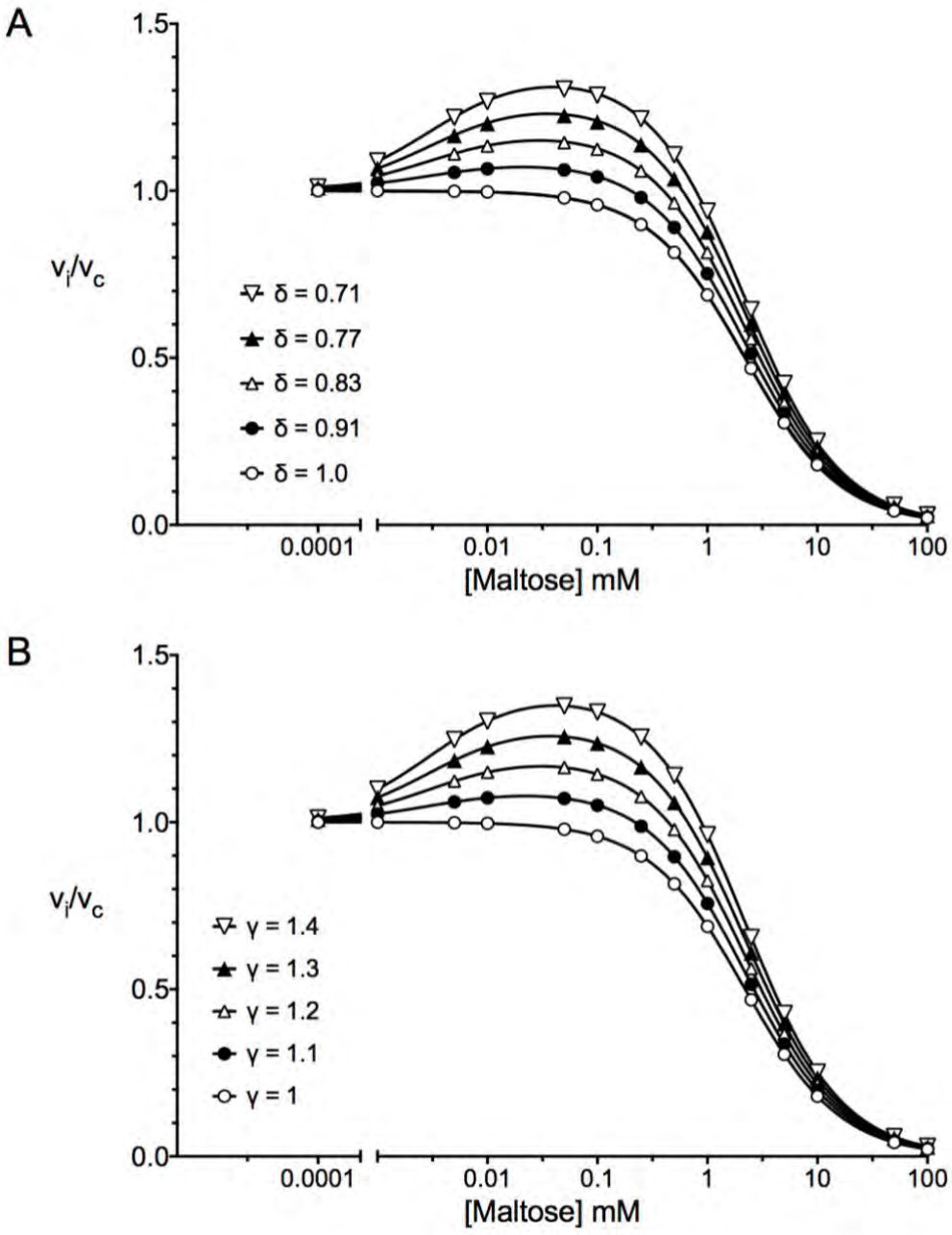
A
1.5
1.0
0.5
0.0
v_i/v_c
δ = 0.71
δ = 0.77
δ = 0.83
δ = 0.91
δ = 1.0
0.0001
0.01
0.1
1
10
100
[Maltose] mM
B
1.5
1.0
0.5
0.0
v_i/v_c
γ = 1.4
γ = 1.3
γ = 1.2
γ = 1.1
γ = 1
0.0001
0.01
0.1
1
10
100
[Maltose] mM

Figure 3.11: A. Intramolecular cis-allostery - the affinity affect. Subsaturating levels of extracellular maltose stimulate GLUT1-mediated 3-O-methylglucose uptake in human erythrocytes then, as extracellular maltose levels increase, sugar uptake is inhibited. Ordinate: vi/vc. Abscissa: [Maltose] in mM (note the log scale). Equation 1 from Model 4 was used to simulate these data. The following constants were used: [S] = 0.1 mM, K_S = 1 mM, K_A = 0.05 mM, K_I = 2 mM, K_{II} = 0.001 mM, $\alpha = \Omega = \gamma = \pi = \varphi = 1$, δ is varied (see legend). These parameters result in the following: $Const_1$ = 0.99, $Const_2$ (varies from 330 mM^{-1} to 464.8 mM^{-1} with increasing δ), $Const_3$ (varies from 330.45 to 342.7 $mM^{-1}$with increasing δ), $Const_4$ = 150 mM^{-2}. Curves were computed by nonlinear regression using equation 1. **B**. Intramolecular cis-allostery - the k_{cat} affect. As in Figure 11 A but now $\delta = 1$ and γ is varied (see legend). These parameters result in the following: $Const_1$ = 0.99, $Const_2$ (varies from 330 mM^{-1} to 462 mM^{-1} with increasing γ), $Const_3$ = 330.45 mM^{-1}, $Const_4$ = 150 mM^{-2}. Curves were computed by nonlinear regression using equation 1.

Figure 3.12 (intermolecular trans-allostery) illustrates how subsaturating levels of cytochalasin B (CB, a ligand that readily crosses the cell membrane to act at an endofacial site on GLUT1 (162,169)) first stimulate GLUT1-mediated 3-O-methylglucose uptake in human erythrocytes then, as CB levels increase, how sugar uptake is inhibited (149,162). This was modeled assuming a dimer of GLUT1 dimers. Each dimer is independent of its neighbor although subunit occupancy states are communicated across the dimer/dimer interface. When one e1 subunit of a dimer contains a bound inhibitor (L or CB) its cognate e2 partner (the adjacent subunit in the same dimer) like its liganded partner, is locked and thus inactive. However the occupancy state of e1.L is transmitted to the adjacent dimer and allows the e2 subunit of the adjacent dimer to bind S_2 with higher affinity (by the factor γ) or to transport S_2 with greater efficiency (by the factor p). Figures 3.12A and B illustrate how varying either γ (the affinity effect) or p (the k_{cat} effect) affect transport. At low [CB], the probability of only 1 e1 subunit of the tetramer being occupied is high, causing transport via the remaining CB-free dimer to become activated by the factor γ. As [CB] is further increased, the second dimer becomes complexed with CB and transport is inhibited. Using parameters that are consistent with previously published affinity constants for 3-O-methylglucose and CB (78,149,162), Figure 3.12 illustrates how reducing γ from 1 to 0.175 (Figure 3.12A) or increasing p from 1 to 4.25 (Figure 3.12B) reproduce the 1.3-fold increase in transport that peaks at approximately 25 nM CB followed by robust transport inhibition with an IC_{50} of approximately 100 - 150 nM.

Equation 2 obtains when not all transport is inhibited by saturating inhibitors and thus allows for the possibility of non-specific, non-protein-mediated or inhibitor-insensitive sugar transport - a phenomenon that is often observed experimentally (168). Under these circumstances vi/vc does not approach 100% inhibition even at saturating [inhibitor].

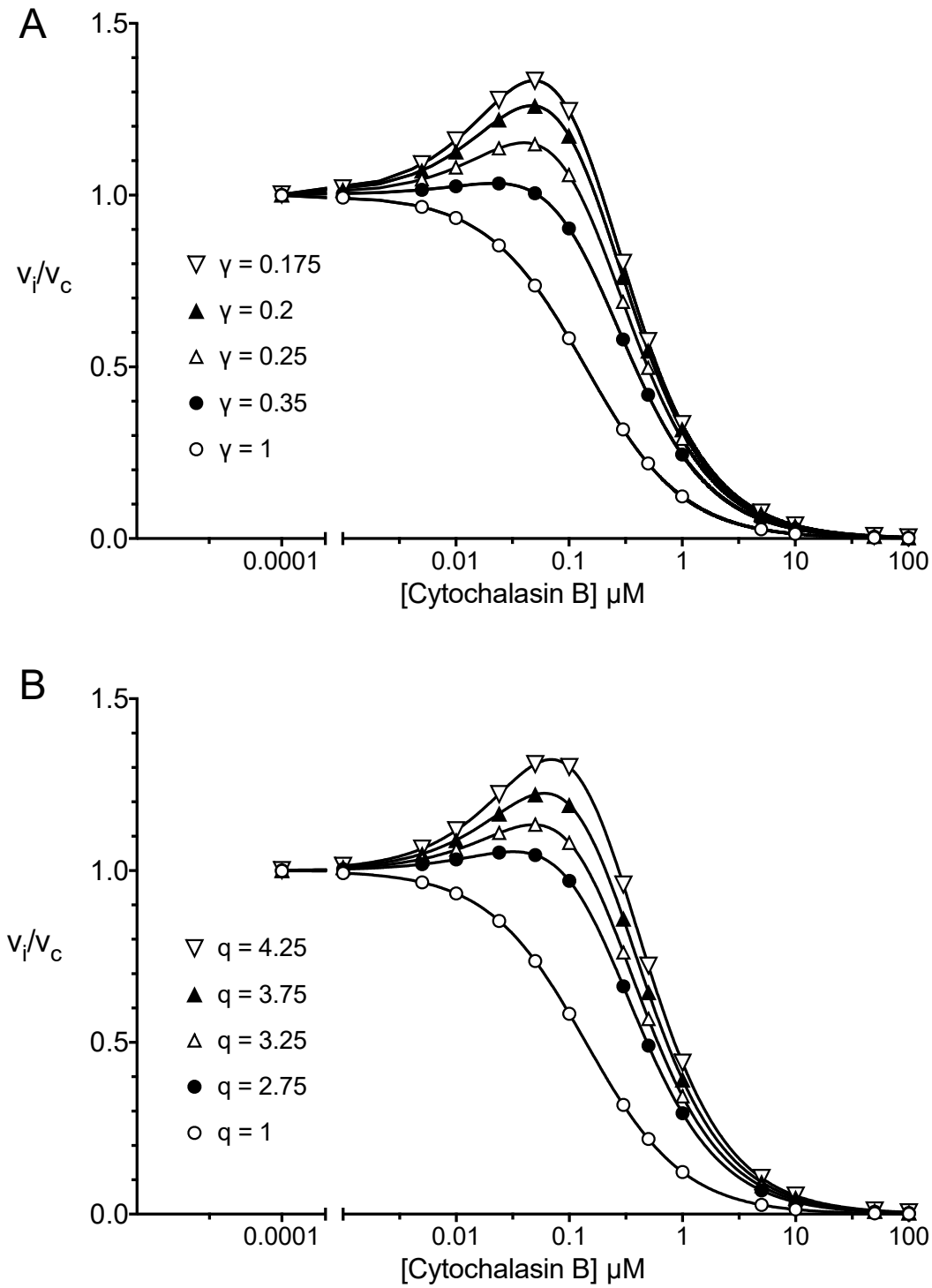
A
1.5
1.0
0.5
0.0
v_i/v_c
γ = 0.175
γ = 0.2
γ = 0.25
γ = 0.35
γ = 1
0.0001
0.01
0.1
1
10
100
[Cytochalasin B] μM
B
1.5
1.0
0.5
0.0
v_i/v_c
q = 4.25
q = 3.75
q = 3.25
q = 2.75
q = 1
0.0001
0.01
0.1
1
10
100
[Cytochalasin B] μM

Figure 3.12: A. Intermolecular trans-allostery - the affinity affect. Subsaturating levels of intracellular cytochalasin B stimulate GLUT1-mediated 3-O-methylglucose uptake in human erythrocytes then, as cytochalasin B levels increase, sugar uptake is inhibited. Ordinate: vi/vc. Abscissa: [cytochalasin B] in µM (note the log scale). Equation 1 from Model 8B was used to simulate these data. The following constants were used: [S] = 100 µM, K_2 = 1000 µM, K_L = 0.14 µM, $\alpha = \beta = \delta = p = q = r = 1$, γ is varied (see legend). These parameters result in the following: $Const_1$ falls from 2.61×10^7 to 7.99×10^5 μM^4 with decreasing γ, $Const_2$ falls from 1.86×10^8 to 3.26×10^7 μM^3 with decreasing γ, $Const_3$ falls from 3.73×10^8 to 1.63×10^7 μM^3 with decreasing γ, $Const_4$ falls from 1.33×10^9 to 8.32×10^7 μM^2 with decreasing γ. Curves were computed by nonlinear regression using equation 1. **B. Intermolecular trans-allostery - the k_{cat} affect**. Subsaturating levels of intracellular cytochalasin B stimulate GLUT1-mediated 3-O-methylglucose uptake in human erythrocytes then, as cytochalasin B levels increase, sugar uptake is inhibited. Ordinate: vi/vc. Abscissa: [cytochalasin B] in µM (note the log scale). Equation 1 from Model 8B was used to simulate these data. The following constants were used: [S] = 100 µM, K_2 = 1000 µM, K_L = 0.14 µM, $\alpha = \beta = \delta = \gamma = p = r = 1$, q is varied (see legend). These parameters result in the following: $Const_1 = 2.61 \times 10^7$ μM^4, $Const_2$ increases from 1.86×10^8 to 7.37×10^8 μM^3 with increasing q, $Const_3 = 3.73 \times 10^8$ μM^3, $Const_4 = 1.33 \times 10^9$ μM^2. Curves were computed by nonlinear regression using equation 1.

Limitations of the analysis

While these considerations support the elimination of models 1, 2, 3, 5, 6 and 7, the remaining models are kinetically indistinguishable. These include model 4 (a fixed site transporter), model 8 (variations of oligomers of alternating access transporters or fixed site transporters) and model 9 (an oligomer of allosteric alternating access transporters). As presented, these analyses do not discriminate between alternating access and fixed site transporter models. Other approaches are necessary to accomplish this (79,83,167) and when applied, support the hypothesis that GLUT1 functions as an allosteric fixed site transporter (although they do not consider the possibility that a fixed site transporter could be an oligomeric complex of interacting, alternating access transporters). In the present study, discrimination between models 4, 8 and 9 relies on prior analysis of GLUT1 cytochalasin B binding stoichiometry. This could introduce interpretive problems for two reasons: 1) GLUT1 cytochalasin B binding is also influenced by ATP; 2) The stoichiometry of cytochalasin B binding to GLUT1 monomers, dimers and tetramers may be difficult to measure accurately if GLUT1 affinity for cytochalasin B is affected by its oligomeric state.

Previous studies from this laboratory (78,80,86,87,118,170) have shown that GLUT1 is a nucleotide binding protein, that ATP binding at an endofacial site increases the affinity of the exofacial site for sugars but reduces V_{max} for sugar uptake, reduces cooperativity in cytochalasin B binding to GLUT1 but increases the affinity of the high affinity site for cytochalasin B. Other studies have shown that steroidal ligands (171,172), caffeine and AMP (85) inhibit ATP binding to GLUT1 thereby altering the kinetics of glucose transport and cytochalasin B binding. It is possible therefore that activation of glucose influx at low cytochalasin B concentrations results from a complex interplay between cytochalasin B and nucleotide binding to GLUT1. We think

this unlikely for three reasons: 1) Cytochalasin B and ATP binding to GLUT1 are positively cooperative - cytochalasin B binding at low [cytochalasin B] is enhanced by ATP and ATP binding at subsaturating [ATP] is enhanced by cytochalasin B (80); 2) Low concentrations of extracellular maltose trans-activate cytochalasin B binding to red cell ghosts in the presence and absence of intracellular ATP (78). Sub-saturating [cytochalasin B] stimulates sugar uptake in both ATP-containing and in ATP-free red cell ghosts [78]. These results indicate that trans-allostery is not ATP-dependent but may be modulated by ATP.

The question of GLUT1 cytochalasin B binding stoichiometry is more difficult to address when cells typically express a mixture of GLUT1 monomers, dimers and tetramers (140). What is clear, however is that cis-allostery persists but trans-allostery is lost in both reduced (dimeric) and recombinant, tetramerization-deficient GLUT1 (80,162). Trans-allostery thus requires intermolecular interactions while cis-allostery may be dependent on intramolecular interactions. Detailed analysis by Cunningham and Naftalin (163) of the homology-modeled GLUT1 structure and the T295M GLUT1 deficiency mutation led to the important insight that GLUT1 presents twin glucose entry ports at its external surface which converge on a common catalytic vestibule containing a high affinity glucose binding site. Maltose binding to one entry port could, therefore, increase glucose affinity at the other port and thereby stimulate glucose entry into the catalytic vestibule. Cunningham and Naftalin further noted that the T295M GLUT1 deficiency mutation exhibits high temperature sensitivity and proposed a rationale for this behavior (impaired glucose exchange between intramolecular “vestibules” at low temperatures; (163)). Our own studies also suggest the presence of 2 exofacial sugar binding sites that converge on a catalytic site (149,162) and thus support the Cunningham and Naftalin model. Studies of the temperature-dependence of cis-allostery in the T295M GLUT1 deficiency mutation may allow

further review of their model and the roles of the entry ports in cis-allostery.

Conclusions

GLUT1 allostery is explained only by models in which multiple exofacial ligand and multiple endofacial ligand binding sites co-exist. At least one exofacial site and one endofacial site must also correspond to the catalytic site. The endofacial ligand binding properties of GLUT1 (92,102) and molecular docking studies (85,135,149,162)indicating 1 or fewer cytochalasin B binding sites per GLUT1 molecule eliminate the possibility that more than one e1 ligand can bind to each GLUT1 molecule. This conclusion, in conjunction with the observation that multiple e1 ligand binding sites per transporter are required to explain the transport behavior, suggests that the transporter must comprise an oligomer of interacting GLUT1 proteins. Each subunit (protein) could function as an AAT or an FST. The X-ray crystallography data (6,77,131,133,162) suggest: 1) each GLUT1 molecule is an AAT not FST; 2) the exofacial conformation of GLUT1 presents multiple ligand binding sites; 3) the allosteric endofacial site corresponds to the catalytic site in an adjacent e1 subunit. Previous studies have shown that forskolin-stimulated cytochalasin B binding to GLUT1 is abolished in dimeric (reduced) GLUT1 (80) suggesting that endofacial cis-allostery requires tetrameric GLUT1 and that the endofacial allosteric site is contributed by an adjacent subunit not by the subunit to which ligand binding is measured. If, correct, this behavior (loss of endofacial cis-allostery) should be recapitulated with the TM9 (tetramerization-deficient) mutant, confirming that exofacial cis-allostery is an intramolecular phenomenon but endofacial cis-allostery is intermolecular.

Chapter 4:

Small Molecule Interactions with GLUT1

Parts of this chapter was published in the *American Journal of Physiology-Cell Physiology* in 2015, the *Journal of Biological Chemistry* in 2016 and 2017, and can be found using the following references:

Sage, J., et al., *Caffeine inhibits glucose transport by binding at the GLUT1 nucleotide-binding site.* Am J Physiol Cell Physiol, 2015. **308**: p. C827-C834

Ojelabi, O., et al., *WZB117 inhibits GLUT1-mediated sugar transport by binding reversibly at the exofacial sugar binding site.* J Biol Chem, 2016. **291**: p. 26762-26772.

Lloyd, K., et al., *Reconciling contradictory findings: Glucose transporter 1 (GLUT1) functions as an oligomer of allosteric, alternating access transporters.* J Biol Chem, 2017.

Research was supported using NIH Grants: DK36081 and DK44888

Abstract

The human glucose transporter GLUT1 interacts with and its activity is modulated by a wide variety of ligands. These ligands can bind at the exofacial and/or endofacial surfaces of the transporter. Recent advances in the structural biology of membrane proteins and the crystallization of GLUT1 and GLUT3 in inward and outward facing conformations, respectively, now permit examination of potential ligand binding sites through computational docking. Using computational docking software, we have examined the potential substrate binding pockets for both endofacial and exofacial ligands in order to explore GLUT1 structural determinants of ligand binding affinity and cooperativity.

Introduction

GLUTs comprise the mammalian family of sugar transporters that mediates rapid equilibration of sugars into or out of the cell. The GLUT family of transporters has several different primary substrates including glucose, galactose, fructose, and myoinositol (100). GLUT1, the first glucose transporter isoform to be identified, purified *ex vivo*, reconstituted, and cloned rapidly transports glucose across the cell membrane in all cell types but, most importantly in humans, red blood cells and at the blood brain barrier (17-19). In addition to its role as the glucose transporter, GLUT1 also transports dehydroascorbic acid and galactose at lower efficiencies (173,174).

The pioneers of the field very quickly proposed that GLUT1-glucose interactions involve hydrogen bonding between amino acid side chains and glucose hydroxyl groups. Replacement of an interacting hydroxyl by a hydrogen atom or inversion of a hydroxyl (e.g. as in the C4 epimer of D-glucose, galactose), it was reasoned, would decrease the affinity of GLUT1 for the sugar, assuming that all other groups on the sugar continued to interact with GLUT1. In practice, substitution of the sugar hydroxyls with either hydrogen or R-groups has a strong effect on the ability of the modified ligand to inhibit sugar transport suggesting requirements for spatial compatibility and hydrogen bonding. Replacement of the hydrogen with an R-group at hydroxyls 2, 3, and 4 of glucose decreases affinity of ligand binding at the exofacial, e2 site while replacement at hydroxyls 1 and 6 does not (74,75). Similarly, when measuring ligand interactions at the endofacial or e1 binding site, replacement of hydroxyl 6 with a hydrogen decreases the ligand's ability to inhibit sugar transport but affinity is rescued by fluorine suggesting hydrogen bonding between GLUT1 and the hydroxyl on C6 [74, 75]. Replacement of hydroxyl 1 with an R-group does not affect the ligand's ability to inhibit sugar transport

suggesting that C1 of the hexose is oriented towards cytoplasmic bulk solvent rather than the interior of GLUT1 and thus can tolerate bulky substitutions at C1 [74, 75]. By contrast, replacement of hydroxyl 6 with an R-group prevents ligand binding at the endofacial site.

GLUT1 also interacts with other non-transportable sugars. Glucose transport is inhibited by interaction with maltose, ethylidene glucose and other glucose analogs (79,80). Increasing the size of the sugar (number of hexose units) increases $K_{I(app)}$ for sugar transport inhibition (78). In addition, both maltose and maltotriose, accelerate sugar transport when applied at low concentrations, but inhibit transport at higher concentrations [78].

Unlike normal differentiated cells which use mitochondrial oxidative phosphorylation to sustain cellular function, most cancer cells use anaerobic metabolism to generate the ATP and biomass required for cellular processes and proliferation (50). This has prompted several groups to propose that suppressing anaerobic metabolism may offer an effective anti-cancer strategy. Three approaches have been used to limit glycolysis in cancer cells: glucose deprivation *in vitro, in vitro* and *in vivo* use of glycolysis inhibitors and use of glucose transport inhibitors both *in vitro* and *in vivo,* with all three approaches resulting in cell death (175-178). GLUT1 is upregulated in tumors (179). Several molecules have been developed as inhibitors of GLUT1 mediated glucose transport including WZB117 (2-fluoro-6-(m-hydroxybenzoloxy)phenyl m-hydroxybenzoate), and two compounds from Bayer pharmaceuticals: BAY-588 and BAY-876 (180,181).

A second class of molecules investigated for their effects on cancer tissue are the flavonoids a large class of polyphenolic secondary metabolites found in green tea and red wine. Several studies have shown that quercetin, epigallocatechin gallate (EGCG) and epicatechin gallate (ECG), flavonoids present in both red wine and green tea, inhibit GLUT1 mediated

glucose transport [81,82]. Glucose transport inhibition by these compounds may explain their reported protections against cancer, cardiovascular disease, and diabetes associated with red wine and green tea consumption.

GLUT1 mediated sugar transport is also inhibited by families of structurally diverse small molecules which affect the kinetics of transport in different ways. Cytochalasin B is a mycotoxin that binds at the endofacial surface of GLUT1 and functions as a competitive inhibitor of exchange and net sugar efflux and as a noncompetitive inhibitor of net sugar uptake (182). Additionally, low concentrations of CB stimulate sugar uptake while increasing concentrations inhibit uptake. Similarly, forskolin, a diterpene is a competitive inhibitor of CB binding and exchange transport while acting as a noncompetitive inhibitor of net sugar uptake (183). Interestingly forskolin and forskolin derivatives have different effects on CB binding, ranging from, competitive inhibition, stimulation at low concentrations and followed by inhibition at high concentrations, and stimulation at all concentrations (84).

GLUT1 is allosterically inhibited by ATP, which binds at a single, ATPase-null nucleotide binding site. ATP binding leads to a conformational change that involves the cytoplasmic C-terminus and the large intracellular loop 6-7 resulting in a decrease in both K_m and V_{max} for zero-trans sugar uptake characteristic of uncompetitive inhibition, an increase in K_m for net exit (characteristic of competitive inhibition of exit) and a reduction in K_m for exchange transport (characteristic of mixed-type inhibition) (86,87,184,185). Caffeine, a methylxanthine, binds to GLUT1 and acts as a competitive inhibitor of ATP inhibition of GLUT1 mediated glucose transport (85). Interestingly caffeine acts as a competitive inhibitor of CB binding while ATP does not [85].

Utilizing our knowledge of the sidedness of action of different GLUT1 inhibitors, the

GLUT1 e1 crystal structure(s), and homology models of GLUT1 based upon the GLUT3 e2 crystal structure in combination with the known structures of GLUT1 ligands and molecular docking analysis may permit definition of the determinants of GLUT1-ligand interactions. Integrating this understanding with experimentally determined binding and inhibition constants may then allow us to determine the regions of the GLUTs involved in ligand binding and how it is that multiple ligands can complex with one subunit of GLUT1 to modify transport in such diverse ways.

Experimental Procedures

Homology Modeling

We modeled GLUT1 e2, e2-occluded and e1-occluded structures respectively using the human GLUT3 (4ZWC) structure (134) and the XylE e2-occluded (4GBZ) and e1-occluded (4JA3) structures (6,131). We removed ligands and used chain A as the template for each modeled structure. Sequence alignments were generated using ClustalX. Homology models were built using Modeller-9.9 and analyzed using PROCHECK. The GLUT1 e1 structure (4PYP (77)) was used directly.

Cavity analysis

Cavities for ligand docking were calculated using the CastP server (http://sts.bioe.uic.edu/castp/) [150] and the grid was centered on the residues forming the cavity.

Stochastic Docking

β-D-Glucose, maltose, maltotriose, maltotetraose, caffeine, ATP, quercetin, EGCG, ECG, forskolin(s) and cytochalasin(s) structures were obtained from ZINC (http://zinc.docking.org). The WZB117, BAY-588, and BAY-876 structures were generated using the 3D structure

generator Corina from Molecular Networks GmbH (http://www.molecular-networks.com). Docking was performed using the Schrodinger software suite. No restraints were used during the docking. The protein structure was preprocessed with the Protein Preparation Wizard, bond orders were assigned, hydrogens added and the H-bond network was optimized. The system was energy minimized using the OPLS 2005 force field. Ligand structures were prepared with the LigPrep module and the pKa of the ligands was calculated using the Epik module. Computational docking was performed by the GLIDE module in standard-precision (SP) mode and default values for grid generation. Grids were mapped using CastP cavity analysis and ligand positions from the original crystal structures. Up to 32 poses were generated for each ligand.

Results

Homology Modeled GLUT1 structures

GLUT1 and GLUT3 structures have been described previously (77,134). The current study presents and interrogates e2 homology-modeled GLUT1 structure and e1 GLUT1 crystal structure(s).

GLUT1 Central Hydrophilic Cavity

The GLUT1 translocation pore is described in chapter 2. The hydrophilic cavity of GLUT1 complexed with CB, pdb code 5EQI, (3294.9, $Å^3$) is larger than the cavity of GLUT1 pdb code 4PYP (2854.9 $Å^3$ (Figure 4.1)).

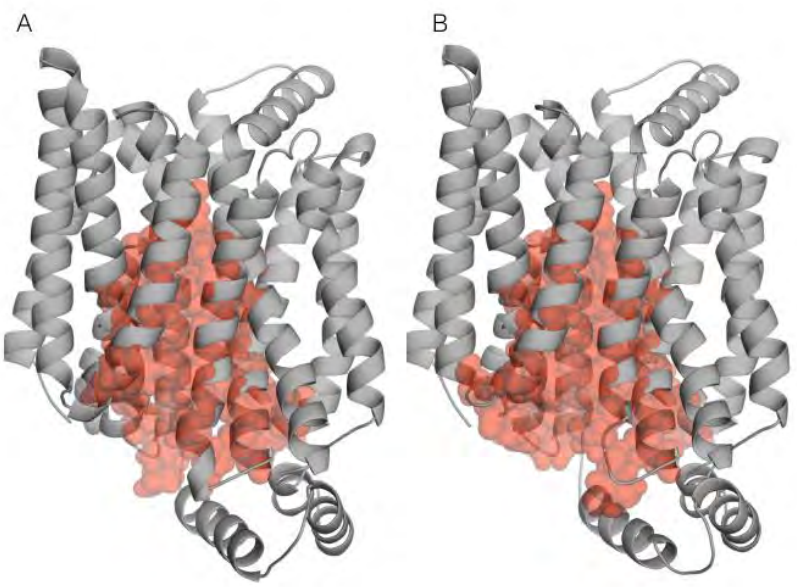

Figure 4.1: GLUT1 e1 structures with the translocation cavity. GLUT1 is shown as a cartoon representation. The amino acids lining the inward open translocation cavity are shown as red spheres. 4PYP, the GLUT1 structure complexed with a glycodetergent is shown in A, with a cavity volume of 2854.9 $Å^3$. Shown in panel B is 5EQI, GLUT1 complexed with CB, with a cavity volume of 3294.9 $Å^3$.

Glucose Interaction Sites

GLUT1 β-D-glucose interaction sites are described in chapter 2.

GLUT1 Ligands

GLUT1 ligands have been characterized based upon their interaction at exofacial (e2) or endofacial (e1) binding sites. Figures 4.2 and 4.3 show the chemical structures of exofacial and endofacial that were docked to GLUT1.

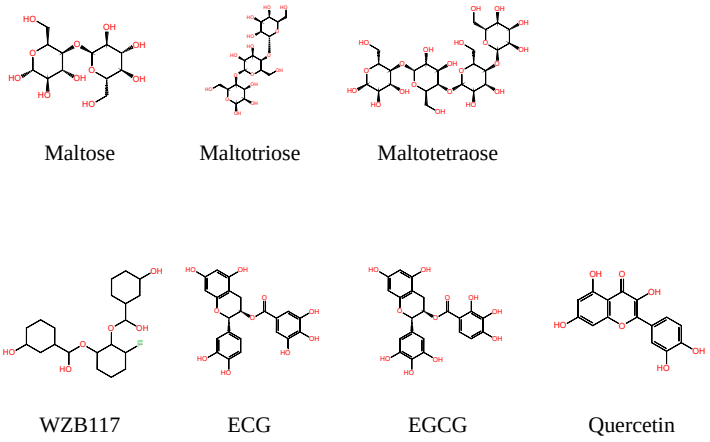

Figure 4.2: Chemical structures of exofacial ligands. The chemical structures of the e2 ligands maltose, maltotriose, maltotetraose, WZB117, ECG, EGCG, and quercetin.

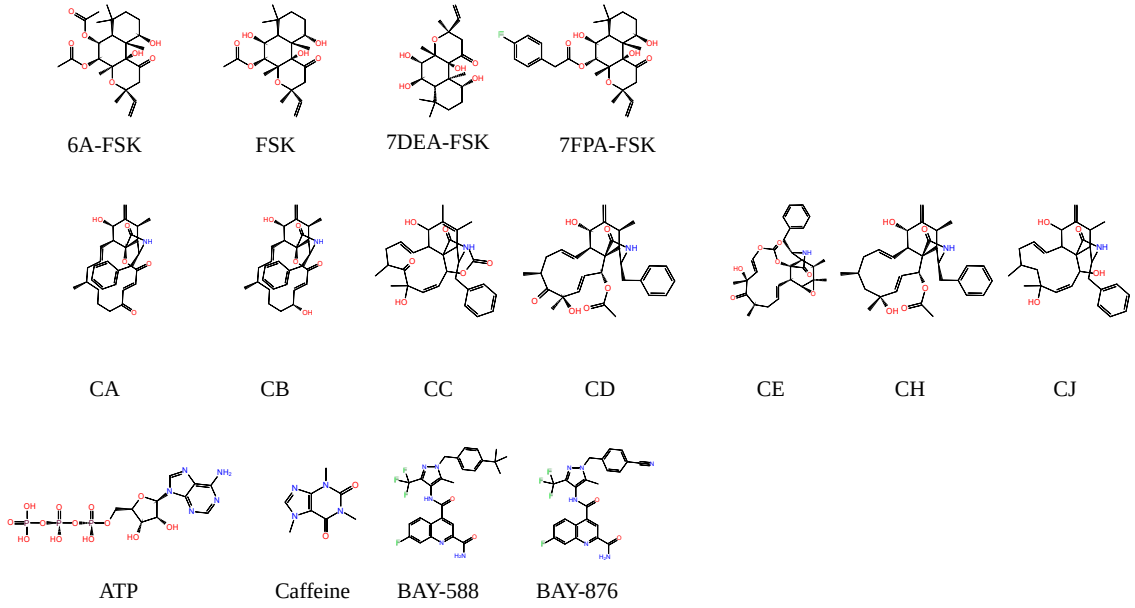

Figure 4.3: Chemical structures of endofacial ligands. The chemical structures of the e1 ligands FSK, 6A-FSK, 7DEA-FSK, 7FPA-FSK, cytochalasins (CA, CB, CC, CD, CE, CH, CJ) ATP, Caffeine, BAY-588, and BAY-876.

ATP Docking to the GLUT1 e1 Conformation

Thirty different poses of ATP, caffeine, and CB interaction with GLUT1 were generated to examine their interactions with the GLUT1 e1 conformation. From these, the highest affinity conformation is shown for ATP, caffeine, and CB, respectively (Figure 4.4). However, ATP and caffeine compete for binding to GLUT1, suggesting that ATP and caffeine share identical or overlapping binding sites [85]. Caffeine is also a competitive inhibitor of CB binding to GLUT1 but CB and ATP binding are not mutually exclusive (85). This suggests that if competitive inhibition is achieved through steric overlap then the caffeine binding site bridges the CB and ATP binding sites. ATP and caffeine were also docked to the 5EQI structure (Figure 4.5). The ligand (CB) was removed and the CastP cavity map was used to generate the grid. CB inhibition studies with caffeine and ATP show that caffeine competitively inhibits CB binding but ATP does not, suggesting that while ATP and caffeine share a common binding site, the caffeine binding site overlaps with CB while ATP does not. We therefore searched the docked positions of ATP, caffeine, and CB to find conformations where ATP and caffeine xanthine rings overlap while the methyl groups of caffeine overlap with the docked CB position (Figure 4.6). The CB pose was chosen that does not overlap with the ATP pose but does with the caffeine pose. All positions of ATP docked to the 5EQI structure overlap with the CB ligand present in the crystal structure. (Figure 4.6).

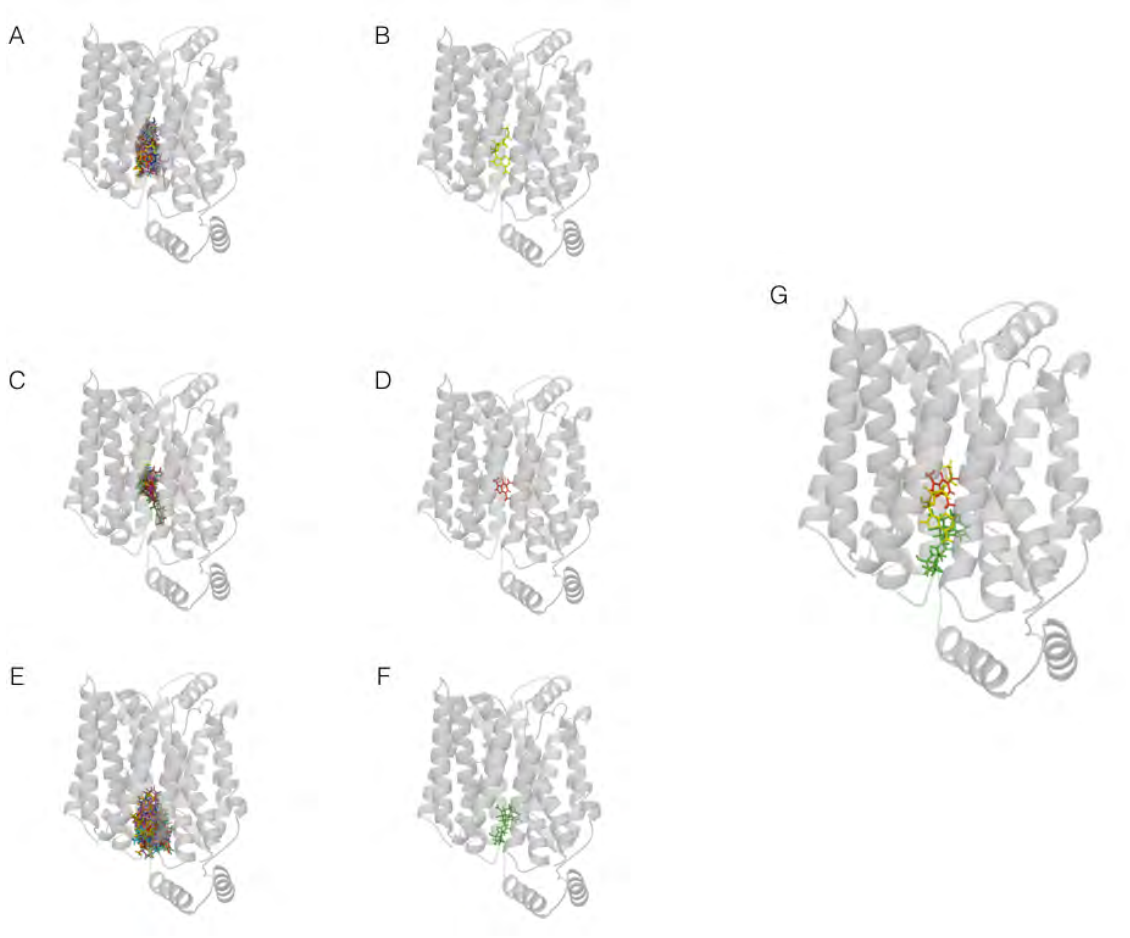

Figure 4.4: Docking of ATP (A, B), caffeine (C, D), and CB (E, F) to the GLUT1 e1 structure, 4PYP. All docked poses are shown in panels A, C, and E for ATP (30), caffeine (27), and CB (29) respectively. The highest affinity pose is shown in panels B, D, and F for ATP, caffeine, and CB respectively. Panel G shows the highest affinity poses for ATP (yellow), caffeine (red), and CB (green) together.

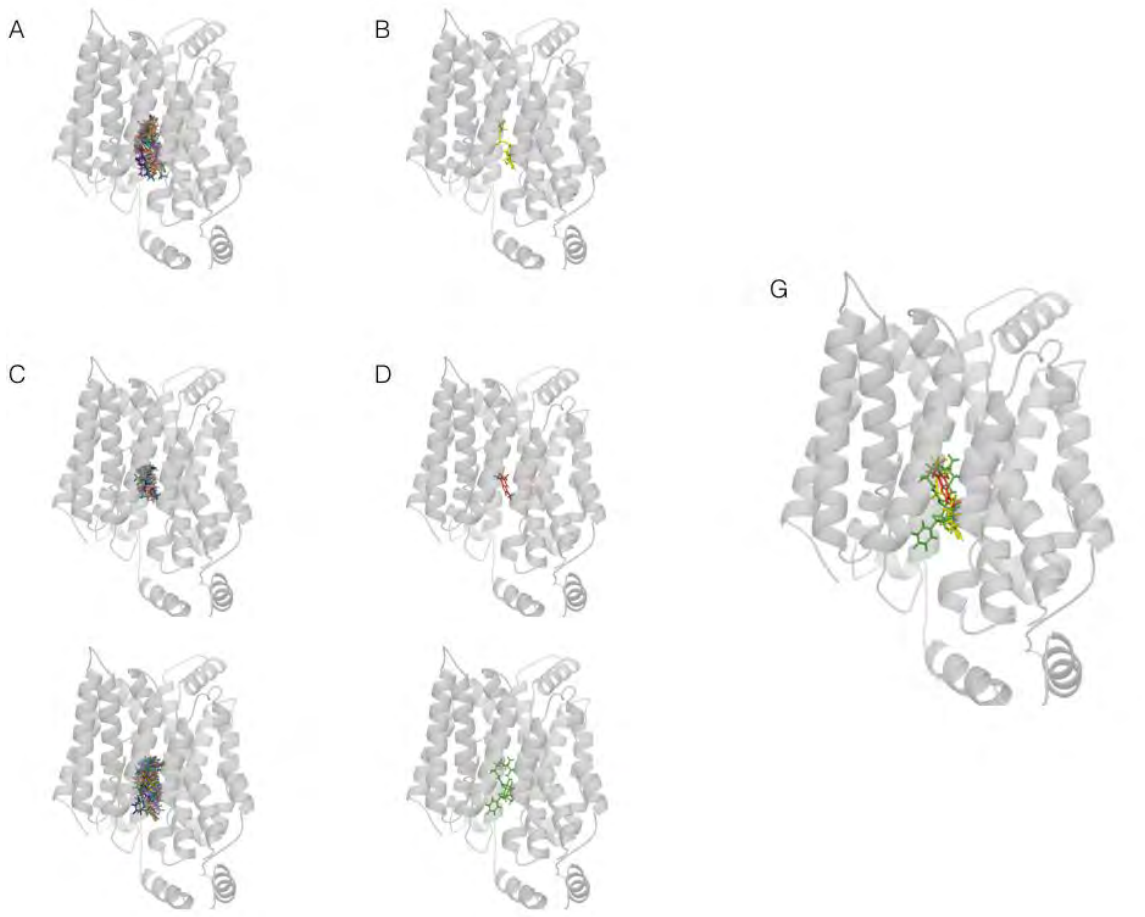

Figure 4.5: Docking of ATP (A, B), caffeine (C, D), and CB (E, F) to the GLUT1 e1 structure, 5EQI. All docked poses are shown in panels A, C, and E for ATP (30), caffeine (30), and CB (26) respectively. The highest affinity pose is shown in panels B, D, and F for ATP, caffeine, and CB respectively. Panel G shows the highest affinity poses for ATP (yellow), caffeine (red), and CB (green) together.

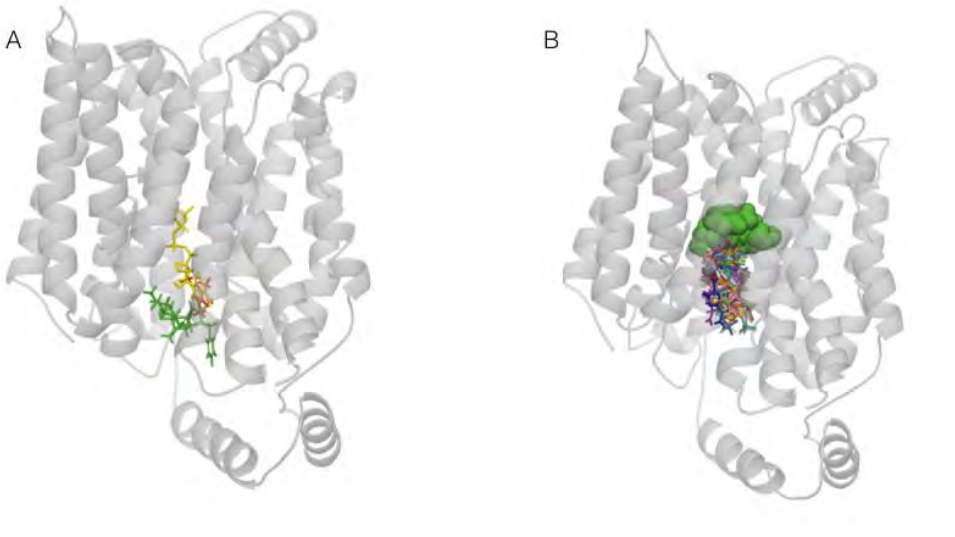

Figure 4.6: ATP, Caffeine, and CB docked to e1 conformations. A.) Docking poses of ATP (yellow), caffeine (red) and CB (green) to the 4PYP crystal structure, with caffeine and the ATP xanthine groups occupying the same site. The caffeine methyl group overlaps with CB while ATP does not overlap with CB. B.) Docking of ATP to the 5EQI GLUT1 crystal structure. ATP positions are shown as sticks in rainbow colors. CB is shown as green spheres in the position it occupies in the crystal structure.

GLUT1 e1 Inhibitor docking to 4PYP

Cytochalasin and forskolin derivatives bind to the e1 conformation of GLUT1. The binding of cytochalasins to GLUT1 has been characterized by inhibition of CB binding and reveals that multiple cytochalasin binding sites coexist in the transporter complex. The size of the macrocyclic ring of the cytochalasin does not always affect $K_{D(app)}$ for binding of the first ligand but decreasing the size of the ring increases the impact (negative cooperativity) on binding of the second cytochalasin (84). This is reflected in the different docking positions for cytochalasin docking to the 4PYP structure (Figure 4.7).

The cytochalasins exercise both homo- and hetero-cooperativity such that the binding of one cytochalasin can either stimulate or inhibit the binding of a second identical or nonidentical cytochalasin respectively. Cytochalasins with highly negative homo-cooperativity bind near the glucose "core" binding site (e.g. CC) while cytochalasins with moderately negative homo-cooperativity and positive hetero-cooperativity in relation to CB do not bind as deeply in the e1 cavity (e.g. CA). As with the cytochalasins, the forskolins also display experimental negative homo-cooperativity with positive homo-cooperativity and bind near the "core" binding site (Figure 4.8).

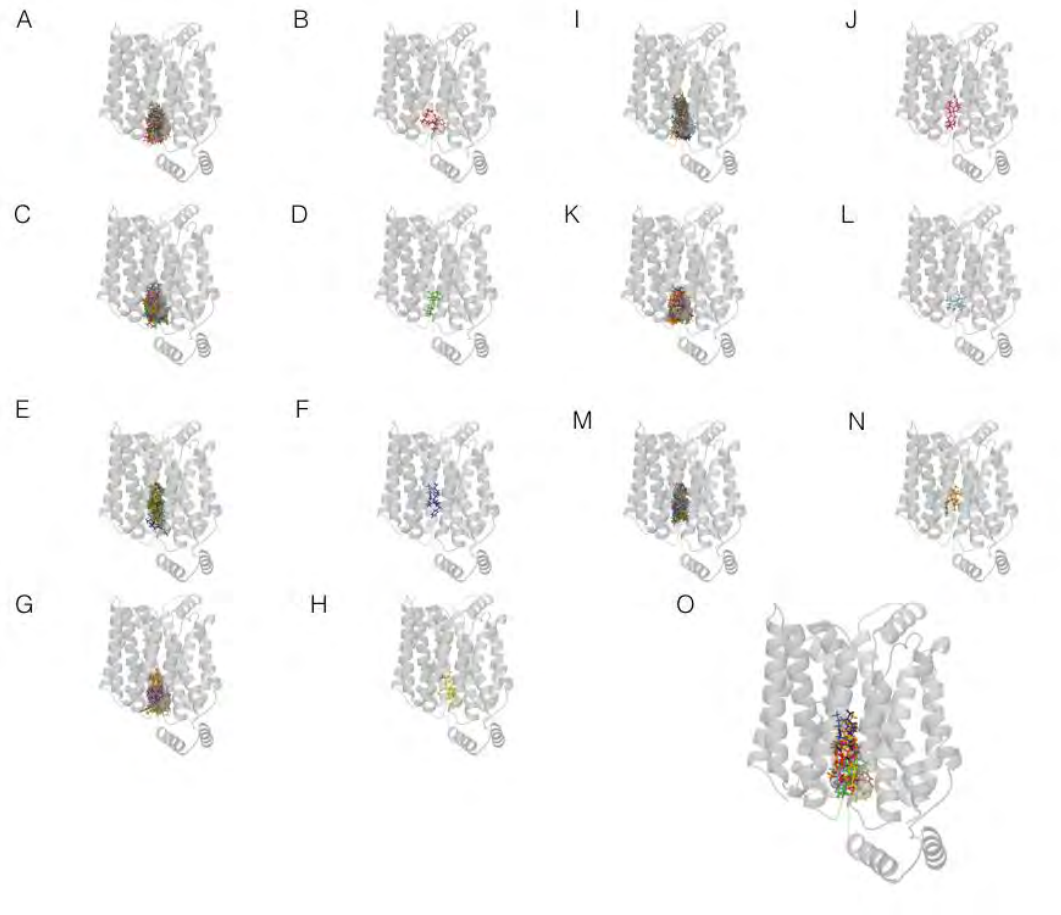

Figure 4.7: Docking of Cytochalasins to the GLUT1 e1 structure, 4PYP. Docking of CA (A, B), CB (C, D), CC (E, F), CD (G, H), CE (I, J), CH (K, L), and CJ (M, N) to the GLUT1 e1 structure, 4PYP. All docked poses of CA (27), CB (29), CC (30), CD (27), CE (28), CH (29), and CJ (30) are shown in panels A, C, E, G, I, K, and M, respectively. The highest affinity pose of each of these ligands is shown by: CA (B), CB (D), CC (F), CD (H), CE (J), CH (L), and CJ (N). Each of the highest affinity poses are shown in panel O with CA (red), CB (green), CC (blue), CD (yellow), CE (magenta), CH (cyan), and CJ (orange).

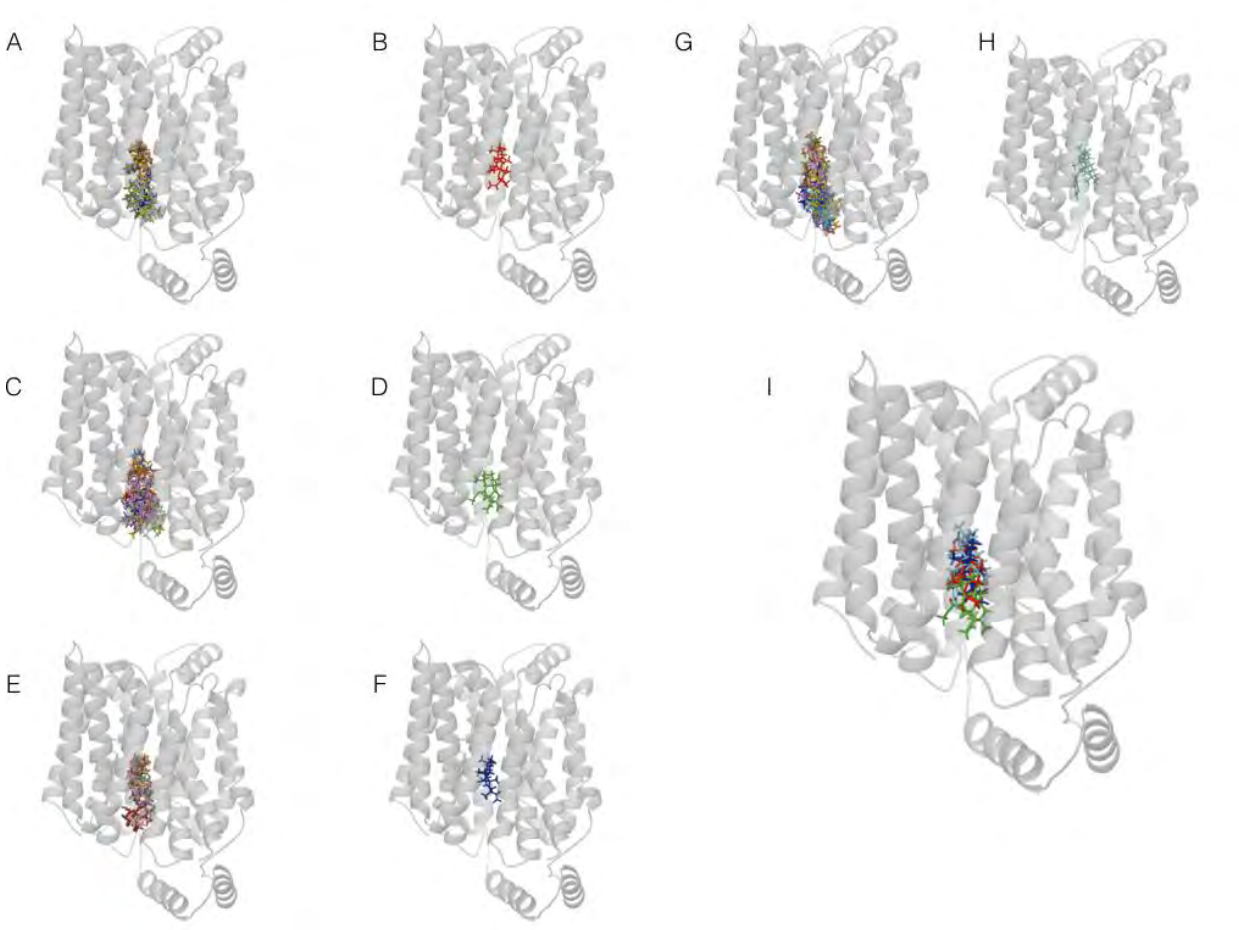

Figure 4.8: Docking positions of FSK and forskolin derivatives to the GLUT1 e1 structure, 4PYP. Docking of FSK (A, B) and the forskolin derivatives 6A-FSK (C, D) 7DeA-FSK (E, F) and 7FPA-FSK (G, H) to the GLUT1 e1 structure, 4PYP. All docking poses are shown in panels A, C, E, and G for FSK (26), 6A-FSK (26), 7DeA-FSK (26), and 7FPA-FSK (16), respectively. The highest affinity pose(s) are shown in panels B, D, F, and H for FSK, 6A-FSK, 7DeA-FSK, and 7FPA-FSK, respectively. Panel I shows the highest affinity poses for each forskolin, FSK (red), 6A-FSK (green), 7DeA-FSK (blue), and 7FPA-FSK (cyan).

GLUT1 e1 Drugs

Transport studies with the potential anti-cancer drugs BAY-588 and BAY-876 suggest that both interact with GLUT1 by non-competitively inhibiting sugar uptake and competitively inhibiting sugar exit. This suggest that BAY interacts with GLUT1 at the endofacial face or interacts only with the e1 conformation of GLUT1. $K_{I(app)}$ for BAY-876 inhibition of transport is almost 50-fold lower than $K_{I(app)}$ for BAY-588 inhibition of GLUT1 suggesting that replacement of the nitrile group with a tert-butyl group on the benzene ring severely decreases affinity (Figure 4.9).

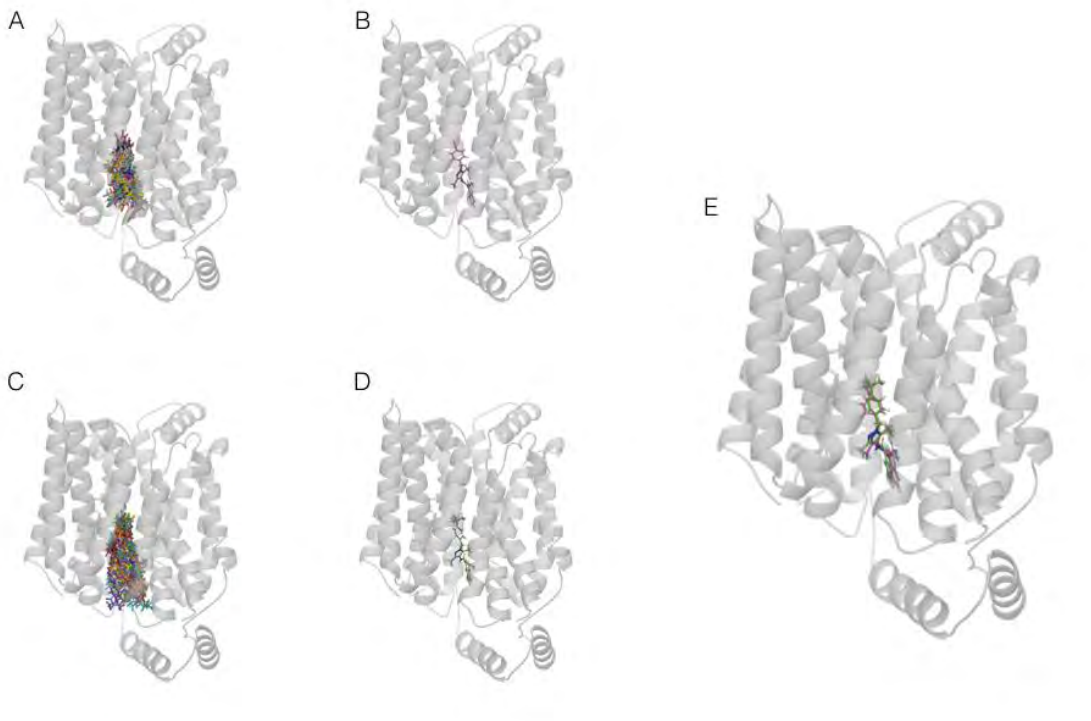

Figure 4.9: Docking positions of BAY-876 and BAY-588 to the GLUT1 e1 structure, 4PYP. BAY-876 (A, B) and BAY-588 (C, D) to the GLUT1 e1 structure, 4PYP. All docking poses are shown in panels A and C for BAY-876 (27) and BAY-588 (30), respectively. The highest affinity position is shown in panel B for BAY-876. Panel D shows a middle affinity docked pose of BAY-588 that matches the pose of the highest affinity BAY-876. Panel E shows BAY-876 (magenta) and BAY-588 (green) in one structure.

GLUT1 e1 Inhibitor docking to 5EQI

The GLUT1 crystal structure pdb code 5EQI is a structure of GLUT1 complexed with a CB molecule. In this structure, the CB molecule forms a hydrogen-bond with W388 and is complexed in the core interaction region (Figure 4.10) (135). While *in silico* docking of CB to 5EQI (using the CB ligand to generate the docking grid) does produce a complex in which the docked CB overlaps with the observed CB binding site in the crystal structure, the docked position(s) of CB do not precisely match the crystal structure (Figure 4.10). Additionally, none of the docked conformations form an H-Bond with W388. GLIDE uses the position of the ligand in the structure to generate the three-dimensional search space, but does not specify coordinating residues. This amino acid (W388) is considered crucial for CB binding because its mutagenesis to alanine in *X. laevis* oocytes decreases GLUT1 photolabeling by CB significantly (186). Similarly, Docking of CB to 5EQI using the hydrophilic cavity rather than the co-crystalized ligand for grid generation produces CB poses that do not align with the co-crystalized CB. Docking of other cytochalasins to 5EQI was undertaken using either ligand replacement (Figure 4.11) or cavity maps (Figure 4.12) for grid generation. The ligand replacement methodology places the cytochalasin molecule deeper in the translocation cavity.

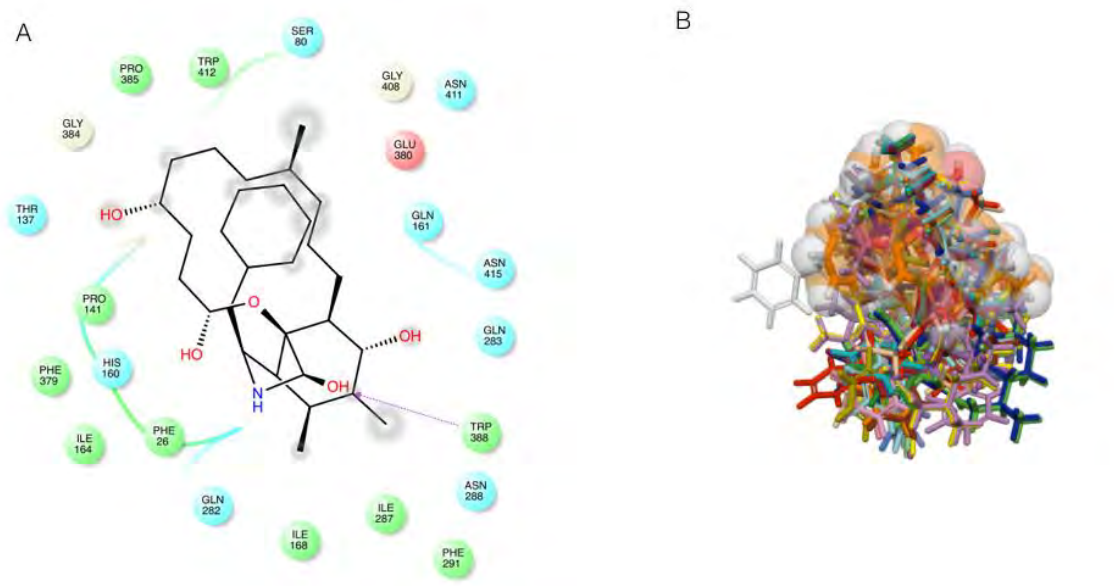

Figure 4.10: Docking of CB to 5EQI using ligand replacement for grid generation. Panel A shows a 2D interaction map of CB co-crystalized with GLUT1 (5EQI). Panel B shows co-crystalized CB as spheres (orange) with the poses of docked CB as rainbow sticks.

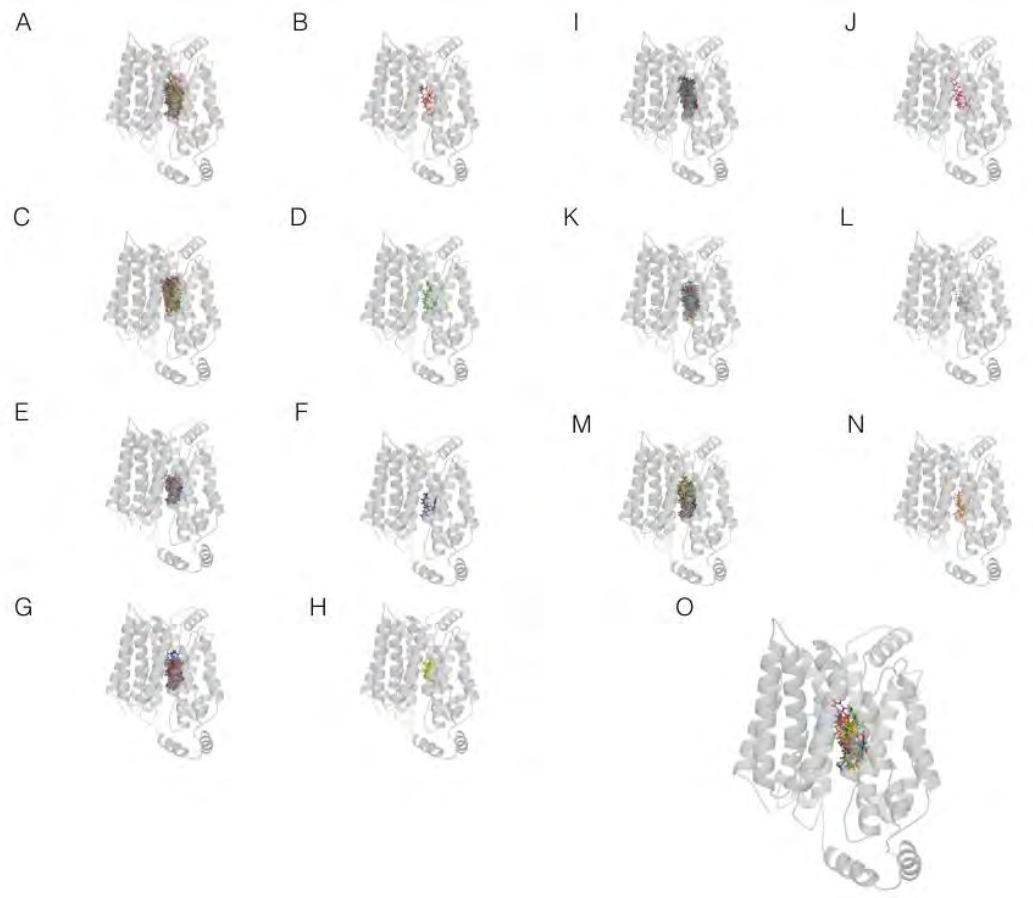

Figure 4.11: Docking of Cytochalasins to the GLUT1 e1 structure, 5EQI. Docking of CA (A, B), CB (C, D), CC (E, F), CD (G, H), CE (I, J), CH (K, L), and CJ (M, N) to the GLUT1 e1 structure, 5EQI using co-crystalized CB for grid generation through ligand replacement. All docked poses of CA (29), CB (26), CC (30), CD (28), CE (27), CH (29), and CJ (30) are shown in panels A, C, E, G, I, K, and M, respectively. The highest affinity position of each of these ligands is shown by: CA (B), CB (D), CC (F), CD (H), CE (J), CH (L), and CJ (N). Each of the highest affinity poses are shown in panel O with CA (red), CB (green), CC (blue), CD (yellow), CE (magenta), CH (cyan), and CJ (orange).

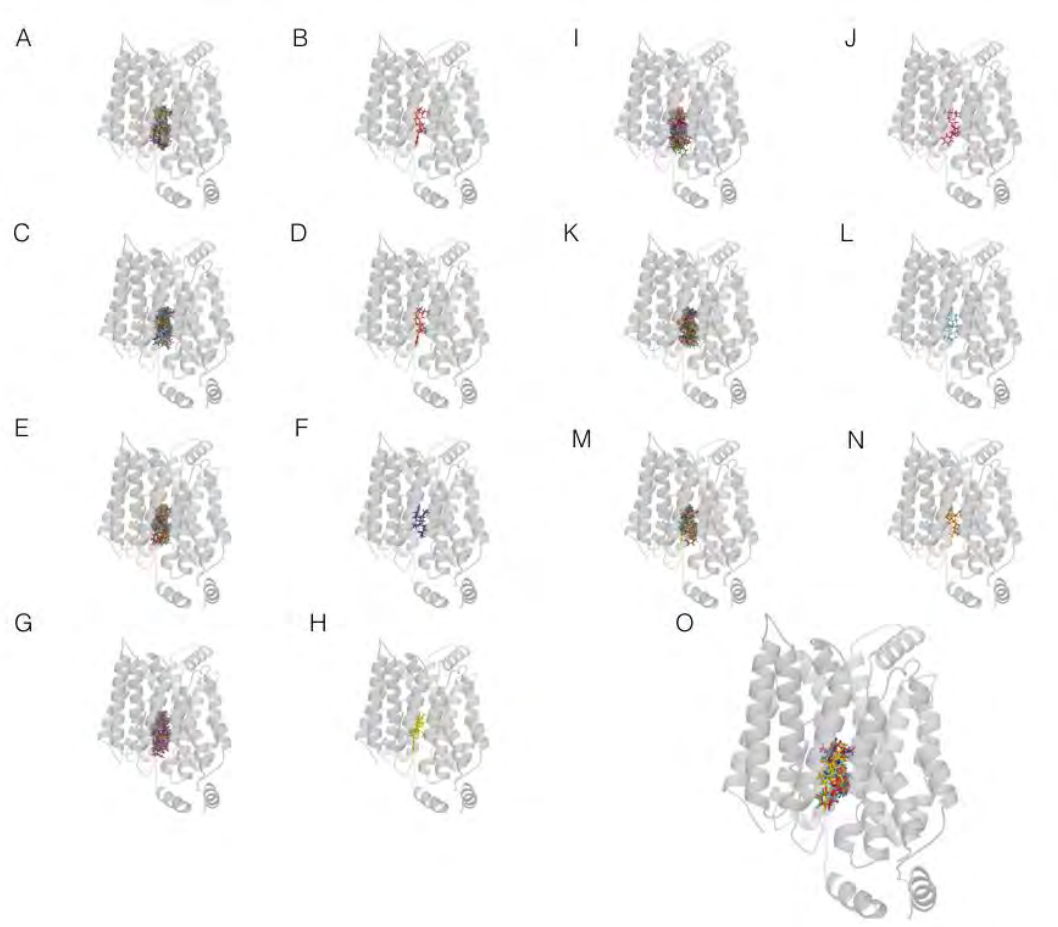

Figure 4.12: Docking of Cytochalasins to the GLUT1 e1 structure, 5EQI. Docking of CA (A, B), CB (C, D), CC (E, F), CD (G, H), CE (I, J), CH (K, L), and CJ (M, N) to the GLUT1 e1 structure, 5EQI using the hydrophilic cavity for grid generation. All docked poses of CA (29), CB (26), CC (30), CD (28), CE (27), CH (29), and CJ (30) are shown in panels A, C, E, G, I, K, and M, respectively. The highest affinity pose of each of these ligands is shown by: CA (B), CB (D), CC (F), CD (H), CE (J), CH (L), and CJ (N). Each of the highest affinity poses are shown in panel O with CA (red), CB (green), CC (blue), CD (yellow), CE (magenta), CH (cyan), and CJ (orange).

GLUT1 e2 Sugars

GLUT1 interacts with, does not transport and is inhibited by several sugars at its external face. The oligosaccharides maltose, maltotriose, and maltotetraose, formed by the concatenation of multiple glucose molecules all bind to and inhibit GLUT1 mediated transport (78). The strength of inhibition/binding decreases as the size of the oligosaccharide increases [78]. The sugars all bind at the "core" glucose binding site. (Figure 4.13)

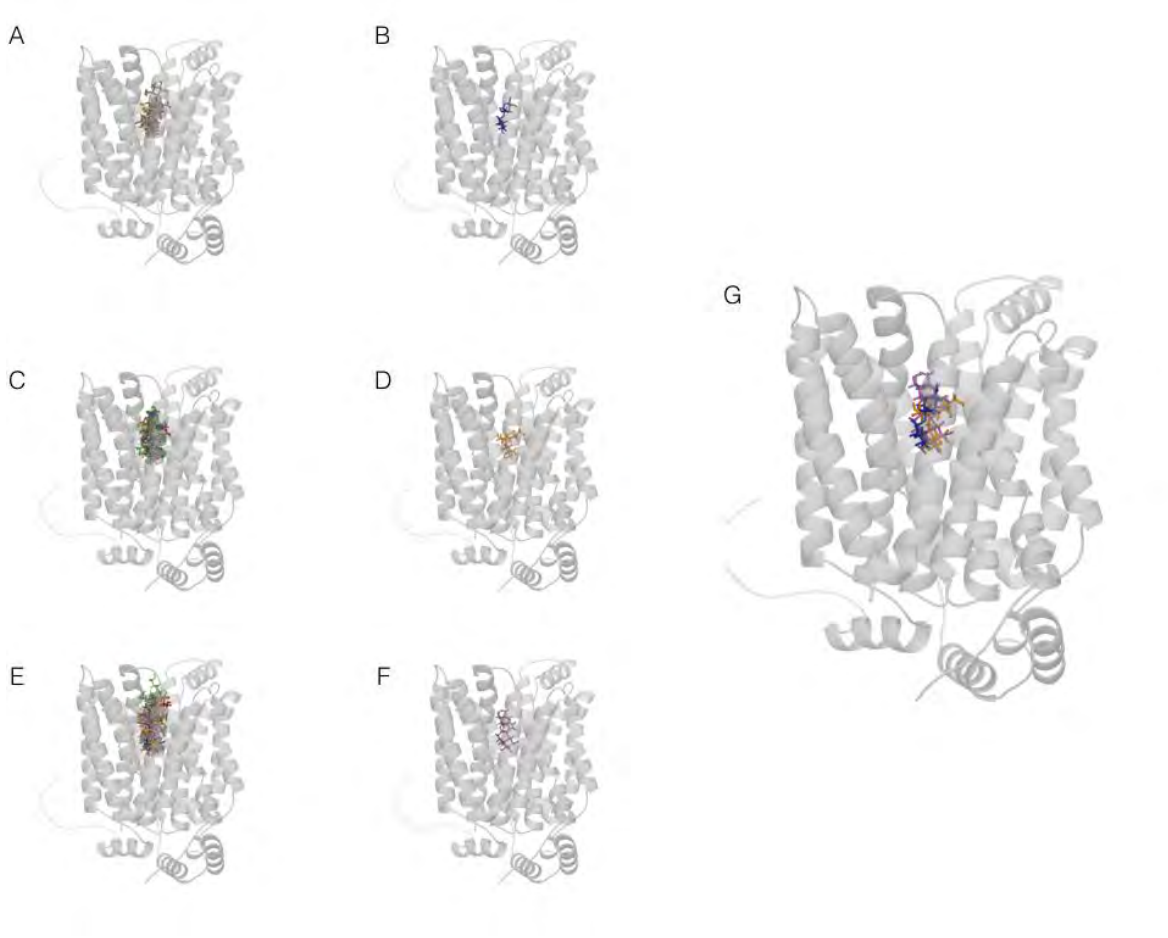

Figure 4.13: Docking positions of maltose, maltotriose, and maltotetraose to the homology modeled GLUT1 e2 structure. Maltose (A, B), maltotriose (C, D), and maltotetraose (E, F) to the homology modeled GLUT1 e2 structure. All docking poses are shown in panels A, C, and E for maltose (30), maltotriose (30), and maltotetraose (30), respectively. The highest affinity pose is shown in panel B, D, and F for maltose, maltotriose, and maltotetraose, respectively. Panel G shows the highest affinity pose for maltose (blue), maltotriose (orange), and maltotetraose (magenta) in one structure.

GLUT1 e2 inhibitors

In addition to the sugar molecules, GLUT1 is inhibited by the flavonoids: ECG, EGCG, and quercetin. These inhibitors appear to interact with the exofacial ligand binding sites of GLUT1. Docking analysis reveals that all three flavonoids interact with the core β-D-glucose interaction site and that increasing the size of the ligand leads to additional interactions with the N-terminal half of GLUT1 (Figure 4.14). GLUT1 is also inhibited by the potential cancer therapeutic WZB117 which binds to the exofacial conformation of GLUT1. The highest affinity position interacts with the core and intermediate β-D-glucose sites. Alternative poses interact with the core and peripheral β-D-glucose sites or intermediate and peripheral β-D-glucose sites (Figure 4.15).

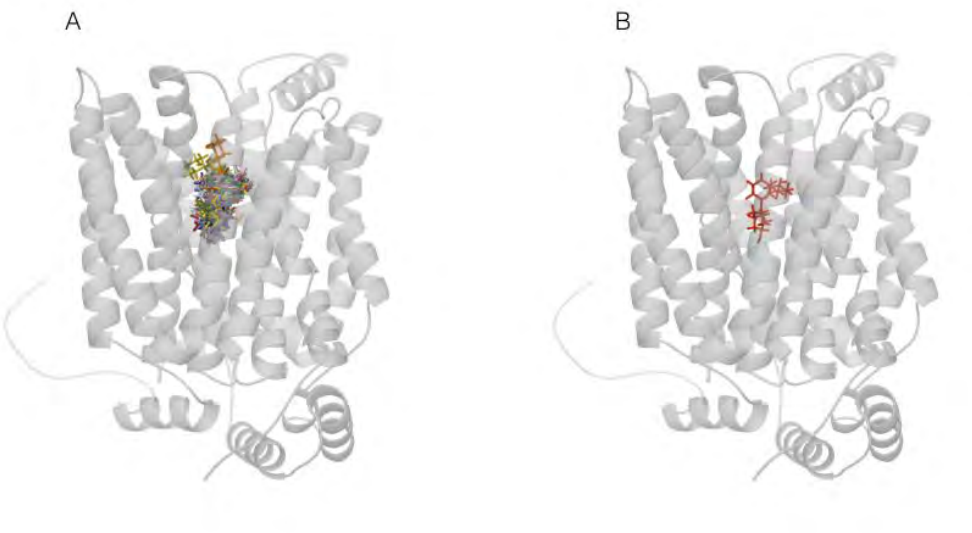

Figure 4.14: Docking of WZB117 (rainbows) to the homology modeled GLUT1 e2 structure. Panel A shows all poses of WZB117 (32). Panel B shows the highest affinity pose of WZB117 in red.

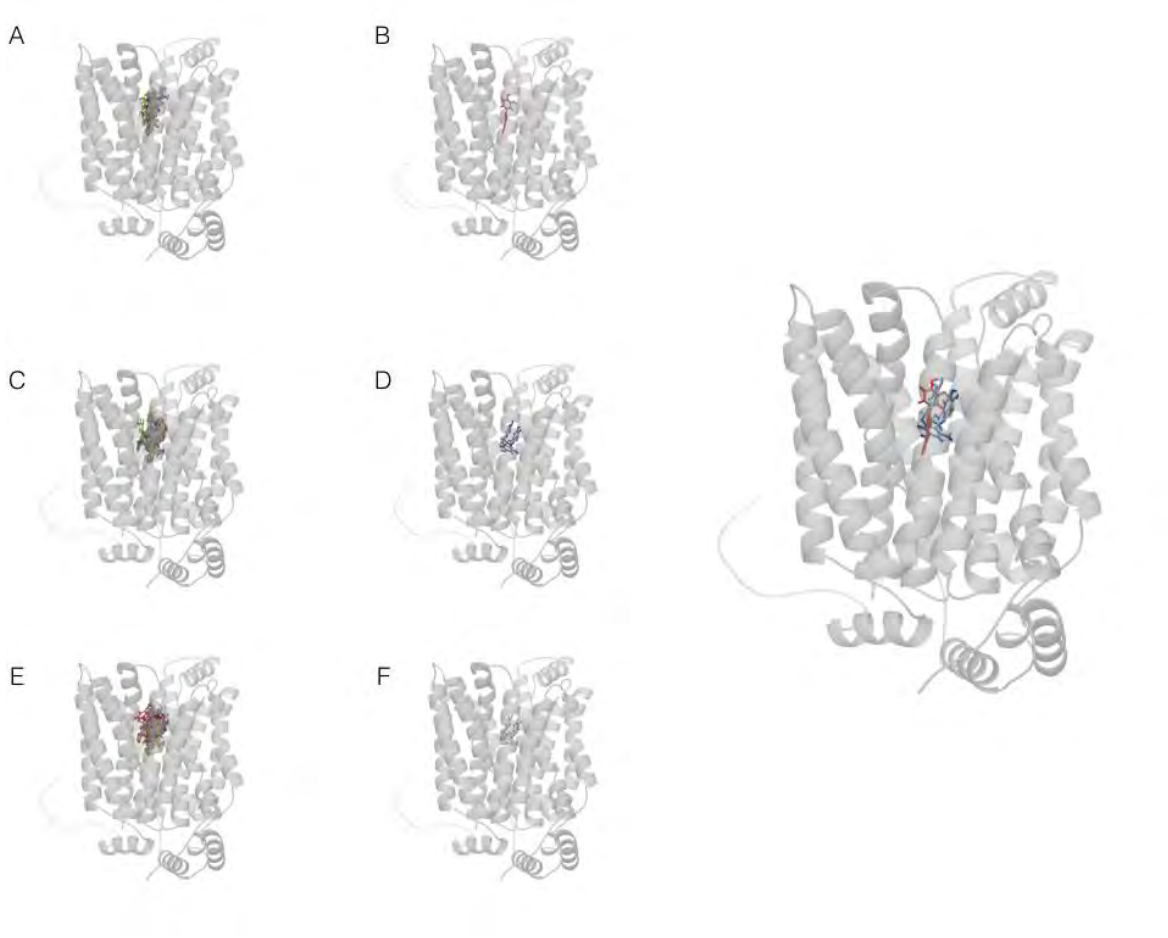

Figure 4.15: Docking positions of quercetin, ECG, and EGCG to the homology modeled GLUT1 e2 structure. Quercetin (A, B), ECG (C, D), and EGCG (E, F) to the homology modeled GLUT1 e2 structure. All docking poses are shown in panels A, C, and E for quercetin (30), ECG (30), and EGCG (30), respectively. The highest affinity pose is shown in panel B, D, and F for quercetin, ECG, and EGCG, respectively. Panel G shows the highest affinity poses for quercetin (red), ECG (blue), and EGCG (cyan) in one structure.

Discussion

Comparisons of the docking of cytochalasins to 5EQI and 4PYP demonstrate one of the main caveats to molecular docking to static structures. The docking analysis requires grid generation for the compound to encompass the binding site, accurate prediction of the ligand's positional, conformational and configurational space (pose) and scoring of the ligand:protein interaction. Additionally, the interaction is based on a static structure of a highly dynamic protein. While, docking of CB to the 5EQI structure faithfully reproduces the binding region it does not reproduce the ligand pose seen in the crystal structure (Figure 4.10). While, the docked ligand may not match the crystallographic position of the ligand, evaluating all of the potential conformations can generate a map of the binding pocket and testable hypothesis for amino acids involved in conferring affinity and specificity. Additionally, as demonstrated with β-D-glucose docking in chapter 2, it is necessary to incorporate biochemical data into the evaluation of the binding sites and docking poses.

The e1 conformation of GLUT1 has been crystalized with both glyco-detergent (4PYP), and CB (5EQI) in the transport pore (77,135). Molecular docking was undertaken with these structures by using the ligand as a guide molecule, in the case of 5EQI, and by choosing a grid based upon the residues lining the translocation pore with both 5EQI and 4PYP. Differences in docking between the conformations can be attributed to the change in pore size, change in ligand, or changes in the docking grid size due to the more specific grid localization using CB.

Cytochalasins were docked to both 4PYP and 5EQI. Analysis of CB docking to the 4PYP structure suggests important roles for residues in helices 4, 5, and 10 including W388 hypothesized to interact with CB (Figure 4.16) [186]. Similarly, the interaction map with CA follows a very similar pattern in side chain interactions, but a decrease in potential hydrogen

bonds resulting from the change from a hydroxyl to a ketone group in the macrocyclic ring, possibly explaining the decreased affinity seen with CA compared to CB CC, CJ and CE all have very high negative homo-cooperatively when compared to CB suggesting that binding of any of these ligands prevents binding of a second ligand. Examination of the interaction maps for CC, CE, CJ, suggest increased interactions in helices 1, 7, 8 and 11 suggesting that binding at this site may affect binding of a second cytochalasin molecule. Since GLUT1 e1 cannot dock two cytochalasins simultaneously, this must mean that binding one molecule of CC, CE, or CJ, affects binding of a second molecule to adjacent GLUT1-e1 conformers in the oligomeric complex. Docking to the 5EQI site utilized co-crystalized CB for grid generation. This CB docking analysis suggests interactions with residues in the glucose binding core (Q282, Q283, chapter 2) and in TMs 4, 5, 10 and 11 (Figure 4.17). Elimination of tryptophan in helices 10 and 11 (W388 and W412) eliminates CB photolabeling of GLUT1 suggesting these residues are important for CB binding [186]. Additionally, the presence of CB in the glucose binding core suggests that CB induced sugar occlusion must involve additional GLUT1 subunits in the oligomeric complex because this seems extremely unlikely to occur in individual monomers (119). Docking of additional cytochalasins to GLUT1 assumes that all of the cytochalasins bind at the same general site. CJ has the highest affinity and additional interactions with H2 and H7 and to N415 relative to CB. CE and CH have similar affinities to CB. CE has a similar docking interaction profile to CB with the main differences being decreased interactions at H11 (G408, W412). CH is also characterized by decreased interactions at H11 (G408, W412) but increased interactions in helices 5, 7, 8, and 10. CA has a slight increase in affinity and a decrease in potential hydrogen bonding resulting from the replacement of the hydroxyl group with a ketone. Of the cytochalasins examined, CC and CD have the lowest affinity for GLUT1 and increased

interactions with residues H8 (N317 and N321) in comparison to the other cytochalasins suggesting that the introduced acetyl group interacts with these residues. CB was also docked to the e2 structure with high affinity (GlideScore = -7.059) demonstrating the necessity of combining experimental determinations of ligand sidedness with computational modeling.

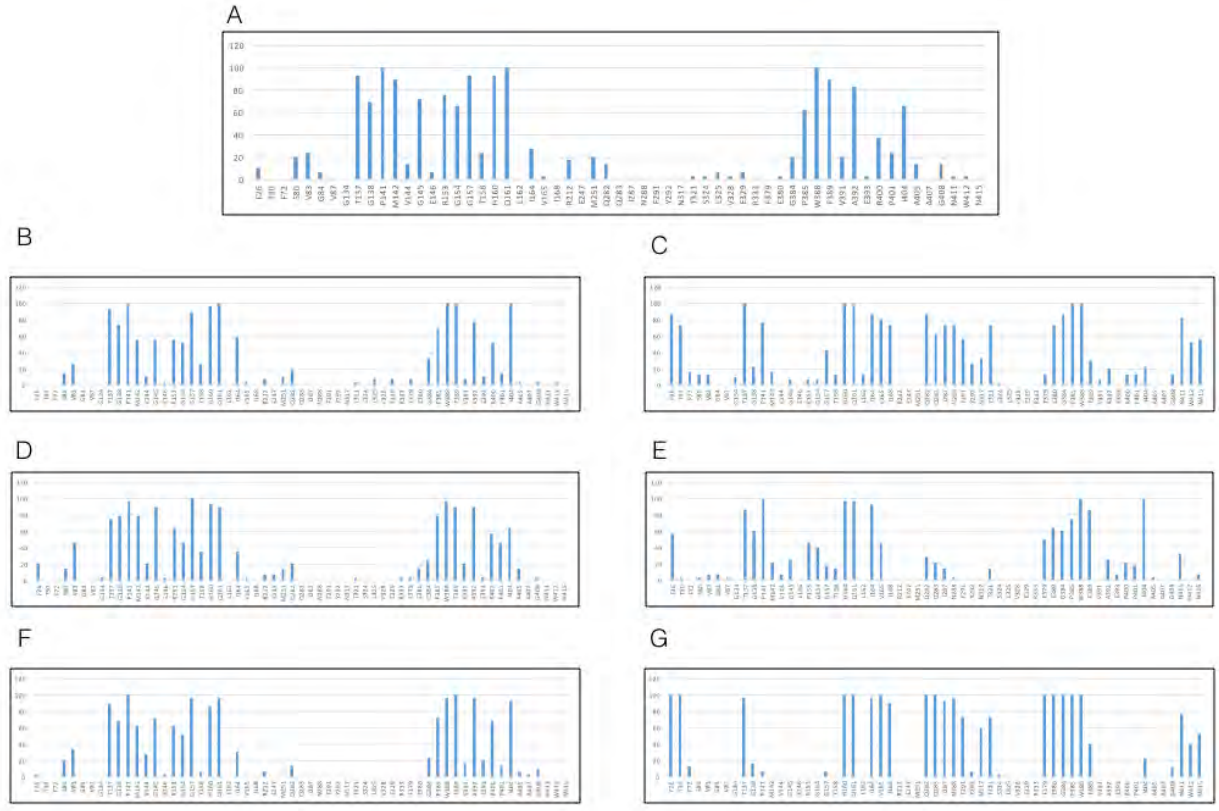

Figure 4.16: Quantitation of amino acid interactions with cytochalasins. CB (A), CA (B), CC (C), and CD (D), CE (E), CH (F), CJ (G) to the GLUT1 e1 structure 4PYP. Percentages are normalized to number of docking poses generated.

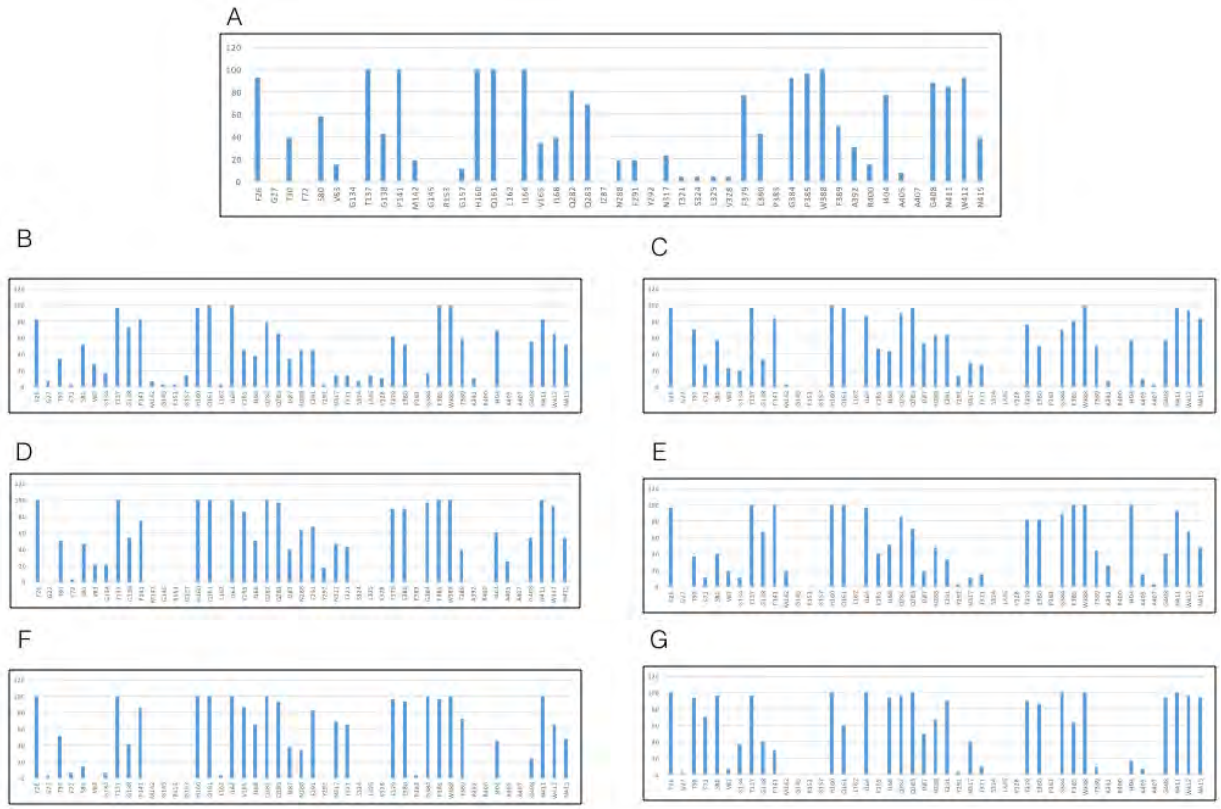

Figure 4.17: Quantitation of amino acid interactions with cytochalasins. CB (A), CA (B), CC (C), and CD (D), CE (E), CH (F), CJ (G) to the GLUT1 e1 structure 5EQI. Percentages are normalized to number of docking poses generated.

Forskolin and forskolin derivatives were only docked to the 4PYP structure. The forskolin binding pocket is characterized by interactions with H4 (T137), H5 (H160, Q161, I164), H7 (Q282, Q283, I287, N288) and H10 (F379, E380, G384, P385, W388) with potential hydrogen bonding to Q282 and W388 (Figure 4.18). Changing the ester group to an alcohol (7DeA-FSK) leads to an increase in both the calculated and experimentally determined affinity compared to forskolin and adds residues N288 and F291 to the potential binding pocket while increasing the hydrogen bonding potential in H10 (E380, W388) and H2 (H160, Q161). Adding a large benzyl fluoride group (7FPA-FSK) to the ester leads to an increase in affinity compared to forskolin while increasing potential interactions with helices 2, and 11 and decreasing interactions with H7. 7FPA-FSK also has fewer potential hydrogen bonds than forskolin. Converting a hydroxyl to an ester (6A-FSK) significantly decreases interactions with H7 while increasing interactions with H4 compared to forskolin. Potential hydrogen bonding to H160 is increased relative to forskolin. Docking of BAY-588 and BAY-876 to the cavity follows similar binding patterns. However, BAY-588 has more side chain interactions in helices 4 and 5 (Figure 4.17). Additionally, BAY-876 has potential hydrogen bonding via its cyano group with Q283 and N288. This is not observed in docked BAY-588 and may account for the increased affinity observed in BAY-876 compared to BAY-588. Calculated K_D for the highest affinity poses of suggests BAY-876 (K_D = 0.764 µM) has ~2-fold higher affinity than BAY-588 (K_D = 1.23 µM). However, when the highest affinity BAY-876 pose is matched to a BAY-588 (K_D = 7.85 µM) pose the change in calculated K_D is 10-fold (Table 4.1).

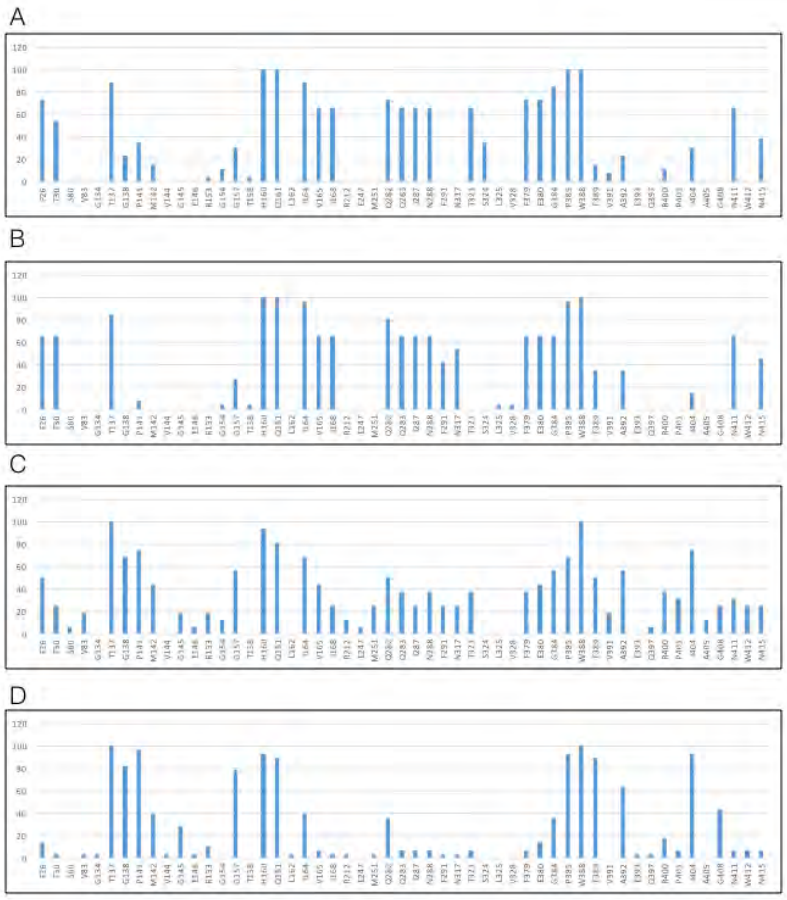

Figure 4.18: Quantitation of amino acid interactions with forskolins. Forskolin (A), 7DEA-FSK (B), 7FPA-FSK (C), and 6A-FSK (D) to the GLUT1 e1 structure 4PYP. Percentages are normalized to number of docking poses generated.

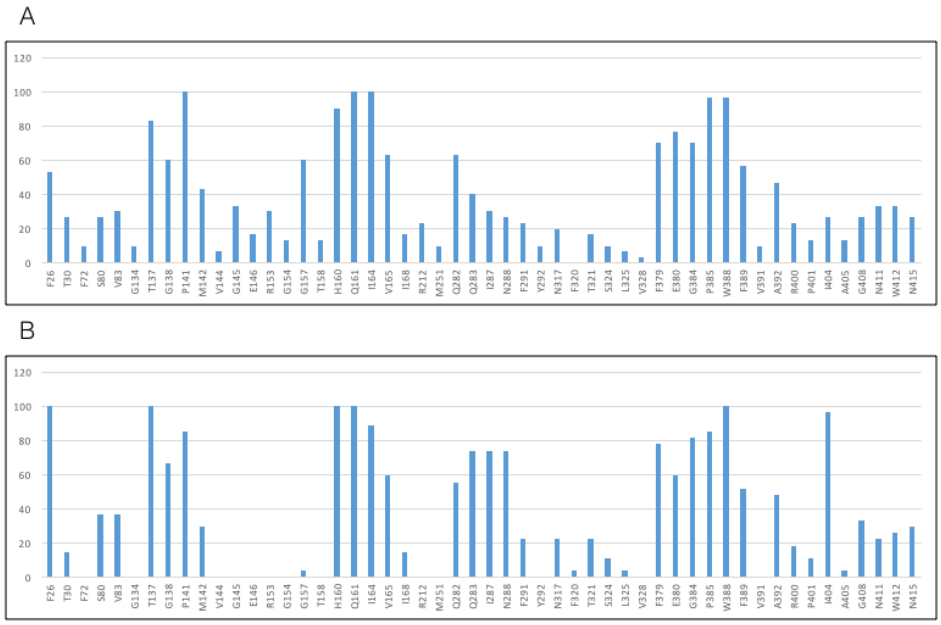

Figure 4.19: Quantitation of amino acid interactions with BAY588 and BAY876 to the GLUT1 e1 structure 4PYP. BAY588 (A) and BAY876 (B) Percentages are normalized to number of docking poses generated.

ATP and caffeine were docked to both the 5EQI structure and the 4PYP structure. Docking of ATP and caffeine to 4PYP suggests potential interactions with helices 5, 7, 10 and 11 (Figure 4.20). When compared to ATP, caffeine has fewer interactions with helices 5 and 10 suggesting that the methylxanthine ring is interacting with residues in helices 4 (T137), 7 (Q282, Q283, I287, N288), 10 (F379, W388) and 11 (N411, W412, N415). Additionally, GLUT1 helices 8 and 9 (residues 301-364) were identified as ATP interacting domains when photolabeled with

8-Azido[γ-^{32}P]ATP (184). Docking studies suggest that potential interaction sites with ATP in this conformation are at N317 and T321. ATP has a similar binding profile when docked to the 5EQI structure with additional potential interactions in helices 1, 2, and 8 and fewer potential interactions in H5. Caffeine follows the same pattern in both 4PYP and 5EQI with only an increase in potential interactions with N317 and fewer interactions with T137.

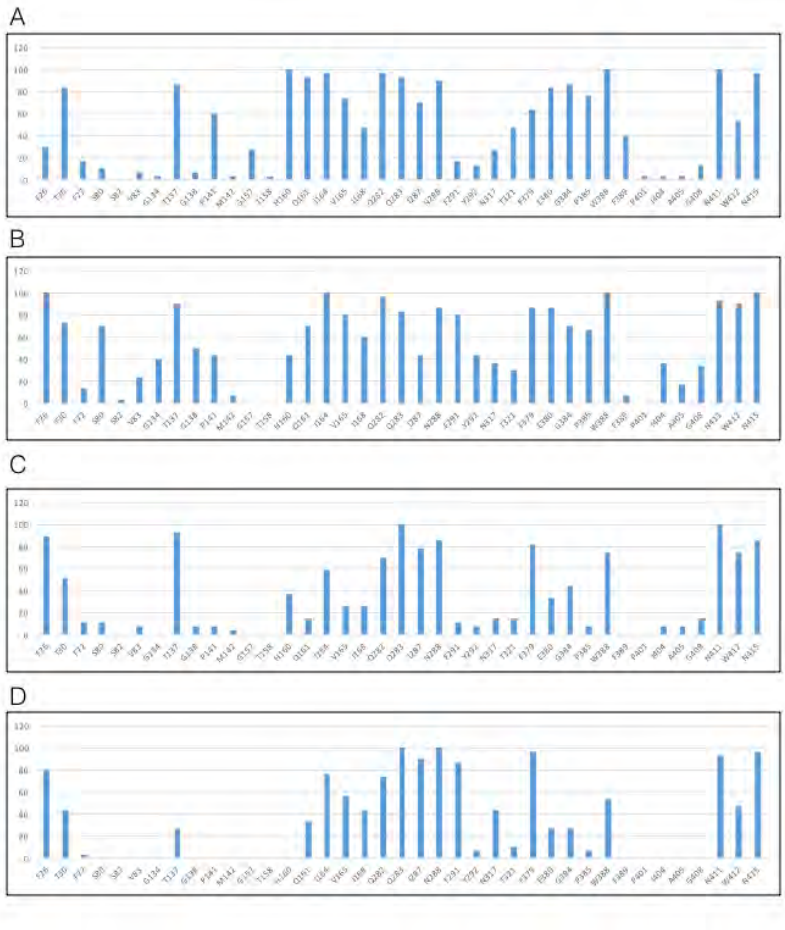

Figure 4.20: Quantitation of amino acid interactions with ATP and Caffeine to GLUT1 e1 structures. ATP to the GLUT1 e1 structures 4PYP (A) and 5EQI (B). Quantitation of amino acid interactions with caffeine to the GLUT1 e1 structures 4PYP (C) and 5EQI (D). Percentages are normalized to number of docking poses generated.

Maltose appears to bind to GLUT1 through potential H-bonding to Q282, Q283, N317, N380 and N415. Increasing the number of hexoses in the oligosaccharide leads to an increase in inhibition constant for GLUT1 mediated glucose transport, and a decrease in affinity for the oligosaccharide [78]. Examination of all of the docked poses suggests that when the size of the oligosaccharide increases there is a decrease in side chain interaction with H8 and H10 and an increase in interactions with helices 1, 2, and 11 (Figure 4.21). Additionally, potential hydrogen bonding is increased to residues in the N-terminal half of GLUT1 and decreases in the C-terminal half.

The high affinity of WZB117-GLUT1 interactions can be attributed to the large number of hydrogen bonds made including potential interactions with Q161, Q282, Q283, and N415. The substrate binding pocket can be defined most strongly with residues T30, F72, S73, I168, I287, F291, F379, and N415. (Figure 4.22). Quercetin and ECG have $K_{I(app)}$ of ~ 2µM while EGCG has lower affinity with $K_{I(app)}$ of 10 µM. Comparison of docking does poses does not explain the differences in affinity for ECG and EGCG (Figure 4.23).

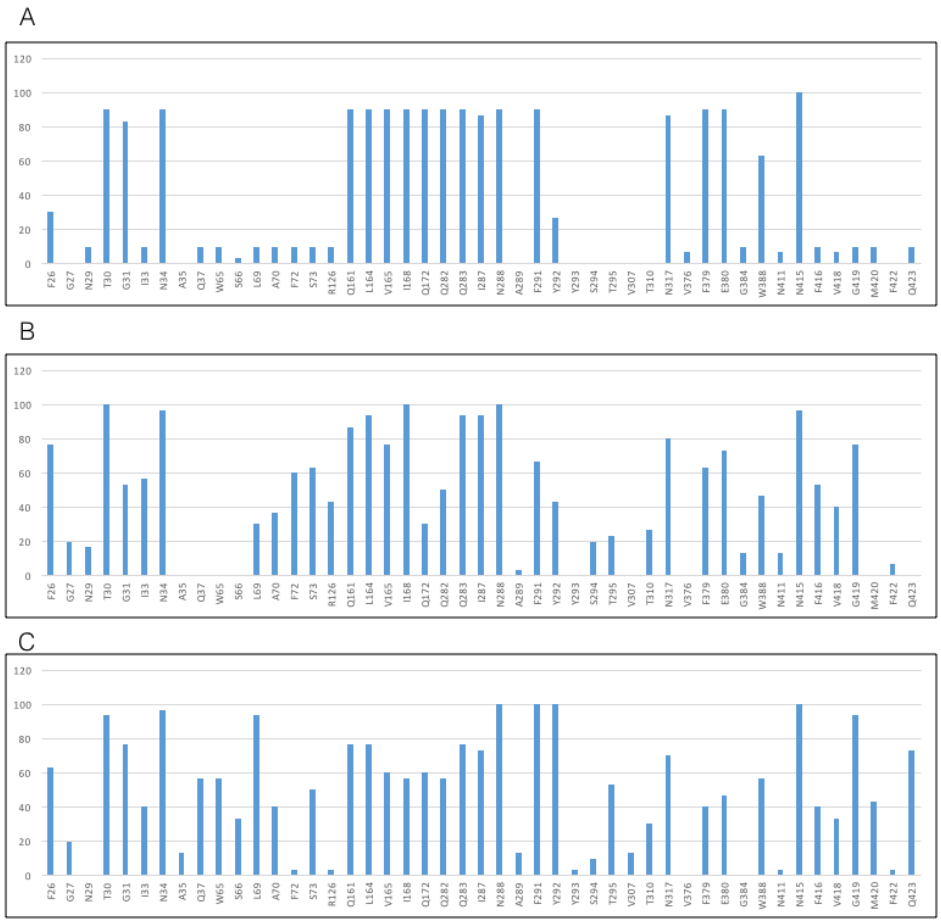

Figure 4.21: Quantitation of amino acid interactions with maltose, maltotriose, and maltotetraose to the homology modeled e2 structure. Maltose (A), maltotriose (B), and maltotetraose (C). Percentages are normalized to number of docking poses generated.

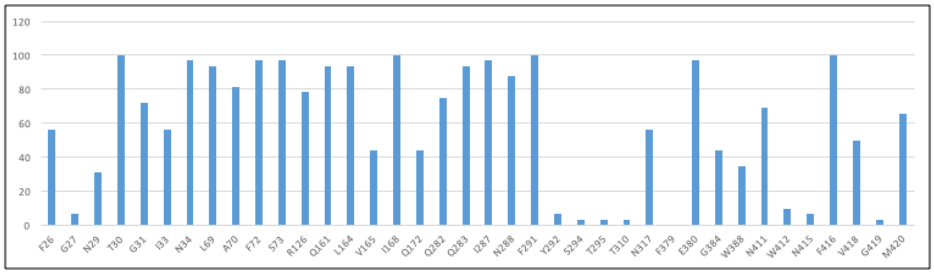

Figure 4.22: Quantitation of amino acid interactions with WZB117 to the homology modeled e2 structure. Percentages are normalized to number of docking poses generated.

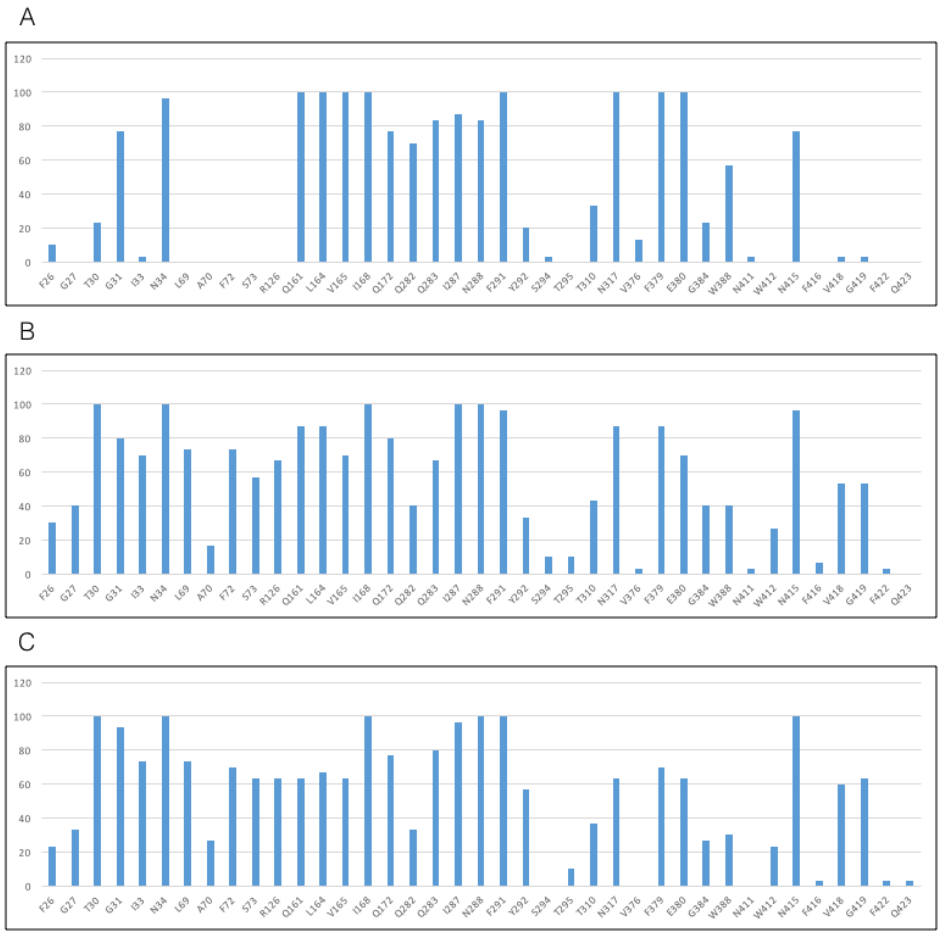

Figure 4.23: Quantitation of amino acid interactions with quercetin, ECG, and EGCG to the homology modeled GLUT1 e2 structure. Quercetin (A), ECG (B), and EGCG (C). Percentages are normalized to number of docking poses generated.

GLIDE software was developed to optimize ligand docking to rigid protein structures using co-crystallized ligand complexes as comparative standards(153,154). GlideScores for computed docking poses are useful for selecting the best docked poses but can under- or over-estimate ΔG by 2 kcal/mol (30-fold) (155). Interpretation of $K_{I(app)}$ for transport and ligand binding is extremely model-dependent and includes both binding, transport (catalytic), and allosteric constants. Comparisons between computed GlideScores and calculated affinity constants are summarized in Table 4.1. The WZB-117 pose best matches GlideScore with experimental affinity. When comparing similar compounds (BAY, FSK compounds) the relative affinities of the molecules matches without the calculated and experimental affinities being equal. Alternatively, the calculated affinities do not match the experimental affinities for the cytochalasins docked to either 5EQI or 4PYP, suggesting that determining cytochalasin affinity for GLUT1 less well predicted by GlideScore.

Table 4.1: Summary of Docked Ligands. Sidedness and experimental $K_{I(app)}$ for EGCG, ECG, Quercetin, BAY-588, and BAY-876 were determined by Ogooluwa Ojelabi and are unpublished. The GlideScore of the highest scoring pose were used for calculating K_D.

Ligand	Sidedness	Affinity	GlideScore kcal/mol 4PYP	GlideScore kcal/mol 5EQI	GlideScore kcal/mol e2	Calculated K_D µM 4PYP	Calculated K_D µM 5EQI	Calculated K_D µM e2
ATP	e1	$K_{D(app)}$ = 0.6-2 mM [86]	-7.192	-6.252	-	5.27	25.82	-
Caffeine	e1	$K_{I(app)}$ = 0.91 ± 0.34 mM [85]	-6.917	-6.645	-	8.39	13.29	-
Bay588	e1	$K_{I(app)}$ = 581.55 nM	-8.054	-	-	1.23	-	-
Bay876	e1	$K_{I(app)}$ = 13.15 nM	-8.335	-	-	0.76	-	-
Cytochalasin B	e1	$K_{D(app)}$ = 98 ± 8.5 nM [84]	-7.174	-7.607	-7.059	5.44	2.62	6.60
Cytochalasin A	e1	$K_{I(app)}$ = 815 ± 96 nM [84]	-6.163	-7.589	-	30.01	2.70	-
Cytochalasin C	e1	$K_{I(app)}$ = 1591 ± 431 nM [84]	-8.048	-8.413	-	1.24	1.87	-
Cytochalasin D	e1	$K_{I(app)}$ = 1969 ± 98 nM [84]	-6.482	-7.805	-	17.50	0.67	-
Cytochalasin E	e1	$K_{I(app)}$ = 99 ± 8 nM [84]	-6.64	-6.968	-	13.40	7.70	-
Cytochalasin H	e1	$K_{I(app)}$ = 98 ± 3 nM [84]	-6.304	-7.163	-	23.64	5.54	-
Cytochalasin J	e1	$K_{I(app)}$ = 12 ± 3 nM [84]	-8.979	-8.929	-	0.26	0.28	-
Forskolin	e1	$K_{D(app)}$ = 3282 ± 960 nM [84]	-5.93	-	-	44.48	-	-
6AFSK	e1	$K_{I(app)}$ = 949 ± 164 nM [84]	-5.982	-	-	40.74	-	-
7FPAFSK	e1	$K_{I(app)}$ = 142 ± 78 nM [84]	-6.228	-	-	26.88	-	-
7DeAFSK	e1	$K_{I(app)}$ = 2 ± 2 nM [84]	-7.5	-	-	3.13	-	-
Maltose	e2	$K_{D(app)}$ = 29.3 µM [78]	-	-	-6.215	-	-	27.48
Maltotriose	e2	$K_{D(app)}$ = 32.2 µM [78]	-	-	-6.472	-	-	17.80
Maltotetraose	e2	$K_{D(app)}$ = 128 µM [78]	-	-	-6.972	-	-	7.65
WZB117	e2	$K_{I(app)}$ = 0.233 ± 0.042 µM [149]	-	-	-8.647	-	-	0.45
EGCG	e2	$K_{I(app)}$ = 9.563 ± 1.80 µM	-	-	-8.428	-	-	0.65
ECG	e2	$K_{I(app)}$ = 1.902 ± 0.315 µM	-	-	-8.274	-	-	0.84
Quercetin	e2	$K_{I(app)}$ = 1.476 ± 0.337 µM	-	-	-7.51	-	-	3.08

In conclusion, molecular docking analysis is a useful tool for understanding the structural components of GLUT1 involved in ligand binding and glucose transport. It can be used to develop testable hypotheses of side chain interactions involved in ligand binding (chapter 2) and to explain biological phenomena (e.g. CB occlusion of glucose in GLUT1, changes in affinity of forskolin ligands based on side-chain interactions). Molecular docking can be used to predict interacting residues and binding pockets for similar ligands. However, differences in docking poses obtained using similar or even the same crystal structures demonstrate the necessity for undertaking biochemical experimentation to verify the interactions predicted by docking analysis. Similarly, incorporation of experimental knowledge into side-chain pose predictions (e.g. as with β-D-glucose, chapter 2) greatly improves the reliability of predictions.

Chapter 5:

Analysis of GLUT1 Transmembrane Domain Glycines

Research was supported using NIH Grants: DK36081 and DK44888

Abstract

GLUT1 catalyzes rapid, equilibrative glucose transport across the cell membrane. Kinetic and ligand binding studies have led to the development of multiple models for explaining GLUT1 mediated glucose transport. The alternating access carrier model proposes that the transporter alternately presents sugar import and export sites. Recent developments in membrane protein crystallography and the crystallization of GLUT1 and GLUT3 in inward and outward open conformations appear to confirm the alternating access carrier hypothesis. Understanding the transition between inward and outward open conformations would help to bridge the gap between kinetic and structural analyses. Transitions between the inward and outward conformations suggest that the N-terminal half of the protein is a rigid body while the C-terminal half of GLUT1 is a more dynamic structure. The N-terminal half of GLUT1 contains multiple GXXXG motifs which are hypothesized to enhance packing in trans-membrane alpha helices. Additionally, GLUT1 has highly dynamic glycine residues, possibly existing as hinges regulating the transition between inward and outward conformations. Combining this structural modeling with glycine-to-alanine mutagenesis suggests that several membrane-resident glycine residues play significant roles in GLUT1-mediated transport as either hinge glycines or GXXXG motifs.

Introduction

Glucose serves as the preferred metabolic substrate in brain and exercising skeletal muscle. Understanding the mechanism by which glucose enters and exits cells is critical to developing a further understanding of energy metabolism. Two families of proteins mediate glucose uptake into cells: the GLUTs and the SGLTs. SGLTs are active transporters that utilize an inwardly directed Na electrochemical gradient to couple net uphill glucose transport to downhill Na transport while the GLUTs are passive transporters that carry sugar down a concentration gradient only (13). The GLUTs are divided into three classes based upon tissue distribution and substrate specificity (100). GLUT1, a class I transporter, is a ubiquitously expressed glucose transporter and, in humans, is the primary glucose transporter in the blood brain barrier, glia and erythrocytes (187).

GLUT1 makes up 10-20% of the integral membrane content of erythrocytes where it is the only expressed glucose transporter (52). The availability of red cells combined with their high GLUT1 content, uniformity of cell size and surface area has resulted in a wealth of detailed kinetic analyses of GLUT1 mediated sugar transport and ligand binding (141). Recent structural studies of GLUTs suggest that the protein acts as an alternating access transporter, presenting either an inward open, e1, or outward open, e2 binding site at any time but not both sites simultaneously (77,134,135).

However, structural studies cannot fully explain the kinetic behavior of the transporter which functions as if it simultaneously presents multiple exofacial and endofacial substrate binding sites (79,83,113,120,122). A more detailed understanding of the physical basis of transitions between the GLUT1 e1 and e2 conformations could provide further insight into the transport cycle. To that end, identification of conformationally dynamic residues in the

transmembrane alpha helices and exploration of their roles by mutagenesis could be an intriguing path of research.

Due to its lack of a side chain, glycine is a unique amino acid that introduces conformational flexibility into the backbone of a protein. Wide scale genome analysis of membrane resident proteins shows that glycine is frequently found in transmembrane helices, including in conserved positions (188,189). Different studies have shown glycine(s) fulfilling both structural and functional roles in membrane transport proteins. Glycine residues have been shown to function as a gating hinge in potassium channels (190,191). Introduction of glycine into lactose permease can confer conformational flexibility (192), and a conserved glycine in GAT-1 is involved in conformational transition during its transport cycle (193). By contrast, glycine-rich-motifs in transmembrane domains have been shown to enhance packing and oligomerization, such as the GXXXG and GXXXXXXG motifs (194-196).

GLUT1 contains 41 (8.3% of total amino acids) glycine residues with 31 (9.2% of transmembrane domain resident amino acids) residing in transmembrane regions. Eight glycines, six in transmembrane regions, are 100% conserved across the 14 members of the GLUT family. GLUT1 structure can be divided into two symmetrical halves with the halves separated by a large intracellular loop. These halves are thought to have arisen through a gene duplication event (197,198). GLUT1 contains 6 GXXXG packing motifs (H1 (2), H2, H4 (2), H5) and 2 GXXXXXXG packing motifs (H1, H4). Interestingly while the first half of GLUT1 contains 8 packing motifs, the second half which contains the oligomerization domain H9 does not contain any packing motifs. To analyze the conformationally dynamic residues we mutated glycine with Δ dihedral angles (phi/psi > 20°) to alanine. Additionally, we mutated the GXXXG domains and all glycine residues that are 100% conserved to alanine.

Our results identify several membrane-resident glycine residues that support GLUT1-mediated catalysis either by serving as hinge glycines or through their role as helix-stabilization GXXXG motifs.

Experimental Procedures

Reagents

[^{3}H]-2-deoxy-D-glucose ([^{3}H]-2DG) was purchased from American Radiolabeled Chemicals (St. Louis, MO). HEK-293 cells were purchased from ATCC. DPBS, DMEM, carbenicillin, Lipofectamine 2000, NuPage BisTris gels and MES buffer were obtained from Life Technologies. Unlabeled 2DG, Maltose, Cytochalasin B (CB), and phloretin were purchased from Sigma-Aldrich (St. Louis, MO). All primers were purchased from Integrated DNA Technologies. HiSpeed Maxi Kits were from Qiagen. QuikChange Multisite-directed Mutagenesis kits were obtained from Agilent. PVDF membranes were obtained from ThermoFisher. Bovine serum albumim was from American Bioanalytical. Protease inhibitor mixture tablets were from Roche Applied Science. SuperSignal Pico West, NeutrAvidin Gel, micro-BCA kits, spin columns, and EZ-Link Sulfo-NHS-ss-Biotin were from Pierce.

Solutions

Solubilization buffer comprised PBS medium with 0.5% Triton X-100 and 5 mM $MgCl_2$. Stop solution comprised ice-cold PBS-Mg medium plus CB (CB; 10 μM) and phloretin (100 μM). Sample buffer contained 0.125 M Tris-HCl (pH 6.8), 4% SDS, 20% glycerol, and 50 mM DTT. Transfer buffer comprised 12 mM Tris base, 96 mM glycine, 20% methanol.

Antibodies

A goat polyclonal antibody anti-GLUT4 C-terminal residues 480–492 (Santa Cruz G1416) was used at 1:10,000 dilution as described previously (86). Horseradish peroxidase-conjugated

donkey anti-goat secondary antibody (Jackson ImmunoResearch) was used at 1:50,000 dilution.

Tissue Culture

HEK293 cells were maintained in Dulbecco's modified Eagle's medium (DMEM) supplemented with 10% fetal bovine serum, 100 units/mL penicillin, and 100 μg/mL streptomycin in a 37 ℃ humidified 5% CO_2 incubator as described previously (149). All experiments were performed with confluent cells. Plates were subcultured into 12-well plates at a ratio of 1:2-1:5 2-4 days prior to transfections. Passages 4-20 were used for all experiments.

Mutagenesis

GLUT1-encoding cDNA was inserted into the EcoRV-NotI restriction sites of PCDNA 3.1(+). As described previously (140), the C-terminal 13 amino acids of this GLUT1 construct are substituted using the C-terminal 13 amino acids of GLUT4 to facilitate detection of heterologously expressed GLUT1 against a low level background expression of endogenous GLUT1. Mutagenesis was as described previously (116) using QuikChange Multi-site-directed Mutagenesis kits and was verified by sequencing. The GLUT1 construct in which H9 is substituted with GLUT3 H9 sequence was described previously (140)**.**

Transient Transfection

Cells (70-90% confluence) were transfected with 2 μg (12 well plates) or 5 μg of DNA per well (6 well plates). Transfections were performed 36-48 hr prior to analysis of sugar uptake or protein expression. Sugar uptake and cell-surface biotinylation measurements were performed in tandem. GLUT1 and GLUT1 glycine mutations GLUT c4 DNA heterologous expression in HEK293 cells was as described previously (116,140).

Cell-Surface Expression Measurements

Three days post-transfection, 6-Well plates of HEK cells were washed twice with ice-cold

PBS and incubated on ice with ice-cold PBS containing 5 mM EZ-Link Sulfo-NHS-ss-Biotin for 30 min with gentle rocking. Reactions were quenched by adjusting each well to 12.5 mM Trizma (Tris base). Cells were harvested, re-suspended in biotin lysis buffer, and lysates were bound to Neutravidin Gel in spin columns according to kit instructions. Protein was eluted from spin columns using reductant, the eluate protein concentration was determined spectrophotometrically. Normalized loads were analyzed by Western blotting.

Western Blotting

GLUT1 expression in whole cell lysates and cell surface expression by biotinylation were analyzed by western blot as previously described (73). Total and isolated biotinylated proteins were normalized for total protein concentration by BCA and resolved by SDS-PAGE on a 10% NuPage gel in NuPage running buffer. Gels were transferred onto PVDF membranes blocked with 3% bovine serum albumin in PBS-T, probed with primary antibody overnight at 4 °C, probed with secondary antibody for 1 hr at room temperature, and developed using SuperSignal Pico West Chemiluminescent substrate. Blots were imaged on a FujiFilm LAS-3000 and relative band densities were quantitated using ImageJ32 software.

2-deoxy-D-glucose Uptake

2-deoxy-D-glucose (2-DG) uptake was measured as described previously (140). Briefly, 36-48 hr post transfections, confluent 12-well plates of HEK-293 cells were serum- and glucose-starved for 2 hr at 37 °C in FBS and penicillin/streptomycin-free DMEM lacking glucose. Cells were washed with 1.0 mL of DPBS-Mg at 37 °C for 15 min, then exposed to 0.4 ml of [^{3}H]2-DG uptake solution at various 2-DG concentrations (0.1 - 20 mM) for 5 min at 37°C. Uptake was stopped by addition of 1 ml of ice-cold stop solution. Cells were washed twice with ice-cold stop solution and lysed with Triton lysis buffer. Total protein content was analyzed in duplicate by

BCA. Each sample was counted in duplicate by liquid scintillation spectrometry. Each mutant was analyzed in triplicate on at least 3 separate occasions.

Homology Modeling

We modeled GLUT1 e2 open using the human GLUT3 (4ZWC) structure. We removed ligands and used chain A as the template for each modeled structure. Sequence alignments were generated using ClustalX. Homology models were built using Modeller-9.9 and analyzed using PROCHECK. The GLUT1 e1 structure (4PYP (77)) was used directly.

Results

Homology Modeled GLUT1 structures

GLUT1 and GLUT3 structures have been described previously (77,134). The current study presents and interrogates the e2 open homology-modeled GLUT1 structure and the e1 open GLUT1 crystal structure. A compelling argument can be made for the alternating access model for facilitative sugar transport simply from inspection of the outward and inward conformations of GLUT1 (Figure 5.1). These conformations suggest a striking physical correspondence to the proposed kinetic intermediates of the alternating access carrier's catalytic cycle named e2 and e1 (99,124,145), argue strongly for sugar movements through a central translocation pore and are henceforth termed GLUT1-e2, and GLUT1-e1. The transporters exist as a 12 transmembrane (TM) domain protein where the first 6 TMs of the N-terminal half are separated from the C-terminal half by a large intracellular loop. Analysis of conformational changes between the e2 and e1 conformations suggest the N-terminal half exists as a rigid body while the C-terminal half is more dynamic.

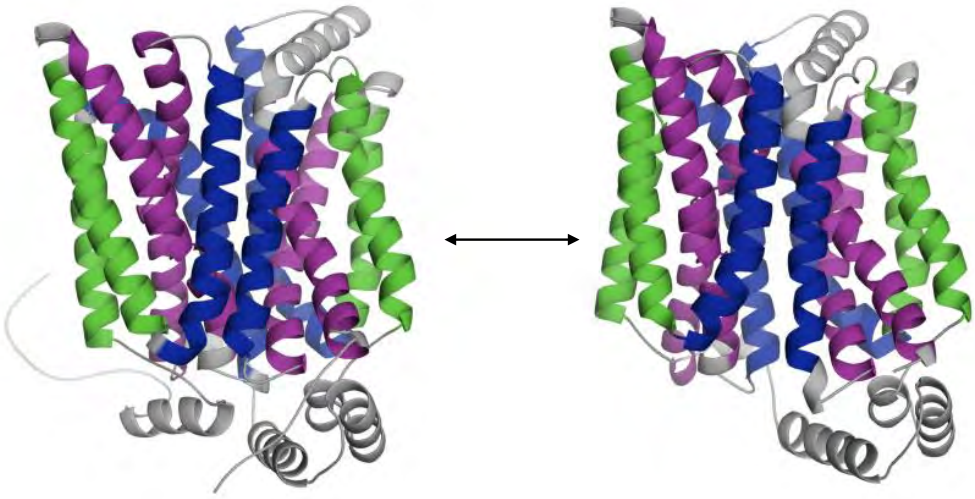

Figure 5.1: GLUT1 e2 and e1 structures. Transmembrane domains are colored such that the pore forming TMs 1, 4, 7, and 10 are pink, and 2, 5, 8, 11 are blue. The scaffold TMs 3, 6, 9, and 12 are green.

Backbone Dynamics in Transmembrane Domains

Amino acids in alpha helices have (Φ/Ψ) angles of (-64 ± 7º, -41 ± 7º). However, glycine due to its lack of a side chain does not generally follow these constraints and can be more conformationally dynamic. Analysis of the Δ(Φ/Ψ) between the e2 and e1 open conformations of GLUT1 suggests highly dynamic alpha-helical regions between the outward and inward open conformations (Figure 5.2).

GLUT Sequence Analysis

The GLUTs are divided into three classes based upon sequence alignments: class I: GLUT1-4, GLUT14; class II GLUT5, 7, 9, and 11, and class III, GLUT6, 8, 10, 12, and 13. Sequence alignments show varying degrees of glycine conservation across the 14 GLUTs ranging from 7% to 100% conserved. Sequence alignments of GLUTs reveal that 6 transmembrane resident glycine residues are 100% conserved and these are located in TM1 (G27), TM4 (G130), TM5 (G154, G167), TM7 (G286) and TM10 (G382) (Figure 5.3).

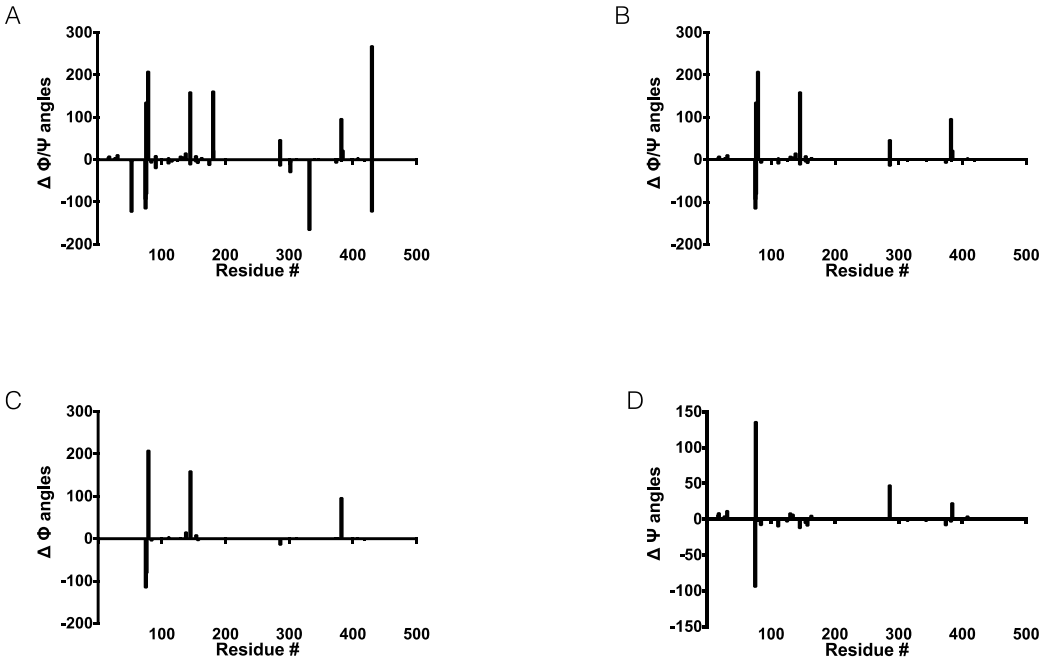

Figure 5.2: Δ Φ/Ψ angles in GLUT1 glycine calculated between GLUT1-e1 and GLUT1-e2. Δ is calculated as e1 angle minus e2 angle. A. ΔΦ/Ψ angles for all glycines. B. ΔΦ/Ψ angles for transmembrane domain glycines. C. ΔΦ angles for transmembrane domain glycines. D. ΔΨ angles for transmembrane domain glycines.

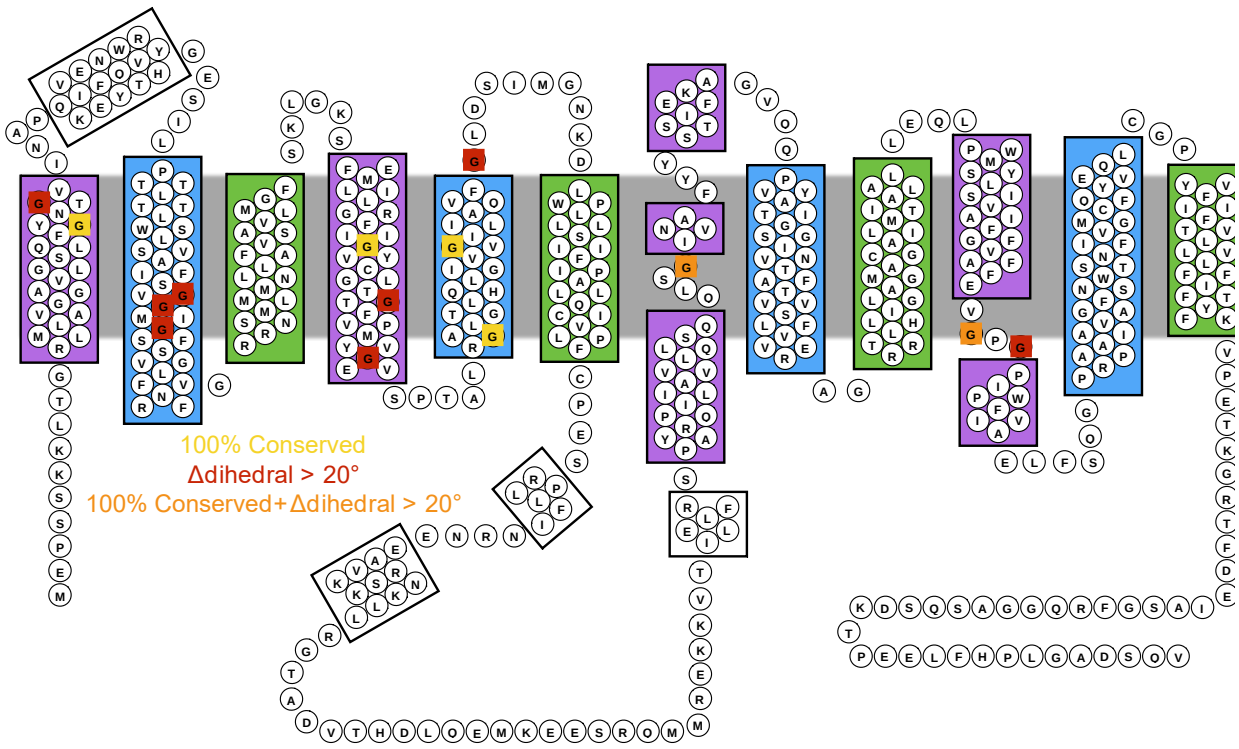

Figure 5.3: GLUT1 topology based off of the 4PYP crystal structure. The amphipathic transport pore domains are colored in purple and blue. The hydrophobic, scaffold domains are colored in green. Glycines that are conserved in all GLUTs are yellow. Glycines where either the Φ or Ψ angle change by > 20° between e1 and e2 conformations are colored red. 100% conserved glycines with Δ Φ/Ψ > 20° are colored orange.

Mutagenesis of Δ(Φ/Ψ) Mutants

Examination of alpha-helix residues with a $\Delta(\Phi/\Psi) > 20°$ for either the Φ or Ψ angles identifies residues in TM1 (G31), TM2 (G75, G76, G79), TM4 (G138, G145) TM5 (G175), TM7 (G286), and TM10 (G382, G384) (Figure 5.4). Mutation of G76 and G384 to alanine had the most pronounced effect on cell surface normalized (Table 5.1) 2DG uptake (Table 5.2). Mutation of G76 to alanine resulted in a decrease in uptake to 29.7 ± 5.9% compared to wtGLUT1. Mutation of G384 to alanine resulted in a decrease in uptake to 22.2 ± 6.5 % of wtGLUT1 uptake.

Mutagenesis of Conserved Glycines

Mutagenesis of the 6 conserved glycines, reveals that the G130A mutation has the greatest impact on transport, decreasing cell-surface expression normalized (Table 5.1) 2DG uptake (at 0.1 mM sugar) to 23.6 ± 5.9% of wtGLUT1. Mutation of G27 to alanine reduces uptake to 33.1 ± 5.9% of wtGLUT1 uptake while the G154A mutation reduces uptake to 44.2 ± 6.5% of wtGLUT1 uptake (Figure 5.5). The G167A, G286A and G382A mutations reduce uptake by a less substantial amount.

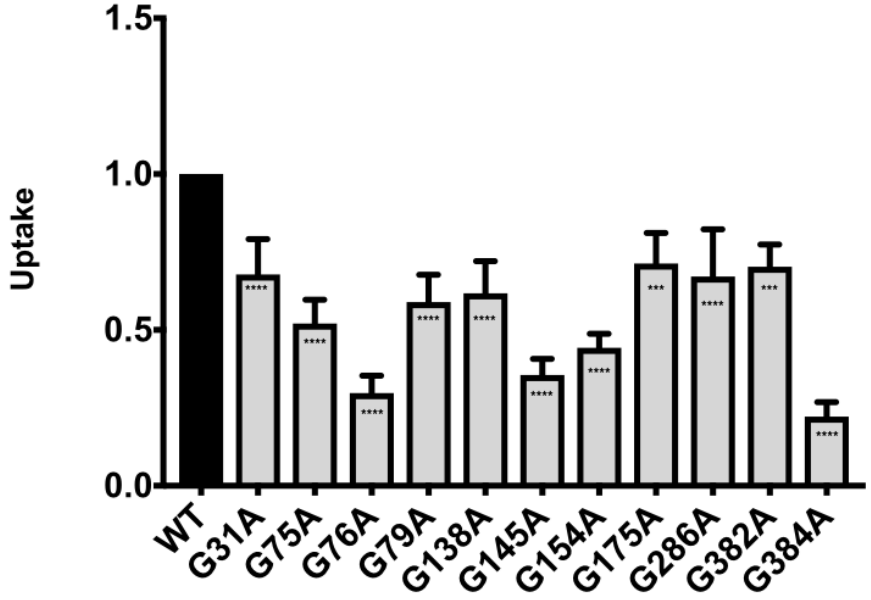

Figure 5.4. Measurement of 2DG uptake in wtGLUT1 and glycine point mutants where Δ Φ/Ψ is > 20°. Uptake is adjusted to cell-surface expression. One-way ANOVA between WT and mutant was performed to determine statistical significance. p value < 0.0001 = **** and p value between 0.0001 and 0.001 = ***.

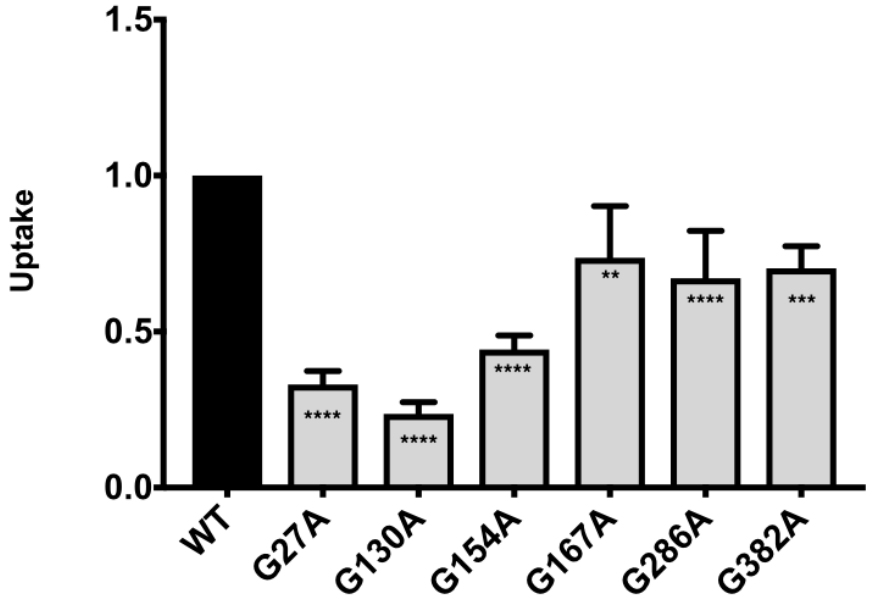

Figure 5.5: Measurement of uptake of 2DG into HEK cells transfected with wtGLUT1 or GLUT1 glycine mutants where the glycine is 100% conserved across the GLUT family.

2DG uptake is normalized to cell-surface expression. One-way ANOVA between WT and mutant was performed to determine statistical significance. p value < 0.0001 = ****, p value between 0.0001 and 0.001 = ***, and p value between 0.001 to 0.01 = **.

Mutagenesis of GXXXG Residues

GXXXG domains promote helix packing and protein-protein interactions [194-196]. GLUT1 contains 6 such motifs in its N-terminal half (Figure 5.6). Mutagenesis of these glycines to alanine and its impact on cell surface expression normalized (Table 5.1) 2DG uptake are summarized in Figure 5.7. G18A, G22A, and G134A were not explored. G163A was constructed but cell-surface biotinylation measurements were unsuccessful. Mutation of G31, G75, G79, G138, G163, or G167 to alanine decrease cell-surface expression normalized 2DG uptake by less than 50% of wtGLUT1. However, mutation of G27, G130, and G145 inhibit cell surface expression-normalized 2DG uptake by 67 ± 5.9%, 76 ± 5.9 % and 64 ± 6.5% respectively.

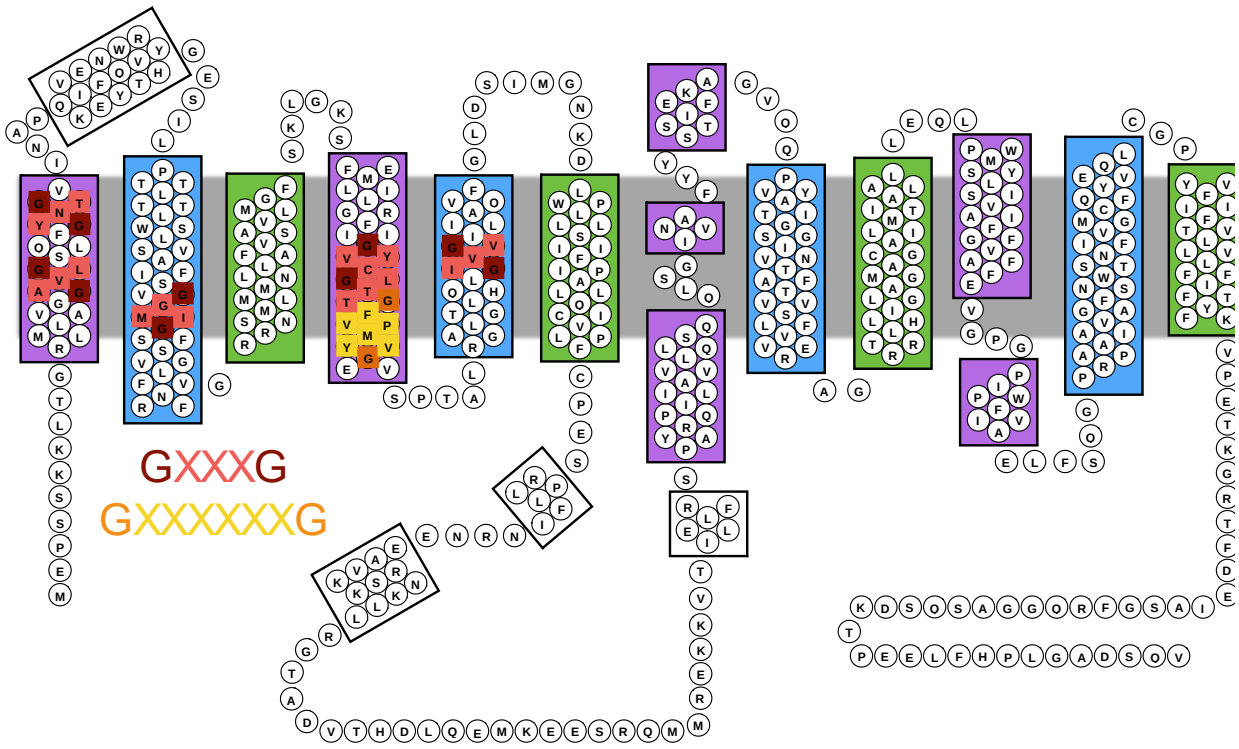

Figure 5.6: GLUT1 topology based off of the 4PYP crystal structure. The amphipathic transport pore domains are colored in purple and blue. The hydrophobic, scaffold domains are colored in green. Glycines in GXXXG motif are colored maroon, while residues comprising the XXX are pink. Glycines in GXXXXXXG motif are colored orange while residues comprising the XXXXXX are yellow.

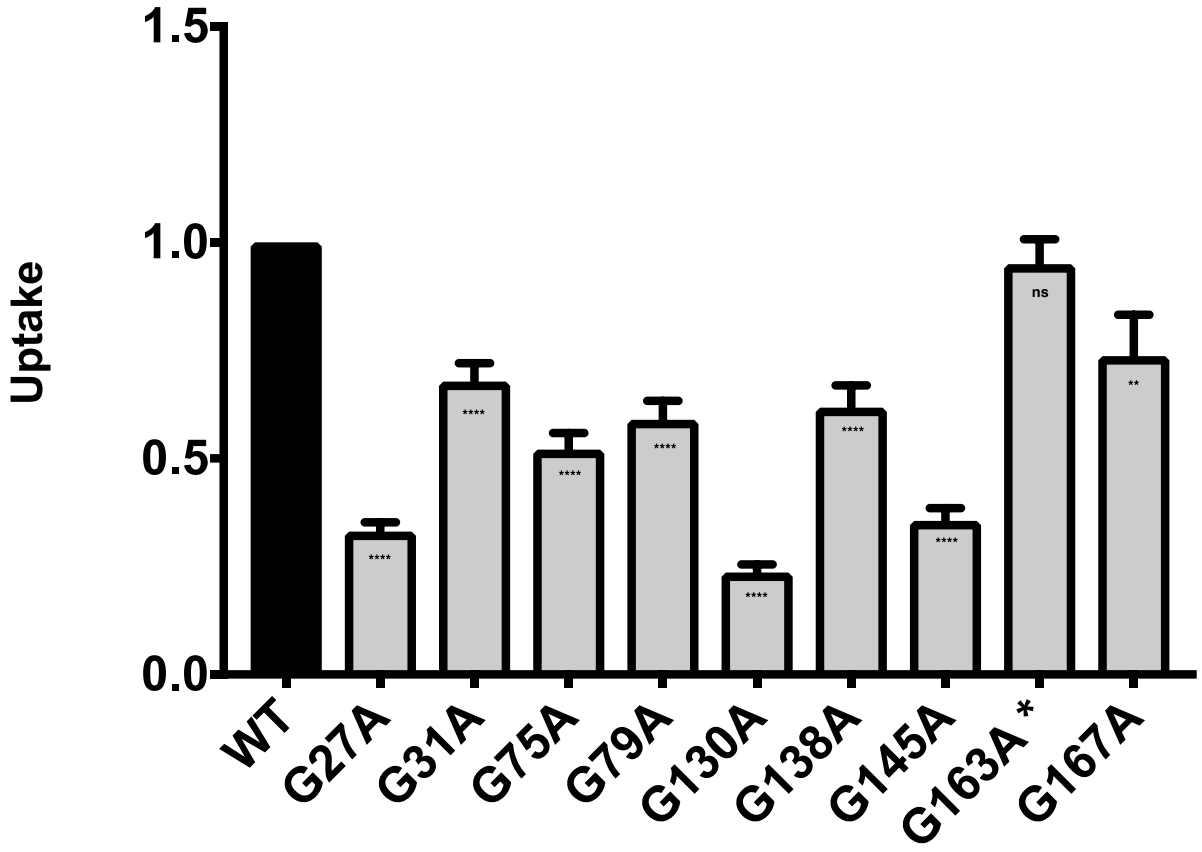

Figure 5.7. Measurement of 2DG uptake in wtGLUT1 and GXXXG glycine point mutants. G18A, G22A, and G134A were not measured. G163A does not have cell-surface biotinylation measured. One-way ANOVA between WT and mutant was performed to determine statistical significance. p value < 0.0001 = ****, p value between 0.0001 and 0.001 = ***, and p value between 0.001 to 0.01 = **.

Table 5.1: Cell Surface Expression of Glycine Mutants. The quantification of western blots of cell surface biotinylated wtGLUT1 and GLUT1 glycine mutants are listed. Each average is computed from three separate experiments. Results are normalized to wtGLUT1 expression.

Sample	Average Cell Surface Expression
WT	1
G27A	2.76026735
G31A	1.15914591
G75A	1.50370343
G76A	1.52999604
G79A	1.33965169
G130A	1.92409894
G138A	1.22494908
G145A	1.99651374
G154A	1.66175401
G167A	1.30768416
G175A	1.16212615
G286A	1.32601458
G312A	1.00381441
G382A	1.44598959
G384A	1.94188772

Michaelis Menten Kinetics of Transport by Glycine Mutants.

The concentration dependence of the initial rate of 2DG uptake by HEK293 cells expressing wtGLUT1 or GLUT1 expressing glycine to alanine mutants is well approximated by Michaelis-Menten kinetics. The steady-state kinetics of 2DG uptake were measured for G27A, G31A, G75A, G76A, G130A, G138A, G154A, G286A, G312A, and G384A. Uptake was normalized to cell-surface expression and compared to simultaneous measurements of 2DG uptake in wtGLUT1. A minimum of two dose responses was carried out for each mutant. The data presented in Figures 5.8. 5.9, 5.10, and 5.11 show the average of all measurements for each mutant while paired two- or one-tailed T-tests were carried out to compare $K_{m(app)}$ and V_{max} in each individual uptake measurement. G31A, G75A, G138A, G154A, G286A, and G312A mutations do not show statistically significant differences for either $K_{m(app)}$ or V_{max} when using either two-tailed or one-tailed T-tests (Figure 5.8). G75A and G130A show an increase in $K_{m(app)}$ and a decrease in V_{max} (Figure 5.9). G27A shows a decrease in V_{max} and no statistically significant change in $K_{m(app)}$ (Figure 5.10). Mutation of G384 to alanine decreases V_{max} but has no significant effect on $K_{m(app)}$ (Figure 5.11).

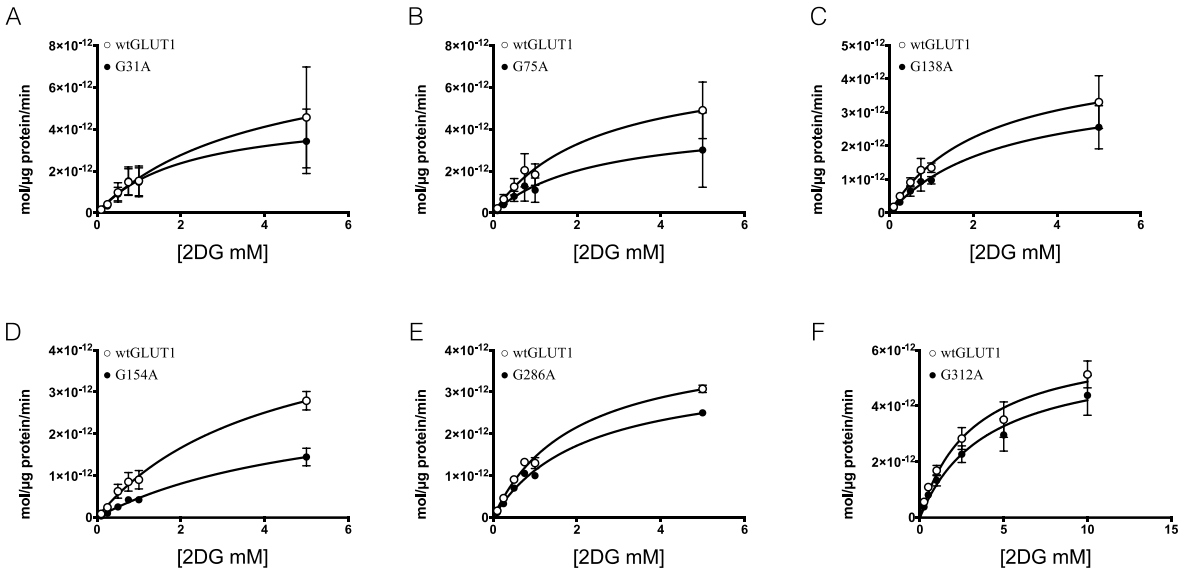
A
wtGLUT1
G31A
mol/µg protein/min
[2DG mM]
B
wtGLUT1
G75A
mol/µg protein/min
[2DG mM]
C
wtGLUT1
G138A
mol/µg protein/min
[2DG mM]
D
wtGLUT1
G154A
mol/µg protein/min
[2DG mM]
E
wtGLUT1
G286A
mol/µg protein/min
[2DG mM]
F
wtGLUT1
G312A
mol/µg protein/min
[2DG mM]

Figure 5.8: Net 2DG dose responses for glucose uptake into wtGLUT1 (○) and glycine mutants (●). A. Uptake of wtGLUT1 ($K_{m(app)}$ = 3.821 ± 3.811 mM; V_{max} = 8.04x10^{-12} ± 4.353x10^{-12} mol/mg protein/min) and G31A ($K_{m(app)}$ = 2.11 ± 1.482 mM; V_{max} = 4.874x10^{-12} ± 1.635x10^{-12} mol/mg protein/min). B. Uptake of wtGLUT1 ($K_{m(app)}$ = 2.429 ± 1.314 mM; V_{max} = 7.263x10^{-12} ± 1.927x10^{-12} mol/mg protein/min) and G75A ($K_{m(app)}$ = 2.399 ± 2.477 mM; V_{MAX} = 4.432x10^{-12} ± 2.232x10^{-12} mol/mg protein/min). C. Uptake of wtGLUT1 ($K_{M(app)}$ = 2.251 ± 0.8074 mM; V_{max} = 4.784x10^{-12} ± 8.292x10^{-13} mol/mg protein/min) and G138A ($K_{m(app)}$ = 2.664 ± 1.102 mM; V_{max} = 3.912x10^{-12} ± 8.083x10^{-13} mol/mg protein/min). D. Uptake of wtGLUT1 ($K_{m(app)}$ = 4.095 ± 1.166 mM; V_{max} = 5.069x10^{-12} ± 7.978x10^{-13} mol/mg protein/min) and G154A ($K_{m(app)}$ = 5.488 ± 2.051 mM; V_{max} = 3.033x10^{-12} ± 6.782x10^{-13} mol/mg protein/min). E. Uptake of wtGLUT1 ($K_{m(app)}$ = 1.938 ± 0.1993 mM; V_{max} = 4.253x10^{-12} ± 2.057x10^{-13} mol/mg protein/min) and G286A ($K_{m(app)}$ = 2.152 ± 0.224 mM; V_{max} = 3.569x10^{-12} ± 1.78x10^{-13} mol/mg protein/min). F. Uptake of wtGLUT1 ($K_{m(app)}$ = 3.114 ± 0.9515 mM; V_{max} = 6.384x10^{-12} ± 7.873x10^{-13} mol/mg protein/min) and G312A ($K_{m(app)}$ = 3.96 ± 1.577 mM; V_{max} = 5.868x10^{-12} ± 1.022x10^{-12} mol/mg protein/min). Measurements for this mutant were made 0.25-10 mM 2DG.

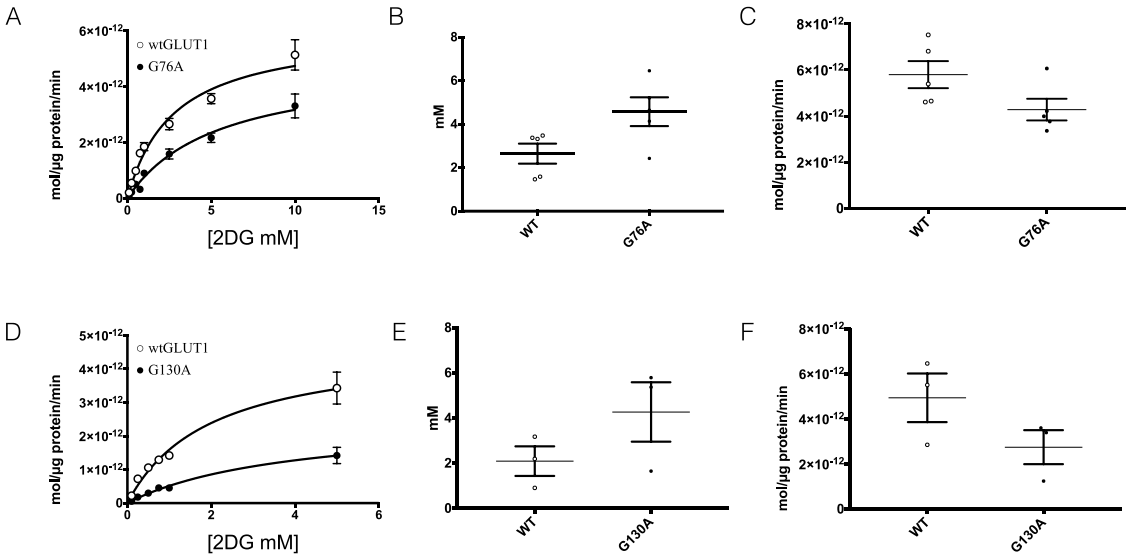
A
B
C
D
E
F
wtGLUT1
G76A
G130A
mol/µg protein/min
[2DG mM]
mM
WT
G76A
G130A

Figure 5.9: Net 2DG dose responses for glucose uptake into wtGLUT1 (○) and glycine mutants (●). A. Uptake of wtGLUT1 ($K_{m(app)}$ = 2.745 ± 0.4961 mM; V_{max} = 6.042x10^{-12} ± 4.481x10^{-13} mol/mg protein/min) and G76A ($K_{m(app)}$ = 5.382 ± 1.379 mM; V_{max} = 4.878x10^{-12} ± 6.326x10^{-13} mol/mg protein/min). B. The results of 5 separate experiments are shown as scatter dot plots for $K_{m(app)}$ for G76A. Results are shown as mean ± SEM. Paired t-test analysis indicates that $K_{m(app)}$ increases 2-fold (p = 0.0324). C. The results of 5 separate experiments are shown as scatter dot plots for V_{max} for G76A. Results are shown as mean ± SEM. Paired t-test analysis indicates that V_{max} decreases (p = 0.0062). D. Uptake of wtGLUT1 ($K_{m(app)}$ = 1.985 ± 0.4394 mM; V_{max} = 4.752x10^{-12} ± 4.968x10^{-13} mol/mg protein/min) and G130A ($K_{m(app)}$ = 3.932 ± 1.399 mM; V_{max} = 2.529x10^{-12} ± 4.923x10^{-13} mol/mg protein/min). E. The results of 3 separate experiments are shown as scatter dot plots for $K_{m(app)}$ for G130A. Results are shown as mean ± SEM. Paired t-test analysis indicates that $K_{m(app)}$ increases 2-fold (p = 0.0489). F. The results of 3 separate experiments are shown as scatter dot plots for V_{max} for G130A. Results are shown as mean ± SEM. Paired t-test analysis indicates that V_{max} decreases by half (p = 0.0387).

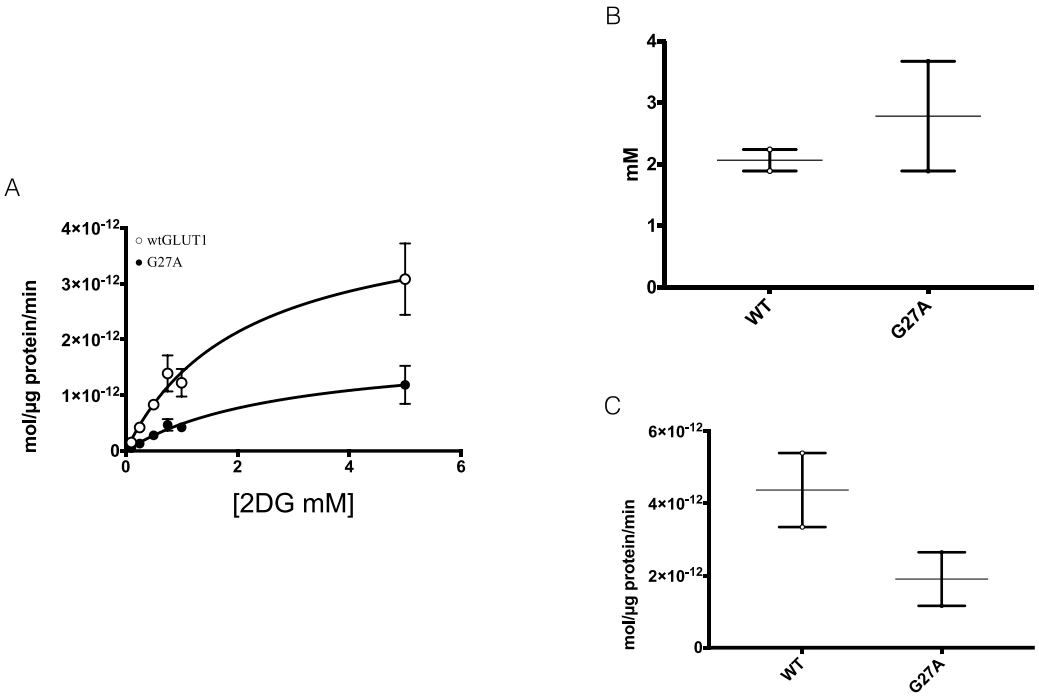

Figure 5.10: Net 2DG dose responses for glucose uptake into wtGLUT1 (○) and glycine mutants (●). A. Uptake of wtGLUT1 ($K_{m(app)}$ = 2.097 ± 0.7206 mM; V_{max} = 4.363x10^{-12} ± 7.151x10^{-13} mol/mg protein/min) and G27A ($K_{m(app)}$ = 2.823 ± 1.313 mM; V_{max} = 1.85x10^{-12} ± 4.352x10^{-13} mol/mg protein/min). B. The results of 2 separate experiments are shown as scatter dot plots for $K_{m(app)}$ for G27A. Results are shown as mean ± SEM. Paired t-test analysis indicates that $K_{m(app)}$ does not change significantly. C. The results of 2 separate experiments are shown as scatter dot plots for V_{max} for G27A. Results are shown as mean ± SEM. Paired t-test analysis indicates that V_{max} decreases (p = 0.0363).

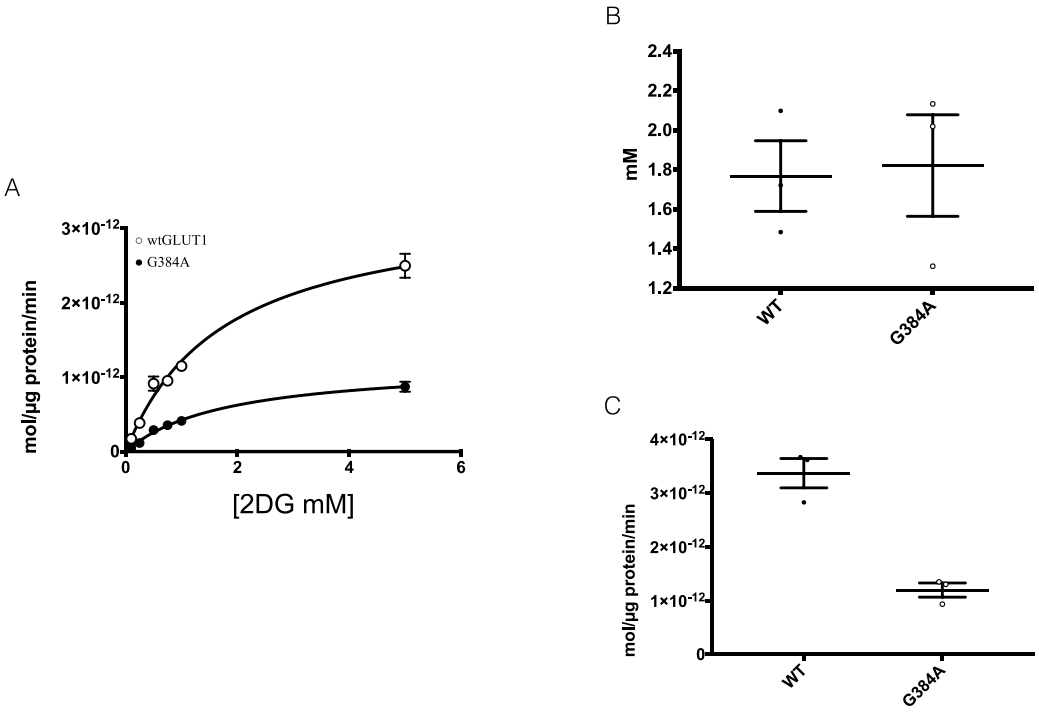

Figure 5.11: Net 2DG dose responses for glucose uptake into wtGLUT1 (○) and glycine mutants (●). A. Uptake of wtGLUT1 ($K_{m(app)}$ = 1.758 ± 0.2325 mM; V_{max} = 3.355x10^{-12} ± 2.051x10^{-13} mol/mg protein/min) and G384A ($K_{m(app)}$ = 1.801 ± 0.2137 mM; V_{max} = 1.85x10^{-12} ± 6.527x10^{-14} mol/mg protein/min). B. The results of 3 separate experiments are shown as scatter dot plots for $K_{m(app)}$ for G384A. Results are shown as mean ± SEM. Paired t-test analysis indicates that $K_{m(app)}$ does not change significantly. C. The results of 2 separate experiments are shown as scatter dot plots for V_{max} for G384A. Results are shown as mean ± SEM. Paired t-test analysis indicates that V_{max} decreases (p = 0.0042).

Discussion

This study uses homology modeling, sequence analysis and site-directed mutagenesis to examine the role of transmembrane domain glycines in GLUT1 mediated glucose transport 1 and asks: 1) Does disrupting GXXXG domains shown to be involved in helix packing in other membrane proteins, affect sugar transport? 2) Does mutagenesis of glycine residues conserved across the GLUT family disrupt GLUT1 mediated glucose transport? 3) Do "dynamic" glycine residues (those characterized by large changes in backbone dihedral angles) play important roles in GLUT1 mediated glucose transport? Our results suggest that the mutation of 100% conserved glycine residues to alanine does not disrupt the transport cycle unless the residue is also found in a GXXXG motif or is one of the highly "dynamic" glycine residues.

The available structural biology data supports the alternating carrier access model for glucose transport (77,133-135). This model posits that the glucose transporter alternately presents outward and inward faces and facilitates glucose transport through a conformational change between the two states (99,124,145). Examination of the structures suggests the N-terminal helices undergo a rigid body movement during the conformational change between N- and C-termini while the C-terminal helices move more independently.

While measurements of 2DG uptake at a single, subsaturating [2DG] (100 μM) suggests that mutation of any of the selected glycine residue to alanine, with the exception of G167, significantly reduces sugar uptake, a detailed Michaelis-Menten analysis presents a more complicated picture. 2DG dose response experiments of glycine mutants suggest that only when a reduction in 2DG uptake of > 50% is observed is this associated with a significantly altered $K_{m(app)}$ or V_{max} (Table 5.2). The 100 μM assay is sensitive to changes in $K_{m(app)}$ but not V_{max}, however changes in cell surface expression have a significant effect on single point uptake. This

could explain the false positives in so many mutants. The overexpression of glycine mutants related to wtGLUT1 lead to lower normalized uptake without having an effect on the $K_{M(app)}$.

When steady-state Michaelis-Menten measurements are analyzed, four glycine point mutants, G27A, G76A, G130A, and G384A, have significant changes compared to wtGLUT1 (Table 5.2). These four mutants, also have the lowest uptake of 100 µM 2DG relative to wtGLUT1. Both G27A and G384A have a significant decrease in V_{max} compared to wtGLUT1 but no change in $K_{m(app)}$. Altered V_{max} compared to wtGLUT1 can best be characterized as resulting from a decreased turnover rate of the transporter. The affinity for glucose isn't changed but the conformational change mediating sugar translocation decreases. G384 may be acting as a gate catalyzing or facilitating the conformational change. Additionally, this residue is located in a proline and glycine rich motif GXXP possibly conferring backbone flexibility similar to alamethicin voltage gated channels (199). Replacement of the P or G residues in the central domain of alamethicin reduces the high-amplitude hinge motion of the helix (199). The G27A mutation was analyzed only twice. In both experiments, V_{max} decreases while $K_{m(app)}$ increases in one experiment but is unchanged in the second. This necessitates more replicates to fully characterize this mutation.

Table 5.2: Summarizing the effects of glycine to alanine mutants in GLUT1. %2DG uptake when compared to WT is summarized in column 4. One-way ANOVA between WT and mutant was performed to determine statistical significance. p value < 0.0001 = ****, p value between 0.0001 and 0.001 = ***, and p value between 0.001 to 0.01 = **. Column 5 shows changes in $K_{M(app)}$ vs WT. Column 6 shows changes in V_{MAX} vs WT. Statistically significant changes as evaluated by T-test ($p < 0.05$) are shown by arrows. X symbolizes untested residues. The ° in columns 5 and 6 symbolize one-way T-test.

Glycine #	Δ Φ/Ψ > 20°	% Conserved	GXXXG	% Uptake vs WT	$K_{mapp)}$ vs WT	V_{max} vs WT
18	-	7	+	X	X	X
22	-	62	+	X	X	X
27	-	100	+	33.1****	-	↓°
31	+	54	+	67.8 ****	-	-
75	+	92	+	52.0 ****	-	-
76	+	62	-	29.7 ****	↑°	↓
79	+	62	+	58.9 ****	X	X
130	-	100	+	23.6 ****	↑°	↓
134	-	85	+	X	X	X
138	+	31	+	61.7 ****	-	-
145	+	54	+	35.5 ****	X	X
154	+	100	-	44.2 ****	-	-
163	-	23	+	95 ns	X	X
167	-	100	+	73.7 **	X	X
175	+	69	-	67.1 ***	X	X
286	+	100	-	68.6 ****	-	-
312	-	54	-	68.9 ***	-	-
382	+	100	-	70.2 ***	X	X
384	+	77	-	22.2 ****	-	↓

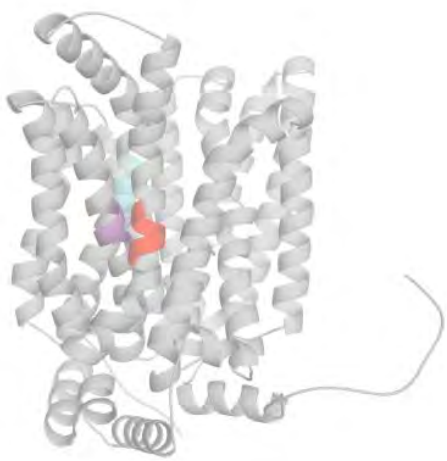

Figure 5.12: GLUT1 homology model of the e2 open conformation. Residues 27-30, 75-79, and 130-134 are shown in cyan, red, and purple, respectively.

G76A and G130A mutations are characterized by increased $K_{m(app)}$ and decreased V_{max}. Mapping residues 75-79 and 130-134 onto the GLUT1 structure suggests that these regions interact as GXXXG stabilizing domains (Figure 5.12). While G76 does not represent a G in the GXXXG domain it is an interior residue that can potentially interact with the adjacent alpha helix. Disrupting the additional interior XXX residues is necessary to confirm that these are interacting domains. Additionally, G130 is implicated in GLUT1 deficiency syndrome potentially due to the disruption of transport by the loss of the GXXXG interaction (200). Both affinity for glucose and GLUT1 catalytic turnover are decreased by disruption of either "stabilization" motif.

While zero-*trans* sugar uptake experiments are useful for analyzing unidirectional sugar uptake they do not provide sufficient information to permit a full understanding of the kinetics of GLUT1-mediated sugar transport. Understanding the role of GLUT1 primary sequence in controlling glucose transport also requires measurements of equilibrium exchange transport in which intra- and extracellular [sugar] is identical and unidirectional sugar fluxes are measured using radioactive tracers. In red cells V_{max} for equilibrium-exchange transport is some 2 to 50-fold greater than V_{max} for zero-trans uptake depending on the temperature at which the experiment is made (the lower the temperature, the greater the difference) (109). Specifically, disruption of GXXXG motifs in TMs 1 and 5 may impact exchange transport because these TMs interact with TM6, a scaffold domain whose GLUT1-specific sequence is absolutely required for accelerated exchange transport (116).

Additionally, design and analysis of the glycine hinge mutations were conducted using the 3D crystal structures of GLUTs 1 and 3 and assuming that the transporter acts as an alternating access transporter. However, GLUT1 forms allosteric oligomers in red cell and HEK 293 cell

membranes. Further analyses of these mutants should examine their impact on GLUT1 quaternary structure and whether their effects persist in the GLUT1-oligomerization deficient mutant in which TM9 of GLUT1 is replaced by TM9 of GLUT3 (116) and which loses the ability to catalyze exofacial *trans*-allostery (162). GXXXG motifs have been hypothesized to act as interacting regions in oligomeric transporters. At this time, the GLUT1 tetramerization domain (TM9) is known but the dimerization domain has not been definitively identified (140). The GXXXG motif in TM2 (G75:G79) is on the exterior lipid facing region of the protein suggesting a potential role in oligomerization. Studies examining the oligomeric state of GXXXG mutants by size-exclusion chromatography may help to identify the dimerization determinant(s).

Chapter 6:

Discussion and Future Directions

Recent advances in membrane protein crystallography coupled with the crystallization of the glucose transporters GLUT1, GLUT3, and GLUT5 and additional, related major facilitator superfamily proteins enable new analysis of GLUT1 mediated transport, ligand binding and allostery (6,77,131,133,134). GLUT1 kinetic and ligand binding studies have accumulated over decades a mountain of evidence on how GLUT1 mediates glucose transport (100,141). This evidence has led to the development of multiple models to explain GLUT1 mediated glucose transport. Specifically, two competing, compelling models have been proposed: the alternating access carrier (99,124,145) and the fixed-site carrier [125,126]. Neither model provides an adequate description of GLUT1 mediated glucose transport. Structural analyses favor the alternating access carrier model but this model cannot account for GLUT1 allostery observed with transport and ligand binding (77,133-135).

As more sugar transporter structures become available the number of analyses that support the alternating access carrier model increase. These studies have interpreted transporter structure in the context of the alternating access model in which the transporter cycles between states alternately presenting either an exofacial (e2) or endofacial (e1) sugar binding cavity (77,133-135). Sugar binding promotes a gated transition in which bound sugar is occluded or shielded from the interstitium (e2o) or cytoplasm (e1o) (119). Occlusion then triggers rigid body movements leading to conversion of the occluded state to the opposite open state. The catalytic cycle concludes via the reverse sequence of conformational changes with or without a bound sugar.

This thesis utilizes sugar transporter crystallographic information to probe potential ligand interaction sites and the residues involved in the gated transitions between outward and inward conformations. Additionally, it interrogates transporter behaviors that are not explained by

structural studies, specifically the well-documented GLUT1 transport allostery, to combine structural evidence and transport physiology into a new model for GLUT1 function.

Ligand Interaction Sites

Molecular docking reveals that the GLUT1-e2 exofacial cavity presents 3 potential, non-overlapping β-D-Glc interaction sites. Maltose interaction sites overlap with both the core and peripheral β-D-Glc interaction sites. This suggest that GLUT1-e2 can simultaneously accommodate core β-D-Glc and peripheral maltose. These three β-D-Glc interaction sites may represent progressive steps in β-D-Glc binding or co-existent interaction sites. Molecular docking indicates that it is highly unlikely the GLUT1-e1 or GLUT1-e2 simultaneously interacts with both endofacial and exofacial ligands. Docking analysis of the GLUT1 e1 and GLUT1 e1o structures suggests that the CB binding site overlaps with β-D-Glc core site. This steric hindrance implies that GLUT1 cannot bind an occluded sugar and CB simultaneously. Thus the experimental observation of CB-promoted glucose occlusion can only be explained if CB binding to one GLUT1 subunit in an oligomeric complex promotes glucose occlusion within an adjacent subunit (119). Molecular docking analysis is a useful tool for understanding GLUT1 domains involved in ligand binding and glucose transport. It can be used to develop testable hypothesis of side chain interactions (Q282) and to explain biological phenomena (e.g. CB occlusion of glucose in GLUT1 [119], changes in affinity of forskolin ligands (84) and BAY compounds based on side-chain interactions).

GLUT1 transmembrane domain glycines

Analysis of the crystal structures of sugar transporters, suggest that GLUT1 functions as an alternating access carrier where the N-terminal helices undergo a rigid body movement during the transition between the outward and inward conformations while the C-terminal helices move

more independently. Glycine is frequently found in transmembrane alpha helices and is hypothesized to play multiple roles (structural and functional) in membrane transporters. This includes acting as a gating hinge [190, 191], conferring conformational flexibility [192], and enhancing packing and oligomerization through GXXXG/GXXXXXXG motifs [194-196].

GLUT1 contains 31 transmembrane domain resident glycines, 9.2% of total transmembrane domain amino acids. This study, utilized glycine to alanine mutations, to stabilize "dynamic" glycine residues, conserved glycine residues and to disrupt GXXXG motfis. Mutation of glycines conserved across all GLUTs does not appear to have a significant effect unless these glycines are "dynamic" or GXXXG resident. Alternatively, stabilization of G384, which resides in a GXXP motif significantly reduces V_{max} for net sugar import. This glycine may act as a gating residue for the GLUT1 translocation conformational change. Disruption of the GXXXG motifs in TM2 (G76A) and TM4 (G130A) significantly reduces both affinity and V_{MAX} for zero-trans uptake. Interestingly, inspection of the GLUT1 e1 and homology-modelled GLUT1 e2 structures suggests these two motifs may be interacting. While demonstrating that GXXXG domains can play a role in mediating glucose transport, zero-*trans* uptake experiments are not, in themselves, sufficient for understanding this role. More detailed kinetic analyses (e.g. examining accelerated exchange transport) and reviewing the roles of GXXXG motifs in TMs 1 and 5 may provide an interesting area for future study as these TMs interact with the scaffold domain TM6 implicated in GLUT1 mediated accelerated exchange (116).

GLUT1 Allostery and Oligomerization

Molecular docking reveals a core binding site in GLUT1 e2, e2o, e1o, and e1 conformations. Analysis of this pocket suggests that Q282 plays a key role in forming hydrogen bonds with sugar molecules. We asked if conversion of the Q282 side chain to alanine affected

zero-*trans* 2DG uptake by the transporter. Mutation of this residue doubles $K_{m(app)}$ for 2DG uptake while not affecting V_{max} signifying a change in transporter substrate affinity. We next examined if the core site mutation has an effect on GLUT1 allostery. The Q282A mutant eliminates maltose stimulation of 2DG uptake (*cis*-allostery). However, the Q282A mutant decreases CB stimulation of 2DG uptake (*trans*-allostery) without eliminating it. This suggests that *cis*- and *trans*-allostery involve different mechanisms. GLUT1 tetramerization deficient mutants $GLUT1_{(GLUT3\text{-}H9)}$ catalyze *cis*-allostery. Addition of the Q282A mutant to the tetramerization deficient mutant eliminates maltose stimulation of 2DG uptake. However, the $GLUT1_{(GLUT3\text{-}H9)}$ mutation eliminates CB stimulation of 2DG uptake. Similarly, the Q282A mutant in $GLUT1_{(GLUT3\text{-}H9)}$ does not exhibit *trans*-allostery.

Cis- and *trans*-allostery require that GLUT1 must bind inhibitor and sugar simultaneously. For *cis*-allostery, GLUT1 presents 2 co-existent exofacial maltose interaction sites, and glucose competes for maltose binding at both sites. However, *trans*-allostery is more difficult to explain as GLUT1 only presents one e1 CB interaction site. This suggests that GLUT1 is an alternating access carrier capable of exofacial *cis*-allostery but, if analysis of the structural data is taken at face value, that GLUT1 is incapable of *trans*-allostery.

GLUT1 forms mixtures of dimeric and tetrameric complexes in both red blood cells and HEK 293 cells and the oligomeric distribution is affected by cellular redox state such that reducing conditions favor dimeric GLUT1 (140). Tetrameric GLUT1 presents 0.5 CB binding sites per molecule of GLUT1 while reduced, dimeric GLUT1 presents 1 CB site per GLUT1 molecule (17,95,96). Additionally, extracellular reductant inhibits sugar transport in RBCs and eliminates *trans*- but not *cis*-allsotery (80).

The molecular mechanisms by which Q282 and transmembrane helix 9 promote cis- and

trans-allostery are unknown. Our observations support a model where dimeric GLUT1 comprises two physically independent GLUT1 molecules. Each subunit displays cis- but not trans-allostery in net sugar uptake, binds 1 molecule of CB and because transport is rate-limited by conformational changes between unliganded e1 and e2 starts, transport is characterized by a low k_{cat}. Tetrameric GLUT1 exists as a noncovalent dimer of two associated and functionally coupled GLUT1 molecules. Intra-dimer interactions produce a functional, anti-parallel arrangement of subunits. If one GLUT1 molecule presents an e2 conformation its cognate partner in the dimer must present an e1 conformation. When an e2 subunit undergoes a transport cycle from eS2 to eS1, its dimeric partner undergoes the reverse conformational change. This couples transport via one subunit to the regeneration of an e2 sugar uptake site on the second subunit, bypasses slow relaxation and accelerates net sugar transport. Each subunit functions as an allosteric alternating access transporter for sugar import. Trans-allostery in sugar import is obtained when one e1 subunit interacts with an endofacial ligand with high affinity. The dimer presenting this liganaded e1 conformation is locked in an inhibited state but its occupancy state is communicated to the adjacent dimer, increasing that dimer's affinity for β-D-Glc or k_{cat} for transport. Raising the endofacial ligand concentration leads to occupation of both e1 subunits and inhibition of uptake.

In conclusion, each GLUT1 molecule appears to present a core, catalytic sugar binding site. The exofacial conformer of GLUT1 presents at least one and possibly two additional sugar interaction sites. Occupancy of additional sugar interaction sites affects transport via the catalytic site. Trans-allostery requires at least one subunit to bind an endofacial ligand and one to bind an extracellular, imported sugar. Disrupting the oligomeric state prevents trans-allostery but not cis-allostery. Disrupting the core sugar interaction site eliminates cis-allostery but not trans-

allostery. This model is consistent with the emerging body of structural data, but unlike the simplified analyses accompanying the structural analyses, is also compatible with the transporter's biochemical and transport behavior.

Future Directions

This study has advanced our understanding of previously unexplained phenomena observed in GLUT1 mediated glucose transport. It additionally has shown some of the gaps present in current structural analysis of MFS transporters. Future work on GLUT1 most necessarily will involve further analysis of oligomeric structure. This could be accomplished through computational protein:protein docking of GLUT1, utilizing software optimized for membrane proteins. This would allow for determination of domains involved in mediating the dimeric interface. Alternatively, cryo-EM could be used to analyze both GLUT1 dimers and tetramers with the caveat that the use of detergents that stabilize GLUT1 oligomeric structure (122) should be preferred. Structural biologists traditionally crystalize mono-dispersed proteins (201) (202) but the use of detergents that cause GLUT1 tetramers to dissociate [122] may prevent the analysis of physiologically relevant GLUT1 structures. Structural analysis of GLUT1 has progressed significantly but it is biased towards an inward open conformation. Further characterization of GLUT1 crystal structures requires obtaining outward open and occluded conformations.

Analysis of both GLUT1 allostery and conformational changes are currently hampered by GLUT1 oligomeric structure. While, GLUT1 cis-allostery is observed in both dimers and tetramers, it is not currently possible to determine if cis-allostery is an intra- or an intermolecular phenomena. Development of a monomeric GLUT1 molecule can assist in studying cis-allostery. Additionally, while *cis*-allostery has been demonstrated in the dimeric GLUT3, *trans*-allostery

has not been explored. Further probing of the oligomeric state and allosteric behavior of the GLUTs to determine if this behavior is unique to GLUT1 or carried across the family. Similarly studying residues involved in GLUT1 conformational changes should be undertaken in both dimeric GLUT1 TM9 background and in a potential GLUT1 monomer. Disruption of GXXXG motifs, should be tested for oligomeric size as GXXXG motifs have been speculated to be involved in oligomerization. Similarly, the glycine mutants were tested for zero-trans uptake, expanding this to include equilibrium exchange will allow for characterization of the turnover rate potentially mitigated by glycine flexibility.

Ligand interaction maps generated by ligand docking to GLUT1 provide an interesting avenue for testing ligand affinity for GLUT1 and for other GLUTs. Specifically, inhibitors can be designed to use the GLUT1 binding pockets, and then compared to binding pockets of the other GLUTs to allay specificity concerns. The variability of poses generated by molecular docking also demonstrates an area of concern for this analysis. Ligand docking may be best used to develop testable hypotheses and to explain biological data. However, highest scoring protein-ligand interactions do not always correspond with biochemical data, (β-D-glucose poses) confirming that best practice demands that we test potential ligand side chain interactions in the experimental setting.

Bibliography

1. Overington, J. P., Al-Lazikani, B., and Hopkins, A. L. (2006) How many drug targets are there? *Nat Rev Drug Discov* **5**, 993
2. Melchior, D. L., Scavitto, F. J., and Steim, J. M. (1980) Dilatometry of dipalmitoyllecithin-cholesterol bilayers. *Biochemistry* **19**, 4828-4834
3. Lieb, W. R., and Stein, W. D. (1986). Academic Press, New York. pp 69-112
4. Singer, S. J., and Nicolson, G. L. (1972) The fluid mosaic model of the structure of cell membranes. *Science* **175**, 720-731
5. Blobel, G. (1980) Intracellular protein topogenesis. *Proc Natl Acad Sci U S A* **77**, 1496-1500
6. Quistgaard, E., Löw, C., Moberg, P., Trésaugues, L., and Nordlund, P. (2013) Structural basis for substrate transport in the GLUT-homology family of monosaccharide transporters. *Nat Struct Mol Biol* **20**, 766-768
7. Marger, M. D., Saier Jr, M. H., and Sobrevia, L. (1993) A major superfamily of transmembrane facilitators that catalyse uniport, symport and antiport. *Trends Biochem Sci* **18**, 13-20
8. Abramson, J., Smirnova, I., Kasho, V., Verner, G., Kaback, H. R., Iwata, S., and Stroud, R. M. (2003) Structure and mechanism of the lactose permease of Escherichia coli. *Science* **301**, 610-615
9. Huang, Y., Lemieux, M. J., Song, J., Auer, M., and Wang, D. N. (2003) Structure and mechanism of the glycerol-3-phosphate transporter from Escherichia coli. *Science* **301**, 616-620
10. Wright, E. M. (2009) *Diseases of Renal Glucose Handling*, Academic Press
11. Richter, E. A. (2010) *Glucose Utilization*, John Wiley & Sons, Inc.
12. Thorens, B., and Mueckler, M. (2010) Glucose transporters in the 21st Century. *Am J Physiol Endocrinol Metab* **298**, E141-145
13. Deng, D., and Yan, N. (2016) GLUT, SGLT, and SWEET: Structural and mechanistic investigations of the glucose transporters. *Protein Sci* **25**, 546-558
14. Joost, H., and Thorens, B. (2001) The extended GLUT-family of sugar/polyol transport facilitators: nomenclature, sequence characteristics, and potential function of its novel members (review). *Mol Membr Biol* **18**, 247-256
15. Augustin, R. (2010) The protein family of glucose transport facilitators: It's not only about glucose after all. *IUBMB Life* **62**, 315-333
16. Mann, G. E., Yudilevich, D. L., and Sobrevia, L. (2003) Regulation of Amino Acid and Glucose Transporters in Endothelial and Smooth Muscle Cells. *Physiol Rev* **83**, 183-252
17. Zoccoli, M. A., Baldwin, S. A., and Lienhard, G. E. (1978) The monosaccharide transport system of the human erythrocyte. Solubilization and characterization on the basis of cytochalasin B binding. *J Biol Chem* **253**, 6923-6930
18. Kasahara, M., and Hinkle, P. C. (1977) Reconstitution and purification of the D-glucose transporter from human erythrocytes. *J Biol Chem* **252**, 7384-7390
19. Mueckler, M., Caruso, C., Baldwin, S. A., Panico, M., Blench, I., Morris, H. R., Allard, W. J., Lienhard, G. E., and Lodish, H. F. (1985) Sequence and structure of a human glucose transporter. *Science* **229**, 941-945
20. Uldry, M., Ibberson, M., Hosokawa, M., and Thorens, B. (2002) GLUT2 is a high affinity glucosamine transporter. *FEBS Lett* **524**, 199-203

21. Gould, G. W., Thomas, H. M., Jess, T. J., and Bell, G. I. (1991) Expression of human glucose transporters in Xenopus oocytes: kinetic characterization and substrate specificities of the erythrocyte, liver, and brain isoforms. *Biochemistry* **30**, 5139-5145
22. Thorens, B., Weir, G. C., Leahy, J. L., Lodish, H. F., and Bonner, W. S. (1990) Reduced expression of the liver/beta-cell glucose transporter isoform in glucose-insensitive pancreatic beta cells of diabetic rats. *Proc Natl Acad Sci U S A* **87**, 6492-6496
23. Thorens, B. (1992) Molecular and cellular physiology of GLUT-2, a high-Km facilitated diffusion glucose transporter. [Review]. *Int Rev Cytol* **137**, 209-238
24. Roncero, I., Alvarez, E., Chowen, J. A., Sanz, C., Rábano, A., Vázquez, P., and Blázquez, E. (2004) Expression of glucose transporter isoform GLUT-2 and glucokinase genes in human brain. *J Neurochem* **88**, 1203-1210
25. McCulloch, L. J., van de Bunt, M., Braun, M., Frayn, K. N., Clark, A., and Gloyn, A. L. (2011) GLUT2 (SLC2A2) is not the principal glucose transporter in human pancreatic beta cells: Implications for understanding genetic association signals at this locus. *Mol Genet Metab* **104**, 648-653
26. Simpson, I. A., Dwyer, D., Malide, D., Moley, K. H., Travis, A., Vannucci, S. J. r.-S., Ellen M., Vannucci, S. J., and Smith, Q. R. (2008) The facilitative glucose transporter GLUT3: 20 years of distinction. *Am J Physiol Endocrinol Metab* **295**, E242-253
27. Nagamatsu, S., Kornhauser, J. M., Burant, C. F., Seino, S., Mayo, K. E., and Bell, G. I. (1992) Glucose transporter expression in brain. cDNA sequence of mouse GLUT3, the brain facilitative glucose transporter isoform, and identification of sites of expression by in situ hybridization. *J Biol Chem* **267**, 467-472
28. Huang, S., and Czech, M. P. (2007) The GLUT4 Glucose Transporter. *Cell Metab* **5**, 237-252
29. Kahn, B. B. (1996) Glucose Transport: Pivotal Step in Insulin Action. *Diabetes* **45**, 1644-1654
30. Kayano, T., Burant, C. F., Fukumoto, H., Gould, G. W., Fan, Y. S., Eddy, R. L., Byers, M. G., Shows, T. B., Seino, S., and Bell, G. I. (1990) Human facilitative glucose transporters. Isolation, functional characterization, and gene localization of cDNAs encoding an isoform (GLUT5) expressed in small intestine, kidney, muscle, and adipose tissue and an unusual glucose transporter pseudogene-like sequence (GLUT6). *J Biol Chem* **265**, 13276-13282
31. Burant, C. F., Takeda, J., Brot, L. E., Bell, G. I., and Davidson, N. O. T. (1992) Fructose transporter in human spermatozoa and small intestine is GLUT5. *J Biol Chem* **267**, 14523-14526
32. Kane, S., Seatter, M., and Gould, G. (1997) Functional studies of human GLUT5: effect of pH on substrate selection and an analysis of substrate interactions. *Biochem Biophys Res Commun* **238**, 503-505
33. Douard, V., and Ferraris, R. (2008) Regulation of the fructose transporter GLUT5 in health and disease. *Am J Physiol Endocrinol Metab* **295**, E227-237
34. Augustin, R., Carayannopoulos, M., Dowd, L., Phay, J., Moley, J., and Moley, K. (2004) Identification and characterization of human glucose transporter-like protein-9 (GLUT9): alternative splicing alters trafficking. *J Biol Chem* **279**, 16229-16236
35. Anzai, N., Ichida, K., Jutabha, P., Kimura, T., Babu, E., Jin, C. J., Srivastava, S., Kitamura, K., Hisatome, I., Endou, H., and Sakurai, H. (2008) Plasma Urate Level Is Directly Regulated by a Voltage-driven Urate Efflux Transporter URATv1 (SLC2A9) in Humans.

J Biol Chem **283**, 26834-26838
36. Bibert, S., Hess, S. K., Firsov, D., Thorens, B., Geering, K., Horisberger, J.-D., and Bonny, O. (2009) Mouse GLUT9: evidences for a urate uniporter. *Am J Physiol Renal Physiol* **297**, F612-F619
37. Ibberson, M., Uldry, M., and Thorens, B. (2000) GLUTX1 (GLUT8), a Novel Mammalian Glucose Transporter Expressed in the Central Nervous System and Insulin-sensitive Tissues. *J Biol Chem* **275**, 4607-4612
38. Mueckler, M., and Thorens, B. (2013) The SLC2 (GLUT) Family of Membrane Transporters. *Mol Aspects Med* **34**, 121-138
39. Uldry, M., Ibberson, M., Horisberger, J., Chatton, J., Riederer, B., and Thorens, B. (2001) Identification of a mammalian H(+)-myo-inositol symporter expressed predominantly in the brain. *EMBO J* **20**, 4467-4477
40. Manolescu, A., Witkowska, K., Kinnaird, A., Cessford, T., and Cheeseman, C. (2007) Facilitated hexose transporters: new perspectives on form and function. *Physiology (Bethesda)* **22**, 234-240
41. Seidner, G., Alvarez, M. G., Yeh, J. I., O'Driscoll, K. R., Klepper, J., Stump, T. S., Wang, D., Spinner, N. B., Birnbaum, M. J., and De Vivo, D. C. (1998) GLUT-1 deficiency syndrome caused by haploinsufficiency of the blood-brain barrier hexose carrier. *Nat Genet* **18**, 188-191
42. Klepper, J. (2012) GLUT1 deficiency syndrome in clinical practice. *Epilepsy Res* **100**, 272-277
43. Gras, D., Roze, E., Caillet, S., Méneret, A., Doummar, D., Billette de Villemeur, T., Vidailhet, M., and Mochel, F. (2014) GLUT1 deficiency syndrome: an update. *Rev Neurol (Paris)* **170**, 91-99
44. Santer, R., Schneppenheim, R., Suter, D., Schaub, J., and Steinmann, B. (1998) Fanconi-Bickel syndrome--the original patient and his natural history, historical steps leading to the primary defect, and a review of the literature. *Eur J Pediatr* **157**, 783-797
45. Santer, R., Groth, S., Kinner, M., Dombrowski, A., Berry, G., Brodehl, J., Leonard, J., Moses, S., Norgren, S., Skovby, F., Schneppenheim, R., Steinmann, B., and Schaub, J. (2002) The mutation spectrum of the facilitative glucose transporter gene SLC2A2 (GLUT2) in patients with Fanconi-Bickel syndrome. *Hum Genet* **110**, 21-29
46. Kahn, S. E., Hull, R. L., and Utzschneider, K. M. (2006) Mechanisms linking obesity to insulin resistance and type 2 diabetes. *Nature* **444**, 840
47. Bryant, N. J., Govers, R., and James, D. E. (2002) Regulated transport of the glucose transporter GLUT4. *Nat Rev Mol Cell Biol* **3**, 267-277
48. Cushman, S. W., and Wardzala, L. J. (1980) Potential mechanism of insulin action on glucose transport in the isolated rat adipose cell. *J Biol Chem* **255**, 4755-4762
49. Suzuki, K., and Kono, T. (1980) Evidence that insulin causes translocation of glucose transport activity to the plasma membrane from an intracellular storage site. *Proc Natl Acad Sci U S A* **77**, 2542-2545
50. Vander Heiden, M., Cantley, L., and Thompson, C. (2009) Understanding the Warburg effect: the metabolic requirements of cell proliferation. *Science* **324**, 1029-1033
51. Barron, C. C., Bilan, P. J., Tsakiridis, T., and Tsiani, E. (2016) Facilitative glucose transporters: Implications for cancer detection, prognosis and treatment. *Metabolism* **65**, 124-139
52. Gorga, F., and Lienhard, G. (1982) Changes in the intrinsic fluorescence of the human

erythrocyte monosaccharide transporter upon ligand binding. *Biochemistry* **21**, 1905-1908
53. Gerritsen, M., Burke, T., Allen, L., Silverstein, S., and Stern, D. (1988) Glucose starvation is required for insulin stimulation of glucose uptake and metabolism in cultured microvascular endothelial cells. *Microvasc Res* **35**, 153-166
54. Ibberson, M., Riederer, B., Uldry, M., Guhl, B., Roth, J., and Thorens, B. (2002) Immunolocalization of GLUTX1 in the testis and to specific brain areas and vasopressin-containing neurons. *Endocrinology* **143**, 276-284
55. Cura, A., and Carruthers, A. (2012) AMP Kinase regulation of Sugar Transport in Brain Capillary Endothelial Cells During Acute Metabolic Stress. *Am J Physiol Cell Physiol* **303**, C808-C814
56. Carruthers, A. (1986) Anomalous asymmetric kinetics of human red cell hexose transfer: role of cytosolic adenosine 5'-triphosphate. *Biochemistry* **25**, 3592-3602
57. Lin, S., and Spudich, J. A. (1974) Biochemical studies on the mechanism of action of cytochalasin B. Cytochalasin B binding to red cell membranes in relation to glucose transport. *J Biol Chem* **249**, 5778-5783
58. Shanahan, M., Morris, D., Edwards, B., and Ruoho, A. (1987) [3H]forskolin. Direct photoaffinity labeling of the erythrocyte D-glucose transporter. *J Biol Chem* **262**, 5978-5984
59. Vannucci, S., Maher, F., and Simpson, I. (1997) Glucose transporter proteins in brain: delivery of glucose to neurons and glia. *Glia* **21**, 2-21
60. Guo, X., Geng, M., and Du, G. (2005) Glucose transporter 1, distribution in the brain and in neural disorders: its relationship with transport of neuroactive drugs through the blood-brain barrier. *Biochem Genet* **43**, 175-187
61. Luiken, J., Coort, S., Koonen, D., van der Horst, D., Bonen, A., Zorzano, A., and Glatz, J. (2004) Regulation of cardiac long-chain fatty acid and glucose uptake by translocation of substrate transporters. *Pflugers Arch* **448**, 1-15
62. Maher, F., Vannucci, S., and Simpson, I., IA. (1994) Glucose transporter proteins in brain. *FASEB J* **8**, 1003-1011
63. Simpson, I. A., Vannucci, S. J., DeJoseph, M. R., and Hawkins, R. A. (2001) Glucose Transporter Asymmetries in the Bovine Blood-Brain Barrier. *J Biol Chem* **276**, 12725-12729
64. Holman, G. D., Kozka, I. J., Clark, A. E., Flower, C. J., Saltis, J., Habberfield, A. D., Simpson, I. A., and Cushman, S. W. (1990) Cell surface labeling of glucose transporter isoform GLUT4 by bis- mannose photolabel. Correlation with stimulation of glucose transport in rat adipose cells by insulin and phorbol ester. *J Biol Chem* **265**, 18172-18179
65. Cooper, D. R., Khalakdina, A., Watson, J. E., and Knauf, P. A. (1993) Chronic effects of glucose on insulin signaling in A-10 vascular smooth muscle cells. *Arch Biochem Biophys* **302**, 490-498
66. Shetty, M., Loeb, J. N., Vikstrom, K., and Ismail, B. F. (1993) Rapid activation of GLUT-1 glucose transporter following inhibition of oxidative phosphorylation in clone 9 cells. *J Biol Chem* **268**, 17225-17232
67. Jacquez, J. A. (1983) Modulation of glucose transport in human red blood cells by ATP. *Biochim Biophys Acta* **727**, 367-378
68. Diamond, D., and Carruthers, A. (1993) Metabolic control of sugar transport by derepression of cell surface glucose transporters: an insulin-independent, recruitment-

independent mechanism of regulation. *J Biol Chem* **268**, 6437-6444
69. D'Angelo, G. (1982) Evidence for an Erythrocyte Glucose Transport System in the Belukha Whale (Delphinapterus Leucas). *Cetology* **42**, 1-9
70. Gaposchkin, C., and Garcia-Diaz, J. (1996) Modulation of cultured brain, adrenal, and aortic endothelial cell glucose transport. *Biochim Biophys Acta* **1285**, 255-266
71. Loike, J., Cao, L., Brett, J., Ogawa, S., Silverstein, S., and Stern, D. (1992) Hypoxia induces glucose transporter expression in endothelial cells. *Am J Physiol* **263**, C326-333
72. Elbrink, J., and Bihler, I. (1975) Membrane transport. Its relation to cellular metabolic rates. *Science* **188**, 1177–1184
73. Cura, A., and Carruthers, A. (2010) Acute modulation of sugar transport in brain capillary endothelial cell cultures during activation of the metabolic stress pathway. *J Biol Chem* **285**, 15430-15439
74. Barnett, J. E., Holman, G. D., Chalkley, R. A., and Munday, K. A. (1975) Evidence for two asymmetric conformational states in the human erythrocyte sugar-transport system. *Biochem J* **145**, 417-429
75. Barnett, J., Holman, G., and Munday, K. (1973) Structural requirements for binding to the sugar-transport system of the human erythrocyte. *Biochem J* **131**, 211-221
76. Leitch, J., and Carruthers, A. (2009) Alpha- and Beta-Monosaccharide transport in human erythrocytes. *Am J Physiol Cell Physiol* **296**, C151-161
77. Deng, D., Xu, C., Sun, P., Wu, J., Yan, C., Hu, M., and Yan, N. (2014) Crystal structure of the human glucose transporter GLUT1. *Nature* **510**, 121-125
78. Hamill, S., Cloherty, E. K., and Carruthers, A. (1999) The human erythrocyte sugar transporter presents two sugar import sites. *Biochemistry* **38**, 16974-16983
79. Helgerson, A. L., and Carruthers, A. (1987) Equilibrium ligand binding to the human erythrocyte sugar transporter. Evidence for two sugar-binding sites per carrier. *J Biol Chem* **262**, 5464-5475
80. Cloherty, E. K., Levine, K. B., and Carruthers, A. (2001) The red blood cell glucose transporter presents multiple, nucleotide-sensitive sugar exit sites. *Biochemistry* **40**, 15549-15561
81. Naftalin, R. J., Afzal, I., Cunningham, P., Halai, M., Ross, C., Salleh, N., and Milligan, S. R. (2003) Interactions of androgens, green tea catechins and the antiandrogen flutamide with the external glucose-binding site of the human erythrocyte glucose transporter GLUT1. *Br J Pharmacol* **140**, 487-499
82. Ojelabi, O., De Zutter, J. K., and Carruthers, A. (2018) The flavonoids inhibit GLUT1 by interacting with the exofacial substrate binding site. *Manuscript in preparation*
83. Carruthers, A., and Helgerson, A. (1991) Inhibitions of sugar transport produced by ligands binding at opposite sides of the membrane. Evidence for simultaneous occupation of the carrier by maltose and cytochalasin B. *Biochemistry* **30**, 3907-3915
84. Robichaud, T., Appleyard, A., Herbert, R., Henderson, P., and Carruthers, A. (2011) Determinants of ligand binding affinity and cooperativity at the GLUT1 endofacial site. *Biochemistry* **50**, 3137-3148
85. Sage, J., Cura, A., Lloyd, K., and Carruthers, A. (2015) Caffeine inhibits glucose transport by binding at the GLUT1 nucleotide-binding site. *Am J Physiol Cell Physiol* **308**, C827-C834
86. Blodgett, D., De Zutter, J., Levine, K., Karim, P., and Carruthers, A. (2007) Structural Basis of GLUT1 Inhibition by Cytoplasmic ATP. *J Gen Physiol* **130**, 157-168

87. Carruthers, A., and Helgerson, A. L. (1989) The human erythrocyte sugar transporter is also a nucleotide binding protein. *Biochemistry* **28**, 8337-8346
88. Glynn, I. M., Richards, D. E. d., D. E.. L., and du, P. J. (1982) Occlusion of rubidium ions by the sodium-potassium pump: Its implications for the mechanism of potassium transport,. *J Physiol (Lond)* **330**, 17-43
89. Stein, W. D. (1986) *Transport and diffusion across cell membranes*, Academic Press, New York
90. Skou, J. C. (1974) Effect of ATP on Na:K affinity and catalytic activity of (Na+ plus K+)-activated enzyme system. *Ann N Y Acad Sci* **242**, 168-184
91. Baldwin, S., Baldwin, J., Gorga, F., and Lienhard, G. (1979) Purification of the cytochalasin B binding component of the human erythrocyte monosaccharide transport system. *Biochim Biophys Acta* **552**, 183-188
92. Gorga, F., and Lienhard, G. (1981) Equilibria and kinetics of ligand binding to the human erythrocyte glucose transporter. Evidence for an alternating conformation model for transport. *Biochemistry* **20**, 5108-5113
93. Sogin, D. C., and Hinkle, P. C. (1980) Binding of cytochalasin B to human erythrocyte glucose transport. *Biochemistry* **19**, 5417–5420
94. Carruthers, A. (1986) ATP regulation of the human red cell sugar transporter. *J Biol Chem* **261**, 11028-11037
95. Hebert, D. N., and Carruthers, A. (1992) Glucose transporter oligomeric structure determines transporter function. Reversible redox-dependent interconversions of tetrameric and dimeric GLUT1. *J Biol Chem* **267**, 23829-23838
96. Sogin, D., Hinkle, P., and Singer, S. (1978) Characterization of the glucose transporter from human erythrocytes. *J Supramol Struct* **8**, 447-453
97. Naftalin, R. J., and Holman, G. D. (1977) Transport of sugars in human red cells. in *Membrane transport in red cells* (Ellory, J. C., and Lew, V. L. eds.), Academic Press, New York. pp 257-300
98. Widdas, W. F. (1980) The asymmetry of the hexose transfer system in the human red cell membrane. *Curr Top Memb Transp* **14**, 165-223
99. Lieb, W. R., and Stein, W. D. (1974) Testing and characterizing the simple carrier. *Biochim Biophys Acta* **373**, 178-196
100. Cura, A. J., and Carruthers, A. (2012) Role of Monosaccharide Transport Proteins in Carbohydrate Assimilation, Distribution, Metabolism, and Homeostasis. *Compr Physiol* **2**, 863-91439
101. Mueckler, M., and Makepeace, C. (2009) Model of the exofacial substrate-binding site and helical folding of the human Glut1 glucose transporter based on scanning mutagenesis. *Biochemistry* **48**, 5934-5942
102. Zottola, R. J., Cloherty, E. K., Coderre, P. E., Hansen, A., Hebert, D. N., and Carruthers, A. (1995) Glucose transporter function is controlled by transporter oligomeric structure. A single, intramolecular disulfide promotes GLUT1 tetramerization. *Biochemistry* **34**, 9734-9747
103. Gould, G. W., and Lienhard, G. E. (1989) Expression of a functional glucose transporter in Xenopus oocytes. *Biochemistry* **28**, 9447-9452
104. Keller, K., and Mueckler, M. (1990) Different mammalian facilitative glucose transporters expressed in Xenopus oocytes. *Biomed Biochim Acta* **49**, 1201-1203
105. Levine, K. B., Robichaud, T. K., Hamill, S., Sultzman, L. A., and Carruthers, A. (2005)

Properties of the human erythrocyte glucose transport protein are determined by cellular context. *Biochemistry* **44**, 5606-5616
106. Baker, G. F., Basketter, D. A., and Widdas, W. F. (1978) Asymmetry of the hexose transfer system in human erythrocytes. Experiments with non-transportable inhibitors. *J Physiol (Lond)* **278**, 377-388
107. Bachelard, H. S. (1972) Deoxyglucose and brain glycolysis. *Biochem J* **127**, 83P
108. Jay, T., Dienel, G., Cruz, N., Mori, K., Nelson, T., and Sokoloff, L. (1990) Metabolic stability of 3-O-methyl-D-glucose in brain and other tissues. *J Neurochem* **55**, 989-1000
109. Lowe, A. G., and Walmsley, A. R. (1986) The kinetics of glucose transport in human red blood cells. *Biochim Biophys Acta* **857**, 146-154
110. Carruthers, A., and Melchior, D. (1983) Asymmetric or symmetric? Cytosolic modulation of human erythrocyte hexose transfer. *Biochim Biophys Acta* **728**, 254-266
111. Carruthers, A. (1991) Mechanisms for the facilitated diffusion of substrates across cell membranes. *Biochemistry* **30**, 3898-3906
112. Lacko, L., Wittke, B., and Geck, P. (1973) The temperature dependence of the exchange transport of glucose in human erythocytes. *J Cell Physiol* **82**, 213-318
113. Cloherty, E. K., Heard, K. S., and Carruthers, A. (1996) Human erythrocyte sugar transport is incompatible with available carrier models. *Biochemistry* **35**, 10411-10421
114. Cloherty, E. K., Diamond, D. L., Heard, K. S., and Carruthers, A. (1996) Regulation of GLUT1-mediated sugar transport by an antiport/uniport switch mechanism. *Biochemistry* **35**, 13231-13239
115. Toyoda, N., Flanagan, J. E., and Kono, T. (1987) Reassessment of insulin effects on the Vmax and Km values of hexose transport in isolated rat epididymal adipocytes. *J Biol Chem* **262**, 2737-2745
116. Vollers, S., and Carruthers, A. (2012) Sequence Determinants of GLUT1-mediated Accelerated-Exchange Transport - Analysis by Homology-Scanning Mutagenesis. *J Biol Chem* **51**, 42533-42544.
117. Appleman, J. R., Lienhard, G. E. a., F., and Baltz, T. (1989) Kinetics of the purified glucose transporter. Direct measurement of the rates of interconversion of transporter conformers. *Biochemistry* **28**, 8221-8227
118. Sultzman, L., and Carruthers, A. (1999) Stop-flow analysis of cooperative interactions between GLUT1 sugar import and export sites. *Biochemistry* **38**, 6640-6650
119. Blodgett, D. M., and Carruthers, A. (2005) Quench-Flow Analysis Reveals Multiple Phases of GluT1-Mediated Sugar Transport. *Biochemistry* **44**, 2650-2660
120. Baker, G. F., and Naftalin, R. J. (1979) Evidence of multiple operational affinities for D-glucose inside the human erythrocyte membrane. *Biochim Biophys Acta* **550**, 474-484
121. Ginsburg, H., and Stein, W. (1975) Zero-trans and infinite-cis uptake of galactose in human erythrocytes. *Biochim Biophys Acta* **382**, 353-368
122. Graybill, C., van Hoek, A., Desai, D., Carruthers, A., and Carruthers, A. (2006) Ultrastructure of Human Erythrocyte GLUT1. *Biochemistry* **45**, 8096-8107
123. Hankin, B., Lieb, W., and Stein, W. (1972) Rejection criteria for the asymmetric carrier and their application to glucose transport in the human red blood cell. *Biochim Biophys Acta* **288**, 114-126
124. Widdas, W. F. (1952) Inability of diffusion to account for placental glucose transfer in the sheep and consideration of the kinetics of a possible carrier transfer. *J Physiol (London)* **118**, 23–39

125. Carruthers, A. (1990) Facilitated diffusion of glucose. *Physiol Rev* **70**, 1135-1176
126. Naftalin, R. J., Smith, P. M., Roselaar, S. E. A., and Munday, K. A. (1985) Evidence for non–uniform distribution of D–glucose within human red cells during net exit and counterflow. *Biochim Biophys Acta* **820**, 235–249
127. Hresko, R., Kruse, M., Strube, M., Mueckler, M. F., and MacDonald, R. (1994) Topology of the Glut 1 glucose transporter deduced from glycosylation scanning mutagenesis. *J Biol Chem* **269**, 20482-20488
128. Blodgett, D., Graybill, C., and Carruthers, A. (2008) Analysis of glucose transporter topology and structural dynamics. *J Biol Chem* **283**, 36416-36424
129. Alvarez, J., Lee, D., Baldwin, S., and Chapman, D. (1987) Fourier transform infrared spectroscopic study of the structure and conformational changes of the human erythrocyte glucose transporter. *J Biol Chem* **262**, 3502-3509
130. Salas-Burgos, A., Iserovich, P., Zuniga, F., Vera, J. C., and Fischbarg, J. (2004) Predicting the three-dimensional structure of the human facilitative glucose transporter glut1 by a novel evolutionary homology strategy: insights on the molecular mechanism of substrate migration, and binding sites for glucose and inhibitory molecules. *Biophys J* **87**, 2990-2999
131. Sun, L., Zeng, X., Yan, C., Sun, X., Gong, X., Rao, Y., and Yan, N. (2012) Crystal structure of a bacterial homologue of glucose transporters GLUT1-4. *Nature* **490**, 361-366
132. Dang, S., Sun, L., Huang, Y., Lu, F., Liu, Y., Gong, H., Wang, J., and Yan, N., HG. (2010) Structure of a fucose transporter in an outward-open conformation. *Nature* **467**, 734-738
133. Nomura, N., Verdon, G., Kang, H., Shimamura, T., Nomura, Y., Sonoda, Y., Hussien, S., Qureshi, A., Coincon, M., Sato, Y., Abe, H., Nakada-Nakura, Y., Hino, T., Arakawa, T., Kusano-Arai, O., Iwanari, H., Murata, T., Kobayashi, T., Hamakubo, T., Kasahara, M., Iwata, S., and Drew, D. (2015) Structure and mechanism of the mammalian fructose transporter GLUT5. *Nature* **526**, 397-401
134. Deng, D., Sun, P., Yan, C., Ke, M., Jiang, X., Xiong, L., Ren, W., Hirata, K., Yamamoto, M., Fan, S., and Yan, N. (2015) Molecular basis of ligand recognition and transport by glucose transporters. *Nature* **526**, 391-396
135. Kapoor, K., Finer-Moore, J., Pedersen, B., Caboni, L., Waight, A., Hillig, R., Bringmann, P., Heisler, I., Müller, T., Siebeneicher, H., and Stroud, R. (2016) Mechanism of inhibition of human glucose transporter GLUT1 is conserved between cytochalasin B and phenylalanine amides. *Proc Natl Acad Sci U S A* **113**, 4711-4716
136. Cunningham, P., and Naftalin, R. (2014) Reptation-induced coalescence of tunnels and cavities in Escherichia Coli XylE transporter conformers accounts for facilitated diffusion. *J Membr Biol* **247**, 1161-1179
137. Hebert, D. N., and Carruthers, A. (1991) Cholate-solubilized erythrocyte glucose transporters exist as a mixture of homodimers and homotetramers. *Biochemistry* **30**, 4654-4658
138. Looyenga, B., VanOpstall, C., Lee, Z., Bell, J., Lodge, E., Wrobel, K., Arnoys, E., and Louters, L. (2016) Determination of GLUT1 Oligomerization Parameters using Bioluminescent Förster Resonance Energy Transfer. *Sci Rep* **6**, 29130
139. Burant, C., and Bell, G. (1992) Mammalian facilitative glucose transporters: evidence for similar substrate recognition sites in functionally monomeric proteins. *Biochemistry* **31**, 10414-10420

140. De Zutter, J., Levine, K., Deng, D., and Carruthers, A. (2013) Sequence determinants of GLUT1 oligomerization: analysis by homology-scanning mutagenesis. *J Biol Chem* **288**, 20734-20744
141. Carruthers, A., De Zutter, J., Ganguly, A., and Devaskar, S. (2009) "Will the Original Glucose Transporter Isoform Please Stand Up!". *Am J Physiol Endocrinol Metab* **297**, E836-8489
142. Yan, N. (2017) A Glimpse of Membrane Transport through Structures-Advances in the Structural Biology of the GLUT Glucose Transporters. *J Mol Biol* **429**, 2710-2725
143. Baker, G., and Naftalin, R. (1979) Evidence of multiple operational affinities for D-glucose inside the human erythrocyte membrane. *Biochim Biophys Acta* **550**, 474-484
144. Naftalin, R. J. (1988) Pre-steady-state uptake of D-glucose is inconsistent with a circulating carrier mechanism. *Biochim Biophys Acta* **946**, 431-438
145. Jardetzky, O. (1966) Simple allosteric model for membrane pumps. *Nature* **211**, 969-970
146. Reddy, V. S., Shlykov, M. A., Castillo, R., Sun, E. I., and Saier Jr, M. H. (2012) The major facilitator superfamily (MFS) revisited. *FEBS Journal*
147. Baker, G. F., and Widdas, W. F. (1973) The asymmetry of the facilitated transfer system for hexoses in human red cells and the simple kinetics of a two component model. *J Physiol* **231**, 143-165
148. Basketter, D., and Widdas, W. (1978) Asymmetry of the hexose transfer system in human erythrocytes. Comparison of the effects of cytochalasin B, phloretin and maltose as competitive inhibitors. *J Physiol* **278**, 389-401
149. Ojelabi, O., Lloyd, K., Simon, A., De Zutter, J., and Carruthers, A. (2016) WZB117 inhibits GLUT1-mediated sugar transport by binding reversibly at the exofacial sugar binding site. *J Biol Chem* **291**, 26762-26772
150. Dundas, J., Ouyang, Z., Tseng, J., Binkowski, A., Turpaz, Y., and Liang, J., JM. (2006) CASTp: computed atlas of surface topography of proteins with structural and topographical mapping of functionally annotated residues. *Nucleic Acids Res* **34**, W116-118
151. Lloyd, K., Ojelabi, O., Simon, A., De Zutter, J., and Carruthers, A. (2017) Kinetic Basis of Cis- and Trans-Allostery in GLUT1-Mediated Sugar Transport. *J Membr Biol*
152. Baker, P. F., and Carruthers, A. (1981) Sugar transport in giant axons of Loligo. *J Physiol (London)* **316**, 481-502
153. Halgren, T., Murphy, R., Friesner, R., Beard, H., Frye, L., Pollard, W., and Banks, J. (2004) Glide: a new approach for rapid, accurate docking and scoring. 2. Enrichment factors in database screening. *J Med Chem* **47**, 1750-1759
154. Friesner, R., Banks, J., Murphy, R., Halgren, T., Klicic, J., Mainz, D., Repasky, M., Knoll, E., Shelley, M., Perry, J., Shaw, D., Francis, P., and Shenkin, P. (2004) Glide: a new approach for rapid, accurate docking and scoring. 1. Method and assessment of docking accuracy. *J Med Chem* **47**, 1739-1749
155. Friesner, R., Murphy, R., Repasky, M., Frye, L., Greenwood, J., Halgren, T., Sanschagrin, P., and Mainz, D. (2006) Extra precision glide: docking and scoring incorporating a model of hydrophobic enclosure for protein-ligand complexes. *J Med Chem* **49**, 6177-6196
156. Sogin, D., and Hinkle, P. (1980) Binding of cytochalasin B to human erythrocyte glucose transporter. *Biochemistry* **19**, 5417-5420
157. Lemieux, M. J., Jinmei, S., Myong Jin, K., Yafei, H., Anthony, V., Manfred, A., Xiao-Dan, L., and Da-Neng, W. (2003) Three-dimensional crystallization of the *Escherichia coli*

glycerol-3-phosphate transporter: A member of the major facilitator superfamily. *Protein Sci* **12**, 2748-2756
158. Coderre, P. E., Cloherty, E. K., Zottola, R. J., and Carruthers, A. (1995) Rapid substrate translocation by the multisubunit, erythroid glucose transporter requires subunit associations but not cooperative ligand binding. *Biochemistry* **34**, 9762-9773
159. Pessino, A., Hebert, D. N., Woon, C. W., Harrison, S. A., Clancy, B. M., Buxton, J. M., Carruthers, A., and Czech, M. P. (1991) Evidence that functional erythrocyte-type glucose transporters are oligomers. *J Biol Chem* **266**, 20213-20217
160. Jarvis, S. M., Ellory, J. C., Young, J. D., R.A., and Jung, C. Y. (1986) Radiation inactivation of the human erythrocyte nucleoside and glucose transporters. *Biochim Biophys Acta* **855**, 312-315
161. Baldwin, J., Gorga, J., and Lienhard, G. (1981) The monosaccharide transporter of the human erythrocyte. Transport activity upon reconstitution. *J Biol Chem* **256**, 3685-3689
162. Lloyd, K., Ojelabi, O., De Zutter, J., and Carruthers, A. (2017) Reconciling contradictory findings: Glucose transporter 1 (GLUT1) functions as an oligomer of allosteric, alternating access transporters. *J Biol Chem*
163. Cunningham, P., and Naftalin, R. (2013) Implications of aberrant temperature-sensitive glucose transport via the glucose transporter deficiency mutant (GLUT1DS) T295M for the alternate-access and fixed-site transport models. *J Membr Biol* **246**, 495-511
164. Topham, C., and Brocklehurst, K. (1992) In defence of the general validity of the Cha method of deriving rate equations. The importance of explicit recognition of the thermodynamic box in enzyme kinetics. *Biochem J* **282** 261-265
165. Cha, S. (1968) A simple method for derivation of rate equations for enzyme-catalyzed reactions under the rapid equilibrium assumption or combined assumptions of equilibrium and steady state. *J Biol Chem* **243**, 820-825
166. Baldwin, S., Baldwin, J., and Lienhard, G. (1982) Monosaccharide transporter of the human erythrocyte. Characterization of an improved preparation. *Biochemistry* **21**, 3836-3842
167. Krupka, R., and Devés, R. (1981) An experimental test for cyclic versus linear transport models. The mechanisms of glucose and choline transport in erythrocytes. *J Biol Chem* **256**, 5410-5416
168. Helgerson, A. L., and Carruthers, A. (1989) Analysis of protein-mediated 3-O-methylglucose transport in rat erythrocytes: rejection of the alternating conformation carrier model for sugar transport. *Biochemistry* **28**, 4580-4594
169. Baker, G. F., Widdas, W. F. C., and Kietzke, E. W. (1973) The permeation of human red cells by 4,6-O-ethylidene- -D- glucopyranose (ethylidene glucose). *J Physiol (Lond)* **231**, 129-142
170. Heard, K., Fidyk, N., and Carruthers, A. (2000) ATP-dependent substrate occlusion by the human erythrocyte sugar transporter. *Biochemistry* **39**, 3005-3014
171. Afzal, I., Cunningham, P., and Naftalin, R. J. (2002) Interactions of ATP, oestradiol, genistein and the anti-oestrogens, faslodex (ICI 182780) and tamoxifen, with the human erythrocyte glucose transporter, GLUT1. *Biochem J* **365**, 707-719
172. Afzal, I., Browning, J. A., Drew, C., Ellory, J. C., Naftalin, R. J., and Wilkins, R. J. (2004) Effects of anti-GLUT antibodies on glucose transport into human erythrocyte ghosts. *Bioelectrochemistry* **62**, 195
173. Sage, J., and Carruthers, A. (2014) Human erythrocytes transport dehydroascorbic acid and

sugars using the same transporter complex. *Am J Physiol Cell Physiol* **306**, C910-917
174. Liu, Q., Vera, J. C., Peng, H., Golde, D. W. W., M. C., and Fischbarg, J. (2001) The predicted atp-binding domains in the hexose transporter glut1 critically affect transporter activity. *Biochemistry* **40**, 7874-7881.
175. Baracca, A., Chiaradonna, F., Sgarbi, G., Solaini, G., Alberghina, L., and Lenaz, G. (2010) Mitochondrial Complex I decrease is responsible for bioenergetic dysfunction in K-ras transformed cells. *Biochim Biophys Acta* **1797**, 314-323
176. Chiaradonna, F., Sacco, E., Manzoni, R., Giorgio, M., Vanoni, M., and Alberghina, L. (2006) Ras-dependent carbon metabolism and transformation in mouse fibroblasts. *Oncogene* **25**, 5391-5404
177. Xintaropoulou, C., Ward, C., Wise, A., Marston, H., Turnbull, A., and Langdon, S. (2015) A comparative analysis of inhibitors of the glycolysis pathway in breast and ovarian cancer cell line models. *Oncotarget* **6**, 25677-25695
178. Liu, Y., Cao, Y., Zhang, W., Bergmeier, S., Qian, Y., Akbar, H., Colvin, R., Ding, J., Tong, L., Wu, S., Hines, J., and Chen, X. (2012) A small-molecule inhibitor of glucose transporter 1 downregulates glycolysis, induces cell-cycle arrest, and inhibits cancer cell growth in vitro and in vivo. *Mol Cancer Ther* **11**, 1672-1682
179. Macheda, M. L., Rogers, S., and Best, J. D. (2005) Molecular and cellular regulation of glucose transporter (GLUT) proteins in cancer. *J Cell Physiol* **202**, 654-662
180. Zhang, W., Liu, Y., Chen, X., and Bergmeier, S. (2010) Novel inhibitors of basal glucose transport as potential anticancer agents. *Bioorg Med Chem Lett* **20**, 2191-2194
181. Siebeneicher, H., Cleve, A., Rehwinkel, H., Neuhaus, R., Heisler, I., Müller, T., Bauser, M., and Buchmann, B. (2016) Identification and Optimization of the First Highly Selective GLUT1 Inhibitor BAY-876. *Chemmedchem* **11**, 2261-2271
182. Bloch, R. (1973) Inhibition of glucose transport in the human erythrocyte by cytochalasin B. *Biochemistry* **12**, 4799-4801
183. Sergeant, S., and Kim, H. D. (1985) Inhibition of 3-O-methylglucose transport in human erythrocytes by forskolin. *J Biol Chem* **260**, 14677-14682
184. Levine, K. B., Cloherty, E. K., Fidyk, N. J., and Carruthers, A. (1998) Structural and physiologic determinants of human erythrocyte sugar transport regulation by adenosine triphosphate. *Biochemistry* **37**, 12221-12232
185. Levine, K. B., Cloherty, E. K., Hamill, S., and Carruthers, A. (2002) Molecular determinants of sugar transport regulation by ATP. *Biochemistry* **41**, 12629-12638
186. Inukai, K., Asano, T., Katagiri, H., Anai, M., Funaki, M., Ishihara, H., Tsukuda, K., Kikuchi, M., Yazaki, Y., and Oka, Y. e., W.J. (1994) Replacement of both tryptophan residues at 388 and 412 completely abolished cytochalasin B photolabelling of the GLUT1 glucose transporter. *Biochem J* **302**, 355-361
187. Mann, G., Yudilevich, D., and Sobrevia, L. (2003) Regulation of amino acid and glucose transporters in endothelial and smooth muscle cells. *Physiol Rev S* **83**, 183-252
188. Senes, A., Gerstein, M., and Engelman, D. M. (2000) Statistical analysis of amino acid patterns in transmembrane helices: the GxxxG motif occurs frequently and in association with beta-branched residues at neighboring positions. *J Mol Biol* **296**, 921-936.
189. Liu, Y., Engelman, D. M., and Gerstein, M. (2002) Genomic analysis of membrane protein families: abundance and conserved motifs. *Genome Biology* **3**, research0054.0051-research0054.0012
190. Jiang, Y., Lee, A., Chen, J., Cadene, M., Chait, B. T., and MacKinnon, R. (2002) Crystal

structure and mechanism of a calcium-gated potassium channel. *Nature* **417**, 515-522
191. Ding, S., Ingleby, L., Ahern, C., and Horn, R. (2005) Investigating the putative glycine hinge in Shaker potassium channel. *J Gen Physiol* **126**, 213-226
192. Weinglass, A. B., Smirnova, I. N., and Kaback, H. R. (2001) Engineering Conformational Flexibility in the Lactose Permease of Escherichia coli: Use of Glycine-Scanning Mutagenesis To Rescue Mutant Glu325→Asp. *Biochemistry* **40**, 769-776
193. Zomot, E., Zhou, Y., and Kanner, B. I. (2005) Proximity of Transmembrane Domains 1 and 3 of the γ-Aminobutyric Acid Transporter GAT-1 Inferred from Paired Cysteine Mutagenesis. *J Biol Chem* **280**, 25512-25516
194. Kim, S., Chamberlain, A. K., and Bowie, J. U. (2004) Membrane channel structure of Helicobacter pylori vacuolating toxin: Role of multiple GXXXG motifs in cylindrical channels. *Proc Natl Acad Sci U S A* **101**, 5988-5991
195. Kim, S., Jeon, T.-J., Oberai, A., Yang, D., Schmidt, J. J., and Bowie, J. U. (2005) Transmembrane glycine zippers: Physiological and pathological roles in membrane proteins. *Proc Natl Acad Sci U S A* **102**, 14278-14283
196. Elbaz, Y., Salomon, T., and Schuldiner, S. (2008) Identification of a Glycine Motif Required for Packing in EmrE, a Multidrug Transporter from Escherichia coli. *J Biol Chem* **283**, 12276-12283
197. Henderson, P. J. (1990) The homologous glucose transport proteins of prokaryotes and eukaryotes. [Review]. *Res Microbiol* **141**, 316-328
198. Pao, S. S., Paulsen, I. T., and Saier, M. H., Jr. (1998) Major facilitator superfamily. *Microbiol Mol Biol Rev* **62**, 1-34
199. Jacob, J., Duclohier, H., and Cafiso, D. S. (1999) The role of proline and glycine in determining the backbone flexibility of a channel-forming peptide. *Biophys J* **76**, 1367-1376
200. Wang, D., Pascual, J. M., Yang, H., Engelstad, K., Jhung, S., Sun, R. P., De Vivo, D. C. R. P., Swaroop, K. M., Fischbarg, J., and De Vivo, D. C. (2005) Glut-1 deficiency syndrome: Clinical, genetic, and therapeutic aspects. *Ann Neurol* **57**, 111-118
201. Rosenbusch, J. P., Lustig, A., Grabo, M., Zulauf, M., and Regenass, M. (2001) Approaches to determining membrane protein structures to high resolution: do selections of subpopulations occur? *Micron* **32**, 75-90
202. Newby, Z. E. R., O'Connel, J. D., Gruswitz, F., Hays, F. A., Harries, W. E. C., Harwood, I. M., Ho, J. D., Lee, J. K., Savage, D. F., Miercke, L. J. W., and Stroud, R. (2009) A general protocol for the crystallization of membrane proteins for X-ray structural investigation. *Nat Protoc* **4**, 619-637